doi : 10.17596/0002783

Mirai Cruise Report

MR16−09

Trans South Pacific Project

December 27, 2016 − March 28, 2017

Japan Agency for Marine-Earth Science and Technology (JAMSTEC)

Content

Abe (JAMSTEC), Matsumoto (Univ. of Ryukyu), Fujiwara (JAMSTEC), Sueyoshi, Y. Murakami, Tokunaga, Inagaki, Okumura, K. Yoshida (NME), Kimura, M. Murakami (Mirai Crew)

3.3 Three Component and Total Force Magnetometry

Abe (JAMSTEC), Matsumoto (Univ. of Ryukyu), Fujiwara (JAMSTEC), Sueyoshi, Y. Murakami, Tokunaga, Inagaki, Okumura, K. Yoshida (NME), Kimura, M. Murakami (Mirai Crew)

3.4 Sea Surface Gravity

Abe (JAMSTEC), Matsumoto (Univ. of Ryukyu), Fujiwara (JAMSTEC), Sueyoshi, Y. Murakami, Tokunaga, Inagaki, Okumura, K. Yoshida (NME), Kimura, M. Murakami (Mirai Crew)

3.5 Surface Meteorological Observations

M. Katsumata (JAMSTEC), Sueyoshi, Y. Murakami, Tokunaga, Inagaki, Okumura, K. Yoshida (NME), Kimura, M. Murakami (Mirai Crew)

3.6 Thermo-salinograph and Related Measurements

Uchida, Shiozaki, Sasaoka (JAMSTEC), H. Sato, Tamada, Enoki, Kuwahara, Orui (MWJ)

3.7 pCO_2

Murata (JAMSTEC), Watai, A. Ono, Deguchi, Fujiki (MWJ)

3.8 Satellite Image Acquisition

M. Katsumata (JAMSTEC), Sueyoshi, Y. Murakami, Tokunaga, Inagaki, Okumura, K. Yoshida (NME), Kimura, M. Murakami (Mirai Crew)

3.9 ADCP

Kouketsu (JAMSTEC), Schneider (Univ. of Concepcion), Sueyoshi, Y. Murakami, Tokunaga, Inagaki, Okumura, K. Yoshida (NME), Kimura, M. Murakami (Mirai Crew)

3.10 Ceilometer Observation

M. Katsumata (JAMSTEC), Sueyoshi, Y. Murakami, Tokunaga, Inagaki, Okumura, K. Yoshida (NME), Kimura, M. Murakami (Mirai Crew)

3.11 Marine Aerosols

Noda (Rakuno Gakuen Univ.), Gutierrez (Univ. of Concepcion), O. Yoshida (Rakuno Gakuen Univ.)

3.12 Aerosol Optical Characteristics Measured by Ship-borne Sky Radiometer

Aoki (Toyama Univ.), Hayasaka (Tohoku Univ.)

3.13 C-Band Polarimetric Doppler Weather Radar

M. Katsumata, Geng (JAMSTEC), Sueyoshi, Y. Murakami, Tokunaga, Inagaki, Okumura, K. Yoshida (NME), Kimura, M. Murakami (Mirai Crew)

3.14 Lidar Observation

M. Katsumata, Taniguchi, Geng (JAMSTEC)

3.15 Disdrometers

M. Katsumata, Taniguchi, Geng (JAMSTEC)

3.16 GNSS Precipitable Water

M. Katsumata, Fujita, Taniguchi (JAMSTEC)

3.17 Ship-borne Measurement of Aerosols

Taketani, Kanaya, Miyagawa, Takashima (JAMSTEC), Todo (NIPR), Komazaki (JAMSTEC), Matsui (Nagoya Univ.), Yoshizue (Tokyo Univ. of Sci.)

3.18 Underway CT

Murata (JAMSTEC), Watai, A. Ono, Deguchi, Fujiki (MWJ)

3.19 XCTD

Uchida (JAMSTEC), Okumura, Inagaki, Kimura (NME), M. Murakami (Mirai Crew)

3.20 Radiosonde Observations

M. Katsumata, Geng, Taniguchi (JAMSTEC), Sueyoshi, Y. Murakami (NME)

4. Station Observation

4.1 Single Channel Seismic Survey

Abe (JAMSTEC), Nasu, Kuno, Iijima, Hayashi (NME)

4.2 Sediment Core

Nagashima (JAMSTEC), Lany (AWI), Arz (IOW), Tokunaga, Inagaki, Y. Murakami (NME), Y. Sato, Hatakeyama, Y. Katayama, Takahashi, Miyajima, Yamaguchi (MWJ)

4.3 Dredge

Y. Sato, Hatakeyama, Y. Katayama (MWJ), Abe, Machida (JAMSTEC), Anma (Univ. of Tsukuba), Orihashi (The Univ. of Tokyo)

4.4 Biological Sample

Castro (UdeC)

4.5 Suspended Particles

Gonzalez, Menshel (IDEAL)

4.6 Physiological Characteristics of Phytoplankton Assemblages in the Southern Patagonia Pacific Margin Waters

Iriarte (IDEAL), Shiozaki (JAMSTEC)

4.7 CTDO2 Measurements

Uchida (JAMSTEC), Ito, Tanihara, K. Katayama, Oshitani, Kobayashi (MWJ), Sunamura (The Univ. of Tokyo)

4.8 Bottle Salinity

Uchida (JAMSTEC), Tanihara, Watanabe (MWJ)

4.9 Oxygen

Kumamoto (JAMSTEC), H. Sato, Tamada, Kuwahara, Orui, Htakeyama (MWJ)

4.10 Nutrients

Aoyama (JAMSTEC), Sone, A. Ono, Yokogawa, Ishikawa, Y. Sato (MWJ)

4.11 Density

Uchida, Shiozaki (JAMSTEC)

4.12 Carbon Items

Murata (JAMSTEC), Watai, A. Ono, Deguchi, Fujuki (MWJ)

4.13 Geochemistry and Microbiology: Nitrogen and Carbon Cycles

Yoshikawa (JAMSTEC), O. Yoshida, Chida, Iwamatsu, Koya (Rakuno Gakuen Univ.), Makabe (JAMSTEC)

4.14 Vertical Profiles of Microbial Abundance, Activity and Diversity

Yokokawa (JAMSTEC), Sunamura (The Univ. of Tokyo), Nunoura (JAMSTEC)

4.15 Chlorophyll *a*

Sasaoka, Shiozaki (JAMSTEC), H. Sato, Enoki, Kuwahara, Tamada, Hatakeyama (MWJ)

4.16 Nitrogen Fixation

Shiozaki (JAMSTEC)

4.17 Absorption Coefficients of Particulate Matter and Colored Dissolved Organic Matter (CDOM)

Sasaoka (JAMSTEC)

4.18 Calcium

E. Ono (JAMSTEC)

4.19 Dissolved Organic Matter and the Associated Parameters

Shigemitsu, Yokokawa, Wakita, Murata (JAMSTEC)

4.20 Carbon Isotopes

Kumamoto (JAMSTEC)

4.21 Stable Isotopes of Water

Uchida, K. Katsumata (JAMSTEC)

4.22 Beryllium Isotopes

Kumamoto (JAMSTEC)

4.23 Lowered Acoustic Doppler Current Profiler

Kouketsu, Uchida, K. Katsumata (JAMSTEC)

4.24 Micro Rider

Kouketsu, Uchida, K. Katsumata (JAMSTEC)

4.25 Sound Velocity

Uchida (JAMSTEC), Ito, Tanihara, K. Katayama, Oshitani, Kobayashi (MWJ)

4.26 pH, POC, and HPLC Sampling for SOCCOM Project

K. Katsumata, Sasaoka (JAMSTEC), Boss (Univ. of Maine), Dickson, Becker, Talley (SIO), Key (Princeton Univ.)

4.27 Chlorofluorocarbons and Sulfur Hexafluoride

Sasaki (JAMSTEC), H. Sato, Hoshino, Orui (MWJ)

5. Floats, Drifters and Moorings

5.1 Argo Floats

Masuda, Hosoda, Sato, Hirano (JAMSTEC), Oshitani (MWJ)

5.2 SOCCOM BGC Floats

K. Katsumata (JAMSTEC), Riser, Swift (Univ. of Washington), Johnson (MBARI), Boss (Univ. of Maine), Talley (SIO)

5.3 CO_2 buoys

Murata, Sasaoka (JAMSTEC), Watai, A. Ono, Deguchi, Fujiki (MWJ)

I. Cruise Information

1. Cruise ID

MR16-09

2. Name of vessel

R/V *Mirai*

3. Title of cruise

Trans South Pacific Project

4. Cruise period

Leg 1: 27th December 2016 – 17th January 2017

Leg 2: 20th January – 5th February 2017

Leg 3: 8th February – 5th March 2017

Leg 4: 8th March – 28th March 2017

5. Ports of departure/call/arrival

Leg 1: Suva, Fuji – Puerto Montt, Chile

Leg 2: Puerto Montt, Chile – Punta Arenas, Chile

Leg 3: Punta Arenas, Chile – Auckland, New Zealand

Leg 4: Auckland, New Zealand – Sekinehama, Japan

6. Research area

South Pacific, Chilean coast, Southern Ocean and western North Pacific

7. Research map

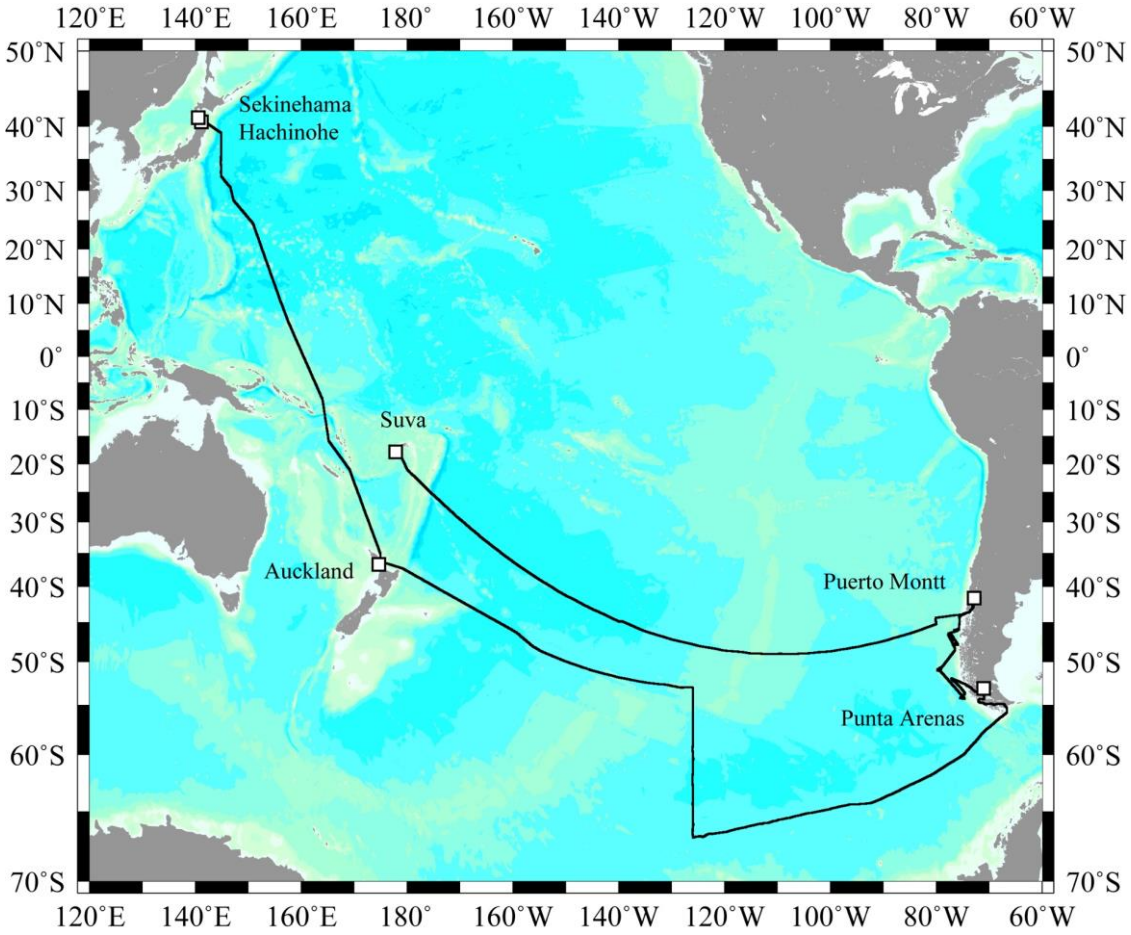

II. Researchers

1. Chief scientists

Leg 1: Akihiko Murata (JAMSTEC)

Leg 2: Naomi Harada (JAMSTEC)

Leg 3: Hiroshi Uchida (JAMSTEC)

Leg 4: Akihiko Murata (JAMSTEC)

2. Representative of the science party and the proposed science plan

(1) Naomi Harada, Akihiko Murata and Natsue Abe: (JAMSTEC): Trans Pacific Project: Ocean Acidification, Marine Biodiversity, Pacific Meridional Overturning Circulation, Crustal Evolution;

(2) Fumikazu Taketani (JAMSTEC): Ship-borne measurements of aerosols in the marine atmosphere: Investigation of potential influence of marine aerosol particles on the climate;

(3) Shuhei Masuda (JAMSTEC): The monitoring of ocean climate change from surface to deep layer in the Southern Ocean by using Argo-type floats;

(4) Taichi Yokokawa (JAMSTEC): Geochemical and microbiological processes throughout water column of the Southern Ocean in the eastern Pacific sector;

(5) Toshiya Fujiwara (JAMSTEC): Regional distribution of seafloor displacement caused by the 2011 Tohoku-oki earthquake: What happened in the northern Japan Trench?

(6) Masaki Katsumata (JAMSTEC): Cumulus-scale air-sea interaction study by shipboard in-situ observations;

(7) Chisato Yoshikawa (JAMSTEC): Geochemical and microbiological investigation for sea surface to sea bottom along Chile margin;

(8) Kazuma Aoki (Toyama University): Aerosol optical characteristics measured by Ship-borne Sky radiometer;

(9) Takeshi Matsumoto (University of the Ryukyus): Cessation of active spreading axes at trenches.

3. List of participants

Name	Charge on board	Affiliation	Occupation
Leg 1: Suva– Puerto Montt			
Akihiko Murata	Chief Scientist	JAMSTEC	Scientist
Masaki Katsumata	Meteorology	JAMSTEC	Scientist
Soichiro Sueyoshi	Chief Technician/ADCP/	NME	Technical Staff

	Meteorology/Geophysics		
Yutaro Murakami	Meteorology/ADCP/ Geophysics	NME	Technical Staff
Tomonori Watai	Chief Technician CO_2-system Properties	MWJ	Technical Staff
Sinichiro Yokogawa	Nutrients	MWJ	Technical Staff
Hiroyasu Sato	DO/TSG	MWJ	Technical Staff
Nagisa Fujiki	CO_2-system Properties	MWJ	Technical Staff

Leg 2: Puerto Montt – Punta Arenas

Naomi Harada	Chief Scientist	JAMSTEC	Scientist
Natsue Abe	Dredge/ Single-channel Seismology	JAMSTEC	Scientist
Kana Nagashima	Sediment	JAMSTEC	Scientist
Takuhei Shiozaki	CTD/Water Sampling	JAMSTEC	Scientist
Miyako Sato	CTD/Water Sampling/ Sediment	JAMSTEC	Technical Staff
Hidetaka Nomaki	Sediment	JAMSTEC	Scientist
Chisato Yoshikawa	Water Sampling	JAMSTEC	Scientist
Shiki Machida	Dredge	JAMSTEC	Scientist
Jun Noda	Aerosol/Water sampling	RGU	Assosiate Professor
Shinya Iwasaki	Sediment	AIST	Researcher
Kanda Chida	Water Sampling	RGU	Graduate Student
Ryo Anma	Dredge/Sediment	Univ of Tsukuba	Lecturer
Yuji Orihashi	Dredge	UT	Assistant Professor
Frank Lamy	Sediment	AWI	Professor
Helge Wolfgang Arz	Sediment	IOW	Professor
Leonardo Román Castro Cifuentes	Plankton Net	UdeC	Professor
Wolfgang Schneider	CTD	UdeC	Professor
Humberto González	Water Sampling	IDEAL	Professor
Jose Luis Iriarte	FRRF	IDEAL	Professor
Eduardo Menschel A.	Water Sampling	IDEAL	Technical Staff
Marcelo Gutiérrez Astete	Aerosol/Water Sampling	UdeC	Researcher
Alejandro Jose Avila Santis	Sediment	UdeC	Technical Staff
Victor Acuña	Sediment/Plankton Net	UdeC	Technical Staff

Wataru Tokunaga	Chief Technician/ADCP/ Meteorology/Bathymetry/Geophysics	NME	Technical Staff
Satsuki Iijima	Meteorology/Bathymetry/ Geophysics/ADCP	NME	Technical Staff
Koichi Inagaki	Meteorology/Bathymetry/ Geophysics/ADCP	NME	Technical Staff
Yutaro Murakami	Meteorology/Bathymetry/ Geophysics/ADCP	NME	Technical Staff
Toshimasa Nasu	Single-channel Seismology	NME	Technical Staff
Hiroyuki Hayashi	Single-channel Seismology	NME	Technical Staff
Mitsuteru Kuno	Single-channel Seismology	NME	Technical Staff
Yusuke Sato	Chief Technician/Sediment/ Dredge	MWJ	Technical Staff
Ei Hatakeyama	Sediment/Dredge	MWJ	Technical Staff
Yuki Miyajima	Sediment/Dredge	MWJ	Technical Staff
Mika Yamaguchi	Sediment/Dredge	MWJ	Technical Staff
Yohei Katayama	Sediment/Dredge	MWJ	Technical Staff
Kazuma Takahashi	Sediment/Dredge	MWJ	Technical Staff
Rei Ito	CTD	MWJ	Technical Staff
Sonoka Tanihara	Water sampling/Salinity	MWJ	Technical Staff
Atsushi Ono	CO2-system Properties	MWJ	Technical Staff
Tomomi Sone	Water Sampling/Nutrients	MWJ	Technical Staff
Haruka Tamada	TSG/Water Sampling/DO	MWJ	Technical Staff

Leg 3: Punta Arenas – Auckland

Hiroshi Uchida	Chief Scientist/Density/ Isotope of Water/Sound Velocity	JAMSTEC	Scientist
Yuichiro Kumamoto	DO/Water Sampling/ Carbon Isotopes/Beryllium Isotopes	JAMSTEC	Scientist
Katsuro Katsumata	SOCCOM Project/ LADCP/Micro Rider	JAMSTEC	Scientist
Kosei Sasaoka	Chlorophyll-a/CDOM/ Absorption Coefficient/CO2 Buoy/ SOCCOM Project	JAMSTEC	Scientist
Etsuro Ono	Calcium/Water Sampling/ CO2 Buoy	JAMSTEC	Scientist

Masahito Shigemitsu	DOM/Water Sampling	JAMSTEC	Scientist
Kenichi Sasaki	CFCs	JAMSTEC	Scientist
Takuma Miyakawa	Aerosols	JAMSTEC	Scientist
Taichi Yokokawa	Microbiology	JAMSTEC	Scientist
Michinari Sunamura	Microbiology	UT	Assistant Professor
Momoka Yoshizue	Aerosols	TUS	Graduate Student
Noriko Iwamatsu	Geochemistry/Microbiology	RGU	Student
Minami Koya	Geochemistry/Microbiology	RGU	Student
Shinya Okumura	Chief technician/ Meteorology/Geophysics/ADCP/XCTD	NME	Technical Staff
Koichi Inagaki	Meteorology/Geophysics/ ADCP/XCTD	NME	Technical Staff
Ryo Kimura	Meteorology/Geophysics/ ADCP/XCTD	NME	Technical Staff
Satoshi Ozawa	Chief Technician/ Water Sampling	MWJ	Technical Staff
Kenichi Katayama	CTD	MWJ	Technical Staff
Akira Watanabe	Water Sampling/Salinity	MWJ	Technical Staff
Shungo Oshitani	CTD/Argo	MWJ	Technical Staff
Rio Kobayashi	CTD	MWJ	Technical Staff
Shinichiro Yokogawa	Nutrients	MWJ	Technical Staff
Tomonori Watai	Total Alkalinity/ Underway DIC	MWJ	Technical Staff
Nagisa Fujiki	DIC/Underway DIC	MWJ	Technical Staff
Ei Hatakeyama	DO/TSG/Chlorophyll-a	MWJ	Technical Staff
Masanori Enoki	DO/TSG/Chlorophyll-a	MWJ	Technical Staff
Hironori Sato	CFCs	MWJ	Technical Staff
Hiroshi Hoshino	CFCs	MWJ	Technical Staff
Misato Kuwahara	DO/TSG/Chlorophyll-a	MWJ	Technical Staff
Koki Uda	Water Sampling	MWJ	Technical Staff
Yoshiaki Sato	Nutrients	MWJ	Technical Staff
Rei Ito	CTD/Argo	MWJ	Technical Staff
Sonoka Tanihara	Salinity	MWJ	Technical Staff
Atsushi Ono	DIC/Underway DIC	MWJ	Technical Staff
Tomomi Sone	Nutrients	MWJ	Technical Staff
Haruka Tamada	DO/TSG/Chlorophyll-a	MWJ	Technical Staff

Yoshiko Ishikawa	Nutrients	MWJ	Technical Staff
Emi Deguchi	Total Alkalinity	MWJ	Technical Staff
Masahiro Orui	CFCs	MWJ	Technical Staff

Leg 4: Auckland – Sekinehama

Akihiko Murata	Chief Scientist	JAMSTEC	Scientist
Kazuho Yoshida	Chief Technician/ADCP/ Meteorology/Geophysics	NME	Technical Staff
Ryo Kimura	Meteorology/ADCP/ Geophysics	NME	Technical Staff
Yoshiko Ishikawa	Chief Technician	MWJ	Technical Staff
Masahiro Orui	DO/TSG/Chlorophyll-a	MWJ	Technical Staff
Emi Deguchi	CO_2-system Properties	MWJ	Technical Staff

JAMSTEC	Japan Agency for Marine-Earth Science and Technology
NME	Nippon Marine Enterprises, Ltd.
MWJ	Marine Works Japan, Ltd.
RGU	Rakuno Gakuen University
TUS	Tokyo University of Science
UdeC	University of Conception, Chile
IDEAL	Centro de Investigación Dinámica de Ecosystemas Marinos de Altas Latitudes, Universidad Austral de Chile
SIO	Scripps Institution of Oceanography, USA
UW	University of Washington, USA
UT	The University of Tokyo
AIST	National Institute of Advanced Industrial Science and Technology
AWI	Alfred Wegener Institute, Germany
IOW	Leibniz-Institute for Baltic Sea Research Warnemünde, Germany

4. List of Principal Investigator and Person in Charge on the Ship

The principal investigator (PI) and the person in charge responsible for major parameters measured on the cruise are listed in Table 4.1.

Table 4.1. List of principal investigator and person in charge on the ship.

Item	Principal Investigator	Person in Charge on the Ship
Underway		
Navigation	Naomi Harada (JAMSTEC) *haradan@jamstec.go.jp*	Souichiro Sueyoshi (NME) (leg 1) Wataru Tokunaga (NME) (leg 2) Shinya Okumura (NME) (leg 3) Kazuho Yoshida (NME) (leg 4)
Bathymetry	Natsue Abe (JAMSTEC) *abenatsu@jamstec.go.jp*	Souichiro Sueyoshi (NME) (leg 1) Wataru Tokunaga (NME) (leg 2) Shinya Okumura (NME) (leg 3) Kazuho Yoshida (NME) (leg 4)
Magnetic Field	Natsue Abe (JAMSTEC) *abenatsu@jamstec.go.jp*	Souichiro Sueyoshi (NME) (leg 1) Wataru Tokunaga (NME) (leg 2) Shinya Okumura (NME) (leg 3) Kazuho Yoshida (NME) (leg 4)
Gravity	Natsue Abe (JAMSTEC) *abenatsu@jamstec.go.jp*	Souichiro Sueyoshi (NME) (leg 1) Wataru Tokunaga (NME) (leg 2) Shinya Okumura (NME) (leg 3) Kazuho Yoshida (NME) (leg 4)
Meteorology	Masaki Katsumata (JAMSTEC) *katsu@jamstec.go.jp*	Souichiro Sueyoshi (NME) (leg 1) Wataru Tokunaga (NME) (leg 2) Shinya Okumura (NME) (leg 3) Kazuho Yoshida (NME) (leg 4)
TSG	Hiroshi Uchida (JAMSTEC) *huchida@jamtec.go.jp*	Hironori Sato (MWJ) (leg 1) Haruka Tamada (MWJ) (leg 2) Masanori Enoki (MWJ) (leg 3) Masahiro Orui (MWJ) (leg 4)
pCO_2	Akihiko Murata (JAMSTEC) *murataa@jamstec.go.jp*	Tomonori Watai (MWJ) (leg 1) Atsushi Ono (MWJ) (leg 2) Emi Deguchi (MWJ) (legs 3, 4)
Underway DIC	Akihiko Murata (JAMSTEC) *murataa@jamstec.go.jp*	Nagisa Fujiki (MWJ)
ADCP	Shinya Kouketsu (JAMSTEC) *skouketsu@jamstec.go.jp*	Souichiro Sueyoshi (NME) (leg 1) Wataru Tokunaga (NME) (lge 2)

		Shinya Okumura (NME) (leg 3)
		Kazuho Yoshida (NME) (leg 4)
Ceilometer	Masaki Katsumata (JAMSTEC)	Souichiro Sueyoshi (NME) (leg 1)
	katsu@jamstec.go.jp	Wataru Tokunaga (NME) (leg 2)
		Shinya Okumura (NME) (leg 3)
		Kazuho Yoshida (NME) (leg 4)
Marine Aerosols	Jun Noda (RGU)	Jun Noda (RGU) (leg 2)
	jnoda@rakuno.ac.jp	Taichi Yokokawa (JAMSTEC) (leg 3)
Sky Radiometer	Kazuma Aoki (Univ. of Toyama)	none
	kazuma@sci.u-toyama.ac.jp	
Doppler Radar	Masaki Katsumata (JAMSTEC)	Souichiro Sueyoshi (NME) (leg 1)
	katsu@jamstec.go.jp	Wataru Tokunaga (NME) (leg 2)
		Shinya Okumura (NME) (leg 3)
		Kazuho Yoshida (NME) (leg 4)
Lidar	Masaki Katsumata (JAMSTEC)	Masaki Katsumata (JAMSTEC) (leg 1)
	katsu@jamstec.go.jp	
Disdrometer	Masaki Katsumata (JAMSTEC)	Masaki Katsumata (JAMSTEC) (leg 1)
	katsu@jamstec.go.jp	
GNSS Precipitable Water		
	Masaki Katsumata (JAMSTEC)	Masaki Katsumata (JAMSTEC) (leg 1)
	katsu@jamstec.go.jp	
XCTD	Hiroshi Uchida (JAMSTEC)	Shinya Okumura (NME)
	huchida@jamstec.go.jp	
Radiosonde	Masaki Katsumata (JAMSTEC)	Souichiro Sueyoshi (NME)
	katsu@jamstec.go.jp	
Satellite Image	Masaki Katsumata (JAMSTEC)	Souichiro Sueyoshi (NME) (leg 1)
	katsu@jamstec.go.jp	Wataru Tokunaga (NME) (leg 2)
		Shinya Okumura (NME) (leg 3)
		Kazuho Yoshida (NME) (leg 4)
MAX-DOAS	Hisahiro Takashima (JAMSTEC)	Takuma Miyakawa (JAMSTEC) (leg 3)
	hisahiro@jamstec.go.jp	
Ozone and CO	Yugo Kanaya (JAMSTEC)	Takuma Miyakawa (JAMSTEC) (leg 3)
	yugo@jamstec.go.jp	
Black Carbon Particles		
	Fumikazu Taketani (JAMSTEC)	Takuma Miyakawa (JAMSTEC) (leg 3)
	taketani@jamstec.go.jp	

Fluorescent Aerosol Particles

Fumikazu Taketani (JAMSTEC) Takuma Miyakawa (JAMSTEC) (leg 3)
taketani@jamstec.go.jp

Aerosol Particle Size Distribution

Takuma Miyakawa (JAMSTEC) Takuma Miyakawa (JAMSTEC) (leg 3)
miyakawat@jamstec.go.jp

Aerosol Particle Sampling for post-analyses

Fumikazu Taketani (JAMSTEC) Takuma Miyakawa (JAMSTEC) (leg 3)
taketani@jamstec.go.jp

Station Observation

Single Channel Seismometer

Natsue Abe (JAMSTEC) Toshimasa Nasu (NME)
abenatsu@jamstec.go.jp

Sediment Core	Kana Nagashima (JAMSTEC) *nagashimak@jamstec.go.jp*	Yusuke Sato (MWJ)
Dredge	Natsue Abe (JAMSTEC) *abenatsu@jamstec.go.jp*	Yusuke Sato (MWJ)
Biological Sample	Leonardo Román Castro Cifuentes (UdeC) *lecastro@oceanografia.udec.cl*	Naomi Harada (JAMSTEC)
Suspended Particles	Humberto González (IDEAL) *hgonzale@uach.cl*	Naomi Harada (JAMSTEC)
FRRF	Jose Luis Iriarte (IDEAL) *jiriarte@uach.cl*	Naomi Harada (JAMSTEC)
CTD/O_2	Hiroshi Uchida (JAMSTEC) *huchida@jamstec.go.jp*	Rei Ito (MWJ) (leg 2) Kenichi Katayama (MWJ) (leg 3)
Salinity	Hiroshi Uchida (JAMSTEC) *huchida@jamstec.go.jp*	Sonoka Tanihara (MWJ)
Oxygen	Yuichiro Kumamoto (JAMSTEC) *kumamoto@jamstec.go.jp*	Hironori Sato (MWJ) (leg 1) Haruka Tamada (MWJ) (legs 2, 3) Masahiro Orui (MWJ) (leg 4)
Nutrients	Michio Aoyama (Fukushima Univ.) *r706@ipc.fukushima-u.ac.jp*	Tomomi Sone (MWJ)
Density	Hiroshi Uchida (JAMSTEC) *huchida@jamstec.go.jp*	Takuhei Shiozaki (JAMSTEC) (leg 2) Hiroshi Uchida (JAMSTEC) (leg 3)

CFCs/SF_6/N_2O	Ken'ichi Sasaki (JAMSTEC) *ksasaki@jamstec.go.jp*	Ken'ichi Sasaki (JAMSTEC)
DIC	Akihiko Murata (JAMSTEC) *murataa@jamstec.go.jp*	Atsushi Ono (MWJ)
Alkalinity	Akihiko Murata (JAMSTEC) *murataa@jamstec.go.jp*	Atsushi Ono (MWJ) (leg 2) Tomonori Watai (MWJ) (leg 3)
Chlorophyll *a*	Kosei Sasaoka (JAMSTEC) *sasaoka@jamstec.go.jp*	Hironori Sato (MWJ) (leg 1) Takuhei Shiozaki (JAMSTEC) (leg 2) Kosei Sasaoka (JAMSTEC) (leg 3) Masahiro Orui (MWJ) (leg 4)
CDOM/Absorption Coefficients	Kosei Sasaoka (JAMSTEC) *sasaoka@jamstec.go.jp*	Kosei Sasaoka (JAMSTEC)
Calcium	Etsuro Ono (JAMSTEC) *onoet@jamstec.go.jp*	Etsuro Ono (JAMSTEC)
DOM	Masahiro Shigemitsu (JAMSTEC) *ma-shige@jamstec.go.jp*	Masahiro Shigemitsu (JAMSTEC)
$\Delta^{14}C/\delta^{13}C$	Yuichiro Kumamoto (JAMSTEC) *kumamoto@jamstec.go.jp*	Yuichiro Kumamoto (JAMSTEC)
Beryllium Isotopes	Yuichiro Kumamoto (JAMSTEC) *kumamoto@jamstec.go.jp*	Yuichiro Kumamoto (JAMSTEC)
$\delta^{18}O/\delta D$	Hiroshi Uchida (JAMSTEC) *huchida@jamstec.go.jp*	Hiroshi Uchida (JAMSTEC)
N_2O/CH_4	Osamu Yoshida (RGU) *yoshida@rakuno.ac.jp*	Kanta Chida (RGU) (leg 2) Noriko Iwamatsu (RGU) (leg 3)
Cell Abundance	Michinari Sunamura (UT) *sunamura@eps.s.u-tokyo.ac.jp*	Hidetaka Nomaki (JAMSTEC) (leg 2) Michinari Sunamura (UT) (leg 3)
Microbial Diversity	Taichi Yokokawa (JAMSTEC) *taichi.yokokawa@jamstec.go.jp*	Hidetaka Nomaki (JSMTEC) (leg 2) Taichi Yokokawa (JAMSTEC) (leg 3)
Microbial Carbon Uptake	Taichi Yokokawa (JAMSTEC) *taichi.yokokawa@jamstec.go.jp*	Taichi Yokokawa (JAMSTEC) (leg 3)
$\delta^{13}C/CH_4$	Akiko Makabe (JAMSTEC) *makabea@jamstec.go.jp*	Chisato Yoshikawa (JAMSTEC) (leg 2) Minami Koya (RGU) (leg 3)
$\delta^{15}N$ $\delta^{18}O/N_2O$	Akiko Makabe (JAMSTEC) *makabea@jamstec.go.jp*	Chisato Yoshikawa (JAMSTEC) (leg 2) Noriko Iwamatsu (RGU) (leg 3)
$\delta^{15}N$ $\delta^{18}O/NO_3$	Chisato Yoshikawa (JAMSTEC) *yoshikawac@jamstec.go.jp*	Chisato Yoshikawa (JAMSTEC) (leg 2) Minami Koya (RGU) (leg 3)

$\delta^{15}N$/chlorophyll	Chisato Yoshikawa (JAMSTEC) *yoshikawac@jamstec.go.jp*	Chisato Yoshikawa (JAMSTEC) (leg 2)
LADCP	Shinya Kouketsu (JAMSTEC) *skouketsu@jamstec.go.jp*	Katsuro Katsumata (JAMSTEC)
Micro-Rider	Shinya Kouketsu (JAMSTEC) *skouketsu@jamstec.go.jp*	Katsuro Katsumata (JAMSTEC)
Sound Velocity	Hiroshi Uchida (JAMSTEC) *huchida@jamstec.go.jp*	Rei Ito (MWJ) (leg 2) Hiroshi Uchida (JAMSTEC) (leg 3)
pH	Andrew Dickson (SIO) *adickson@ucsd.edu*	Katsuro Katsumata (JAMSTEC)
POC	Susan Becker (SIO) *sbecker@ucsd.edu*	Kosei Sasaoka (JAMSTEC)
HPLC	Susan Becker (SIO) *sbecker@ucsd.edu*	Kosei Sasaoka (JAMSTEC)

Floats, Drifters, Moorings

ARGO Float	Shuhei Masuda (JAMSTEC) *smasuda@jamstec.go.jp*	Shungo Oshitani (MWJ)
SOCCOM BGC Float	Stephen Riser (UW) *riser@ocean.washington.edu*	Katsuro Katsumata (JAMSTEC)
CO_2 Buoy	Akihiko Murata (JAMSTEC) *murataa@jamstec.go.jp*	Akihiko Murata (JAMSTEC) (leg 1) Kosei Sasaoka (JAMSTEC) (leg 3)

JAMSTEC	Japan Agency for Marine-Earth Science and Technology
NME	Nippon Marine Enterprises, Ltd.
MWJ	Marine Works Japan, Ltd.
RGU	Rakuno Gakuen University
TUS	Tokyo University of Science
UdeC	University of Conception, Chile
IDEAL	Centro de Investigación Dinámica de Ecosystemas Marinos de Altas Latitudes, Universidad Austral de Chile
SIO	Scripps Institution of Oceanography, USA
UW	University of Washington, USA
UT	The University of Tokyo

III. Observation

1. Cruise Narrative

We are now at a transient stage moving from Holocene, which is characterized by a stable climate, to a new era: Anthropocene. Impacts due to human activities upon surface environment of the earth are appearing as catastrophic climate changes and the related collapse of ecosystem. In addition, as demonstrated by a series of great earthquakes occurred off Chilean coast, off Sumatra and off East Japan, and volcanic activities linked to the earthquakes, it can be said that we are now in the era, when the interior of the earth or crust is in an active phase. Therefore, the present cruise was aimed at clarifying what happened, in this Anthropocene, era of great earth changes, in the fields on surface environment of the earth and those in the interior of it, focusing emergent and confronting issues: 1) Changes in heat and material transports by ocean circulation; 2) Detection of progressive ocean acidification and the response of marine biology, and relationship between biodiversity of marine organisms and changes in living environment; 3) Interaction among mantle, ocean ridge, and subduction system.

In the cruise, 8 science plans (see II 2) adopted by the *Mirai* science committee were also conducted together with the main mission: Trans South Pacific Project.

2. Cruise Track and Log

Cruise tracks and positions at each day are shown in the following figures, separately for respective legs.

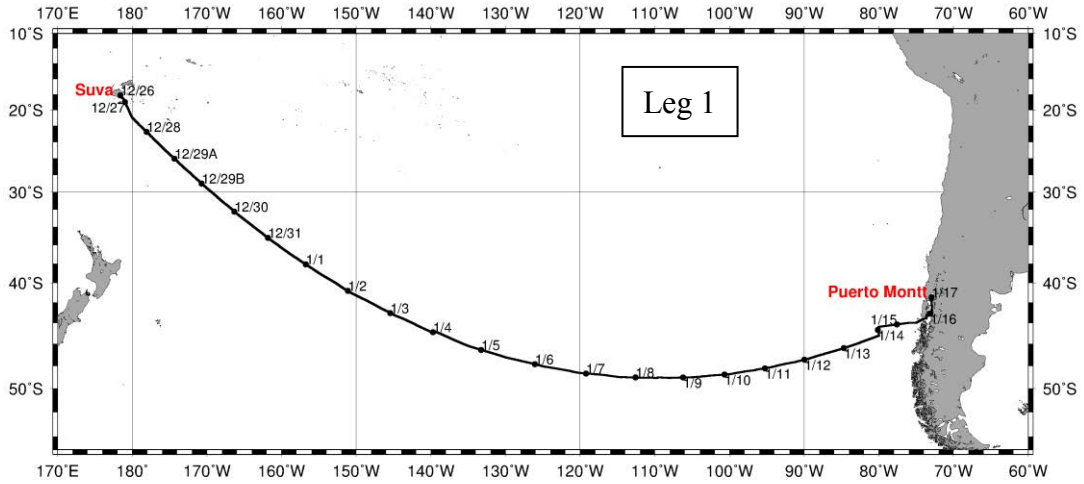

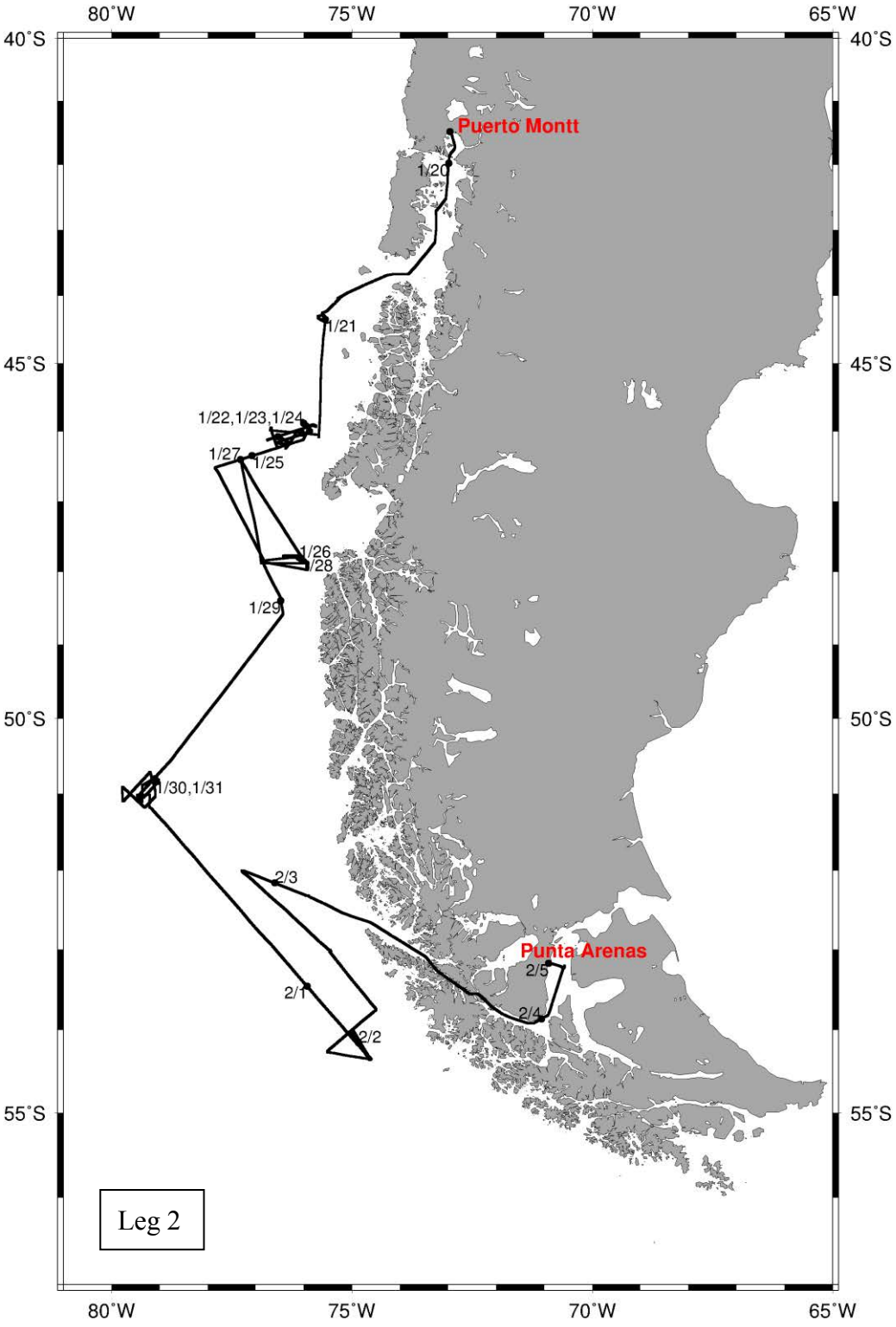
80°W
75°W
70°W
65°W
40°S
45°S
50°S
55°S
Puerto Montt
1/20
1/21
1/22,1/23,1/24
1/27
1/25
1/26
1/28
1/29
1/30,1/31
2/3
2/1
2/2
Punta Arenas
2/5
2/4
Leg 2

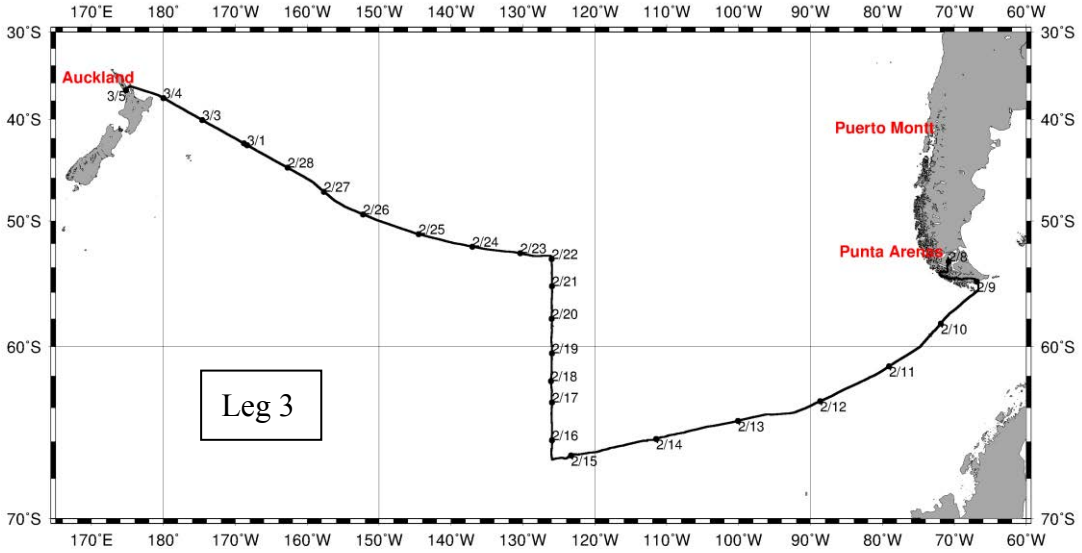
170°E
180°
170°W
160°W
150°W
140°W
130°W
120°W
110°W
100°W
90°W
80°W
70°W
60°W
30°S
40°S
50°S
60°S
70°S
Auckland
3/5
3/4
3/3
3/1
2/28
2/27
2/26
2/25
2/24
2/23
2/22
2/21
2/20
2/19
2/18
2/17
2/16
2/15
2/14
2/13
2/12
2/11
2/10
2/9
2/8
Puerto Montt
Punta Arenas
Leg 3

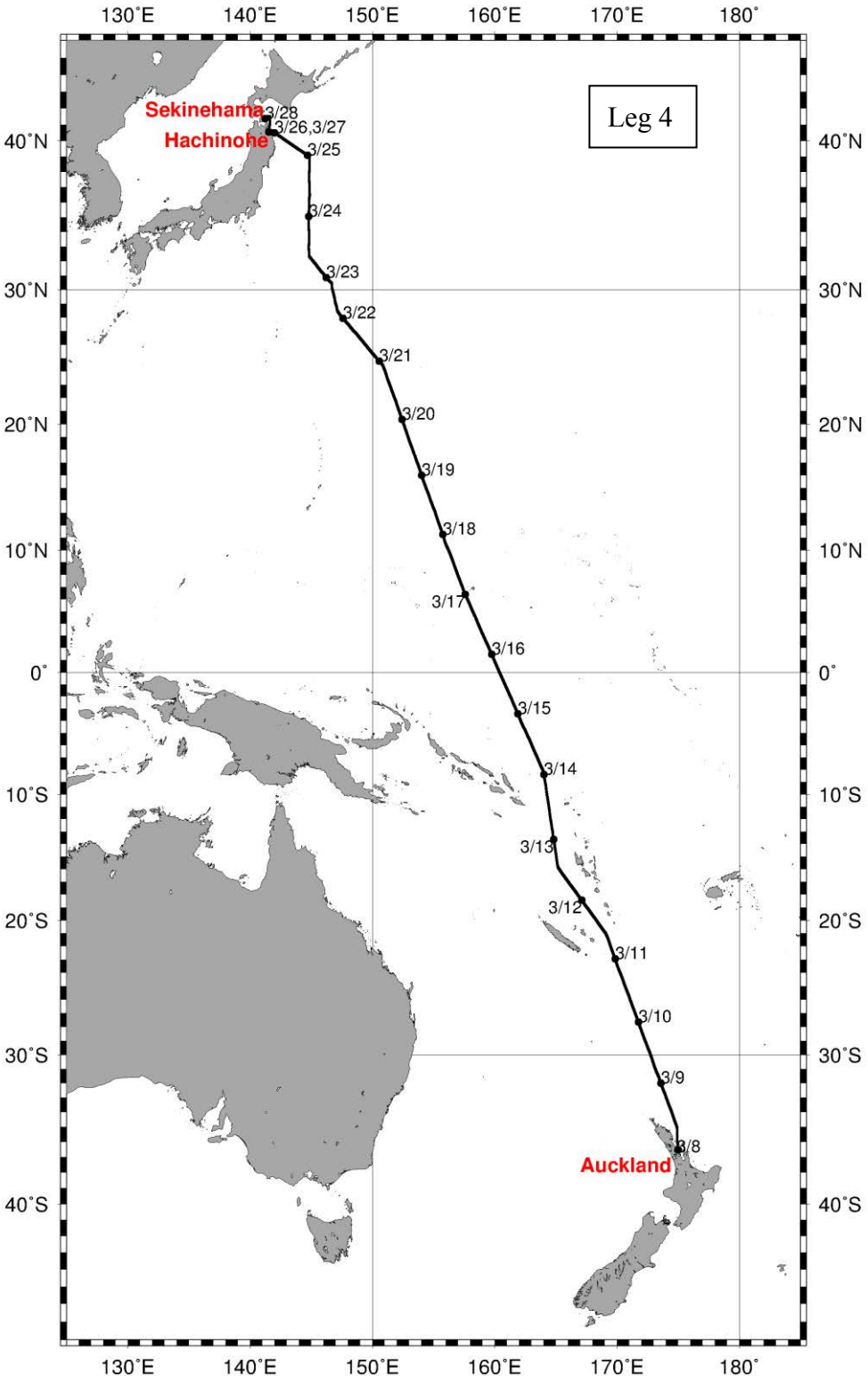
Leg 4
Sekinehama
Hachinohe
3/28
3/26,3/27
3/25
3/24
3/23
3/22
3/21
3/20
3/19
3/18
3/17
3/16
3/15
3/14
3/13
3/12
3/11
3/10
3/9
3/8
Auckland
130˚E
140˚E
150˚E
160˚E
170˚E
180˚
40˚N
30˚N
20˚N
10˚N
0˚
10˚S
20˚S
30˚S
40˚S

3 Underway Observation

3.1 Navigation

(1) Personnel

Akihiko Murata	***JAMSTEC: Principal investigator[*1]***	***- leg1,2,3,4 -***
Souichiro Sueyoshi	***Nippon Marine Enterprises Ltd., (NME)***	***- leg1 -***
Yutaro Murakami	***NME***	***- leg1,2 -***
Wataru Tokunaga	***NME***	***- leg2 -***
Koichi Inagaki	***NME***	***- leg2,3 -***
Shinya Okumura	***NME***	***- leg3 -***
Kazuho Yoshida	***NME***	***- leg4 -***
Ryo Kimura	***MIRAI crew / NME***	***- leg1,3,4 -***
Masanori Murakami	***MIRAI crew***	***- leg2,3,4 -***

[*1] leg1,4: On-board, leg2,3: Not on-board

(2) System description

Ship's position and velocity were provided by Navigation System on R/V MIRAI. This system integrates GNSS position, Doppler sonar log speed, Gyro compass heading and other basic data for navigation. This system also distributed ship's standard time synchronized to GPS time server via Network Time Protocol. These data were logged on the network server as "SOJ" data every 5 seconds. Sensors for navigation data are listed below;

i) GNSS system:

R/V MIRAI has four GNSS systems, all GNSS positions were offset to radar-mast position, datum point. Anytime changeable manually switched as to GNSS receiving state.

a) StarPack-D & Multi-Fix (version 6), Differential GNSS system.
   Antenna: Located on compass deck, starboard.

b) StarPack-D & Multi-Fix (version 6), Differential GNSS system.
   Antenna: Located on compass deck, portside.

c) Standalone GPS system.
   Receiver: Trimble SPS751
   Antenna: Located on navigation deck, starboard.

d) Standalone GPS system.
   Receiver: Trimble SPS751
   Antenna: Located on navigation deck, portside.

ii) Doppler sonar log:

FURUNO DS-30, which use three acoustic beam for current measurement under the hull.

iii) Gyro compass:

TOKYO KEIKI TG-6000, sperry type mechanical gyrocompass.

iv) GPS time server:

SEIKO Precision TS-2540 Time Server, synchronizing to GPS satellites every 1 second.

(3) Data period (Time in UTC)

Leg1: 17:10, 26 Dec. 2016 to 11:00, 17 Jan. 2017

Leg2: 12:00, 20 Jan. 2017 to 13:00, 05 Feb. 2017

Leg3: 13:10, 08 Feb. 2017 to 21:00, 04 Mar. 2017

Leg4: 21:20, 07 Mar. 2017 to 00:00, 28 Mar. 2017

3.2 Swath Bathymetry (MBES, Sub-bottom profiler)

(1) Personnel

Natsue Abe	*JAMSTEC: Principal investigator*	*- leg2 -*
Takeshi Matsumoto	*Univ. of the Ryukyus: Principal investigator (Not on board)*	*- leg1,2,3,4 -*
Toshiya Fujiwara	*JAMSTEC: Principal investigator (Not on board)*	*- leg4 -*
Souichiro Sueyoshi	*Nippon Marine Enterprises Ltd., (NME)*	*- leg1 -*
Yutaro Murakami	*NME*	*- leg1,2 -*
Wataru Tokunaga	*NME*	*- leg2 -*
Koichi Inagaki	*NME*	*- leg2,3 -*
Shinya Okumura	*NME*	*- leg3 -*
Kazuho Yoshida	*NME*	*- leg4 -*
Ryo Kimura	*MIRAI crew / NME*	*- leg1,3,4 -*
Masanori Murakami	*MIRAI crew*	*- leg2,3,4 -*

(2) Introduction

R/V MIRAI is equipped with a Multi narrow Beam Echo Sounding system (MBES), SEABEAM 3012 (L3 Communications, ELAC Nautik). The objective of MBES is collecting continuous bathymetric data along ship's track to make a contribution to geological and geophysical investigations and global datasets.

Also, R/V MIRAI is equipped with a Sub-Bottom Profiler (SBP), Bathy2010 (SyQwest). The objective of SBP is collecting sub-bottom data along ship's track.

(3) Data Acquisition

The "SEABEAM 3012" on R/V MIRAI was used for bathymetry mapping in the MR16-09 Leg1 to Leg4 cruises.

To get accurate sound velocity of water column for ray-path correction of acoustic multibeam, we used Surface Sound Velocimeter (SSV) data to get the sea surface sound velocity (at 6.62m), and the deeper depth sound velocity profiles were calculated by temperature and salinity profiles from CTD and XCTD data by the equation in Del Grosso (1974) during these cruises. Table 3.2-1 shows system configuration and performance of SEABEAM 3012.

Bathy2010 on R/V MIRAI was used for sub-bottom mapping during the Leg2 cruise. Table 3.2-2 shows system configuration and performance of Bathy2010 system.

Table 3.2-1 SEABEAM 3012 system configuration and performance

Frequency:	12 kHz
Transmit beam width:	2.0 degree
Transmit power:	4 kW
Transmit pulse length:	2 to 20 msec.
Receive beam width:	1.6 degree
Depth range:	50 to 11,000 m
Number of beams:	301 beams
Beam spacing:	Equi-angle
Swath width:	60 to 150 degrees
Depth accuracy:	< 1 % of water depth (average across the swath)

Table 3.2-2 Bathy2010 System configuration and performance

Frequency:	3.5 KHz (FM sweep)
Transmit beam width:	23 degree
Transmit pulse length:	0.5 to 50 msec
Strata resolution:	Up to 8 cm with 300 m of bottom penetration according to bottom type
Depth resolution:	0.1 feet, 0.1 m
Depth accuracy:	±10 cm to 100 m, ± 0.3% to 6,000 m
Sound velocity:	1,500 m/s (fix)

(4) Data processing of MBES (leg3)

i) Sound velocity correction

Bathymetry data were corrected with sound velocity profiles calculated from the nearest CTD or XCTD data in the distance. The equation of Del Grosso (1974) was used for calculating sound velocity. The data correction was carried out using the HIPS software version 9.1.4 (CARIS, Canada)

ii) Editing and Gridding

Editing for the bathymetry data was carried out using the HIPS. Firstly, the bathymetry data during ship's turning were basically deleted, and spike noise of swath data was removed. Then the bathymetry data were checked by "BASE surface (resolution: 50 m averaged grid)".

Finally, all accepted data were exported as XYZ ASCII data (longitude [degree], latitude [degree],

depth [m]), and converted to 150 m grid data using “nearneighbor” utility of GMT (Generic Mapping Tool) software.

Table 3.2-3 Parameters for gridding on “nearneighbor” in GMT

Gridding mesh size:	150 m
Search radius size:	150 m
Minimum number of neighbors for grid:	1

(5) Data Archives

These data obtained in this cruise will be submitted to the Data Management Group (DMG) in JAMSTEC, and will be opened to the public via “Data Research System for Whole Cruise Information in JAMSTEC (DARWIN)” in JAMSTEC web site.
<http://www.godac.jamstec.go.jp/darwin/e>.

(6) Remarks (Time in UTC)

i) The following periods, the MBES observations were carried out.

Leg1: 18:46, 28 Dec. 2016 to 06:00, 15 Jan. 2017
Leg2: 12:11, 21 Jan. 2017 to 14:17, 21 Jan. 2017
14:32, 21 Jan. 2017 to 00:23, 04 Feb. 2017
Leg3: 21:00, 10 Feb. 2017 to 06:59, 03 Mar. 2017
Leg4: 07:03, 09 Mar. 2017 to 09:59, 10 Mar. 2017
10:00, 15 Mar. 2017 to 08:09, 16 Mar. 2017
01:50, 18 Mar. 2017 to 03:43, 26 Mar. 2017

ii) The following periods, the SBP observations were carried out.

Leg2: 12:11, 21 Jan. 2017 to 14:17, 21 Jan. 2017
14:32, 21 Jan. 2017 to 00:23, 04 Feb. 2017

iii) The following periods, data acquisition of MBES was suspended due to system trouble.

Leg4: 07:38, 09 Mar. 2017 to 07:47, 09 Mar. 2017
04:02, 25 Mar. 2017 to 04:11, 26 Mar. 2017

3.3 Three Component and Total Force Magnetometry

(1) Personnel

Natsue Abe	*JAMSTEC: Principal investigator*	*- leg2 -*
Takeshi Matsumoto	*Univ. of the Ryukyus: Principal investigator (Not on board)*	*- leg1, 2, 3, 4 -*
Toshiya Fujiwara	*JAMSTEC: Principal investigator (Not on board)*	*- leg4 -*
Souichiro Sueyoshi	*Nippon Marine Enterprise Ltd., (NME)*	*- leg1 -*
Yutaro Murakami	*NME*	*- leg1, 2 -*
Wataru Tokunaga	*NME*	*- leg2 -*
Koichi Inagaki	*NME*	*- leg2, 3 -*
Shinya Okumura	*NME*	*- leg3 -*
Kazuho Yoshida	*NME*	*- leg4 -*
Ryo Kimura	*MIRAI crew / NME*	*- leg1, 3, 4 -*
Masanori Murakami	*MIRAI crew*	*- leg2, 3, 4 -*

(2) Introduction

Measurement of magnetic force on the sea surface is required for the geophysical investigations of marine magnetic anomaly caused by magnetization in the upper crust. We measured geomagnetic vector by using a three-component magnetometer and total magnetic force by using a cesium magnetometer.

(3) Instruments and Methods

A) Three-component magnetometer

A shipboard three-component magnetometer system (Tierra Tecnica SFG1214) is equipped on-board R/V MIRAI. Three-axes flux-gate sensors with ring-cored coils are fixed on the fore mast. Outputs from the sensors are digitized by a 20-bit A/D converter (1 nT/LSB), and sampled at 8 times per second. Ship's heading, pitch, and roll are measured by the Inertial Navigation System (INS) for controlling attitude of a Doppler radar. Ship's position and speed data are taken from LAN every second.

The relation between a magnetic-field vector observed on-board, **H**ob, (in the ship's fixed coordinate system) and the geomagnetic field vector, **F**, (in the Earth's fixed coordinate system) is expressed as:

$$\mathbf{H}ob = \tilde{\mathbf{A}}\ \tilde{\mathbf{R}}\ \tilde{\mathbf{P}}\ \tilde{\mathbf{Y}}\ \mathbf{F} + \mathbf{H}p \qquad (a)$$

where $\tilde{\mathbf{R}}$, $\tilde{\mathbf{P}}$ and $\tilde{\mathbf{Y}}$ are the matrices of rotation due to roll, pitch and heading of a ship, respectively. $\tilde{\mathbf{A}}$ is a 3 x 3 matrix which represents magnetic susceptibility of the ship, and **H**p is a magnetic field vector produced by a permanent magnetic moment of the ship's body. Rearrangement of Eq. (a) makes

$$\tilde{\mathbf{B}}\ \mathbf{H}ob + \mathbf{H}bp = \tilde{\mathbf{R}}\ \tilde{\mathbf{P}}\ \tilde{\mathbf{Y}}\ \mathbf{F} \qquad (b)$$

where $\tilde{\mathbf{B}} = \tilde{\mathbf{A}}^{-1}$, and $\mathbf{H}bp = -\tilde{\mathbf{B}}\,\mathbf{H}p$. The magnetic field, **F**, can be obtained by measuring $\tilde{\mathbf{R}}$, $\tilde{\mathbf{P}}$, $\tilde{\mathbf{Y}}$ and **H**ob, if $\tilde{\mathbf{B}}$ and **H**bp are known. Twelve constants in $\tilde{\mathbf{B}}$ and **H**bp can be determined by measuring variation of **H**ob with $\tilde{\mathbf{R}}$, $\tilde{\mathbf{P}}$ and $\tilde{\mathbf{Y}}$ at a place where the geomagnetic field, **F**, is known.

B) Cesium magnetometer

We measured the total magnetic force by using a cesium marine magnetometer (G-882, Geometrics Inc.) and recorded by G-882 data logger (Ver.1.0.0, Clovertech Co.). The G-882 magnetometer uses an optically pumped Cesium-vapor atomic resonance system. The sensor fish towed from 450m to 500 m behind the vessel to minimize the effects of the ship's magnetic field. Table 3.3-1 shows system configuration of MIRAI cesium magnetometer system.

Table 3.3-1: System configuration of MIRAI cesium magnetometer system

Dynamic operating range:	20,000 to 100,000 nT	
Absolute accuracy:	< ±2 nT throughout range	
Setting:	Cycle rate;	0.1 sec
	Sensitivity;	0.001265 nT at a 0.1 second cycle rate
	Sampling rate;	1 sec

(3) Data Archive

These data obtained in this cruise will be submitted to the Data Management Group of JAMSTEC, and will be opened to the public via “Data Research System for Whole Cruise Information in JAMSTEC (DARWIN)” in JAMSTEC web site.

<http://www.godac.jamstec.go.jp/darwin/e>

(4) Remarks (Time in UTC)

A) Three component magnetometer

i) The following periods, observations were carried out.

Leg1: 18:45, 28 Dec. 2016 to 06:14, 15 Jan. 2017

Leg2: 12:11, 21 Jan. 2017 to 14:17, 21 Jan. 2017

14:32, 21 Jan. 2017 to 00:23, 04 Feb. 2017

Leg3: 21:00, 10 Feb. 2017 to 06:59, 03 Mar. 2017

Leg4: 07:03, 09 Mar. 2017 to 09:59, 10 Mar. 2017

10:00, 15 Mar. 2017 to 08:09, 16 Mar. 2017

01:50, 18 Mar. 2017 to 00:00, 28 Mar. 2017

ii) The following periods, we made a “figure-eight” turn (a pair of clockwise and anti-clockwise rotation) for calibration of the ship’s magnetic effect.

Leg1: 01:47, 29 Dec. 2016 to 02:08 29 Dec. 2016 around 26-18N, 174-01W
22:00, 03 Jan. 2017 to 22:22, 03 Jan. 2017 around 43-08S, 145-11W
18:00, 11 Jan. 2017 to 18:24. 11 Jan. 2017 around 48-13S, 95-01W
10:10, 14 Jan. 2017 to 10:42, 14 Jan. 2017 around 45-01S, 80-02W

Leg2: 20:29, 21 Jan. 2017 to 21:02, 21 Jan. 2017 around 44-21S, 75-33W
05:35, 31 Jan. 2017 to 05:58, 31 Jan. 2017 around 50-43S, 79-12W

Leg3: 21:07, 10 Feb. 2017 to 21:41, 10 Feb. 2017 around 59-10S, 73-18W
00:57, 03 Mar. 2017 to 01:17, 03 Mar. 2017 around 39-46S, 175-20W

Leg4: 03:00, 18 Mar. 2017 to 03:21, 18 Mar. 2017 around 11-27N, 155-42E
00:41, 25 Mar. 2017 to 01:09, 25 Mar. 2017 around 38-58N, 144-51E
20:08, 25 Mar. 2017 to 20:39, 25 Mar. 2017 around 39-52N, 143-10E

iii) The following period, data were invalid due to trouble of the deck box.

Leg3: 10:47, 18 Feb. 2017 to 13:39, 18 Feb. 2017
20:49, 25 Feb. 2017 to 00:32, 26 Feb. 2017

iv) The following period, time stamps were delayed 7 seconds.

Leg3: 13:39, 18 Feb. 2017 to 22:04, 18 Feb. 2017

v) The following period, data acquisition was suspended due to maintenance.

Leg3: 22:04, 18 Feb. 2017 to 22:05, 18 Feb. 2017
00:32, 26 Feb. 2017 to 00:34, 26 Feb. 2017

B) Cesium magnetometer

i) The following periods, observations were carried out.

Leg1 (Towing distance from stern; 500m):
01:40, 29 Dec. 2016 to 19:01, 04 Jan. 2017
19:50, 04 Jan. 2017 to 15:30, 07 Jan. 2017
16:54, 07 Jan. 2017 to 15:30, 08 Jan. 2017
16:50, 08 Jan. 2017 to 12:30, 14 Jan. 2017

Leg2 (Towing distance from stern; 450m):
20:20, 21 Jan. 2017 to 07:27, 22 Jan. 2017
13:40, 22 Jan. 2017 to 17:15, 22 Jan. 2017
18:43, 22 Jan. 2017 to 23:33, 22 Jan. 2017
02:50, 23 Jan. 2017 to 11:00, 23 Jan. 2017

03:18, 24 Jan. 2017 to 09:35, 24 Jan. 2017

02:09, 25 Jan. 2017 to 05:17, 25 Jan. 2017

11:21, 25 Jan. 2017 to 08:32, 26 Jan. 2017

20:15, 26 Jan. 2017 to 13:36, 27 Jan. 2017

21:12, 27 Jan. 2017 to 06:32, 28 Jan. 2017

21:14, 28 Jan. 2017 to 11:39, 29 Jan. 2017

16:04, 29 Jan. 2017 to 13:33, 30 Jan. 2017

20:18, 30 Jan. 2017 to 07:00, 31 Jan. 2017

20:07, 31 Jan. 2017 to 06:58, 02 Feb. 2017

13:30, 02 Feb. 2017 to 23:53, 02 Feb. 2017

04:34, 03 Feb. 2017 to 18:17, 03 Feb. 2017

Leg3 (Towing distance from stern; 490m)

19:08, 10 Feb. 2017 to 22:55, 14 Feb. 2017

Leg4 (Towing distance from stern; 490m)

01:50, 18 Mar. 2017 to 06:58, 21 Mar. 2017

07:19, 23 Mar. 2017 to 23:30, 25 Mar. 2017

ii) The following period, total magnetic data were invalid due to low signal strength.

Leg2: 23:29, 25 Jan. 2017

19:16, 01 Feb. 2017

19:21, 01 Feb. 2017

20:02, 01 Feb. 2017

3.4 Sea Surface Gravity

(1) Personnel

Natsue Abe	*JAMSTEC: Principal investigator*	*- leg2 -*
Takeshi Matsumoto	*Univ. of the Ryukyus: Principal investigator (Not on board)*	*- leg1, 2, 3, 4 -*
Toshiya Fujiwara	*JAMSTEC: Principal investigator (Not on board)*	*- leg4 -*
Souichiro Sueyoshi	*Nippon Marine Enterprises Ltd., (NME)*	*- leg1 -*
Yutaro Murakami	*NME*	*- leg1, 2 -*
Wataru Tokunaga	*NME*	*- leg2 -*
Koichi Inagaki	*NME*	*- leg2, 3 -*
Shinya Okumura	*NME*	*- leg3 -*
Kazuho Yoshida	*NME*	*- leg4 -*
Ryo Kimura	*MIRAI crew / NME*	*- leg1, 3, 4 -*
Masanori Murakami	*MIRAI crew*	*- leg2, 3, 4 -*

(2) Introduction

The local gravity is an important parameter in geophysics and geodesy. We collected gravity data at the sea surface.

(3) Parameters

Relative Gravity [CU: Counter Unit]

[mGal] = (coef1: 0.9946) * [CU]

QC Filter : 120sec. filtered

(4) Data Acquisition

We measured relative gravity using LaCoste and Romberg air-sea gravity meter S-116 (Micro-G LaCoste, LLC) in the MR16-09 Leg1 to Leg4 cruises.

To convert the relative gravity to absolute one, we measured gravity, using portable gravity meter (CG-5, Scintrex), at Shimizu, Punta Arenas and Sekinehama as the reference points.

(5) Preliminary Results

Absolute gravity table is shown in Table 3.4-1.

Table 3.4-1. Absolute gravity table of the MR16-09 cruise

No.	Date yy/mm/dd	UTC	Port	Absolute Gravity [mGal]	Sea Level [cm]	Ship Draft [cm]	Gravity at Sensor * [mGal]	S-116 Gravity [mGal]
#1	16/11/25	06:18	Shimizu	979729.626	128	645	979730.18	12014.81
#2	17/03/28	08:35	Sekinehama	980371.862	200	600	980372.63	12685.04

*: Gravity at Sensor = Absolute Gravity + Sea Level*0.3086/100 + (Draft-530)/100*0.2222

(6) Data Archive

These data obtained in this cruise will be submitted to the Data Management Group (DMG) in JAMSTEC, and will be opened to the public via "Data Research System for Whole Cruise Information in JAMSTEC (DARWIN)" in JAMSTEC web site. <http://www.godac.jamstec.go.jp/darwin/e>.

(7) Remarks (Time in UTC)

i) The following periods, the observation were carried out.

Leg1: 18:46, 28 Dec. 2016 to 06:13, 15 Jan. 2017

Leg2: 12:11, 21 Jan. 2017 to 14:17, 21 Jan. 2017

14:32, 21 Jan. 2017 to 00:23, 04 Feb. 2017

Leg3: 21:00, 10 Feb. 2017 to 06:59, 03 Mar. 2017

Leg4: 07:03, 09 Mar. 2017 to 09:59, 10 Mar. 2017

10:00, 15 Mar. 2017 to 08:09, 16 Mar. 2017

01:50, 18 Mar. 2017 to 00:00, 28 Mar. 2017

ii) The following period, depth data was available

Leg1: 18:47, 28 Dec. 2016 to 05:39, 15 Jan. 2017

Leg2: 12:11, 21 Jan. 2017 to 14:17, 21 Jan. 2017

14:32, 21 Jan. 2017 to 00:23, 04 Feb. 2017

Leg3: 21:00, 10 Feb. 2017 to 06:59, 03 Mar. 2017

Leg4: 07:05, 09 Mar. 2017 to 07:37, 09 Mar. 2017

07:48, 09 Mar. 2017 to 09:59, 10 Mar. 2017

10:00, 15 Mar. 2017 to 08:09, 16 Mar. 2017

01:50, 18 Mar. 2017 to 04:01, 25 Mar. 2017

04:12, 25 Mar. 2017 to 03:43, 26 Mar. 2017

3.5 Surface Meteorological Observations

(1) Personnel

Masaki Katsumata	***JAMSTEC: Principal investigator[*1]***	***- leg1,2,3,4 -***
Souichiro Sueyoshi	***Nippon Marine Enterprise Ltd., (NME)***	***- leg1 -***
Yutaro Murakami	***NME***	***- leg1,2 -***
Wataru Tokunaga	***NME***	***- leg2 -***
Koichi Inagaki	***NME***	***- leg2,3 -***
Shinya Okumura	***NME***	***- leg3 -***
Kazuho Yoshida	***NME***	***- leg4 -***
Ryo Kimura	***MIRAI crew / NME***	***- leg1,3,4 -***
Masanori Murakami	***MIRAI crew***	***- leg2,3,4 -***

[*1] leg1:On-board, leg2,3,4:Not on-board

(2) Objectives

Surface meteorological parameters are observed as a basic dataset of the meteorology. These parameters provide the temporal variation of the meteorological condition surrounding the ship.

(3) Methods

Surface meteorological parameters were observed from the MR16-09 Leg1 cruise to Leg4 cruise. In these cruises, we used two systems for the observation.

i) MIRAI Surface Meteorological observation (SMet) system

Instruments of SMet system are listed in Table 3.5-1 and measured parameters are listed in Table 3.5-2. Data were collected and processed by KOAC-7800 weather data processor made by Koshin-Denki, Japan. The data set consists of 6-second averaged data.

ii) Shipboard Oceanographic and Atmospheric Radiation (SOAR) measurement system

SOAR system designed by BNL (Brookhaven National Laboratory, USA) consists of major five parts.

a) Portable Radiation Package (PRP) designed by BNL – short and long wave downward radiation.
b) Analog meteorological data sampling with CR1000 logger manufactured by Campbell Inc. Canada – wind, pressure, and rainfall (by a capacitive rain gauge) measurement.
c) Digital meteorological data sampling from individual sensors - air temperature, relative humidity and rainfall (by ORG (optical rain gauge)) measurement.

d) Photosynthetically Available Radiation (PAR) sensor manufactured by Biospherical Instruments Inc. (USA) - PAR measurement.
e) Scientific Computer System (SCS) developed by NOAA (National Oceanic and Atmospheric Administration, USA) – centralized data acquisition and logging of all data sets.

SCS recorded PRP, CR1000 data, air temperature and relative humidity data, ORG data. SCS composed Event data (JamMet) from these data and ship's navigation data every 6 seconds. Instruments and their locations are listed in Table 3.5-3 and measured parameters are listed in Table 3.5-4.

For the quality control as post processing, we checked the following sensors, before and after the cruise.

i. Young rain gauge (SMet and SOAR)
Inspect of the linearity of output value from the rain gauge sensor to change input value by adding fixed quantity of test water.
ii. Barometer (SMet and SOAR)
Comparison with the portable barometer value, PTB220, VAISALA
iii. Thermometer (air temperature and relative humidity) (SMet and SOAR)
Comparison with the portable thermometer value, HM70, VAISALA

(4) Preliminary results

Fig. 3.5-1 to Fig. 3.5-3 show the time series of the following parameters;

Wind (SOAR)
Air temperature (SMet)
Relative humidity (SMet)
Precipitation (SOAR, ORG)
Short/long wave radiation (SOAR)
Pressure (SMet)
Sea surface temperature (SMet)
Significant wave height (SMet)

(5) Data archives

These data obtained in these cruises will be submitted to the Data Management Group of JAMSTEC, and will be opened to the public via "Data Research System for Whole Cruise Information in JAMSTEC (DARWIN)" in JAMSTEC web site.
<http://www.godac.jamstec.go.jp/darwin/e>.

(6) Remarks (Times in UTC)

i) The following periods, the observation were carried out.

Leg1: 18:45, 28 Dec. 2016 to 06:13, 15 Jan. 2017

Leg2: 12:11, 21 Jan. 2017 to 14:17, 21 Jan. 2017

14:32, 21 Jan. 2017 to 00:23, 04 Feb. 2017

Leg3: 21:00, 10 Feb. 2017 to 06:59, 03 Mar. 2017

Leg4: 07:03, 09 Mar. 2017 to 09:59, 10 Mar. 2017

10:00, 15 Mar. 2017 to 08:09, 16 Mar. 2017

01:50, 18 Mar. 2017 to 00:00, 28 Mar. 2017

ii) The following periods, sea surface temperature of SMet data was available.

Leg1: 18:45, 28 Dec. 2016 to 06:13, 15 Jan. 2017

Leg2: 12:11, 21 Jan. 2017 to 14:17, 21 Jan. 2017

14:32, 21 Jan. 2017 to 00:23, 04 Feb. 2017

Leg3: 21:00, 10 Feb. 2017 to 06:59, 03 Mar. 2017

Leg4: 07:03, 09 Mar. 2017 to 09:59, 10 Mar. 2017

10:00, 15 Mar. 2017 to 08:09, 16 Mar. 2017

01:50, 18 Mar. 2017 to 05:30, 26 Mar. 2017

iii) The following period, downwelling shortwave radiation amount of SOAR was invalid due to a PSP sensor failure.

about 13:00, 02 Jan. 2017 to 16:11, 07 Jan. 2017

iv) PSP senor of PRP was replaced to a spare due to a sensor failure at 06:11, 07 Jan. 2017.

v) The following period, FRSR data acquisition was stopped due to a trouble of heater in the FRSR sensor.

08:14, 27 Feb. 2017 to 07:00, 03 Mar. 2017

vi) The following period, FRSR data acquisition was suspended to prevent the shadow-band from freezing.

21:25, 12 Feb. 2017 to 23:28, 22 Feb. 2017

vii) The following periods, downwelling shortwave radiation amount and longwave radiation amount data of SOAR were invalid due to PRP system maintenance.

21:15, 06 Jan. 2017 to 21:51, 06 Jan. 2017

15:55, 07 Jan. 2017 to 16:15, 07 Jan. 2017

viii) The following periods, downwelling shortwave radiation amount and longwave radiation amount data of SOAR were not acquired due to PRP system maintenance.

21:23, 12 Feb. 2017 to 21:24, 12 Feb. 2017

23:24, 22 Feb. 2017 to 23:28, 22 Feb. 2017

07:56, 27 Feb. 2017 to 08:13, 27 Feb. 2017

17:33, 27 Feb. 2017 to 17:50, 27 Feb. 2017

23:22, 27 Feb. 2017 to 23:26, 27 Feb. 2017

ix) The following time, increasing of SMet capacitive rain gauge data were invalid due to transmitting for MF/HF or VHF radio.

21:27, 06 Jan. 2017

20:17, 03 Feb. 2017

20:21, 03 Feb. 2017

23:20, 18 Mar. 2017

15:01, 23 Mar. 2017

15:04, 23 Mar. 2017

x) The following time, increasing of SMet optical rain gauge data were invalid due to maintenance.

02:50, 25 Feb. 2017

20:29, 01 Mar. 2017

20:30, 01 Mar. 2017

06:21, 23 Mar. 2017

Table 3.5-1 Instruments and installation locations of MIRAI Surface Meteorological observation system

Sensors	Type	Manufacturer	Location (altitude from surface)
Anemometer	KE-500	Koshin Denki, Japan	Foremast (24 m)
Tair/RH	HMP155	Vaisala, Finland	
with 43408 Gill aspirated radiation shield		R.M. Young, USA	Compass deck (21 m) starboard and portside
Thermometer: SST	RFN2-0	Koshin Denki, Japan	4th deck (-1m, inlet -5m)
Barometer	Model-370	Setra System, USA	Captain deck (13 m) weather observation room
Capacitive rain gauge	50202	R. M. Young, USA	Compass deck (19 m)
Optical rain gauge	ORG-815DS	Osi, USA	Compass deck (19 m)
Radiometer (short wave)	MS-802	Eko Seiki, Japan	Radar mast (28 m)
Radiometer (long wave)	MS-202	Eko Seiki, Japan	Radar mast (28 m)
Wave height meter	WM-2	Tsurumi-seiki, Japan	Bow (10 m) Stern (8m)

Table 3.5-2 Parameters of MIRAI Surface Meteorological observation system

Parameter	Units	Remarks
1 Latitude	degree	
2 Longitude	degree	
3 Ship's speed	knot	MIRAI log DS-30, Furuno
4 Ship's heading	degree	MIRAI gyro, TG-6000, TOKYO-KEIKI
5 Relative wind speed	m/s	6sec./10min. averaged
6 Relative wind direction	degree	6sec./10min. averaged
7 True wind speed	m/s	6sec./10min. averaged
8 True wind direction	degree	6sec./10min. averaged
9 Barometric pressure	hPa	adjusted to sea surface level 6sec. averaged
10 Air temperature (starboard side)	degC	6sec. averaged
11 Air temperature (port side)	degC	6sec. averaged
12 Dewpoint temperature (starboard side)	degC	6sec. averaged
13 Dewpoint temperature (port side)	degC	6sec. averaged
14 Relative humidity (starboard side)	%	6sec. averaged
15 Relative humidity (port side)	%	6sec. averaged
16 Sea surface temperature	degC	6sec. averaged
17 Rain rate (optical rain gauge)	mm/hr	hourly accumulation
18 Rain rate (capacitive rain gauge)	mm/hr	hourly accumulation
19 Down welling shortwave radiation	W/m^2	6sec. averaged
20 Down welling infra-red radiation	W/m^2	6sec. averaged
21 Significant wave height (bow)	m	hourly
22 Significant wave height (aft)	m	hourly
23 Significant wave period (bow)	second	hourly
24 Significant wave period (aft)	second	hourly

Table 3.5-3 Instruments and installation locations of SOAR system

Sensors (Meteorological)	Type	Manufacturer	Location (altitude from surface)
Anemometer	05106	R.M. Young, USA	Foremast (25 m)
Barometer	PTB210	Vaisala, Finland	
with 61002 Gill pressure port		R.M. Young, USA	Foremast (23 m)
Capacitive rain gauge	50202	R.M. Young, USA	Foremast (24 m)
Tair/RH	HMP155	Vaisala, Finland	
with 43408 Gill aspirated radiation shield		R.M. Young, USA	Foremast (23 m)
Optical rain gauge	ORG-815DR	Osi, USA	Foremast (24 m)

Sensors (PRP)	Type	Manufacturer	Location (altitude from surface)
Radiometer (short wave)	PSP	Epply Labs, USA	Foremast (25 m)
Radiometer (long wave)	PIR	Epply Labs, USA	Foremast (25 m)
Fast rotating shadowband radiometer		Yankee, USA	Foremast (25 m)

Sensor (PAR)	Type	Manufacturer	Location (altitude from surface)
PAR sensor	PUV-510	Biospherical Instru ments Inc., USA	Navigation deck (18m)

Table 3.5-4 Parameters of SOAR system (JamMet)

	Parameter	Units	Remarks
1	Latitude	degree	
2	Longitude	degree	
3	SOG	knot	
4	COG	degree	
5	Relative wind speed	m/s	
6	Relative wind direction	degree	
7	Barometric pressure	hPa	
8	Air temperature	degC	
9	Relative humidity	%	
10	Rain rate (optical rain gauge)	mm/hr	
11	Precipitation (capacitive rain gauge)	mm	reset at 50 mm
12	Down welling shortwave radiation	W/m^2	
13	Down welling infra-red radiation	W/m^2	
14	Defuse irradiance	W/m^2	
15	PAR	$microE/cm^2/sec$	

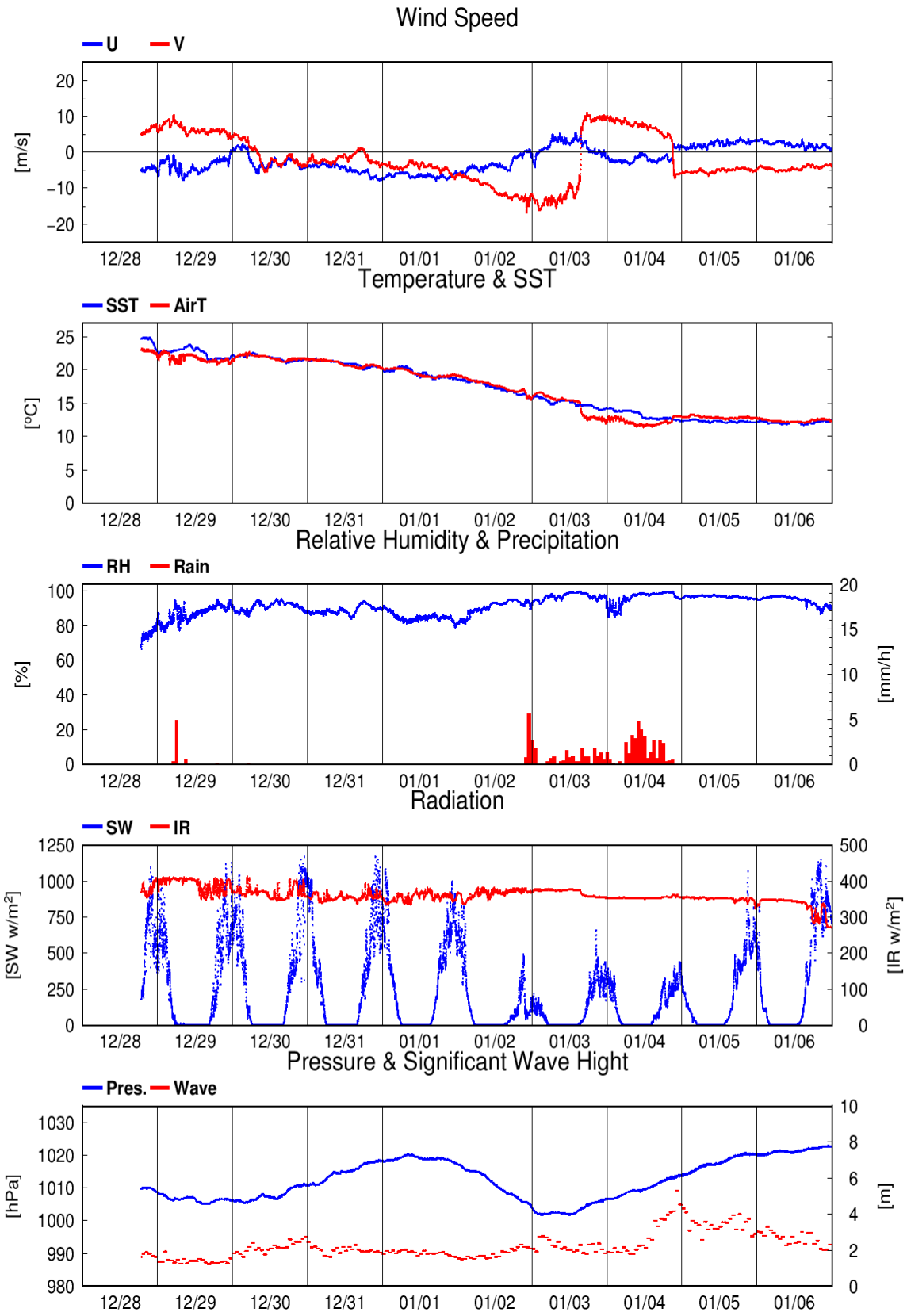

Fig. 3.5-1 Time series of surface meteorological parameters during the MR16-09 Leg1 cruise

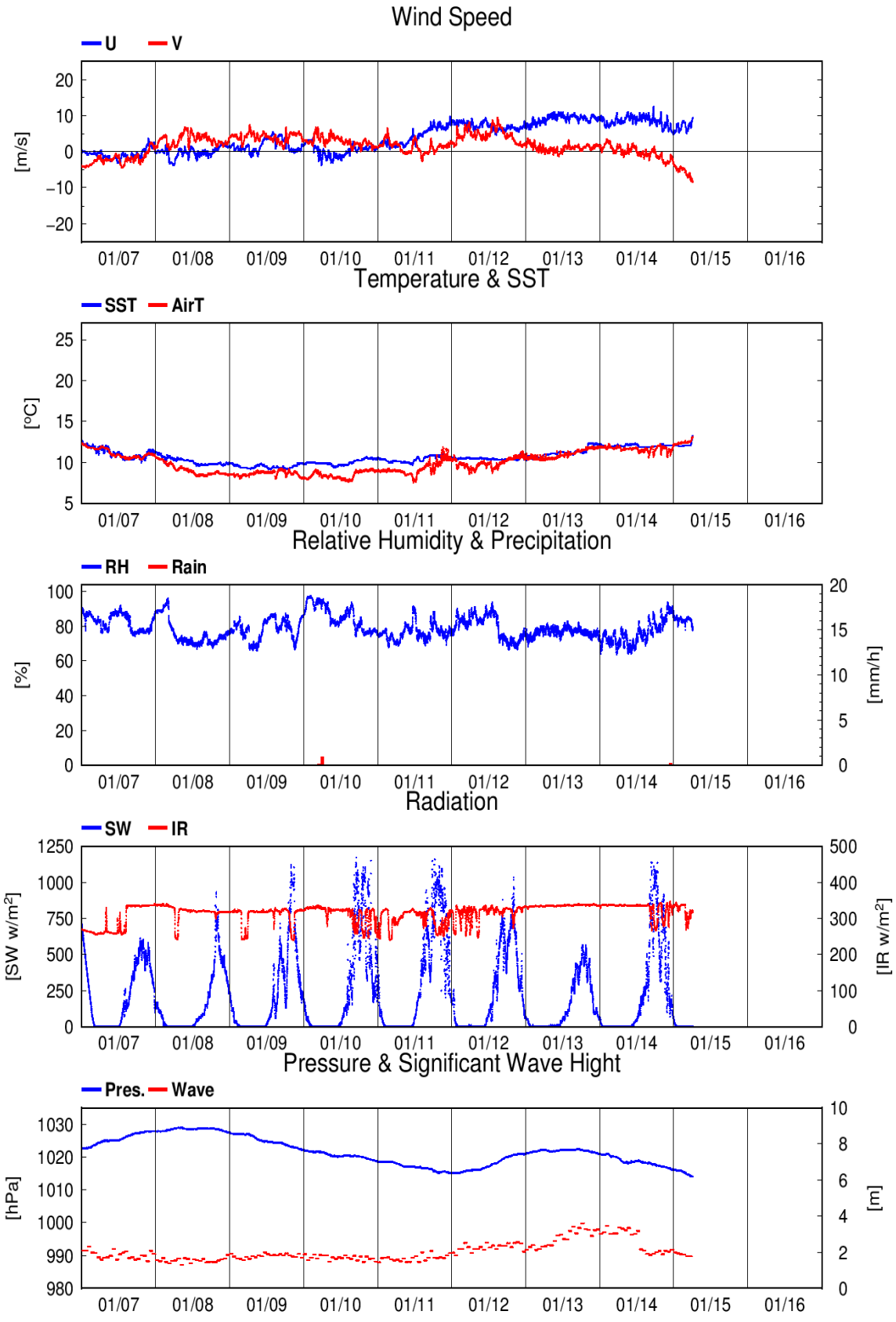

Fig. 3.5-1 (Continued)

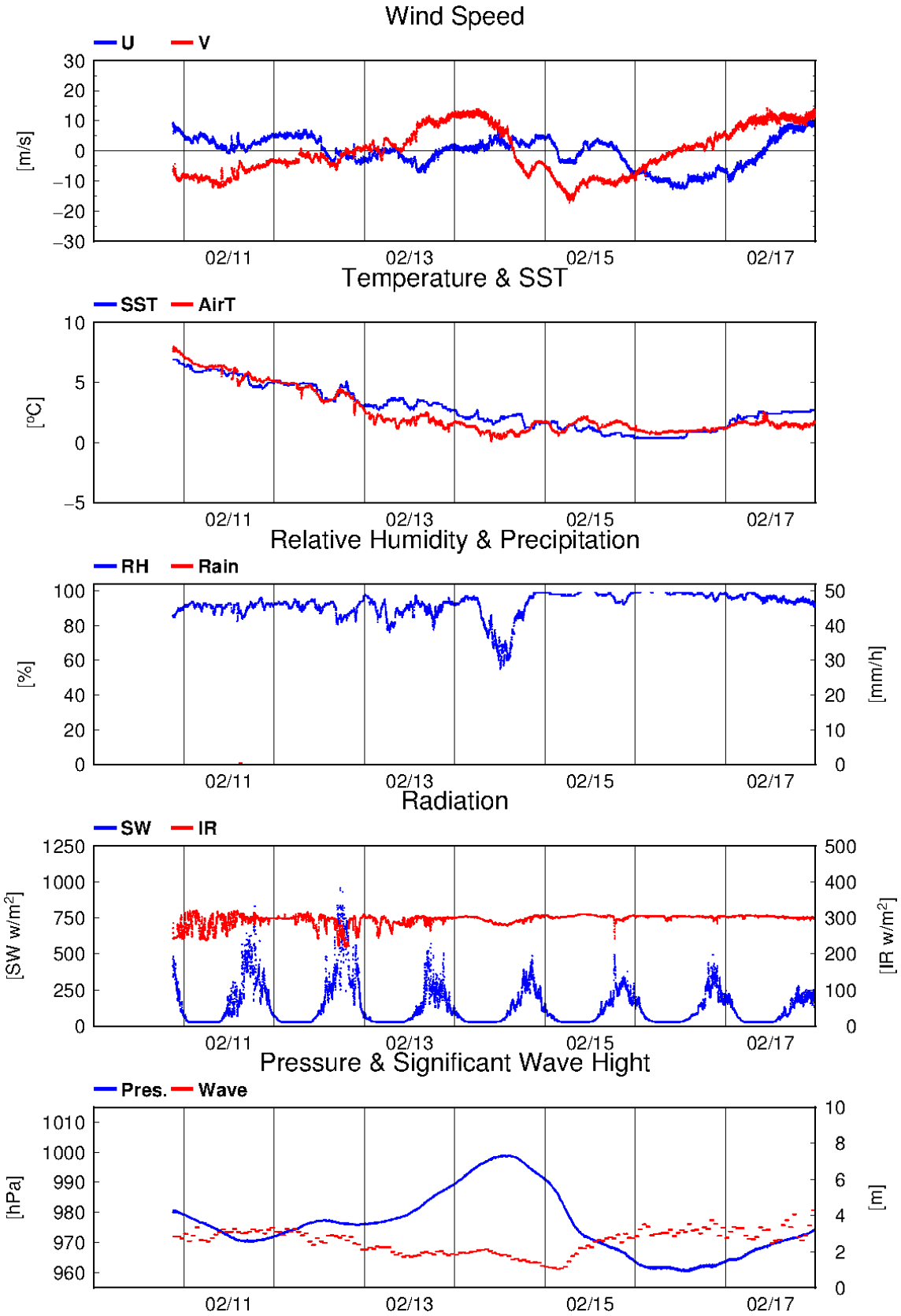

Fig. 3.5-2 Time series of surface meteorological parameters during the MR16-09 Leg3 cruise

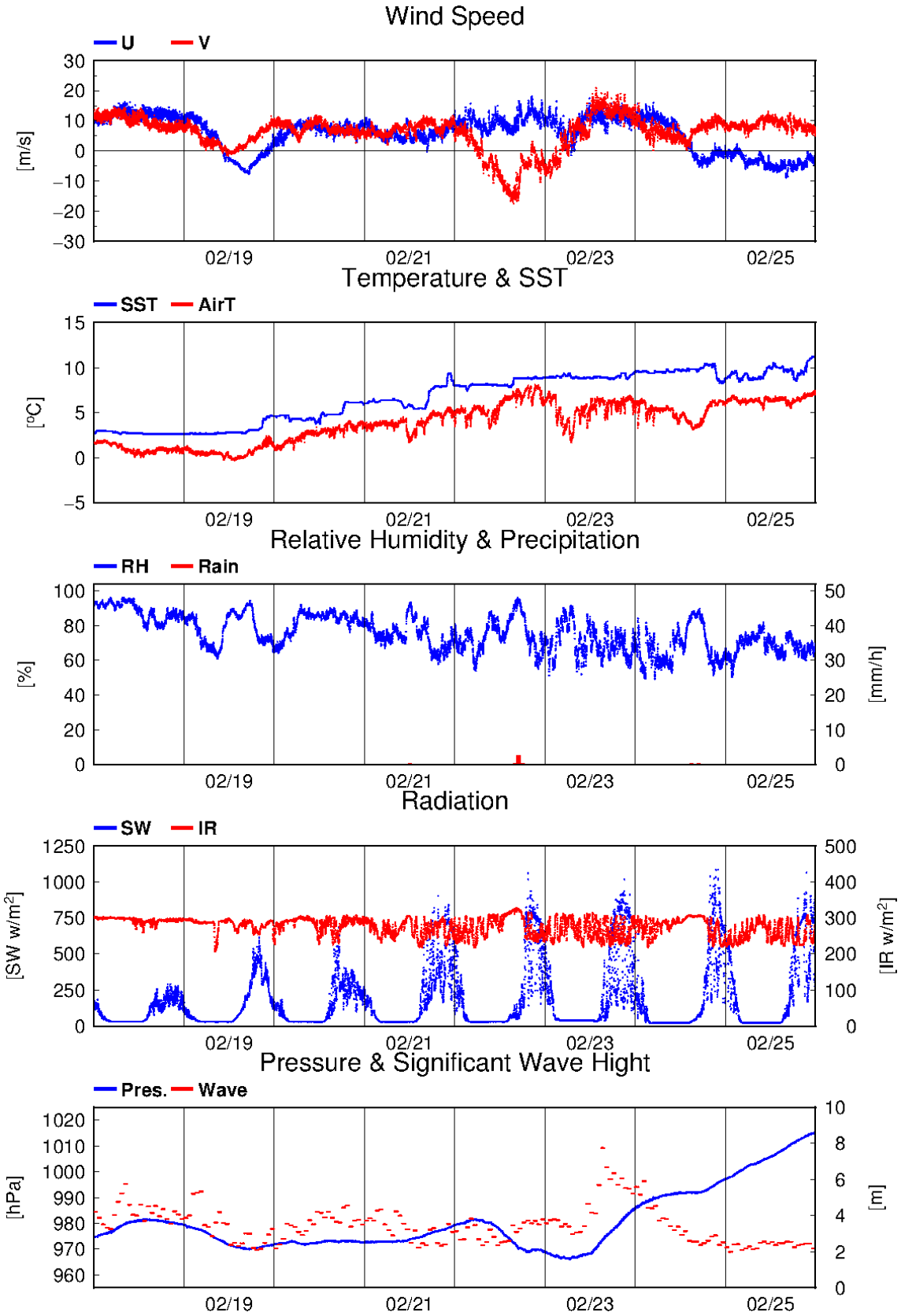

Fig. 3.5-2 (Continued)

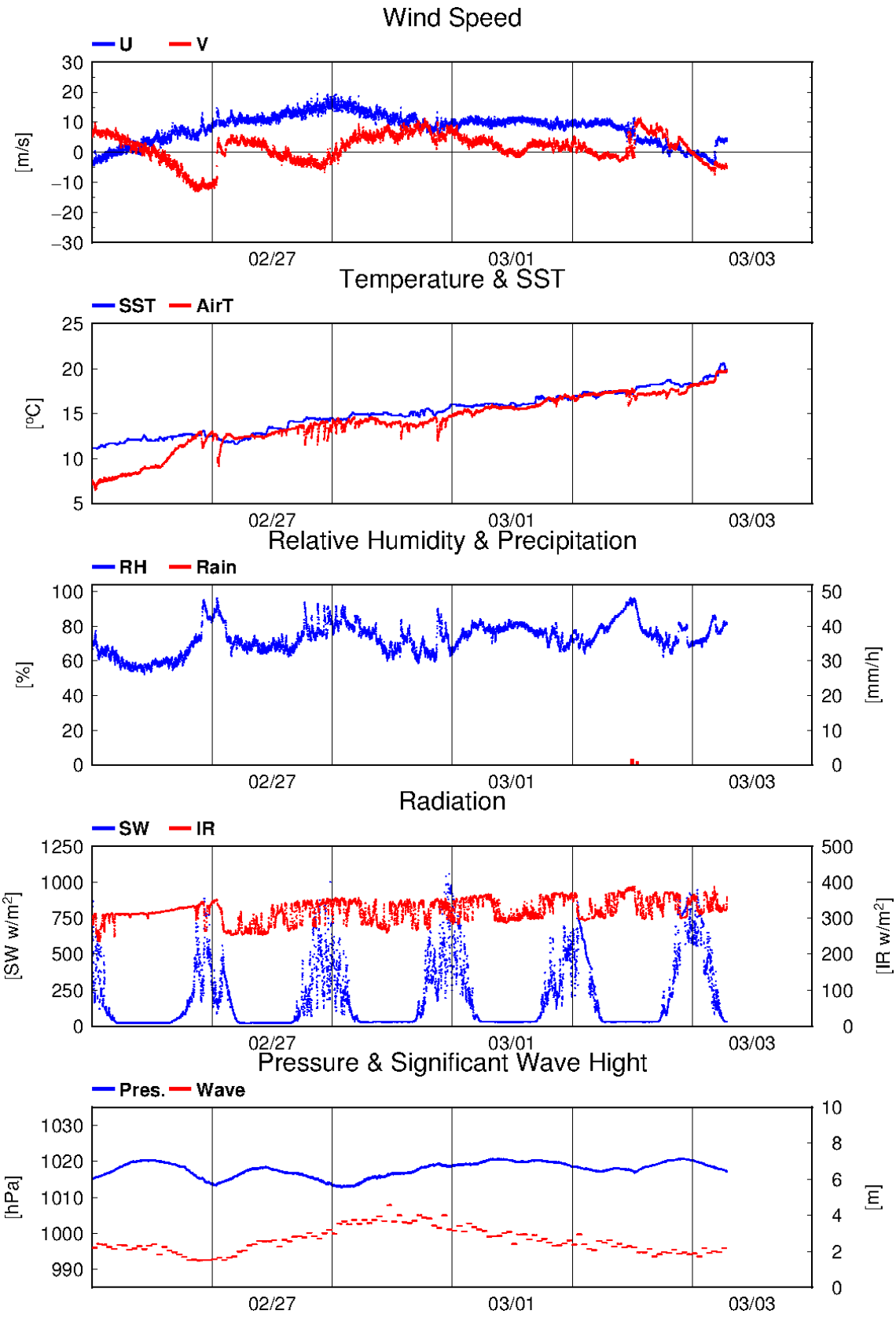

Fig. 3.5-2 (Continued)

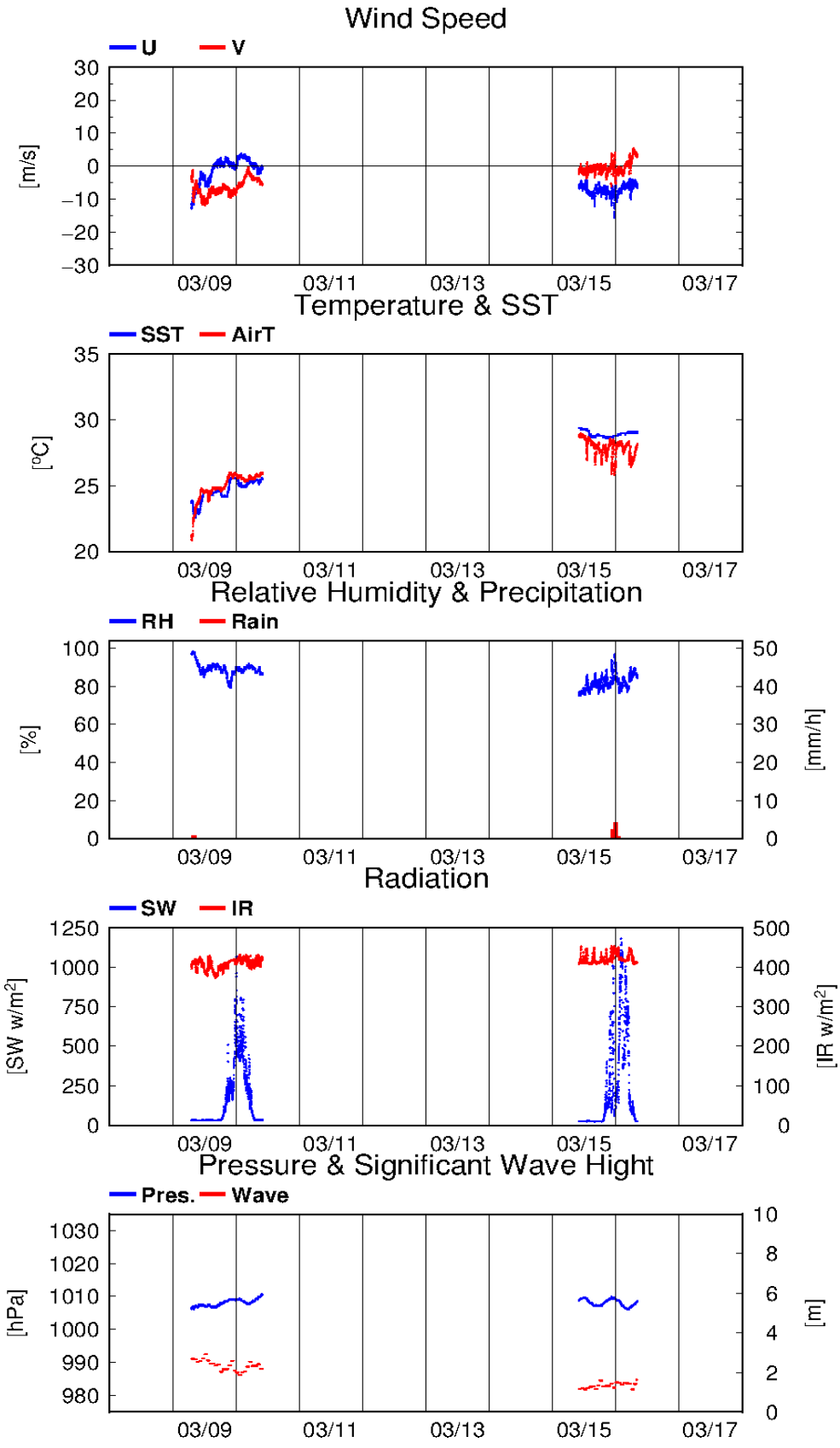

Fig. 3.5-3 Time series of surface meteorological parameters during the MR16-09 Leg4 cruise

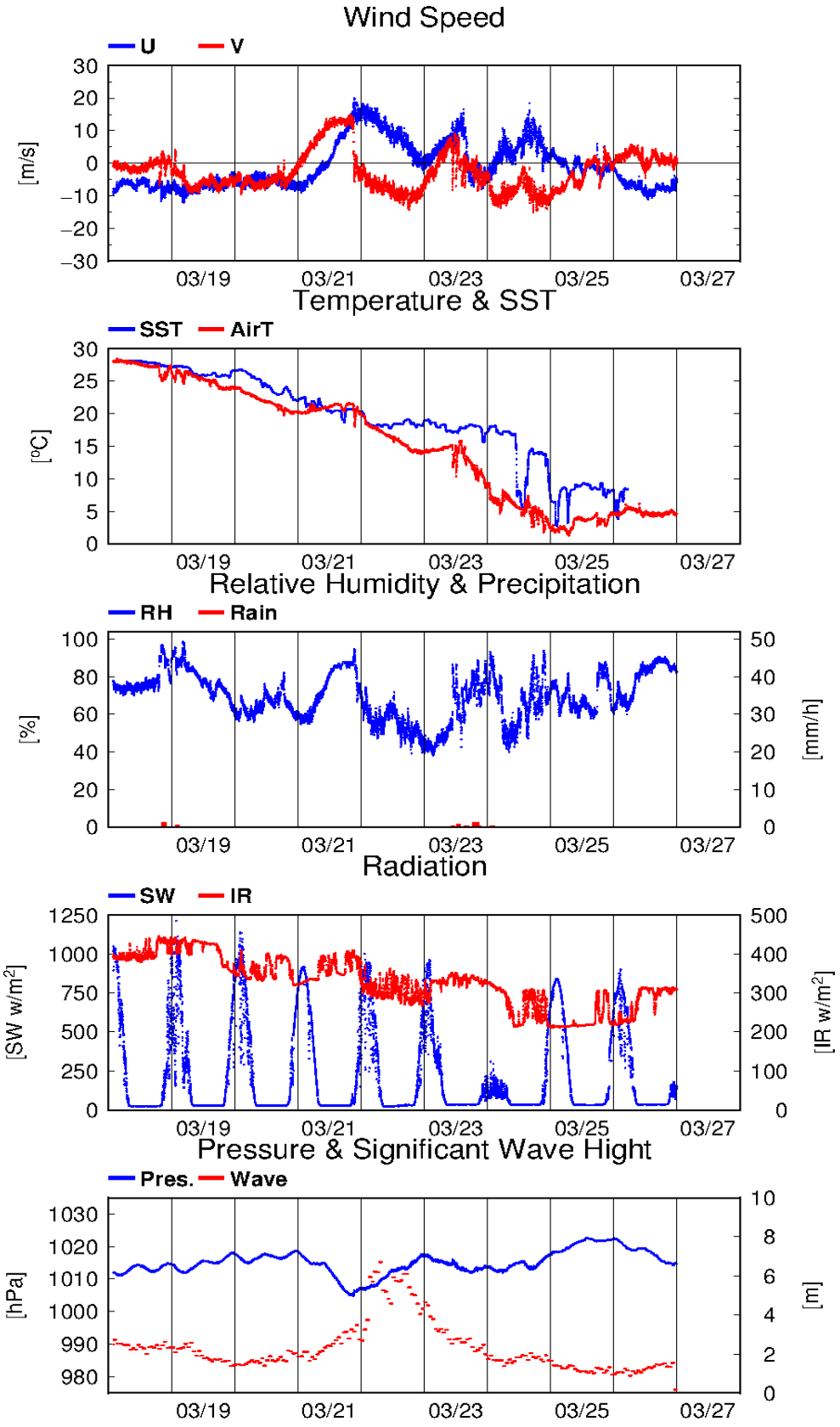

Fig. 3.5-3 (Continued)

3.6 Thermo-Salinograph and Related Measurements

May 17, 2017

(1) Personnel

Hiroshi Uchida (JAMSTEC)

Takuhei Shiozaki (JAMSTEC)

Kosei Sasaoka (JAMSTEC)

Hironori Sato (MWJ)

Haruka Tamada (MWJ)

Masanori Enoki (MWJ)

Misato Kuwahara (MWJ)

Masahiro Orui (MWJ)

(2) Objectives

The objective is to collect sea surface salinity, temperature, dissolved oxygen, fluorescence and turbidity data continuously along the cruise track.

(3) Materials and methods

The Continuous Sea Surface Water Monitoring System (Marine Works Japan Co, Ltd.) has seven sensors and automatically measures salinity, temperature, dissolved oxygen, fluorescence, and turbidity in sea surface water every one minute. This system is located in the sea surface monitoring laboratory and bottom of the ship and connected to shipboard LAN system. Measured data along with time and location of the ship were displayed on a monitor and stored in a desktop computer. The sea surface water was continuously pumped up to the laboratory from about 5 m water depth and flowed into the system through a vinyl-chloride pipe. One thermometer is located just before the sea water pump at bottom of the ship. The flow rate of the surface seawater was controlled to be about 1.2 L/min. Periods of measurement, maintenance and problems are listed in Table 3.6.1.

Software and sensors used in this system are listed below.

i. Software

Seamoni-kun Ver.1.50

ii. Sensors

Temperature and conductivity sensor

Model:	SBE 45, Sea-Bird Electronics, Inc.
Serial number:	4557820-0319
Pre-cruise calibration:	19 May 2016, Sea-Bird Electronics, Inc.

Bottom of ship thermometer

Model:	SBE 38, Sea-Bird Electronics, Inc.

Serial number: 3852788-0457

Pre-cruise calibration: 8 March 2016, Sea-Bird Electronics, Inc.

Dissolved oxygen sensor

Model: RINKO-II, JFE Adantech Co. Ltd.

Serial number: 0013

Pre-cruise calibration: 24 April 2016, JAMSTEC

Model: OPTODE 3835, Aanderaa Data Instruments, AS.

Serial number: 1915

Pre-cruise calibration: 13 May 2015, JAMSTEC

Fluorometer and turbidity sensor

Model: C3, Turner Designs, Inc.

Serial number: 2300384

Table 3.6.1. Events of the Continuous Sea Surface Water Monitoring System operation.

System Date [UTC]	System Time [UTC]	Event
Leg 1		
2016/12/28	18:46	Logging start
2017/01/06	00:11~00:57	Logging stop for filter cleaning
2017/01/15	06:12	Logging stop
Leg 2		
2017/01/21	12:11	Logging start
2017/01/21	14:18~14:31	All data unavailable
2017/01/28	11:01~11:43	Logging stop for filter cleaning
2017/01/28	12:02~12:03	C3 data unavailable
2017/01/28	19:14~19:15	All data unavailable
2017/01/28	19:15~19:18	C3 data unavailable
2017/01/28	20:15~21:21	Logging stop for entering into Chilean territorial waters
2017/01/31	08:50~08:55	Flow rate for RINKO/Optode was zero
2017/02/03	23:59	Logging stop
Leg 3		
2017/02/10	21:15	Logging start

2017/02/16	03:17~04:10	Logging stop for filter cleaning
2017/02/16	08:16~15:46	Flow rate for RINKO/Optode might be small
2017/02/16	20:55~	Flow rate for SBE 45 was unstable
2017/02/17	~12:07	
2017/02/17	12:08~13:25	Logging stop for filter cleaning
2017/03/03	07:00	Logging stop
Leg 4		
2017/03/09	07:03	Logging start
2017/03/10	10:00~	Logging stop for entering into foreign EEZs
2017/03/15	~09:59	
2017/03/16	08:10~	Logging stop for entering into foreign EEZs
2017/03/18	~01:49	
2017/03/25	23:00	Logging stop

(4) Pre-cruise calibration

Pre-cruise sensor calibrations for the SBE 45 and SBE 38 were performed at Sea-Bird Electronics, Inc.

Pre-cruise sensor calibrations for the oxygen sensors were performed at JAMSTEC. The oxygen sensors were immersed in fresh water in a 1-L semi-closed glass vessel, which was immersed in a temperature-controlled water bath. Temperature of the water bath was set to 1, 10, 20 and 29ºC. Temperature of the fresh water in the vessel was measured by a thermistor thermometer (expanded uncertainty of smaller than 0.01ºC, ARO-PR, JFE Advantech, Co., Ltd.). At each temperature, the fresh water in the vessel was bubbled with standard gases (4, 10, 17 and 25% oxygen consisted of the oxygen-nitrogen mixture, whose relative expanded uncertainty is 0.5%) for more than 30 minutes to insure saturation. Absolute pressure of the vessel headspace was measured by a reference quartz crystal barometer (expanded uncertainty of 0.01% of reading) and ranged from about 1040 to 1070 hPa. The data were averaged over 5 minutes at each calibration point (a matrix of 24 points). As a reference, oxygen concentration of the fresh water in the calibration vessel was calculated from the oxygen concentration of the gases, temperature and absolute pressure at the water depth (about 8 cm) of the sensor's sensing foil as follows:

$$O_2\ (\mu mol/L) = \{1000 \times c(T) \times (A_p - pH_2O)\} / \{0.20946 \times 22.3916 \times (1013.25 - pH_2O)\}$$

where c(T) is the oxygen solubility, A_p is absolute pressure [in hPa], and pH_2O is the water vapor pressure [in hPa].

The RINKO was calibrated by the modified Stern-Volmer equation slightly modified from a method by Uchida et al. (2010):

$$O_2\ (\mu mol/L) = [(V_0 / V)^E - 1] / K_{sv}$$

where V is raw phase difference, V_0 is raw phase difference in the absence of oxygen, K_{sv} is Stern-Volmer constant. The coefficient E corrects nonlinearity of the Stern-Volmer equation. The V_0 and the K_{sv} are assumed to be functions of temperature as follows.

$$K_{sv} = C_0 + C_1 \times T + C_2 \times T^2$$

$$V_0 = 1 + C_3 \times T$$

$$V = C_4 + C_5 \times V_b$$

where T is CTD temperature (°C) and V_b is raw output. The oxygen concentration is calculated using accurate temperature data from the SBE 45 instead of temperature data from the RINKO. The calibration coefficients were as follows:

C_0 = 5.123682697760924e–3

C_1 = 2.216599487021134e–4

C_2 = 4.123214071344090e–6

C_3 = –6.672929550710492e–4

C_4 = 2.395966849477748e–2

C_5 = 0.1951644347447042

E = 1.5

(5) Data processing and post-cruise calibration

Data from the Continuous Sea Surface Water Monitoring System were obtained at 1 minute intervals. These data were processed as follows. Spikes in the temperature and salinity data were removed using a median filter with a window of 3 scans (3 minutes) when difference between the original data and the median filtered data was larger than 0.1ºC for temperature and 0.5 for salinity. Data gaps were linearly interpolated when the gap was ≤ 13 minutes. Fluoromete and turbidity data were low-pass filtered using a median filter with a window of 3 scans (3 minutes) to remove spikes. Raw data from the RINKO oxygen sensor, fluorometer and turbidity data were low-pass filtered using a Hamming filter with a window of 15 scans (15 minutes).

Salinity (S [PSU]), dissolved oxygen (O [μmol/kg]), and fluorescence (Fl [RFU]) data were corrected using the water sampled data. Details of the measurement methods are described in Sections 4.8, 4.9 and 4.15 for salinity, dissolved oxygen, and chlorophyll-a, respectively. Corrected salinity (S_{cor}), dissolved oxygen (O_{cor}), and estimated chlorophyll *a* (Chl-a) were calculated from following equations

$$S_{cor}\ [PSU] = c_0 + c_1 S + c_2 t$$

$$O_{cor}\ [\mu mol/kg] = c_0 + c_1 O + c_2 T + c_3 t$$

$$Chl\text{-}a\ [\mu g/L] = c_0 + c_1 Fl$$

where S is practical salinity, t is days from a reference time (2016/12/28 18:46 [UTC]), T is temperature in ºC. The best fit sets of calibration coefficients (c_0~c_3) were determined by a least square technique to minimize the deviation from the water sampled data. The calibration coefficients were listed in Table

3.6.2. Comparisons between the Continuous Sea Surface Water Monitoring System data and water sampled data are shown in Figs. 3.6.1, 3.6.2 and 3.6.3. The calibration coefficients were basically determined for each leg.

For leg 3, salinity data were shifted at routine maintenance (2017/02/16 03:17~04:10). Therefore, the coefficient c_0 was changed before and after the maintenance.

For fluorometer data, water sampled data obtained at night [PAR (Photosynthetically Available Radiation) < 50 μE/(m^2 sec)] were used for the calibration, since sensitivity of the fluorometer to chlorophyll *a* is different at nighttime and daytime (Section 2.4 in Uchida et al., 2015). Sensitivity of the fluorometer to chlorophyll *a* may also have regional differences. Therefore, the calibration coefficients were change in leg 2.

For leg 2, chlorophyll *a* data obtained at 10 m depths of CTD/water sampling casts were also used to calibrate the fluorometer data.

(6) References

Uchida, H., G. C. Johnson, and K. E. McTaggart (2010): CTD oxygen sensor calibration procedures, The GO-SHIP Repeat Hydrography Manual: A collection of expert reports and guidelines, IOCCP Rep., No. 14, ICPO Pub. Ser. No. 134.

Uchida, H., K. Katsumata, and T. Doi (2015): WHP P14S, S04I Revisit Data Book, JASTEC, Yokosuka, 187 pp.

Table 3.6.2. Calibration coefficients for the salinity, dissolved oxygen, and chlorophyll *a*.

	c_0	c_1	c_2	c_3
Salinity				
Leg 1	4.130002e–2	0.9988262	3.781427e–4	
Leg 2	–7.173855e–3	0.9997166	4.655501e–4	
Leg 3	–5.867472e–5	0.9992261	4.396308e–4	(for ~ 2017/02/16 04:00)
	–5.160587e–3	0.9992261	4.396308e–4	(for 2017/02/16 04:00 ~)
Leg 4	–9.554012e–3	0.9994091	2.991207e–4	
Dissolved oxygen				
Leg 1	–10.49821	0.9774294	0.4408163	7.269963e–2
Leg 2	–8.846670	0.9636318	0.4452296	0.1050298
Leg 3	3.415634	0.9044650	–5.714148e–3	0.2063646
Leg 4	53.65725	0.8189659	–0.3604695	–0.1434302
Chlorophyll a				
Leg 1	0.0	2.615018e–2	(for Fl < 8)	
	–0.1071907	3.954902e–2	(for Fl >= 8)	
Leg 2 (for ~ 2017/01/25 19:50 or 2017/01/29 19:50 ~)				
	0.0	6.722433e–2	(for Fl < 7)	
	–0.3219685	0.1132198	(for Fl >= 7)	
(for 2017/01/25 19:50 ~ 2017/01/29 19:50)				
	0.0	0.1164691	(for Fl < 8)	
	–3.496350	0.5535129	(for Fl >= 8 and Fl < 12)	
	2.689773	3.800260e–2	(for Fl >= 12)	
Leg 3	0.0	5.766692e–2	(for Fl < 8)	
	–0.1513446	7.658499e–2	(for Fl >= 8)	
Leg 4	0.0	0.1164691	(for Fl < 8)	
	–3.496350	0.5535129	(for Fl >= 8 and Fl < 12)	
	2.689773	3.800260e–2	(for Fl >= 12)	

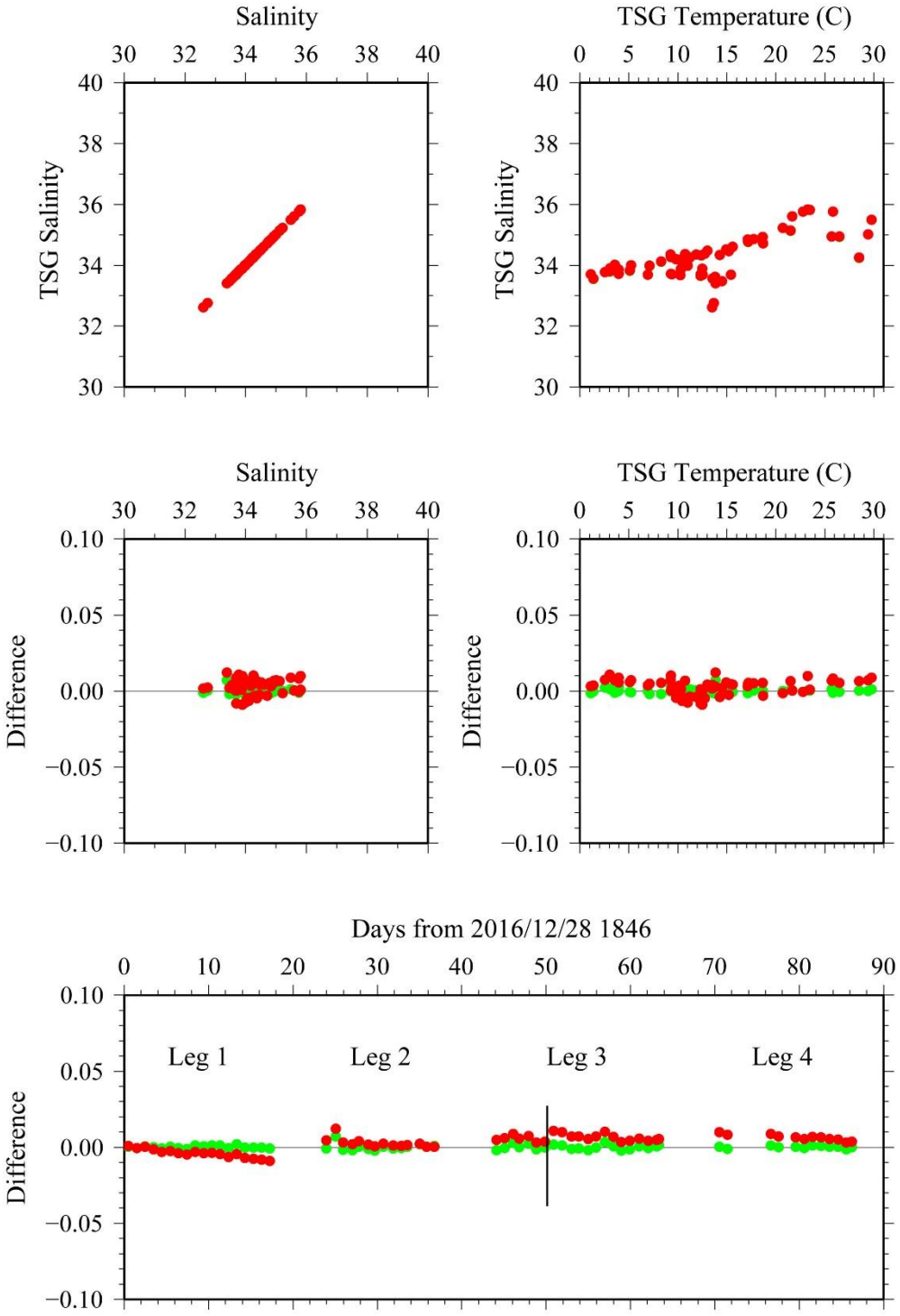

Figure 3.6.1. Comparison between TSG salinity (red: before correction, green: after correction) and sampled salinity.

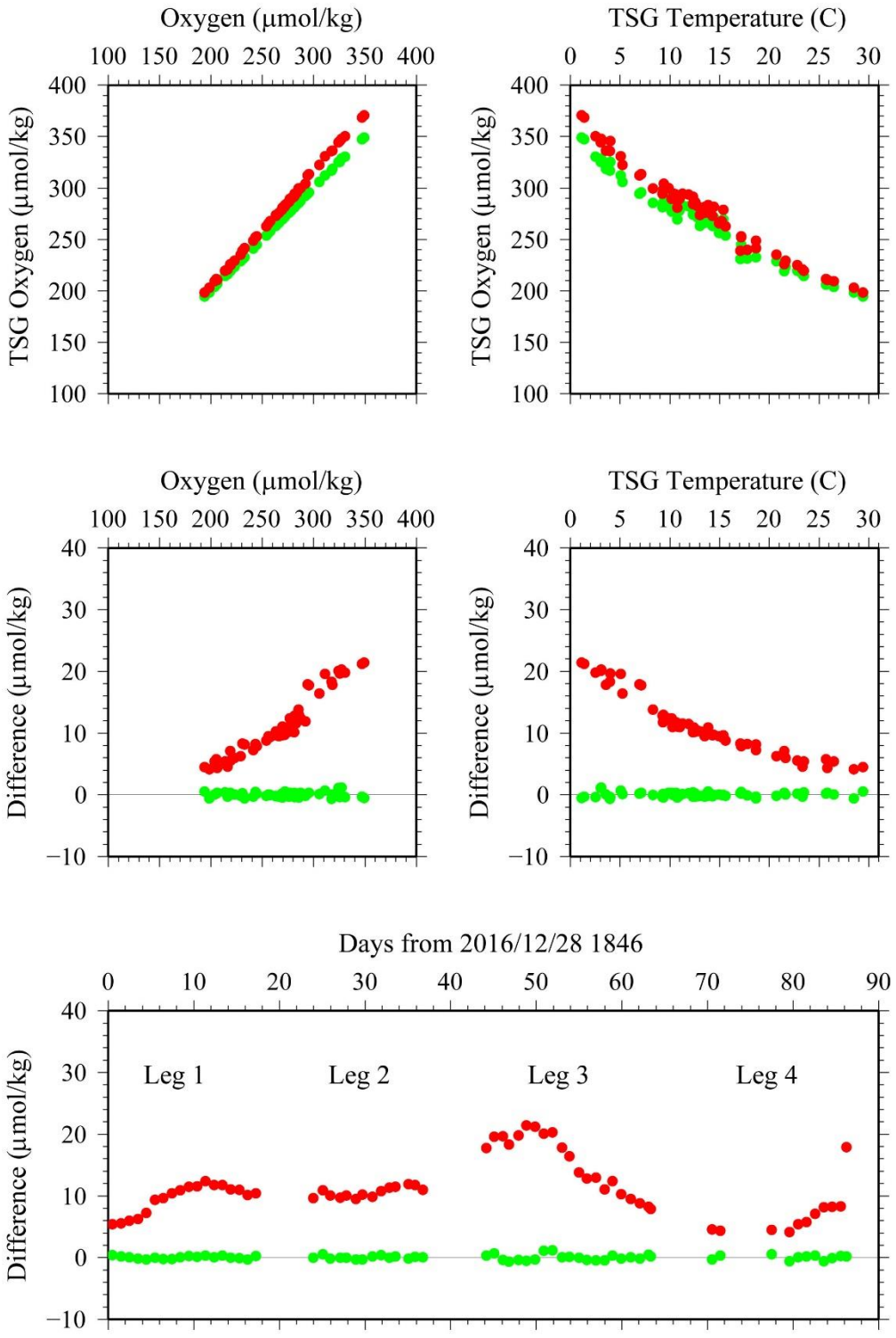

Figure 3.6.2. Comparison between TSG oxygen (red: before correction, green: after correction) and sampled oxygen.

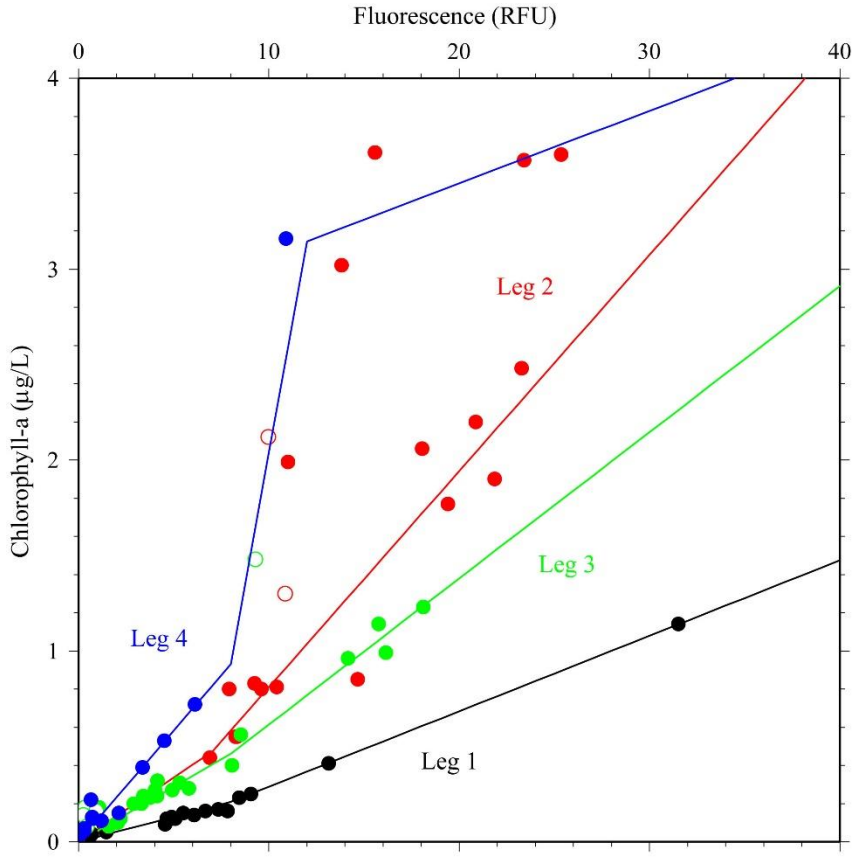

Figure 3.6.3. Comparison between TSG fluorescence and sampled chlorophyll-a. Open dots show that PAR data were greater than 50 µE/(m^2 sec). Calibration functions are also shown as lines.

3.7 pCO_2

(1) Personnel

Akihiko Murata (JAMSTEC)
Tomonori Watai (MWJ)
Atsushi Ono (MWJ)
Emi Deguchi (MWJ)
Nagisa Fujiki (MWJ)

(2) Objective

Concentrations of CO_2 in the atmosphere are now increasing at a rate of about 2.0 ppmv y^{-1} owing to human activities such as burning of fossil fuels, deforestation, and cement production. It is an urgent task to estimate as accurately as possible the absorption capacity of the oceans against the increased atmospheric CO_2, and to clarify the mechanism of the CO_2 absorption, because the magnitude of the anticipated global warming depends on the levels of CO_2 in the atmosphere, and because the ocean currently absorbs 1/3 of the 6 Gt of carbon emitted into the atmosphere each year by human activities.

In this cruise, we measured pCO_2 (partial pressure of CO_2) in the atmosphere and surface seawater continuously along cruise tracks in the South Pacific in order to quantify how much CO_2 is absorbed in the region.

(3) Apparatus

Concentrations of CO_2 in the atmosphere and the sea surface were measured continuously during the cruise using an automated system with a non-dispersive infrared (NDIR) analyzer (Li-COR LI-7000). The automated system (Nippon ANS) was operated by about one and a half hour cycle. In one cycle, standard gasses, marine air and an air in a headspace of an equilibrator were analyzed subsequently. The nominal concentrations of the standard gas were 230, 290, 370 and 430 ppmv. The standard gases will be calibrated after the cruise.

The marine air taken from the bow was introduced into the NDIR by passing through a mass flow controller, which controlled the air flow rate at about 0.6 – 0.8 L/min, a cooling unit, a perma-pure dryer (GL Sciences Inc.) and a desiccant holder containing $Mg(ClO_4)_2$.

A fixed volume of the marine air taken from the bow was equilibrated with a stream of seawater that flowed at a rate of 4.0 – 5.0 L/min in the equilibrator. The air in the equilibrator was circulated with a pump at 0.7-0.8L/min in a closed loop passing through two cooling units, a perma-pure dryer (GL Science Inc.) and a desiccant holder containing $Mg(ClO_4)_2$.

(4) Results

Concentrations of CO_2 (xCO_2) of marine air and surface seawater are shown in Fig. 3.7.1, together with SST.

(a)

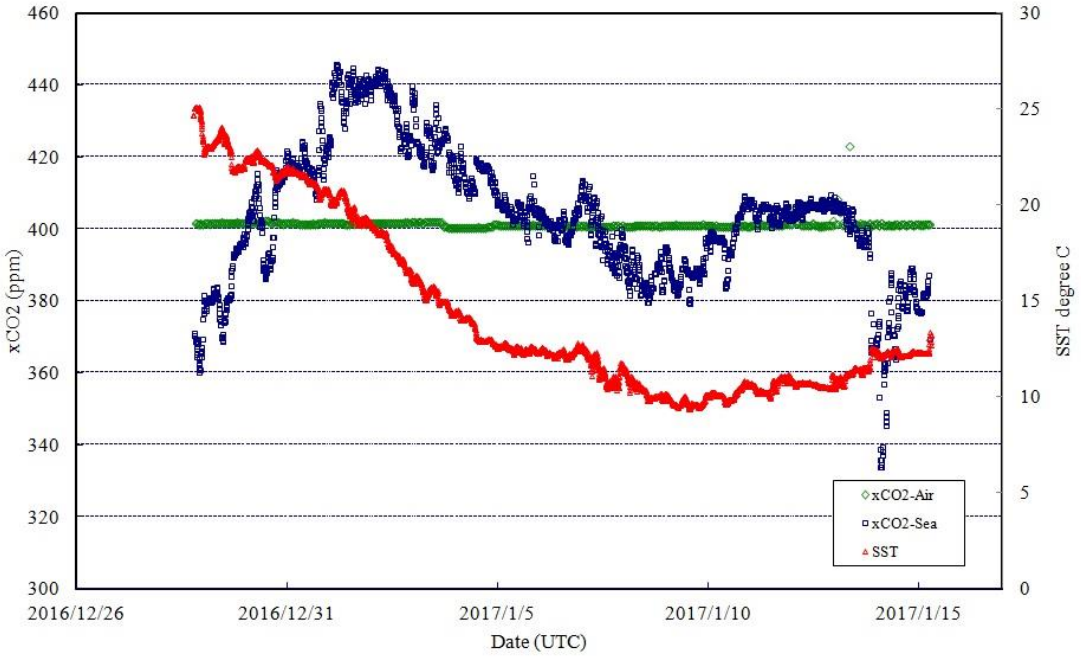

(b)

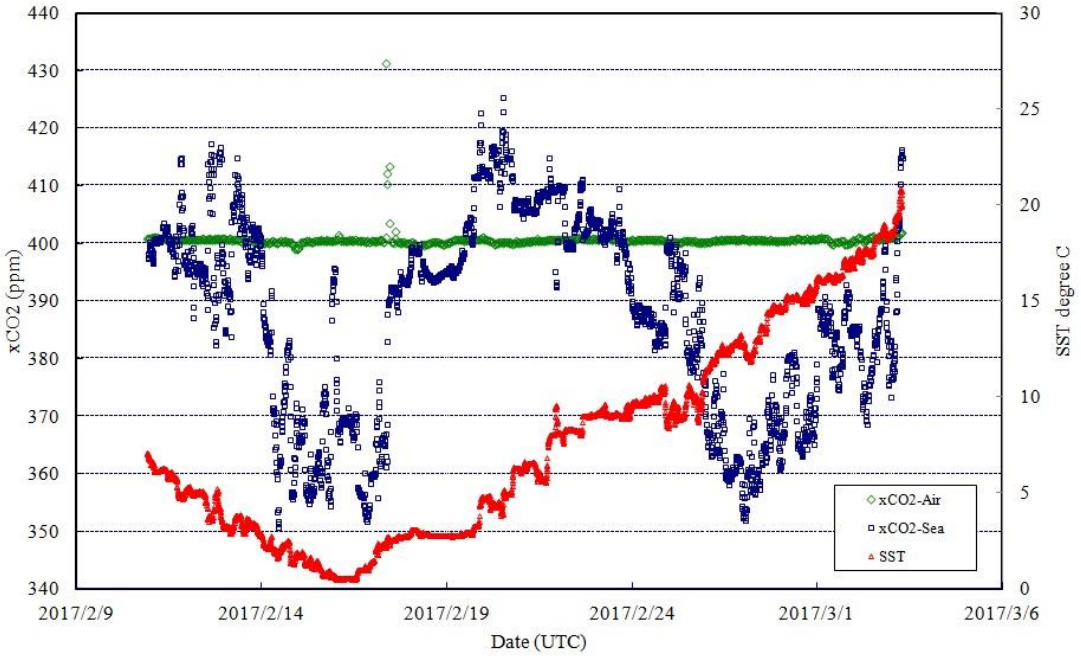

(c)

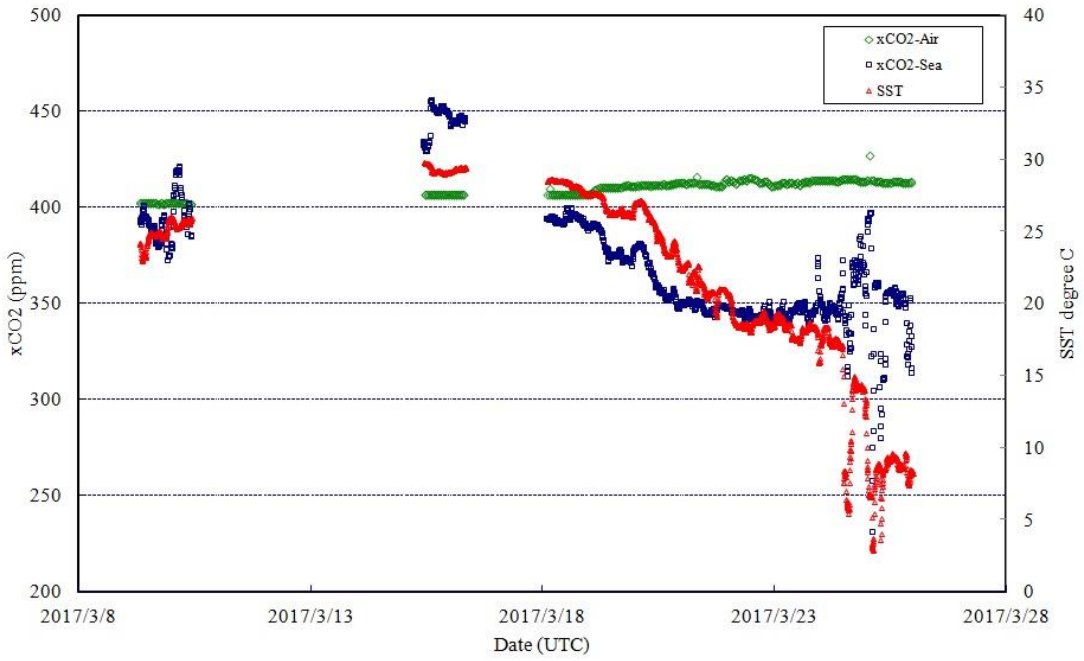

Fig. 3.7.1. Preliminary results of concentrations of CO_2 (xCO_2) in atmosphere (green) and surface seawater (blue), and SST (red) observed during (a) leg 1, (b) leg 3, and (c) leg 4 of MR16-09.

3.8 Satellite Image Acquisition

(1) Personnel

Masaki Katsumata	*JAMSTEC: Principal investigator*[*1]	*- leg1,2,3,4 -*
Souichiro Sueyoshi	*Nippon Marine Enterprise Ltd., (NME)*	*- leg1 -*
Yutaro Murakami	*NME*	*- leg1,2 -*
Wataru Tokunaga	*NME*	*- leg2 -*
Koichi Inagaki	*NME*	*- leg2,3 -*
Shinya Okumura	*NME*	*- leg3 -*
Kazuho Yoshida	*NME*	*- leg4 -*
Ryo Kimura	*MIRAI crew / NME*	*- leg1,3,4 -*
Masanori Murakami	*MIRAI crew*	*- leg2,3,4 -*

*[*1] leg1: On-board, leg2,3,4: Not on-board*

(2) Objectives

The objectives are to collect cloud data in a high spatial resolution mode from the Advance Very High Resolution Radiometer (AVHRR) on the NOAA and MetOp polar orbiting satellites, and to verify the data from Doppler radar on board.

(3) Methods

We received the down link High Resolution Picture Transmission (HRPT) signal from satellites, which passed over the area around the R/V MIRAI. We processed the HRPT signal with the in-flight calibration and computed the brightness temperature. A cloud image map around the R/V MIRAI was made from the data for each pass of satellites.

We received and processed polar orbiting satellites data from the MR16-09 Leg1 cruise to Leg4 cruise.

(4) Data archives

These data obtained in these cruises will be submitted to the Data Management Group of JAMSTEC, and will be opened to the public via “Data Research System for Whole Cruise Information in JAMSTEC (DARWIN)” in JAMSTEC web site.

<http://www.godac.jamstec.go.jp/darwin/e>.

3.9 ADCP

(1) Personnel

Shinya Kouketsu	***JAMSTEC: Principal Investigator(Not on board)***	***- leg1,2,3,4 -***
Wolfgang Schneider	***Univ. of Concepcion: Principal Investigator***	***- leg2 -***
Souichiro Sueyoshi	***Nippon Marine Enterprises Ltd., (NME)***	***- leg1 -***
Yutaro Murakami	***NME***	***- leg1,2 -***
Wataru Tokunaga	***NME***	***- leg2 -***
Koichi Inagaki	***NME***	***- leg2,3 -***
Shinya Okumura	***NME***	***- leg3 -***
Kazuho Yoshida	***NME***	***- leg4 -***
Ryo Kimura	***MIRAI crew / NME***	***- leg1,3,4 -***
Masanori Murakami	***MIRAI crew***	***- leg2,3,4 -***

(2) Objective

To obtain continuous measurement of the current profile along the ship's track.

(3) Methods

Upper ocean current measurements were made in the MR16-09 Leg1 to Leg4 cruises, using the hull-mounted Acoustic Doppler Current Profiler (ADCP) system. For most of its operation the instrument was configured for water-tracking mode. Bottom-tracking mode, interleaved bottom-ping with water-ping, was made to get the calibration data for evaluating transducer misalignment angle in the shallow water. The system consists of following components;

1) R/V MIRAI has installed vessel-mount ADCP (acoustic frequency 76.8 kHz "Ocean Surveyor", Teledyne RD Instruments). It has a phased-array transducer with single ceramic assembly and creates 4 acoustic beams electronically. We mounted the transducer head rotated to a ship-relative angle of 45 degrees azimuth from the keel.

2) For heading source, we use ship's gyro compass (TOKYO KEIKI, Japan), continuously providing heading to the ADCP system directory. Also we have Inertial Navigation System (PHINS, IXBLUE) which provide high-precision heading and attitude information are stored in ".N2R" data files.

3) Differential GNSS system (Multi-Fix, Fugro, Netherlands) providing precise ship's position fixes.

4) We used VmDas version 1.46.5 (TRDI) for data acquisition.

5) To synchronize time stamp of pinging with GPS time, the clock of the logging computer is adjusted to GPS time every 8 minutes.

6) The sound speed at the transducer does affect the vertical bin mapping and vertical velocity measurement, is calculated from temperature, salinity (constant value; 35.0 psu) and depth (6.5 m;

transducer depth) by equation in Medwin (1975).

Data was configured for 8-m intervals starting 23-m below the surface. Every ping was recorded as raw ensemble data (.ENR). Major parameters for the measurement (Direct Command) are shown in Table 3.9-1.

(4) Preliminary results

Fig.3.9-1 to 3.9-4 show surface current profile along the ship's track, averaged four depth cells from 6th to 10th, about 55m to 103 m with 30 minutes average.

(5) Data archive

These data obtained in these cruises will be submitted to the Data Management Group of JAMSTEC, and will be opened to the public via "Data Research System for Whole Cruise Information in JAMSTEC (DARWIN)" in JAMSTEC web site.
<http://www.godac.jamstec.go.jp/darwin/e>.

(6) Remarks (Time in UTC)

i) The following periods, the observations were carried out.

Leg1: 18:46, 28 Dec. 2016 to 06:00, 15 Jan. 2017

Leg2: 12:11, 21 Jan. 2017 to 14:17, 21 Jan. 2017

14:32, 21 Jan. 2017 to 00:23, 04 Feb. 2017

Leg3: 21:00, 10 Feb. 2017 to 06:59, 03 Mar. 2017

Leg4: 07:03, 09 Mar. 2017 to 09:59, 10 Mar. 2017

10:00, 15 Mar. 2017 to 08:09, 16 Mar. 2017

01:50, 18 Mar. 2017 to 00:00, 28 Mar. 2017

ii) The following period, Temperature and Sound Velocity data were constant (0.0°C and 1449m/s) due to system trouble.

02:55, 16 Feb. 2017 to 02:19, 19 Feb. 2017

Table 3.9-1 Major parameters

Bottom-Track Commands
BP = 001 Pings per Ensemble (almost less than 1300m depth)
Leg1: None
Leg2: 22:19, 21 Jan. 2017 to 06:00, 22 Jan. 2017
21:43, 26 Jan. 2017 to 23:19, 26 Jan. 2017

23:02, 28 Jan. 2017 to 01:25, 29 Jan. 2017

22:55, 03 Feb. 2017 to 23:56, 03 Feb. 2017

Leg3: None

Leg4: 07:58, 09 Mar. 2017 to 18:34, 09 Mar. 2017

22:19, 25 Mar. 2017 to 00:00, 28 Mar. 2017

Environmental Sensor Commands

EA = +04500 Heading Alignment (1/100 deg)

EB = +00000 Heading Bias (1/100 deg)

ED = 00065 Transducer Depth (0 - 65535 dm)

EF = +001 Pitch/Roll Divisor/Multiplier (pos/neg) [1/99 - 99]

EH = 00000 Heading (1/100 deg)

ES = 35 Salinity (0-40 pp thousand)

EX = 00000 Coord Transform (Xform:Type; Tilts; 3Bm; Map)

EZ = 10200010 Sensor Source (C; D; H; P; R; S; T; U)

C (1): Sound velocity calculates using ED, ES, ET (temp.)

D (0): Manual ED

H (2): External synchro

P (0), R (0): Manual EP, ER (0 degree)

S (0): Manual ES

T (1): Internal transducer sensor

U (0): Manual EU

Timing Commands

TE = 00:00:02.00 Time per Ensemble (hrs:min:sec.sec/100)

TP = 00:02.00 Time per Ping (min:sec.sec/100)

Water-Track Commands

WA = 255 False Target Threshold (Max) (0-255 count)

WB = 1 Mode 1 Bandwidth Control (0=Wid, 1=Med, 2=Nar)

WC = 120 Low Correlation Threshold (0-255)

WD = 111 100 000 Data Out (V; C; A; PG; St; Vsum; Vsum^2;#G;P0)

WE = 1000 Error Velocity Threshold (0-5000 mm/s)

WF = 0800 Blank After Transmit (cm)

WG = 001 Percent Good Minimum (0-100%)

WI = 0 Clip Data Past Bottom (0 = OFF, 1 = ON)

WJ = 1 Rcvr Gain Select (0 = Low, 1 = High)

WM = 1 Profiling Mode (1-8)

WN = 100 Number of depth cells (1-128)

WP = 00001 Pings per Ensemble (0-16384)

WS= 0800 Depth Cell Size (cm)

WT = 000 Transmit Length (cm) [0 = Bin Length]

WV = 0390 Mode 1 Ambiguity Velocity (cm/s radial)

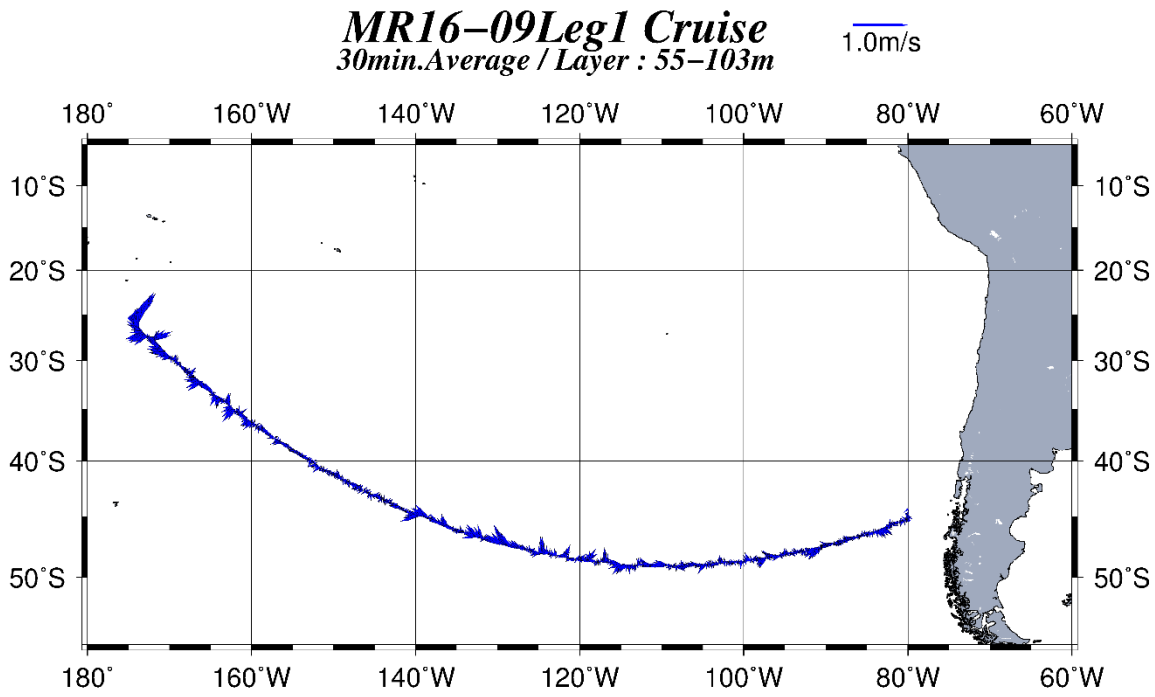

Fig 3.9-1 Current profile along the ship's track, about 55m to 103m depth, averaged every 30 minutes (Leg1).

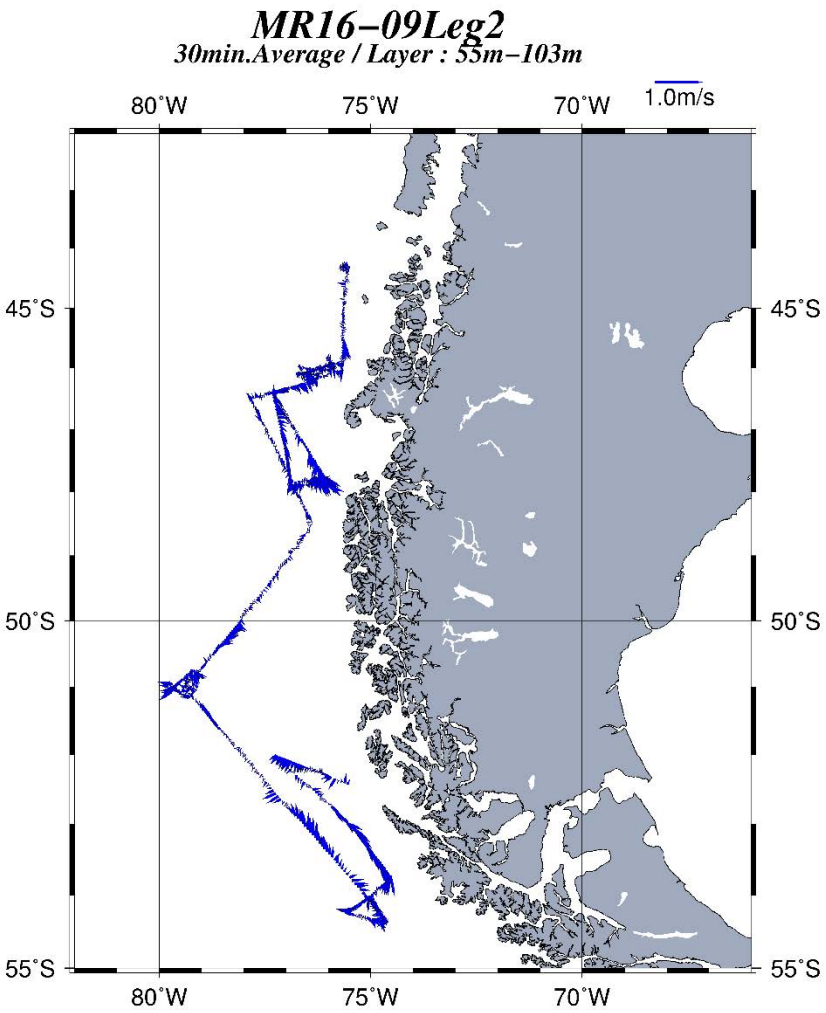

Fig 3.9-2 Current profile along the ship's track, about 55m to 103m depth, averaged every 30 minutes (Leg2).

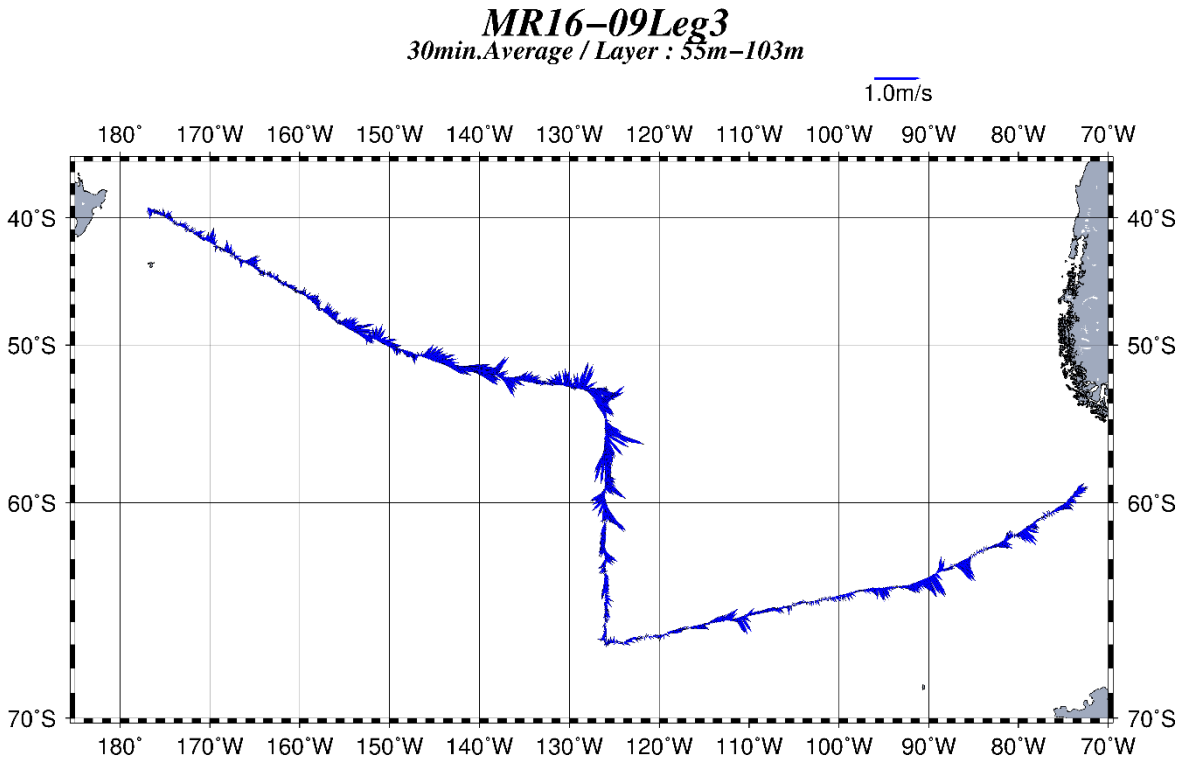

Fig 3.9-3 Current profile along the ship's track, about 55m to 103m depth, averaged every 30 minutes (Leg3).

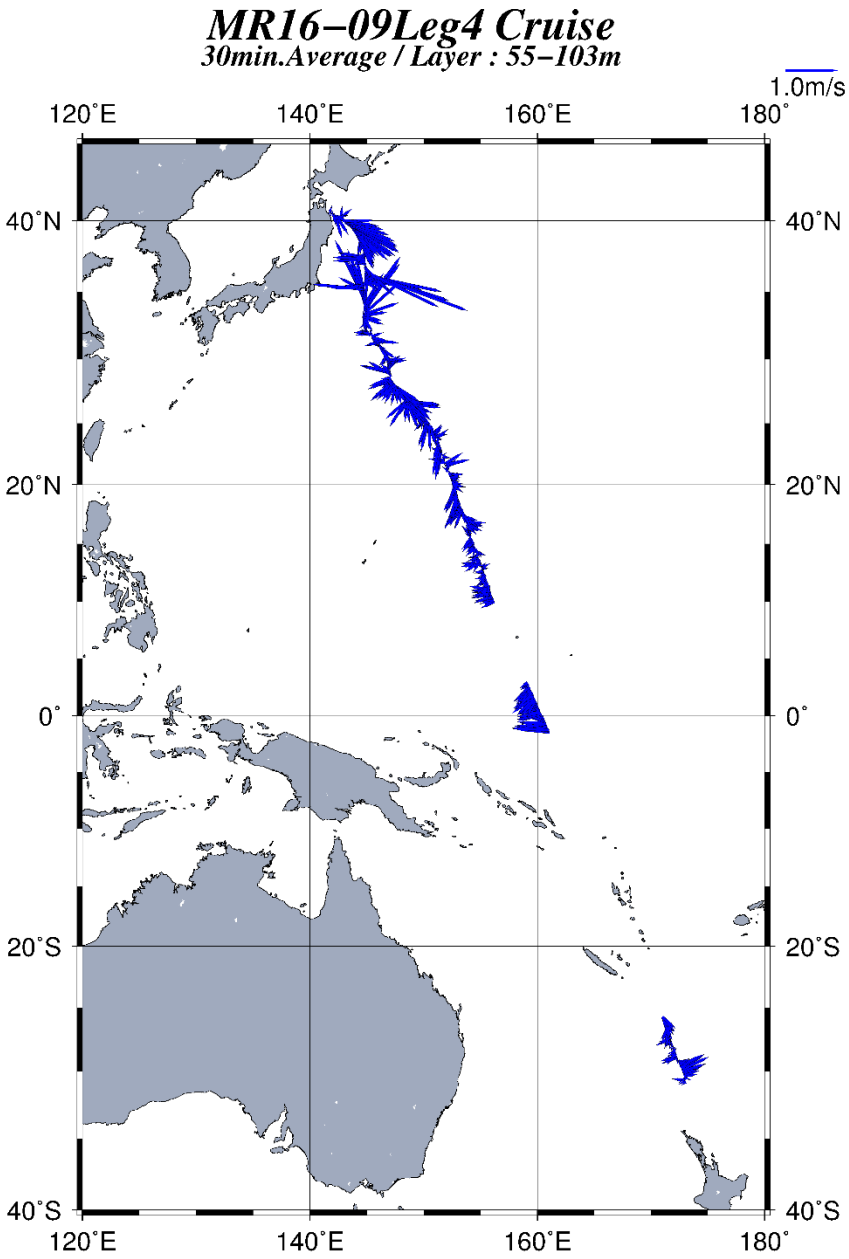

Fig 3.9-4 Current profile along the ship's track, about 55m to 103m depth, averaged every 30 minutes (Leg4).

3.10 Ceilometer observation

(1) Personnel

Masaki Katsumata	*JAMSTEC: Principal investigator*[*1]	*- leg1,2,3,4 -*
Souichiro Sueyoshi	*Nippon Marine Enterprise Ltd., (NME)*	*- leg1 -*
Yutaro Murakami	*NME*	*- leg1,2 -*
Wataru Tokunaga	*NME*	*- leg2 -*
Koichi Inagaki	*NME*	*- leg2,3 -*
Shinya Okumura	*NME*	*- leg3 -*
Kazuho Yoshida	*NME*	*- leg4 -*
Ryo Kimura	*MIRAI crew / NME*	*- leg1,3,4 -*
Masanori Murakami	*MIRAI crew*	*- leg2,3,4 -*

[*1] *leg1: On-board, leg2,3,4: Not on-board*

(2) Objectives

The information of cloud base height and the liquid water amount around cloud base is important to understand the process on formation of the cloud. As one of the methods to measure them, the ceilometer observation was carried out.

(3) Parameters

1. Cloud base height [m].
2. Backscatter profile, sensitivity and range normalized at 10 m resolution.
3. Estimated cloud amount [oktas] and height [m]; Sky Condition Algorithm.

(4) Methods

We measured cloud base height and backscatter profile using ceilometer (CL51, VAISALA, Finland). Major parameters for the measurement configuration are shown in Table 3.10-1;

Table 3.10-1 Major parameters

Laser source:	Indium Gallium Arsenide (InGaAs) Diode
Transmitting center wavelength:	910±10 nm at 25 degC
Transmitting average power:	19.5 mW
Repetition rate:	6.5 kHz
Detector:	Silicon avalanche photodiode (APD)
Responsibility at 905 nm:	65 A/W

Cloud detection range:	0 ~ 13 km
Measurement range:	0 ~ 15 km
Resolution:	10 meter in full range
Sampling rate:	36 sec
Sky Condition:	Cloudiness in octas (0 ~ 9)

(0:Sky Clear, 1:Few, 3:Scattered, 5-7:Broken, 8:Overcast, 9:Vertical Visibility)

On the archive dataset, cloud base height and backscatter profile are recorded with the resolution of 10 m (33 ft).

(5) Preliminary results

Fig.3.10-1 to Fig.3.10-3 show the time series of 1st, 2nd and 3rd lowest cloud base height during these cruises.

(6) Data archives

These data obtained in these cruises will be submitted to the Data Management Group of JAMSTEC, and will be opened to the public via "Data Research System for Whole Cruise Information in JAMSTEC (DARWIN)" in JAMSTEC web site.
<http://www.godac.jamstec.go.jp/darwin/e>.

(7) Remarks (Times in UTC)

i) The following periods, the observation were carried out.

Leg1: 18:45, 28 Dec. 2016 to 06:13, 15 Jan. 2017
Leg2: 12:11, 21 Jan. 2017 to 14:17, 21 Jan. 2017
14:32, 21 Jan. 2017 to 00:23, 04 Feb. 2017
Leg3: 21:00, 10 Feb. 2017 to 06:59, 03 Mar. 2017
Leg4: 07:03, 09 Mar. 2017 to 09:59, 10 Mar. 2017
10:00, 15 Mar. 2017 to 08:09, 16 Mar. 2017
01:50, 18 Mar. 2017 to 00:00, 28 Mar. 2017

ii) The following time, the window was cleaned.

Leg1: 04:58, 29 Dec. 2016
01:55, 04 Jan. 2017
21:03, 11 Jan. 2017
Leg2: 11:51, 27 Jan. 2017
00:57, 03 Feb. 2017

Leg3: 01:18, 14 Feb. 2017

22:13, 21 Feb. 2017

02:48, 25 Feb. 2017

20:26, 01 Mar. 2017

Leg4: 02:12, 15 Mar. 2017

06:21, 23 Mar. 2017

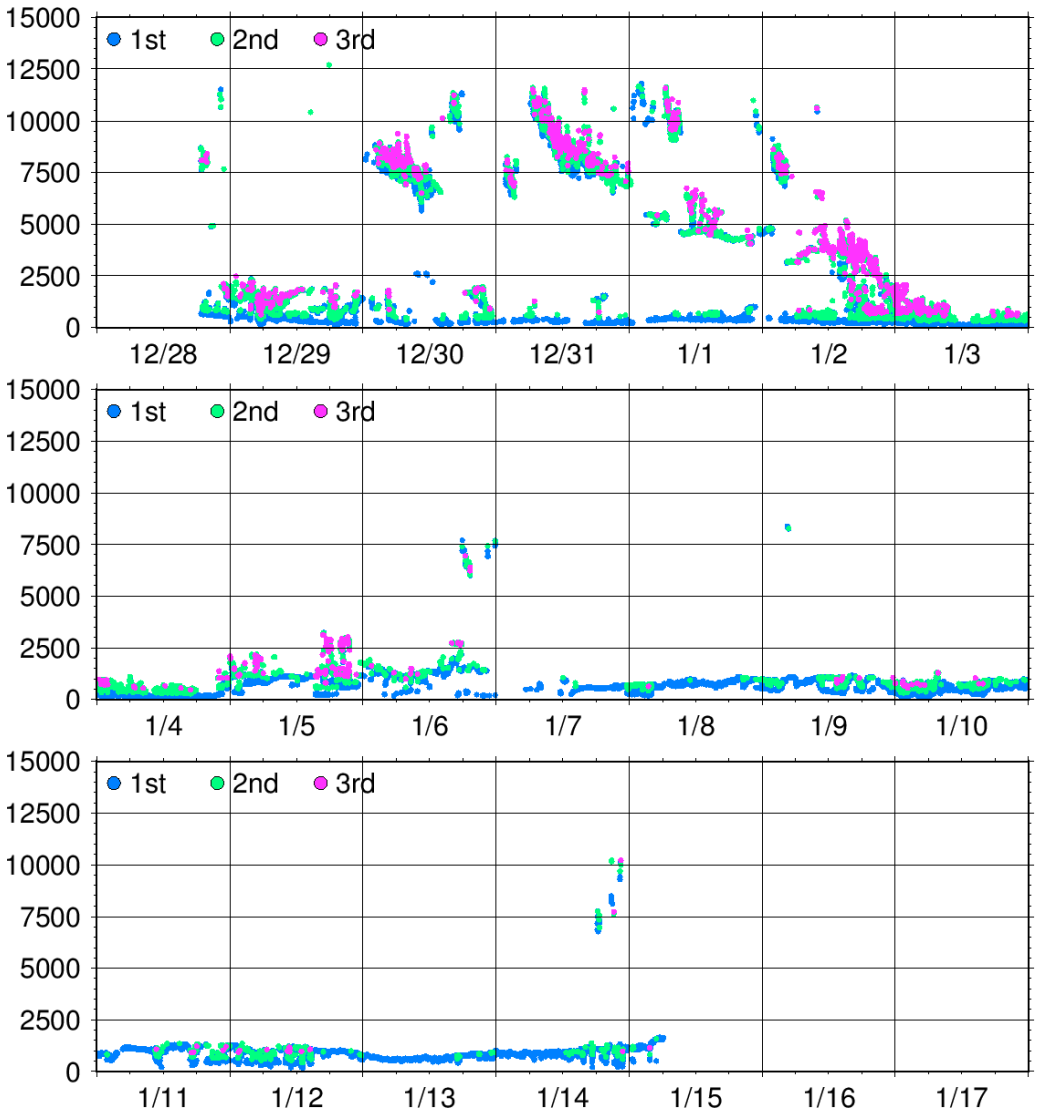

Fig. 3.10-1 1st, 2nd and 3rd lowest cloud base height during MR16-09 Leg1 cruise.

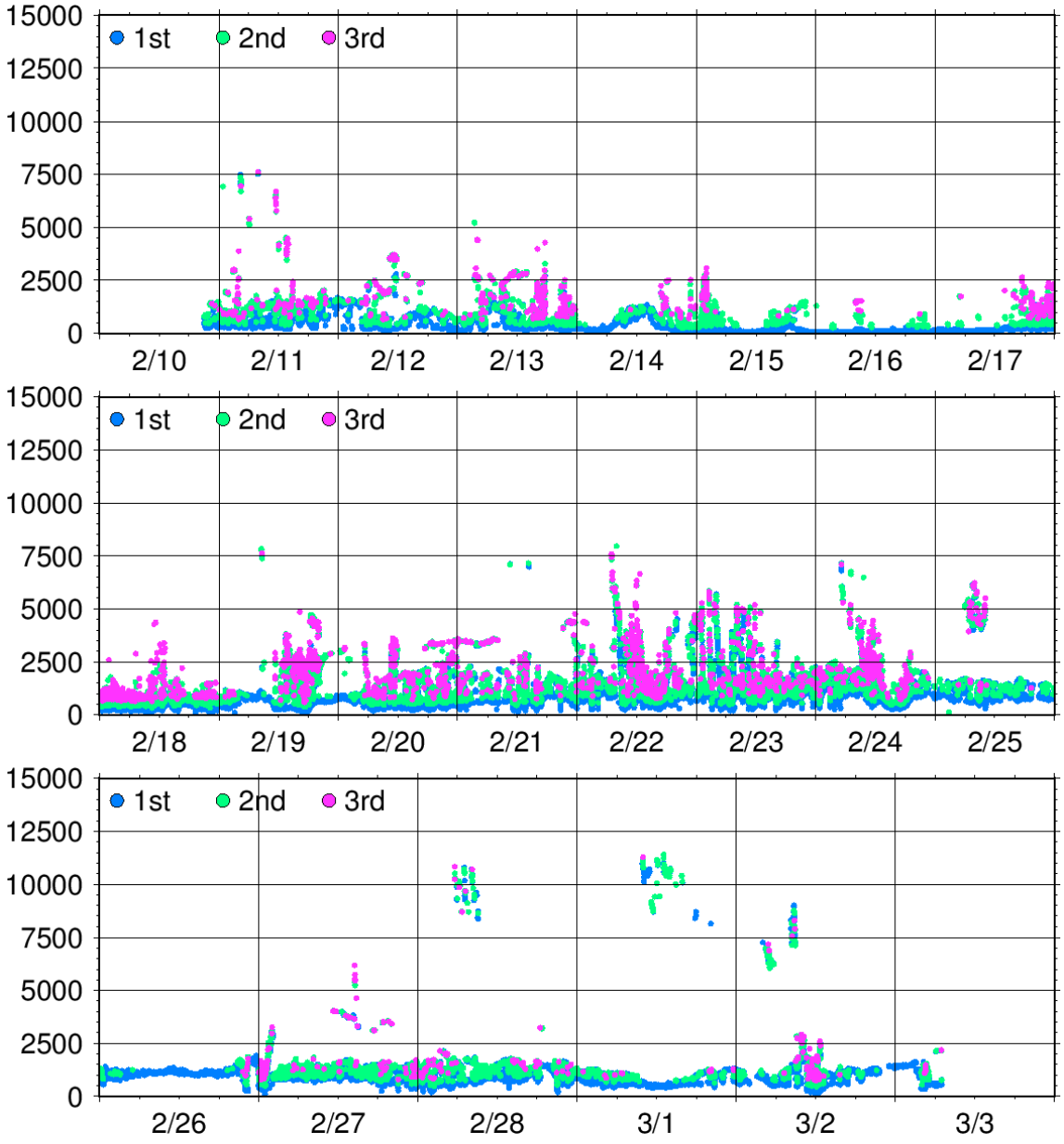

Fig. 3.10-2 . 1st, 2nd and 3rd lowest cloud base height during MR16-09 Leg3 cruise.

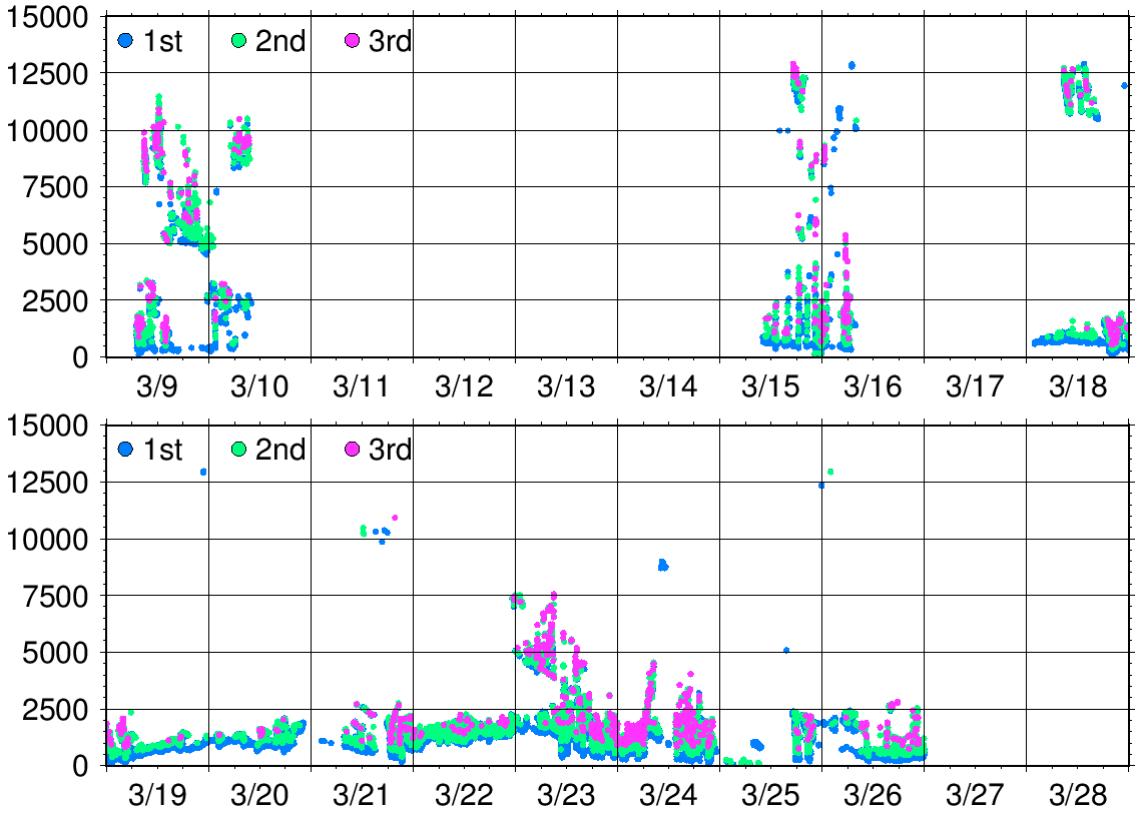

Fig. 3.10-3 . 1st, 2nd and 3rd lowest cloud base height during MR16-09 Leg4 cruise.

3.11 Marine Aerosols

(1) Personnel

Jun Noda	Rakuno Gakuen University	- on board
Marcelo Gutiérrez	University of Concepcion	- on board
Osamu Yoshida	Rakuno Gakuen University	- not on board

(2) Objectives

· To investigate chemical and biological properties of aerosols in a marine environment

· To investigate micron-size particles number and size distribution

· To investigate a biological linkage between marine aerosol and seawater

(3) Parameters

· Chemical and biological compositions of marine aerosols

· Particle number concentration

· Comparison of biological diversities in ocean water and marine aerosols

(4) Instruments and methods

(4-1) Marine aerosol collection

(4-1-1) Aerosol collection with NILU filter unit with NL $PM_{2.5}$ cut off impactor

The NILU (Norwegian Institute for Air Research, Norway) 2-stage filter holder unit with NL $PM_{2.5}$ impactor (Tokyo Dylec, Japan) was equipped with two PTFE (Polytetrafluoroethylene) membrane filters with pore size of 0.8 μm (Top:ϕ=47 with 20 mm hole in the center and Bottom:ϕ=47mm) to collect two size ranges of marine aerosols. The sampling unit was mounted on the roof section of navigation deck close to a high volume sampler. The Filter units withdraw 4L/min. by a vacuum pump and a Mass Flow Controller (MFC) to maintain the flow rate. Also, the MFC counted the total volume of air passed through the filter unit. The sampling intervals were ca. 24 hr during the leg 2. and ca. 24 hr to 7.8 days during the leg 3 (detail information are shown on the Table 3.11-1 and 3.11-2 Logs of marine aerosol sampling on PTFE membrane filters).

(4-2) BioSampler

The BioSampler (SKC, USA) was employed to collect marine aerosols from the right side of the upper deck. The BioSampler has three critical orifice nozzles with designated flow direction to create a vortex inside the collection liquid of 15 ml. Also the nozzles act as critical orifice to maintain the flow rate through the nozzle at ca. 10 L/min. At initial trial, sampling duration was ca. 30 min during the surface water sampling period, which was strictly limited to this period to minimize the workload for the

ship crews. The Biosampler has a greater capacity to collect biological aerosols than the NILU filter method; we expect to have much more DNA and other biogenic substances in the collection liquid.

After the initial trial, there was a discussion about possible prolonged sampling period to ensure more than adequate amount of DNA with onboard Chilean Scientists. After the consultation with the chief scientist and the Chilean side chief scientist, we have decided to conduct sampling of marine aerosols with increased amount of collection liquid and prolonged sampling duration (detail information are shown in the Table 3.11-3. Logs of marine aerosol sampling with BioSampler).

(4-3) Particle number concentration and size distribution

The particle number concentration and size distributions were planned to measure with Optical Particle Sizer (OPS3330). However, the instrument was not functioning during the leg 2, thus none of the data sets was obtained by the OPS 3330.

(5) Station list or Observation log

Table 3.11-1. Log of marine aerosol sampling on PTFE membrane filters

On board ID	Date Collected					Latitude			Longitude		
	YYYY	MM	DD	hh:mm:ss	UTC/JST	Deg.	Min.	N/S	Deg.	Min.	E/W
MR1609-Tel-001	2017	01	21	13:35	UTC	44	17.3760	S	75	35.4831	W
	2017	01	22	13:35	UTC	46	03.9138	S	75	41.4622	W
MR1609-Tel-002	2017	01	22	13:40	UTC	46	03.5267	S	75	41.4220	W
	2017	01	23	13:40	UTC	46	04.2428	S	76	32.01270	W
MR1609-Tel-003	2017	01	23	13:45	UTC	46	04.2314	S	76	32.06210	W
	2017	01	24	13:35	UTC	46	10.7887	S	76	17.68200	W
MR1609-Tel-004	2017	01	24	13:38	UTC	46	10.7960	S	76	17.67470	W
	2017	01	25	13:37	UTC	46	17.7684	S	76	49.21520	W
MR1609-Tel-005	2017	01	25	13:41	UTC	46	17.9294	S	76	49.97760	W
	2017	01	26	13:40	UTC	47	46.0578	S	76	24.98860	W
MR1609-Tel-006	2017	01	26	13:43	UTC	47	46.0370	S	76	24.93060	W
	2017	01	27	13:38	UTC	46	29.5537	S	77	17.37910	W
MR1609-Tel-007	2017	01	27	13:46	UTC	46	29.1496	S	77	17.35700	W
	2017	01	28	13:42	UTC	47	47.6478	S	76	02.48930	W
MR1609-Tel-008	2017	01	28	13:45	UTC	47	47.7123	S	76	02.57160	W
	2017	01	29	13:52	UTC	48	23.2475	S	76	28.13850	W
MR1609-Tel-009	2017	01	29	13:55	UTC	48	23.2536	S	76	28.16440	W
	2017	01	30	13:50	UTC	50	49.0803	S	79	00.68380	W
MR1609-Tel-010	2017	01	30	13:54	UTC	50	48.8939	S	79	01.44170	W
	2017	01	31	13:45	UTC	50	48.3214	S	79	07.15040	W
MR1609-Tel-011	2017	01	31	13:49	UTC	50	48.3250	S	79	07.16240	W
	2017	02	01	13:49	UTC	53	16.2706	S	76	12.13750	W
MR1609-Tel-012	2017	02	01	13:55	UTC	53	17.2478	S	76	10.76840	W
	2017	02	02	13:48	UTC	54	20.4553	S	74	39.49880	W
MR1609-Tel-013	2017	02	02	13:50	UTC	54	20.1487	S	74	39.83210	W
	2017	02	03	19:48	UTC	52	19.0665	S	75	56.76900	W

Table 3.11-2. Logs of marine aerosol sampling on PTFE membrane filters

On board ID	Date Collected					Latitude			Longitude		
	YYYY	MM	DD	hh:mm:ss	UTC/JST	Deg.	Min.	N/S	Deg.	Min.	E/W
MR1609-Tel-022	2017	02	11	19:39	UTC	61	45.6669	S	80	24.0890	W
	2017	02	16	0:03	UTC	66	55.9992	S	125	14.9269	W
MR1609-Tel-023	2017	02	16	0:03	UTC	66	55.9992	S	125	14.9269	W
	2017	02	17	0:04	UTC	65	38.8478	S	125	57.4883	W
MR1609-Tel-024	2017	02	17	0:04	UTC	65	38.8478	S	125	57.4883	W
	2017	02	17	23:57	UTC	63	11.8680	S	126	00.6343	W
MR1609-Tel-025	2017	02	17	23:57	UTC	63	11.8680	S	126	00.6343	W
	2017	02	18	23:53	UTC	62	20.3533	S	126	06.4242	W
MR1609-Tel-026	2017	02	18	23:53	UTC	62	20.3533	S	126	06.4242	W
	2017	02	20	0:06	UTC	60	00.8449	S	125	58.5689	W
MR1609-Tel-027	2017	02	20	0:06	UTC	60	00.8449	S	125	58.5689	W
	2017	02	20	23:53	UTC	57	49.5030	S	125	59.9270	W
MR1609-Tel-028	2017	02	20	23:53	UTC	57	49.5030	S	125	59.9270	W
	2017	02	22	0:21	UTC	55	01.0794	S	125	58.5795	W
MR1609-Tel-029	2017	02	22	0:21	UTC	55	01.0794	S	125	58.5795	W
	2017	02	23	0:00	UTC	53	01.1720	S	126	00.1355	W
MR1609-Tel-030	2017	02	23	0:00	UTC	53	01.1720	S	126	00.1355	W
	2017	03	02	18:36	UTC			S			W

Table 3.11-3. Logs of marine aerosol sampling with BioSampler

On board ID	Date Collected					Latitude			Longitude		
	YYYY	MM	DD	hh:mm:ss	UTC/JST	Deg.	Min.	N/S	Deg.	Min.	E/W
MR1609-Tel-014	2017	01	24	1:23	UTC	46	10.1910	S	76	17.28530	W
	2017	01	24	1:53	UTC	46	10.1935	S	76	17.28690	W
MR1609-Tel-015	2017	01	24	1:55	UTC	46	10.1935	S	76	17.28690	W
	2017	01	24	2:15	UTC	46	10.1948	S	76	17.28910	W
MR1609-Tel-016	2017	01	26	3:10	UTC	47	49.3219	S	76	36.35760	W
	2017	01	26	7:36	UTC	47	45.9932	S	76	12.48200	W
MR1609-Tel-017	2017	01	27	20:00	UTC	46	24.8541	S	77	18.93600	W
	2017	01	28	14:55	UTC	47	47.9249	S	76	02.09790	W
MR1609-Tel-018	2017	01	28	22:23	UTC	47	57.3677	S	76	01.44350	W
	2017	01	29	14:55	UTC	48	23.8232	S	76	28.78540	W
MR1609-Tel-019	2017	01	30	14:15	UTC	50	48.5986	S	79	04.32910	W
	2017	01	31	12:52	UTC	50	48.3102	S	79	06.99480	W
MR1609-Tel-020	2017	01	31	19:00	UTC	50	48.3240	S	79	07.17860	W
	2017	02	02	10:14	UTC	54	20.1017	S	74	38.17960	W
MR1609-Tel-021	2017	02	02	18:43	UTC	53	46.4482	S	74	32.70620	W
	2017	02	03	19:59	UTC	52	19.0874	S	75	56.70720	W

(6) Plan of analyses

(6-1) Chemical analysis

In marine aerosols, the amount of organic fraction has clear dependency with the abundance of chlorophyll concentrations (O'Dowd et al., 2004). There have been several efforts to use different saccharides and other organic components as a tracer to link the primary production in seawater (Russel

et al., 2010, Miyazaki et al., 2016). In this investigation, we would like to analyze the series of saccharides and fatty acids and some inorganic salts to characterize the marine aerosols from the southern Pacific Ocean.

(6-2) Biological analysis

A contribution of marine biological materials on the surface layer has gained much of attention because of the effective ice-nucleating properties (Wilson et al., 2015). From the field and laboratory measurements, Wilson et al., proposed the components from diatom such as *Thalassiosira psudonana* may start the ice nucleation at higher temperature than homogenous nucleation of water at much lower temperature of – 48.3 °C (Willson, et al., 2015, Speedy and Angell, 1976). Thus, understanding the biological components such as plankton in marine flora and marine aerosol is important. For the marine aerosol analysis, the collected particulate matters on the Teflon filters will be extracted and analyzed for microbe diversity by metagenomic analysis. Polymerase chain reaction (PCR) amplification to prepare template DNA for pyrosequencing will be carried out. A data analysis will be performed on each read sequence using previously developed computational tools with some modifications (Nakamura et al., 2008, 2009). In order to have comprehensive metagenomics analyses scheme for marine aerosols and seawater, the analysis method found in Nunoura et al. (2015) will also be taken into consideration.

(6-3) Biological analysis by Chilean scientist

The Chilean scientist plans to extract and quantify DNA from filters containing suspended material collected by BioSampler. Template DNA will be subjected to PCR amplification using general primers to study fungal diversity. If the outcome of these steps will be successful, a further step to do a molecular fingerprint analysis (DGGE, Denaturing Gradient Gel Electrophoresis) will be carried out to compare biological communities collected from BioSampler and surface seawaters. Finally, a deep taxonomic analysis of fungal communities will be performed according to DGGE results.

(7) Expected outcome

From this investigation, we expect to get some understanding of the linkage between microbial flora in seawater and marine aerosols. The previous studies by Russel et al. (2010) and Wilson et al. (2015) clearly indicated that chemical substances produced by the marine flora including plankton might play a particular role to attribute the type of marine aerosols. This kind of an integrated approach helps to understand the mechanism to derive marine aerosols such as ice nuclei formation and lifetime of the cloud.

(8) Data archives

These data obtained in this cruise will be submitted to the Data Management Group of JAMSTEC, and will be opened to the public via “Data Research System for Whole Cruise Information in JAMSTEC

(DARWIN)" in JAMSTEC web site.
<http://www.godac.jamstec.go.jp/darwin/e>

References

Miyazaki, Y. Coburn, S. Ono, K. T.Ho, T. Pierce, R.B. Kawamura, K., and Volkamer, R. 2016. Contribution of dissolved organic matter to submicron water-soluble organic aerosols in the marine boundary layer over the eastern equatorial Pacific. *Atmos. Chem. Phys.*, 16, 7695-7707.

Nakamura, S. Maeda, N. Miron, I.M. Yoh, M. Izutsu, K. Kataoka, C. Honda, T. Yasunaga, T. Nakaya, T. Kawai, J. Hayashizaki, Y. Horii, T. and Iida, T. 2008. Metagenomic diagnosis of bacterial infections, *Emerg. Infect. Dis.*, 14(11):1784-86.

Nakamura, S. Yang, C.S. Sakon, N. Ueda, M. Tougan, T. Yamashita, A. Goto, N. Takahashi, K. Yasunaga, T. Ikuta, K. Mizutani, T. Okamoto, Y. Tagami, M. Morita, R. Maeda, N. Kawai, J. Hayashizaki, Y. Nagai, Y. Horii, T. Iida, T. and Nakaya, T. 2009. Direct metagenomic detection of viral pathogens in nasal and fecal specimens using an unbiased high-throughput sequencing approach, *PLoS One.* 4(1): e4219.

Nunoura, T. Takaki, Y. Hirai, M. Shimamura, S. Makabe, A. Koide, O. Kikuchi, T. Miyazaki, J. Koba, K. Yoshida, N. Sunamura, M. and Takai K. 2015. Hadal biosphere: insight into the microbial ecosystem in the deepest ocean on Earth. *Proc. Natl. Acad. Sci. U.S.A.*, 112(11):1230-1236.

O'Dowd. C.D. Facchini, M.C. Cavalli, F. Ceburnis, D. Mircea, M. Decesari, S. Fuzzi, S. Yoon Y.J. and Putaud, J.P. 2004. Biogenically driven organic contribution to marine aerosol. *Nature*, 431, 676-680.

Russell, L.M. Hawkins, L.N. Frossard, A.A. Quinn, P.K. and Bates, T.S. 2010. Carbohydrate-like composition of submicron atmospheric particles and their production from ocean bubble bursting. *Proc. Natl. Acad. Sci. U.S.A.*, 107(15):6652-6657.

Wilson, T.W. Ladino, L.A. Alpert, P.A. Breckels, M.N. Brooks, I.M. Browse, J. Burrows, S.M. Carslaw, K.S. Huffman, J.A. Judd, C., Kilthau, W.P. Mason, R.H. McFiggans, G. Miller, L.A. Nájera, J.J. Polishchuk, E. Rae, S. Schiller, C.L. Si, M. Temprado, J.V. Whale, T.F. Wong, J.P. Wurl, O. Yakobi-Hancock, J.D. Abbatt, J.P. Aller, J.Y. Bertram, A.K. Knopf, D.A. and Murray, B.J. 2015. A marine biogenic source of atmospheric ice-nucleating particles. *Nature*, 525(7568):234-8.

Speedy, R.J. and Angell, C.A. 1976. Isothermal compressibility of supercooled water and evidence for a thermodynamic singularity at -45°C. *Journal of Chemical Physics*, 65 (3), pp. 851-858.

3.12 Aerosol optical characteristics measured by ship-borne sky radiometer

(1) Personnel

Kazuma Aoki (University of Toyama) Principal Investigator / not onboard

Tadahiro Hayasaka (Tohoku University) Co-worker / not onboard

Sky radiometer operation was supported by Nippon Marine Enterprises, Ltd.

(2) Objective

Objective of this observation is to study distribution and optical characteristics of marine aerosols by using a ship-borne sky radiometer (POM-01 MK-III: PREDE Co. Ltd., Japan). Furthermore, collections of the data for calibration and validation to the remote sensing data were performed simultaneously.

(3) Parameters

- Aerosol optical thickness at five wavelengths (400, 500, 675, 870 and 1020 nm)
- Ångström exponent
- Single scattering albedo at five wavelengths
- Size distribution of volume (0.01 μm – 20 μm)
- # GPS provides the position with longitude and latitude and heading direction of the vessel, and azimuth and elevation angle of the sun. Horizon sensor provides rolling and pitching angles.

(4) Instruments and Methods

The sky radiometer measures the direct solar irradiance and the solar aureole radiance distribution with seven interference filters (0.315, 0.4, 0.5, 0.675, 0.87, 0.94, and 1.02 μm). Analysis of these data was performed by SKYRAD.pack version 4.2 developed by Nakajima *et al*. 1996.

(5) Data archives

Aerosol optical data are to be archived at University of Toyama (K.Aoki, SKYNET/SKY: http://skyrad.sci.u-toyama.ac.jp/) after the quality check and will be submitted to JAMSTEC.

3.13 C-band polarimetric Doppler weather radar

(1) Personnel

Masaki KATSUMATA	(JAMSTEC)	Principal Investigator
		(onboard Leg-1, not on board Leg-2, 3, 4)
Biao GENG	(JAMSTEC)	(not on board)
Soichiro SUEYOSHI	(NME)	(Leg-1)
Yutaro MURAKAMI	(NME)	(Leg-1, 2)
Wataru TOKUNAGA	(NME)	(Leg-2)
Koichi INAGAKI	(NME)	(Leg-2, 3)
Shinya OKUMURA	(NME)	(Leg-3)
Kazuho YOSHIDA	(NME)	(Leg-4)
Ryo KIMURA	(NME)	(Leg-3, 4)
Ryo KIMURA	(Mirai Crew)	(Leg-1)
Masanori MURAKAMI	(Mirai Crew)	(Leg-2, 3, 4)

(2) Objective

The objective of the radar observations in this cruise is to investigate structure and evolution of precipitating systems over the globe, especially those related to the south pacific convergence zone (SPCZ) and stratiform clouds over the Southern Ocean.

(3) Radar specifications

The C-band polarimetric weather Doppler radar on board the R/V Mirai is used. Basic specifications of the radar are as follows:

Frequency:	5370 MHz (C-band)
Polarimetry:	Horizontal and vertical
	(simultaneously transmitted and received)
Transmitter:	Solid-state transmitter
Pulse Configuration:	Using pulse-compression
Output Power:	6 kW (H) + 6 kW (V)
Antenna Diameter:	4 meter
Beam Width:	1.0 degrees
INU (Inertial Navigation Unit):	PHINS (IXBLUE S.A.S.)

(4) Available variables

Radar variables, which are converted from the power and phase of the backscattered signal at

vertically- and horizontally-polarized channels, are as follows:

Radar reflectivity:	Z
Doppler velocity:	Vr
Spectrum width of Doppler velocity:	SW
Differential reflectivity:	ZDR
Differential propagation phase:	ΦDP
Specific differential phase:	KDP
Co-polar correlation coefficients:	ρHV

(5) Operational methodology

The antenna is controlled to point the commanded ground-relative direction, by controlling the azimuth and elevation to cancel the ship attitude (roll, pitch and yaw) detected by the INU. The Doppler velocity is also corrected by subtracting the ship movement in beam direction.

For the maintenance, internal signals of the radar are checked and calibrated at the beginning and the end of the cruise. Meanwhile, the following parameters are checked daily; (1) frequency, (2) peak output power, (3) pulse width, and (4) PRF (pulse repetition frequency).

The operational mode of the radar during the cruise is shown in Tables 3.13-1. A dual PRF mode is used for a volume scan. For a RHI, vertical point, and surveillance PPI scans, a single PRF mode is used.

(6) Results

The Doppler radar observations were conducted all through the cruise, except over the EEZ without permission.

An example of the obtained data are shown in Fig. 3.13-1, for the case when synoptic-scale front passed over the vessel. The meridionally-elongated raining area can be seen in the reflectivity panel. The velocity panel indicates the northerly wind (along front-elongating direction), which can be estimated by strongest approaching (negative) Doppler velocity to the north, and vice versa. Perturbations in the Doppler velocity can be seen to be recognized as wind discontinuous line, wave structure, etc.
Detailed analyses of the obtained data will be performed after the cruise.

(7) Data archive

All data of the Doppler radar observations during this cruise will be submitted to the JAMSTEC Data Management Group (DMG).

Table 3.13-1 Operational mode of the radar

	Surveillance PPI Scan	Volume Scan						RHI Scan	Vertical Point Scan
Repeated Cycle (min.)	30	6						12	
Times in One Cycle	1	1						3	3
Pulse Width (long / short, in microsec)	200 / 2	64 / 1		32 / 1		32 / 1		32 / 1	32 / 1
Scan Speed (deg/sec)	18	18		24		36		9	36
PRF(s) (Hz)	400	dual PRF (ray alternative)						1250	2000
		667	833	938	1250	1333	2000		
Pulses / Ray	16	26	33	27	34	37	55	32	64
Ray Spacing (deg.)	0.7	0.7		0.7		1.0		0.2	1.0
Azimuth (deg)	Full Circle							Option	Full Circle
Bin Spacing (m)	150								
Max. Range (km)	300	150		100		60		100	60
Elevation Angle(s) (deg.)	0.5	0.5		1.0, 1.8, 2.6, 3.4, 4.2, 5.1, 6.2, 7.6, 9.7, 12.2, 15.2		18.7, 23.0, 27.9, 33.5, 40.0		0.0~ 60.0	90

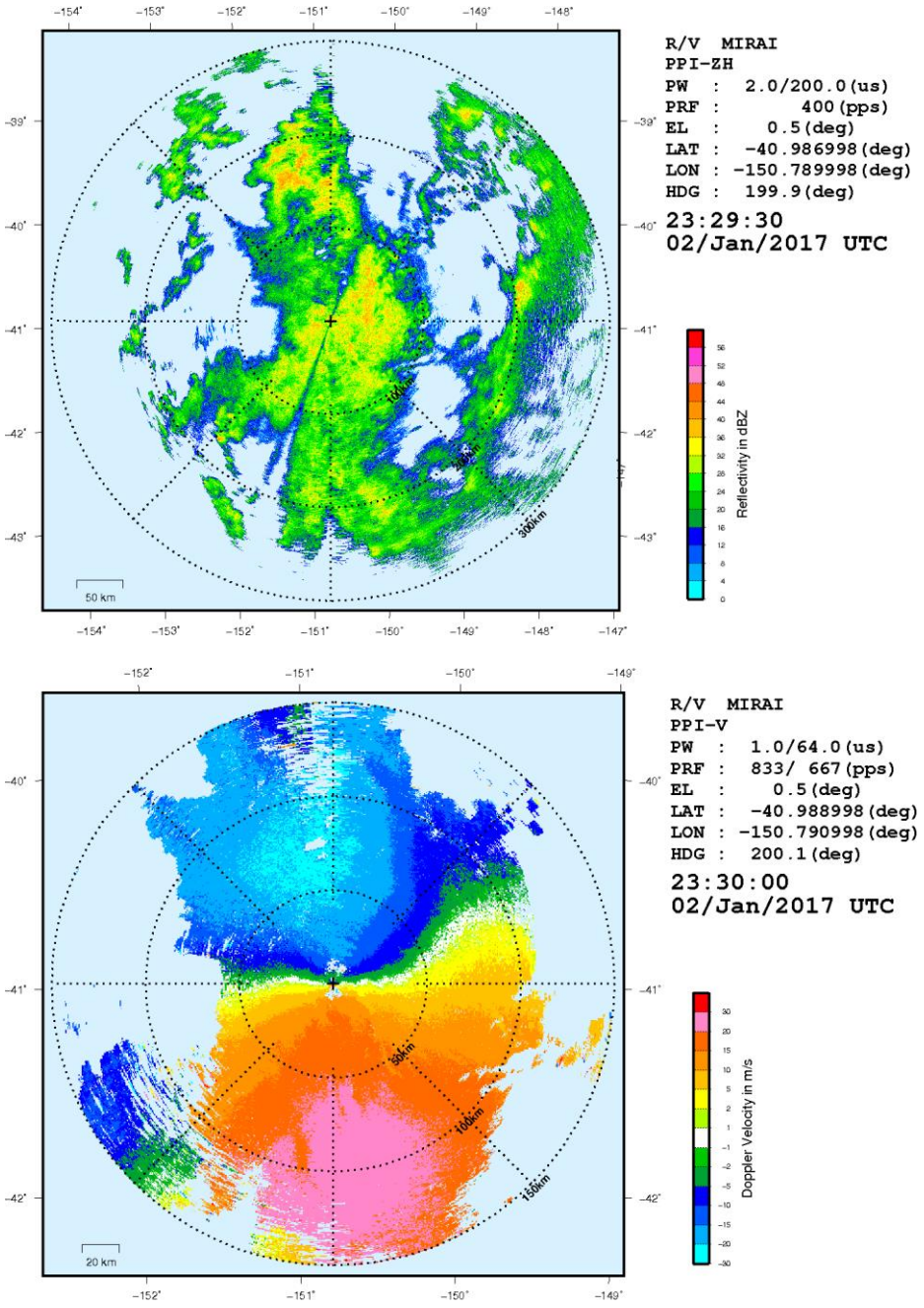

Figure 3.13-1. Example of the obtained data, obtained at 2330UTC Jan.02, 2017, when a synoptic-scale front passed over. Upper panel: Radar reflectivity at an elevation of 0.5 degrees, within 300 km radius. Lower panel: Doppler velocity at same elevation angle but within 150 km radius.

3.14 Lidar Observation

(1) Personal

Masaki KATSUMATA	(JAMSTEC)	Principal Investigator
		(onboard Leg-1, not on board Leg-2, 3)
Kyoko TANIGUCHI	(JAMSTEC)	(not on board)
Biao GENG	(JAMSTEC)	(not on board)

(2) Objective

To capture distributions of cloud, aerosol and water vapor in high temporal and special resolutions.

(3) Instrumentation

The lidar system on R/V Mirai transmits 10Hz pulse laser at 1064 nm, 532nm, and 355nm, and detects backscattered signals at the same wavelengths (Mie signal) continuously up to 21km height. The system splits signals at 532 nm and 355nm into parallel and perpendicular components. These Mie signals indicate vertical distribution of cloud and aerosol. The parallel and perpendicular components provide the depolarization ratio, an indicator of particle roundness. The combination of these parameters provides the information about the clouds and aerosols, including amounts and types.

The system also detects Raman signals at 387nm and 607nm for nitrogen and 660 nm for water vapor. The Raman signals indicate vertical distribution of nitrogen and water vapor molecules. The 660nm and 607nm signals share a 532nm laser as a light source. The ratio of the Raman signals is a proportion to the water vapor mixing ratio, a mass ratio of water vapor and dry air. The observations at 607nm and 660nm are only available at nighttime (from sunset to sunrise).

The system reserves a period of 23:56-00:00 UTC for daily maintenance. Instead of observations, the system obtains the background noise data for calibration. Necessary care such as observation window cleaning also take place in the period.

(4) Preliminary Results

The data were obtained continuously thru Leg-1, 2 and 3, except over the EEZs without permissions. The data will be examined after the cruise.

(5) Data Archive

All data obtained during this cruise will be submitted to the JAMSTEC Data Management Group (DMG).

(6) Acknowledgment

During Leg-2 and 3, the operations are supported by the on-board technical staff of Nippon Marine Enterprise Ltd.

3.15 Disdrometers

(1) Personnel

Masaki KATSUMATA	(JAMSTEC)	Principal Investigator
		(on board Leg-1 / not on board Leg-2, 3, 4)
Kyoko TANIGUCHI	(JAMSTEC)	(not on board)
Biao GENG	(JAMSTEC)	(not on board)

(2) Objectives

The disdrometer can continuously obtain size distribution of raindrops. The objective of this observation is (a) to reveal microphysical characteristics of the rainfall, depends on the type, temporal stage, etc. of the precipitating clouds, (b) to retrieve the coefficient to convert radar reflectivity to the rainfall amount, and (c) to validate the algorithms and the product of the satellite-borne precipitation radars; TRMM/PR and GPM/DPR.

(3) Parameters

Number and size of precipitating particles

(4) Methods

Three different types of disdrometers are utilized to obtain better reasonable and accurate value on the moving vessel. Two of them are installed in one place, the starboard side on the roof of the anti-rolling system of R/V Mirai, as in Fig. 3.15-1. The other one, named “micro rain radar”, is installed at the starboard side of the anti-rolling systems (see Fig. 3.15-2).

The details of the sensors are described below. All the sensors archive data every one minute.

Fig. 3.15-1: The two disdrometers (Parsivel and LPM),

Fig. 3.15-2: The micro rain radar, installed on

installed on the roof of the anti-rolling tank. the starboard side of the anti-rolling tank.

(4-1) Laser Precipitation Monitor (LPM) optical disdrometer

The "Laser Precipitation Monitor (LPM)" (Adolf Thies GmbH & Co) is an optical disdrometer. The instrument consists of the transmitter unit which emit the infrared laser, and the receiver unit which detects the intensity of the laser come thru the certain path length in the air. When a precipitating particle fall thru the laser, the received intensity of the laser is reduced. The receiver unit detect the magnitude and the duration of the reduction and then convert them onto particle size and fall speed. The sampling volume, i.e. the size of the laser beam "sheet", is 20 mm (W) x 228 mm (D) x 0.75 mm (H).
The number of particles are categorized by the detected size and fall speed and counted every minutes. The categories are shown in Table 3.15-1.

(4-2) "Parsivel" optical disdrometer

The "Parsivel" (OTT Hydromet GmbH) is another optical disdrometer. The principle is same as the LPM. The sampling volume, i.e. the size of the laser beam "sheet", is 30 mm (W) x 180 mm (D). The categories are shown in Table 3.15-2.

(4-3) Micro rain radar

The MRR-2 (METEK GmbH) was utilized. The specifications are in Table 3.15-3. The antenna unit was installed at the starboard side of the anti-rolling systems (see Fig. 3.15-2), and wired to the junction box and laptop PC inside the vessel.
The data was averaged and stored every one minute. The vertical profile of each parameter was obtained every 200 meters in range distance (i.e. height) up to 6200 meters, i.e. well beyond the melting layer. The drop size distribution is recorded, as well as radar reflectivity, path-integrated attenuation, rain rate, liquid water content and fall velocity.

(5) Preliminary Results

The data were obtained continuously thru the cruise, except over the EEZs without permissions. The result will be examined after the cruise.

(6) Data Archive

All data obtained during this cruise will be submitted to the JAMSTEC Data Management Group (DMG).

(7) Acknowledgment

The operations are supported by Japan Aerospace Exploration Agency (JAXA) Precipitation Measurement Mission (PMM). During Leg-2 and 3, the operations are supported by the on-board

technical staff of Nippon Marine Enterprise Ltd.

Table 3.15-1: Categories of the size and the fall speed for LPM.

Particle Size		
Class	Diameter [mm]	Class width [mm]
1	≥ 0.125	0.125
2	≥ 0.250	0.125
3	≥ 0.375	0.125
4	≥ 0.500	0.250
5	≥ 0.750	0.250
6	≥ 1.000	0.250
7	≥ 1.250	0.250
8	≥ 1.500	0.250
9	≥ 1.750	0.250
10	≥ 2.000	0.500
11	≥ 2.500	0.500
12	≥ 3.000	0.500
13	≥ 3.500	0.500
14	≥ 4.000	0.500
15	≥ 4.500	0.500
16	≥ 5.000	0.500
17	≥ 5.500	0.500
18	≥ 6.000	0.500
19	≥ 6.500	0.500
20	≥ 7.000	0.500
21	≥ 7.500	0.500
22	≥ 8.000	unlimited

Fall Speed		
Class	Speed [m/s]	Class width [m/s]
1	≥ 0.000	0.200
2	≥ 0.200	0.200
3	≥ 0.400	0.200
4	≥ 0.600	0.200
5	≥ 0.800	0.200
6	≥ 1.000	0.400
7	≥ 1.400	0.400
8	≥ 1.800	0.400
9	≥ 2.200	0.400
10	≥ 2.600	0.400
11	≥ 3.000	0.800
12	≥ 3.400	0.800
13	≥ 4.200	0.800
14	≥ 5.000	0.800
15	≥ 5.800	0.800
16	≥ 6.600	0.800
17	≥ 7.400	0.800
18	≥ 8.200	0.800
19	≥ 9.000	1.000
20	≥ 10.000	10.000

Table 3.15-2: Categories of the size and the fall speed for Parsivel.

Particle Size			Fall Speed		
Class	Average Diameter [mm]	Class spread [mm]	Class	Average Speed [m/s]	Class Spread [m/s]
1	0.062	0.125	1	0.050	0.100
2	0.187	0.125	2	0.150	0.100
3	0.312	0.125	3	0.250	0.100
4	0.437	0.125	4	0.350	0.100
5	0.562	0.125	5	0.450	0.100
6	0.687	0.125	6	0.550	0.100
7	0.812	0.125	7	0.650	0.100
8	0.937	0.125	8	0.750	0.100
9	1.062	0.125	9	0.850	0.100
10	1.187	0.125	10	0.950	0.100
11	1.375	0.250	11	1.100	0.200
12	1.625	0.250	12	1.300	0.200
13	1.875	0.250	13	1.500	0.200
14	2.125	0.250	14	1.700	0.200
15	2.375	0.250	15	1.900	0.200
16	2.750	0.500	16	2.200	0.400
17	3.250	0.500	17	2.600	0.400
18	3.750	0.500	18	3.000	0.400
19	4.250	0.500	19	3.400	0.400
20	4.750	0.500	20	3.800	0.400
21	5.500	1.000	21	4.400	0.800
22	6.500	1.000	22	5.200	0.800
23	7.500	1.000	23	6.000	0.800
24	8.500	1.000	24	6.800	0.800
25	9.500	1.000	25	7.600	0.800
26	11.000	2.000	26	8.800	1.600
27	13.000	2.000	27	10.400	1.600
28	15.000	2.000	28	12.000	1.600
29	17.000	2.000	29	13.600	1.600
30	19.000	2.000	30	15.200	1.600
31	21.500	3.000	31	17.600	3.200

32	24.500	3.000		32	20.800	3.200

Table 3.15-3: Specifications of the MRR-2.

Transmitter power	50 mW
Operating mode	FM-CW
Frequency	24.230 GHz (modulation 1.5 to 15 MHz)
3dB beam width	1.5 degrees
Spurious emission	< -80 dBm / MHz
Antenna Diameter	600 mm
Gain	40.1 dBi

3.16 GNSS precipitable water

(1) Personnel

Masaki KATSUMATA	(JAMSTEC)	Principal Investigator (not on board)
Mikiko FUJITA	(JAMSTEC)	(not on board)
Kyoko TANIGUCHI	(JAMSTEC)	(not on board)

(2) Objective

Recording the GNSS satellite data to estimate the total column integrated water vapor content of the atmosphere.

(3) Method

The GNSS satellite data was archived to the receiver (Trimble NetR9) with 5 sec interval. The GNSS antenna (Margrin) was set on the roof of radar operation room. The observations were carried out all thru the cruise.

(4) Results

We will calculate the total column integrated water from observed GNSS satellite data after the cruise.

(5) Data archive

Raw data is recorded as T02 format and stream data every 5 seconds. These raw datasets are available from Mikiko Fujita of JAMSTEC. Corrected data will be submitted to JAMSTEC Marine-Earth Data and Information Department and will be archived there.

3.17 Ship-borne Measurement of Aerosols

(1) Personnel

Fumikazu Taketani	JAMSTEC	- PI, not on board
Yugo Kanaya	JAMSTEC	- not on board
Takuma Miyakawa	JAMSTEC	- on board (Leg 3)
Hisahiro Takashima	JAMSTEC/Fukuoka Univ.	- not on board
Yutaka Tobo	NIPR	- not on board
Yuichi Komazaki	JAMSTEC	- not on board
Hitoshi Matsui	Nagoya Univ.	- not on board
Momoka Yoshizue	Tokyo Univ. of Sci.	- on board (Leg 3)

(2) Objectives

• To investigate roles of maritime aerosol particles in climate change through indirect effect (i.e., aerosol-cloud interaction).

• To investigate processes of biogeochemical cycles between the atmosphere and sea surface, such as sea spraying process.

(3) Parameters

• Particle size distributions

• Black carbon(BC) and fluorescent aerosol particle number concentrations

• Airborne bacteria concentrations

• Ice nucleation activity of aerosol particles

• Chemical composition of ambient particles

• Chemical composition of rain water

• Aerosol extinction coefficient (AEC)

• Surface carbon monoxide (CO) and ozone(O_3) mixing ratios

(4) Instruments and methods

(4-1) Continuous or temporal aerosol observations:

(4-1-1) Particle size distributions

The size-resolved number concentration of particles was measured by a scanning mobility particle sizer (SMPS) (comprising a 3080 Electrostatic Classifier with 3081 differential mobility analyzer (DMA), a condensation particle counter (CPC) (model 3010, TSI)), and a handheld optical particle counter (OPC) (KR-12A, RION). We temporally operated the OPC at the time of air sampling on the compass deck (see below for details).

(4-1-2) Black carbon (BC)

Size-resolved number and mass BC concentrations were measured by an instrument based on laser-induced incandescence, single particle soot photometer (SP2) (model D, Droplet Measurement Technologies). The laser-induced incandescence technique based on intra-cavity Nd:YVO4 laser operating at 1064 nm were used for detection of single particles of BC.

(4-1-3) Fluorescence measurements of airborne particles

Fluorescent properties of aerosol particles were measured by a single particle fluorescence sensor, Waveband Integrated bioaerosol sensor (WIBS4) (WIBS-4A, Droplet Measurement Technologies). Two pulsed xenon lamps emitting UV light (280 nm and 370 nm) were used for excitation. Fluorescence emitted from a single particle within 310–400 nm and 420–650 nm wavelength bands was detected by photomultiplier tubes (PMT) with the bandpass filters.

The ambient air was commonly sampled from the rooftop of the environmental research room through a 3-m-long conductive silicone tube to the SP2, SMPS, and WIBS4, and was dehumidified using a Nafion aerosol particle dryer to eliminate liquid water contents of airborne particles (typical relative humidity < 15%). They finally were introduced to those instruments installed in the environmental research room. The OPC instrument was temporally placed on the compass deck at the time to collect the particles for the electron microscopic analyses.

(4-2) Aerosol sampling on various types of media

Ambient air samplings were carried out using air samplers on the compass deck. Aerosol particles were collected on the quartz fiber (QF) filter (ϕ = 110 mm) and pre-washed nuclepore membrane filter (ϕ = 47 mm) along cruise track using a high-volume air sampler (HVS, HV-525PM, SIBATA, 500 L/min) and a handmade air sampler (10 L/min) to analyze their composition and ice nuclei ability, respectively. In addition to those samplers, a cascade impactor, which has 5 stages for the size separation, was operated at the flow rate of 9 L/min on the compass deck to investigate the size-resolved chemical compositions. For this sampler, QF filters (ϕ = 25 mm) were used for the collection. To avoid collecting particles derived from the research vessel exhaust, the sampling period was controlled automatically by using a "wind-direction selection system". These sampling logs are listed in Tables 3.17-1~3.17-3.

Electron microscopic analyses, including Scanning Election Microscopy (SEM) and Transmission Electron Microscopy (TEM), are performed in order to investigate the morphology and physicochemical properties of aerosol particles. For these purposes, aerosol particles were collected on a Silicon wafer or TEM grids (quantifoil or formvar) using air samplers as follows.

MPS-3 (California Measurements) for SEM

MPS (EcoMesure) for TEM

Kl-1L (PIXE INTERNATIONAL) for TEM

Sampling was performed on the compass deck for 10 min. These samplings are summarized in Tables 3.17-4. All samples will be analyzed using SEM or TEM placed in a laboratory of JAMSTEC or TUS.

Automated counting of autofluorescent and epifluorescent particles were performed using a Bioplorer (Koyo Sangyo). Aerosol particles were collected on the gold-coated membrane filters using a custom-made sampler at typical flow rate of 0.9-1.0 L/min for 2-3 hrs. The collected aerosol particles were analyzed using the Bioplorer immediately after the sampling. The number concentrations of airborne bacteria was calculated by dividing the counted bacteria on a filter by total sampling volume of air. The samples collected were summarized in Table 3.17-5.

(4-3) MAX-DOAS

Multi-Axis Differential Optical Absorption Spectroscopy (MAX-DOAS), a passive remote sensing technique measuring spectra of scattered visible and ultraviolet (UV) solar radiation, was used for atmospheric aerosol and gas profile measurements. Our MAX-DOAS instrument consists of two main parts: an outdoor telescope unit and an indoor spectrometer (Acton SP-2358 with Princeton Instruments PIXIS-400B), connected to each other by a 14-m bundle optical fiber cable. The line of sight was in the directions of the portside of the vessel and the scanned elevation angles were 1.5, 3, 5, 10, 20, 30, 90 degrees in the 30-min cycle. The roll motion of the ship was measured to autonomously compensate additional motion of the prism, employed for scanning the elevation angle.

For the selected spectra recorded with elevation angles with good accuracy, DOAS spectral fitting was performed to quantify the slant column density (SCD) of NO_2 (and other gases) and O_4 (O_2-O_2, collision complex of oxygen) for each elevation angle. Then, the O_4 SCDs were converted to the aerosol optical depth (AOD) and the vertical profile of aerosol extinction coefficient (AEC) using an optimal estimation inversion method with a radiative transfer model. The tropospheric vertical column/profile of NO_2 and other gases were retrieved using derived aerosol profiles.

(4-4) CO and O_3

Ambient air was continuously sampled on the compass deck and drawn through ~20-m-long Teflon tubes connected to a gas filter correlation CO analyzer (Model 48C, Thermo Fisher Scientific) and a UV photometric ozone analyzer (Model 49C, Thermo Fisher Scientific), located in the Research Information Center. The data will be used for characterizing air mass origins.

(4-5) Rain sampling

Rain samples were collected using a rain sampler. These samples were analyzed to investigate the chemical composition of rain water over Southern Ocean and south Pacific region. These sampling logs are listed in Tables 3.17-6.

(5) Station list or Observation log

Air samplings during MR16-09-leg3 were summarized as follows.

Table 3.17-1: High-volume air sampling for aerosol composition analyses

ID	Date and Time					Latitude (deg, min, N/S)			Longitude (deg, min, E/W)		
MR1609-H-S1	2017	02	11	12:40	UTC	60	59	S	77	55	W
MR1609-H-S2	2017	02	13	15:07	UTC	64	39	S	98	45	W
MR1609-H-S3	2017	02	15	16:31	UTC	66	40	S	121	41	W
MR1609-H-S4	2017	02	16	2:50	UTC	67	00	S	126	00	W
MR1609-H-S5	2017	02	19	20:15	UTC	60	29	S	126	00	W
MR1609-H-S6	2017	02	23	0:00	UTC	53	01	S	126	00	W
MR1609-H-S7	2017	02	25	17:40	UTC	51	18	S	143	45	W
MR1609-H-S8	2017	02	28	1:00	UTC	46	54	S	158	25	W

Table 3.17-2: Low-volume air sampling for the size-resolved aerosol composition analyses

ID	Date and Time					Latitude (deg, min, N/S)			Longitude (deg, min, E/W)		
MR1609-S-1	2017	02	11	12:40	UTC	60	59	S	77	55	W
MR1609-S-2	2017	02	15	16:31	UTC	66	41	S	121	40	W
MR1609-S-3	2017	02	16	2:50	UTC	67	00	S	126	00	W
MR1609-S-4	2017	02	23	0:00	UTC	53	01	S	126	00	W

Table 3.17-3: Low-volume air sampling for airborne ice nuclei analysis

ID	Date and Time					Latitude (deg, min, N/S)			Longitude (deg, min, E/W)		
MR1609-IN-001	2017	02	11	12:40	UTC	60	59	S	77	55	W
MR1609-IN-002	2017	02	13	15:07	UTC	64	39	S	98	45	W
MR1609-IN-003	2017	02	15	16:31	UTC	66	40	S	125	5	W
MR1609-IN-004	2017	02	16	2:50	UTC	67	00	S	126	00	W
MR1609-IN-005	2017	02	18	4:50	UTC	62	59	S	125	59	W
MR1609-IN-006	2017	02	20	23:55	UTC	57	49	S	126	00	W
MR1609-IN-007	2017	02	23	0:00	UTC	53	01	S	126	00	W
MR1609-IN-008	2017	02	24	20:45	UTC	52	14	S	137	17	W
MR1609-IN-009	2017	02	27	17:12	UTC	47	44	S	156	37	W
MR1609-IN-010	2017	03	01	2:10	UTC	44	36	S	163	44	W

Table 3.17-4: Aerosol sampling for electron microscope analyses

ID	Date and Time					Latitude (deg, min, N/S)			Longitude (deg, min, E/W)		
MR1609-SEM-01	2017	02	11	12:35	UTC	60	59	S	77	57	W
MR1609-SEM-02	2017	02	12	13:02	UTC	63	16	S	87	02	W
MR1609-SEM-03	2017	02	13	17:14	UTC	64	45	S	99	46	W
MR1609-SEM-04	2017	02	14	15:21	UTC	65	38	S	109	45	W
MR1609-SEM-05	2017	02	15	16:27	UTC	66	41	S	121	38	W
MR1609-SEM-06	2017	02	16	14:10	UTC	66	21	S	126	03	W
MR1609-SEM-07	2017	02	17	12:00	UTC	64	21	S	126	02	W
MR1609-SEM-08	2017	02	18	23:15	UTC	62	23	S	126	06	W
MR1609-SEM-09	2017	02	19	17:30	UTC	60	29	S	125	59	W
MR1609-SEM-10	2017	02	20	14:43	UTC	58	30	S	125	59	W
MR1609-SEM-11	2017	02	21	18:45	UTC	55	30	S	125	59	W
MR1609-SEM-12	2017	02	22	16:05	UTC	53	30	S	126	01	W
MR1609-SEM-13	2017	02	24	16:35	UTC	52	24	S	135	56	W
MR1609-SEM-14	2017	02	26	0:09	UTC	50	55	S	145	51	W
MR1609-SEM-15	2017	02	26	2:42	UTC	50	45	S	146	41	W
MR1609-SEM-16	2017	02	26	19:20	UTC	49	33	S	151	44	W
MR1609-SEM-17	2017	02	27	1:12	UTC	49	6.7	S	153	21	W
MR1609-SEM-18	2017	02	27	19:07	UTC	47	31	S	157	20	W
MR1609-SEM-19	2017	03	02	2:10	UTC	42	20	S	169	20	W
MR1609-T-01	2017	02	11	19:45	UTC	61	47	S	80	29	W
MR1609-T-02	2017	02	12	20:43	UTC	63	56	S	90	12	W
MR1609-T-03	2017	02	13	23:57	UTC	65	2	S	102	52	W
MR1609-T-04	2017	02	14	23:52	UTC	65	59	S	113	41	W
MR1609-T-05	2017	02	15	0:12	UTC	66	56	S	125	18	W
MR1609-T-06	2017	02	16	21:28	UTC	65	40	S	125	58	W
MR1609-T-07	2017	02	17	18:20	UTC	63	41	S	126	00	W
MR1609-T-08	2017	02	18	23:28	UTC	62	20	S	126	06	W
MR1609-T-09	2017	02	19	23:19	UTC	60	01	S	125	58	W
MR1609-T-10	2017	02	20	19:45	UTC	58	00	S	126	00	W
MR1609-T-11	2017	02	21	18:57	UTC	53	31	S	125	59	W
MR1609-T-12	2017	02	25	0:10	UTC	52	05	S	138	25	W
MR1609-T-13	2017	02	26	2:30	UTC	50	45	S	146	37	W
MR1609-T-14	2017	02	26	17:24	UTC	49	41	S	151	13	W
MR1609-T-15	2017	02	27	17:23	UTC	47	42	S	157	01	W
MR1609-T-16	2017	03	01	18:35	UTC	43	4	S	167	31	W
MR1609-Nit-01	2017	02	11	12:37	UTC	61	01	S	77	60	W
MR1609-Nit-02	2017	02	11	19:45	UTC	61	48	S	81	32	W
MR1609-Nit-03	2017	02	12	20:43	UTC	63	57	S	90	20	W
MR1609-Nit-04	2017	02	14	23:57	UTC	65	03	S	102	59	W
MR1609-Nit-05	2017	02	14	15:21	UTC	65	40	S	109	52	W
MR1609-Nit-06	2017	02	14	22:52	UTC	65	57	S	113	21	W
MR1609-Nit-07	2017	02	15	16:21	UTC	66	41	S	121	43	W
MR1609-Nit-08	2017	02	16	0:11	UTC	66	56	S	125	24	W
MR1609-Nit-09	2017	02	16	14:10	UTC	66	20	S	126	3	W
MR1609-Nit-10	2017	02	16	23:25	UTC	65	39	S	125	57	W
MR1609-Nit-11	2017	02	17	12:15	UTC	64	21	S	126	2	W
MR1609-Nit-12	2017	02	18	20:40	UTC	62	20	S	126	7	W
MR1609-Nit-13	2017	02	19	17:33	UTC	60	29	S	125	60	W
MR1609-Nit-14	2017	02	20	0:01	UTC	60	01	S	125	59	W
MR1609-Nit-15	2017	02	20	14:50	UTC	58	30	S	125	60	W
MR1609-Nit-16	2017	02	20	23:41	UTC	57	49	S	125	60	W
MR1609-Nit-17	2017	02	21	18:45	UTC	55	30	S	125	60	W
MR1609-Nit-18	2017	02	22	0:10	UTC	55	01	S	125	59	W
MR1609-Nit-19	2017	02	22	16:10	UTC	53	30	S	126	1	W
MR1609-Nit-20	2017	02	22	23:40	UTC	53	01	S	126	0	W
MR1609-Nit-21	2017	02	24	16:35	UTC	52	23	S	136	0	W
MR1609-Nit-22	2017	02	25	0:10	UTC	52	05	S	138	29	W
MR1609-Nit-23	2017	02	26	0:09	UTC	50	54	S	145	56	W
MR1609-Nit-24	2017	02	26	17:24	UTC	49	40	S	151	17	W
MR1609-Nit-25	2017	02	27	0:54	UTC	49	07	S	153	20	W
MR1609-Nit-26	2017	02	27	17:24	UTC	47	41	S	157	2	W
MR1609-Nit-27	2017	02	28	1:58	UTC	46	52	S	158	27	W
MR1609-Nit-28	2017	02	28	18:23	UTC	45	17	S	161	59	W
MR1609-Nit-29	2017	03	01	1:57	UTC	44	36	S	163	46	W
MR1609-Nit-30	2017	03	01	18:35	UTC	43	03	S	167	34	W
MR1609-Nit-31	2017	03	02	2:10	UTC	42	18	S	169	25	W
MR1609-Nit-32	2017	03	02	18:30	UTC	40	29	S	173	46	W

*MR1609-SEM-## and MR1609-T-## samples were collected by JAMSTEC

*MR1609-Nit-## samples were collected by TUS

Table 3.17-5: Air sampling for automated counting of airborne bacteria

ID	Date and Time					Latitude (deg, min, N/S)			Longitude (deg, min, E/W)		
MR1609-B-air01	2017	02	11	12:37	UTC	60	59	S	77	54	W
MR1609-B-air02	2017	02	12	13:02	UTC	63	16	S	87	02	W
MR1609-B-air03	2017	02	13	17:16	UTC	64	45	S	99	47	W
MR1609-B-air04	2017	02	13	20:17	UTC	64	54	S	101	11	W
MR1609-B-air05	2017	02	14	15:21	UTC	65	38	S	109	45	W
MR1609-B-air06	2017	02	14	18:13	UTC	65	48	S	111	7	W
MR1609-B-air07	2017	02	14	20:15	UTC	65	54	S	112	5	W
MR1609-B-air08	2017	02	15	16:28	UTC	66	41	S	121	39	W
MR1609-B-air09	2017	02	15	19:00	UTC	66	42	S	122	49	W
MR1609-B-air10	2017	02	16	2:54	UTC	67	00	S	126	00	W
MR1609-B-air11	2017	02	16	14:10	UTC	66	21	S	126	3	W
MR1609-B-air12	2017	02	16	21:29	UTC	65	38	S	125	59	W
MR1609-B-air13	2017	02	17	12:00	UTC	64	21	S	126	2	W
MR1609-B-air14	2017	02	17	18:23	UTC	63	41	S	126	00	W
MR1609-B-air15	2017	02	18	1:00	UTC	63	1	S	126	1	W
MR1609-B-air16	2017	02	18	18:37	UTC	62	20	S	126	6	W
MR1609-B-air17	2017	02	19	17:35	UTC	60	29	S	125	59	W
MR1609-B-air18	2017	02	19	23:20	UTC	60	7	S	125	58	W
MR1609-B-air19	2017	02	20	14:30	UTC	58	29	S	125	59	W
MR1609-B-air20	2017	02	20	19:47	UTC	58	00	S	126	00	W
MR1609-B-air21	2017	02	21	18:50	UTC	55	31	S	125	59	W
MR1609-B-air22	2017	02	22	16:05	UTC	53	30	S	126	2	W
MR1609-B-air23	2017	02	24	16:35	UTC	52	24	S	135	56	W
MR1609-B-air24	2017	02	25	0:10	UTC	52	05	S	138	25	W
MR1609-B-air25	2017	02	26	0:30	UTC	50	45	S	146	37	W
MR1609-B-air26	2017	02	26	17:26	UTC	49	41	S	151	13	W
MR1609-B-air27	2017	02	27	0:55	UTC	49	8	S	153	17	W
MR1609-B-air28	2017	02	27	17:19	UTC	47	43	S	156	59	W
MR1609-B-air29	2017	03	01	2:10	UTC	44	36	S	163	44	W
MR1609-B-air30	2017	03	02	2:17	UTC	42	19	S	169	22	W

Table 3.17-6: Rain sampling for chemical composition analysis

ID	Date and Time					Latitude (deg, min, N/S)			Longitude (deg, min, E/W)		
MR1609-Leg3-rain-001-冷凍	2017	02	11	12:45	UTC	61	01	S	77	60	W
MR1609-Leg3-rain-001-冷蔵	2017	02	11	12:45	UTC	61	01	S	77	60	W
MR1609-Leg3-rain-002-冷凍	2017	02	12	20:45	UTC	63	57	S	90	20	W
MR1609-Leg3-rain-003-冷凍	2017	02	15	16:30	UTC	66	41	S	121	43	W
MR1609-Leg3-rain-003-冷蔵	2017	02	15	16:30	UTC	66	41	S	121	43	W
MR1609-Leg3-rain-004-冷凍	2017	02	16	23:30	UTC	65	39	S	125	57	W
MR1609-Leg3-rain-005-冷凍	2017	02	18	0:27	UTC	63	06	S	126	1	W
MR1609-Leg3-rain-006-冷凍	2017	02	18	23:25	UTC	62	20	S	126	7	W
MR1609-Leg3-rain-007-冷凍	2017	02	20	23:59	UTC	57	48	S	125	60	W
MR1609-Leg3-rain-008-冷凍	2017	02	22	0:27	UTC	55	01	S	125	59	W
MR1609-Leg3-rain-009-冷凍	2017	02	23	0:03	UTC	53	02	S	126	0	W
MR1609-Leg3-rain-009-冷蔵	2017	02	23	0:03	UTC	53	02	S	126	0	W
MR1609-Leg3-rain-010-冷凍	2017	02	24	16:54	UTC	52	23	S	136	1	W
MR1609-Leg3-rain-010-冷蔵	2017	02	24	16:54	UTC	52	23	S	136	1	W
MR1609-Leg3-rain-011-冷凍	2017	02	25	0:29	UTC	52	05	S	138	30	W
MR1609-Leg3-rain-012-冷凍	2017	02	27	17:44	UTC	47	40	S	157	4	W
MR1609-Leg3-rain-012-冷蔵	2017	02	27	17:44	UTC	47	40	S	157	4	W
MR1609-Leg3-rain-013-冷凍	2017	02	28	18:38	UTC	45	18	S	161	58	W
MR1609-Leg3-rain-013-冷蔵	2017	02	28	18:38	UTC	45	18	S	161	58	W
MR1609-Leg3-rain-014-冷凍	2017	03	02	18:43	UTC	40	29	S	173	45	W
MR1609-Leg3-rain-014-冷蔵	2017	03	02	18:43	UTC	40	29	S	173	45	W

(6) Preliminary results

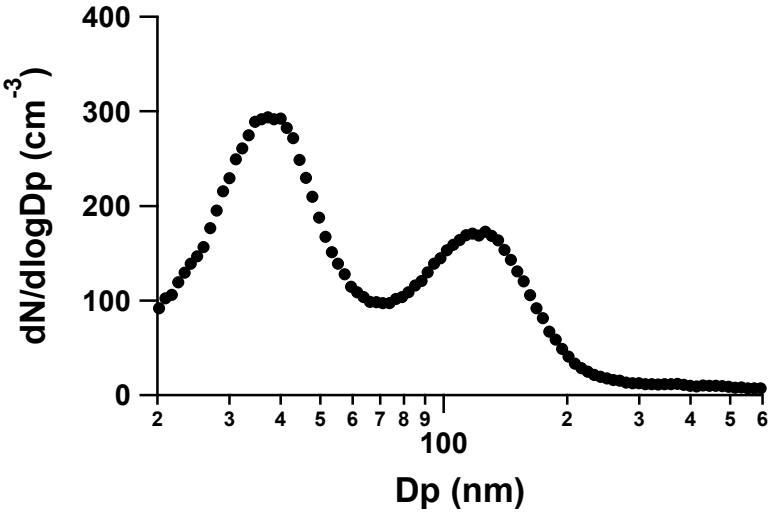

Figure 3.17-1: Average particle size distribution for Feb 11 – 28, 2017. (X axis is Particle diameter in nm; Y axis is the number concentration normalized by size-bin width)

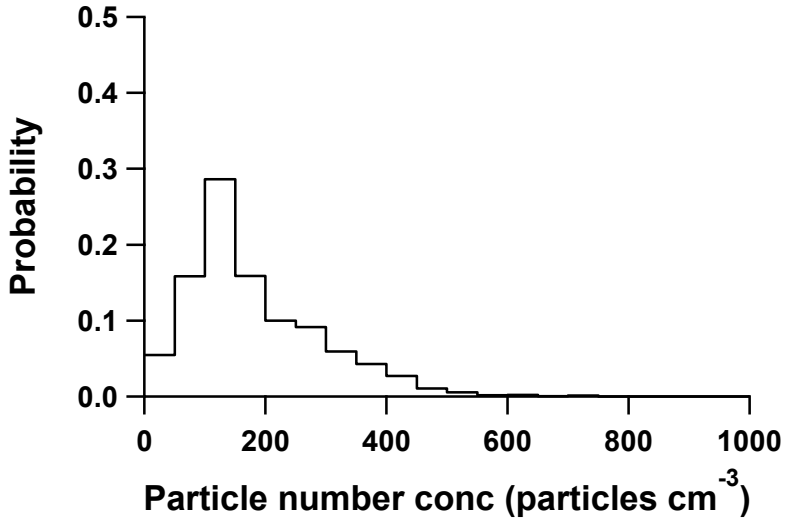

Figure 3.17-2: Histogram of total particle number concentration for Feb 11- 28, 2017.

(7) Data archives

These data obtained in this cruise will be submitted to the Data Management Group of JAMSTEC, and will be opened to the public via "Data Research System for Whole Cruise Information in JAMSTEC (DARWIN)" in JAMSTEC web site.

<http://www.godac.jamstec.go.jp/darwin/e>

3.18 Underway C_T

(1) Personnel

Akihiko Murata (JAMSTEC)

Tomonori Watai (MWJ)

Atsushi Ono (MWJ)

Emi Deguchi (MWJ)

Nagisa Fujiki (MWJ)

(2) Objective

It is doubtless that the ocean moderates global warming by absorbing ~30% of anthropogenic CO_2 emitted into the atmosphere. However, increases of anthropogenic CO_2 in the ocean cause another CO_2 problem called as ocean acidification. Since it is predicted that ocean acidification gives a large influence on ocean biology, especially on calcifying organisms, it is an important task to evaluate progression of ocean acidification.

In the leg 3 of MR16-09 cruise, we measured underway dissolved inorganic carbon (C_T) in the surface seawater continuously along the cruise track. The data for C_T are used to calculate saturation state of calcium carbonate (Ω), which is one of good indicators of ocean acidification, together with data for underway pCO_2 (section 3.7)

(3) Apparatus

Measurement of C_T was made with automated TCO_2 analyzer (Nippon ANS, Inc., Japan). The system comprises of a seawater dispensing system, a CO_2 extraction system and a coulometer (Model 3000A, Nippon ANS, Inc., Japan). Specification of the system is as follows:

Seawater collected from the seawater inlet at 4.5 m deep is transferred into a DURAN® glass bottle of nominal 250 ml after overflowing seawater of 3 time volume of the bottle. The seawater sample is kept at 20°C by a constant temperature bath until measurement. Then the seawater sample is dispensed from the glass bottle into a pipette of about 15 ml volume. The pipette is also kept at 20 °C by a water jacket, in which water from a water bath set at 20°C is circulated. CO_2 dissolved in a seawater sample is extracted in a stripping chamber of the CO_2 extraction system by adding phosphoric acid (~ 10 % v/v) of about 2 ml. The stripping chamber is approx. 25 cm long and has a fine frit at the bottom. The acid is added to the stripping chamber from the bottom of the chamber by pressurizing an acid bottle for a given time to push out the right amount of acid. The pressurizing is made with nitrogen gas (99.9999 %). After the acid is transferred to the stripping chamber, a seawater sample kept in a pipette is introduced to the stripping chamber by the same method as in adding an acid. The seawater reacted with phosphoric acid is stripped of CO_2 by bubbling the nitrogen gas through a fine frit at the bottom of the stripping chamber. The CO_2

stripped in the chamber is carried by the nitrogen gas (flow rates is 140 ml min^{-1}) to the coulometer through a dehydrating module. The module consists of two electric dehumidifiers (kept at ~4°C) and a chemical desiccant ($Mg(ClO_4)_2$).

The measurement sequence such as 1.5% CO_2 gas in N_2 base, system blank (phosphoric acid blank), seawater samples (6) is repeated automatically by PC control.

(4) Results

Concentrations of C_T in surface seawater along the cruise track are shown in Fig. 3.18.1, together with (a) salinity and (b) SST.

(a)

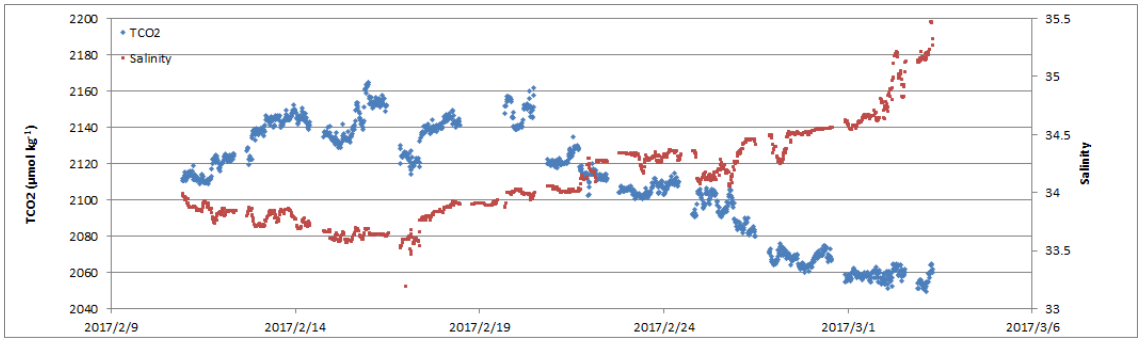

(b)

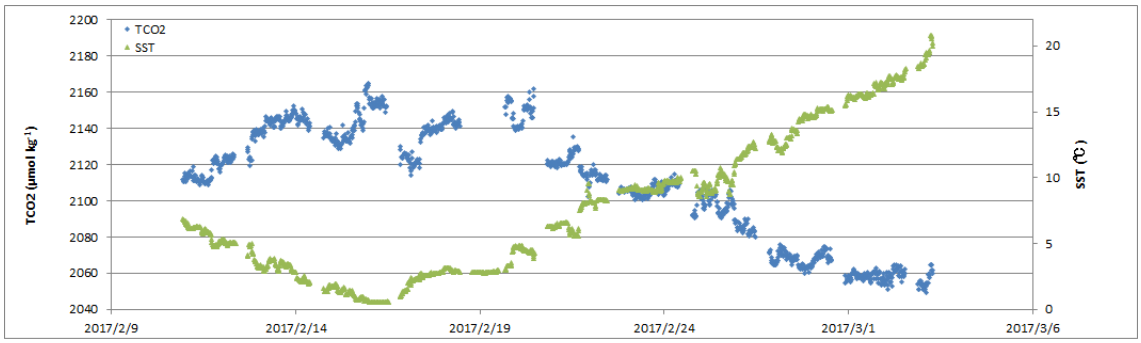

Fig. 3.18.1. Preliminary results of concentrations of C_T in surface seawater (blue), salinity (red), and SST (green) observed during the leg 3 of MR16-09.

3.19 XCTD

March 3, 2017

(1) Personnel

Hiroshi Uchida (JAMSTEC)

Shinya Okumura (NME)

Koichi Inagaki (NME)

Ryo Kimura (NME)

Masanori Murakami (Mirai crew)

(2) Objectives

XCTD (eXpendable Conductivity, Temperature and Depth profiler) measurements were carried out to substitute CTD casts and to evaluate the fall rate equation and the thermal bias by comparing with CTD (Conductivity, Temperature and Depth profiler) measurements.

(3) Instrument and Method

The XCTD used was XCTD-4 (Tsurumi-Seiki Co., Ltd., Yokohama, Kanagawa, Japan) with an MK-150N deck unit (Tsurumi-Seiki Co., Ltd.). The manufacturer's specifications are listed in Table 3.19.1. In this cruise, the XCTD probes were deployed by using 8-loading automatic launcher (Tsurumi-Seiki Co., Ltd.) or a hand launcher (stn. ****). For comparison with CTD, XCTD was deployed at about 10 minutes after the beginning of the down cast of the CTD (P17E_8, 16, 22 and 23). For correction of the sound velocity profile used in the bathymetry observation, XCTD-1 was deployed near station P17E_1. Also, two XCTD-4 were deployed at CO_2 buoy deployment locations at longitude of 140°W and 160°W.

The fall-rate equation provided by the manufacturer was initially used to infer depth Z (m), $Z = at - bt^2$, where t is the elapsed time in seconds from probe entry into the water, and a (terminal velocity) and b (acceleration) are the empirical coefficients (Table 3.19.2).

(4) Data Processing and Quality Control

The XCTD data were processed and quality controlled based on a method by Uchida et al. (2011). Differences between XCTD and CTD depths were shown in Fig. 3.19.1. The terminal velocity error was estimated for the XCTD-4 (Table 3.19.2). The XCTD-4 data were corrected for the depth error by using the estimated terminal velocities. Differences of temperature on pressure surfaces were examined by using side-by-side XCTD and CTD data (Fig. 3.19.3). Average thermal bias below 900 dbar was 0.014 °C. The XCTD data were corrected for the thermal bias. Differences of salinity on reference temperature surfaces were examined by using CTD data (Fig. 3.19.4). The XCTD data were corrected for the

estimated salinity bias.

(5) Results

Temperature-salinity plot using the quality controlled XCTD data is shown in Fig. 3.19.3.

(6) References

Kizu, S., H. Onishi, T. Suga, K. Hanawa, T. Watanabe, and H. Iwamiya (2008): Evaluation of the fall rates of the present and developmental XCTDs. *Deep-Sea Res I*, **55**, 571–586.

Uchida, H., K. Shimada, and T. Kawano (2011): A method for data processing to obtain high-quality XCTD data. *J. Atmos. Oceanic Technol.*, **28**, 816–826.

Uchida, H., A. Murata, and T. Doi (eds.) (2014): WHP P10 Revisit in 2011 Data Book, 179 pp., JAMSTEC.

Uchida, H., K. Katsumata, and T. Doi (eds.) (2015): WHP P14S/S04I Revisit in 2012/2013 Data Book, 187 pp., JAMSTEC.

Uchida, H and T. Doi (eds.) (2016): WHP P01 Revisit in 2014 Data Book, 149 pp., JAMSTEC, ISBN 978-4-901833-22-6.

Table 3.19.1. Manufacturer's specifications of XCTD-4.

Parameter	Range	Accuracy
Conductivity	0 ~ 60 mS cm^{-1}	±0.03 mS cm^{-1}
Temperature	–2 ~ 35 °C	±0.02 °C
Depth	0 ~ 1850 m	5 m or 2%, whichever is greater *

* Depth error is shown in Kizu et al (2008).

Table 3.19.2. Manufacturer's coefficients for the fall-rate equation.

Model	*a* (terminal velocity, m/s)	*b* (acceleration, m/s^2)	*e* (terminal velocity error, m/s)
XCTD-4	3.68081	0.00047	–0.0197

Table 3.19.3. Thermal biases of the XCTD temperature data.

Cruise	Average thermal bias (°C)	Depth range	Source
MR09-01	0.016	>= 1100 dbar	Uchida et al. (2011)
KH-02-3	0.019	>= 1100 dbar	Uchida et al. (2011)
MR11-08	0.014	>= 1100 dbar	Uchida et al. (2014)
MR12-05	0.009	>= 400 dbar	Uchida et al. (2015)
MR14-04	0.011	>= 900 dbar	Uchida et al. (2016)
MR15-05	–0.003	>= 900 dbar	Cruise report of MR15-05
MR16-09	0.014	>= 900 dbar	this report
Mean	0.011 ± 0.007		

Table 3.19.4. Salinity biases of the XCTD data.

XCTD station	Salinity bias	Reference temperature (°C)	Reference salinity	Reference CTD stations
8	–0.007	1.7	34.7306	7, 8, 9
22	0.008	2.4	34.6366	22, 23
23	0.017	2.4	34.6366	22, 23

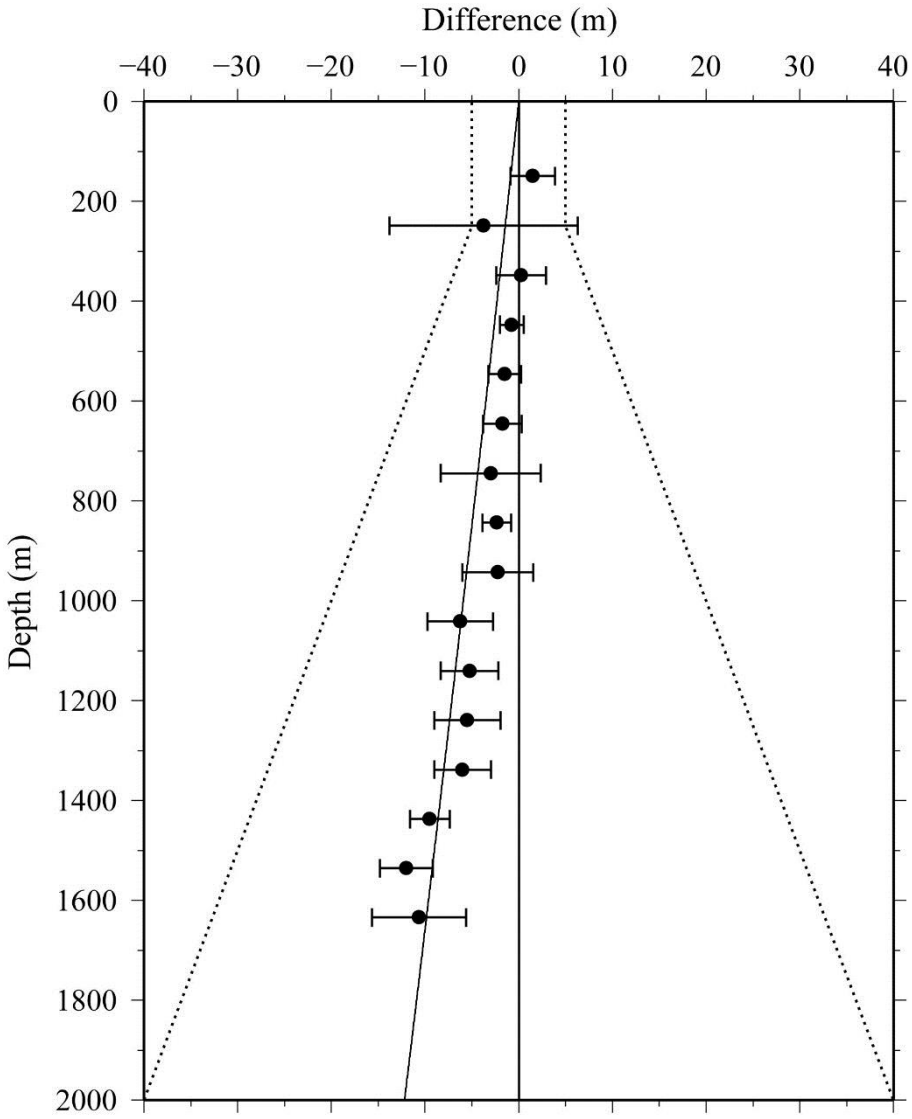

Figure 3.19.1. Differences between XCTD and CTD depths for XCTD-4. Differences were estimated with the same method as Uchida et al. (2011). Standard deviation of the estimates (horizontal bars) and the manufacturer's specification for XCTD depth error (dotted lines) are shown. The regression for the data (solid line) is also shown.

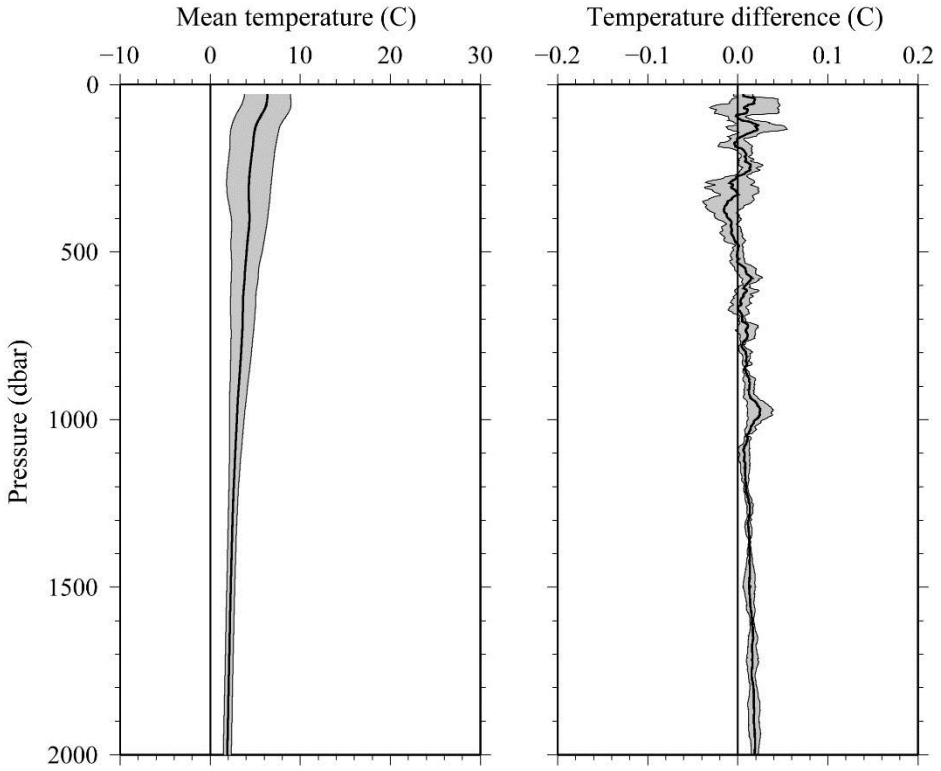

Figure 3.19.2. Comparison between XCTD and CTD temperature profiles. (a) Mean temperature of CTD profiles with standard deviation (shade) and (b) mean temperature difference with standard deviation (shade) between the XCTD and CTD. Mean profiles were low-pass filtered by a running mean with a window of 51 dbar.

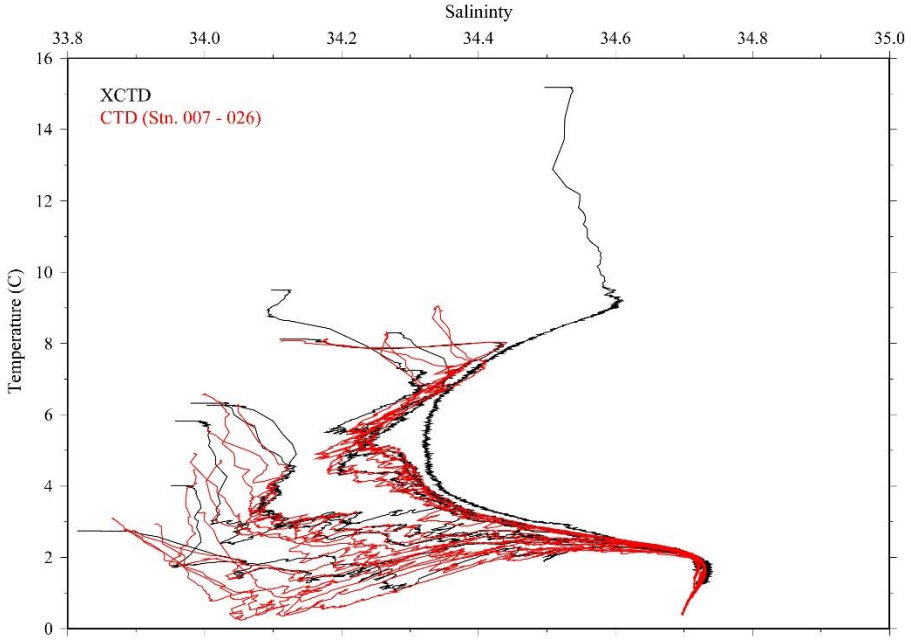

Figure 3.19.3. Comparison of temperature-salinity profiles of CTD data (red lines) used for the XCTD salinity bias estimation and salinity bias-corrected XCTD data (black lines).

3.20 Radiosonde observations

(1) Personnel

Masaki KATSUMATA	(JAMSTEC)	Principal Investigator (on board Leg-1)
Biao GENG	(JAMSTEC)	(not on board)
Kyoko TANIGUCHI	(JAMSTEC)	(not on board)
Soichiro SUEYOSHI	(NME)	Operation Leader
Yutaro MURAKAMI	(NME)	

(2) Objectives

The objective of radiosonde observations is to obtain the atmospheric profile of temperature, humidity, and wind speed/direction, and their temporal and special variations over the tropical ocean.

(3) Operational methodology

The Vaisala GPS radiosonde sensors (RS92-SGPD and RS41-SGP) were launched with the balloon (TA-200). The on-board radiosonde system consists of sounding processing system (SPS-311), ground check device (RI41), processing and recording software (MW41), GPS antenna (GA20), UHF antenna (RB21), and automatic balloon launcher (ASAP). In addition, the pressure sensor (PTB-330) was also utilized for ground check. In case the relative wind to the ship is not appropriate for using the automatic balloon launcher, the radiosonde equipped balloon was launched manually.

(4) Results

The radiosonde observations were conducted from Dec. 29, 2016 to Jan.15, 2017. During this period, 51 radiosondes equipped balloons have been launched (Table 3.20-1). Figure 3.20-1 shows some results of the radiosonde observations. Detailed analyses of the data observed by the radiosonde will be performed after the cruise.

(5) Data Archive

The radiosonde data were sent to the world meteorological community via Global Telecommunication System (GTS) through the Japan Meteorological Agency, immediately after each observation, when the appropriate satellite communication was available.

Raw data are recorded in Vaisala original binary format. The ASCII data are also available. These datasets will be submitted to JAMSTEC Data Integration and Analyses Group.

Table 3.20-1 Radiosonde launch log, with surface values and maximum height.

ID	Nominal Time YYYYMMDD hh	Launched Location Lat. deg.N	Lon deg.E	Surface Values P hPa	T deg.C	RH %	WD Deg.	WS m/s	Max Height m	Sensor Type
RS001	2016122900	-26.051	-174.346	1006.3	22.6	80	147	9.4	22045	
RS002	2016122912	-27.451	-172.664	1004.5	22.0	87	141	7.9	22486	
RS003	2016123000	-29.027	-170.693	1003.7	21.2	93	174	4.5	22898	
RS004	2016123012	-30.633	-168.564	1005.0	21.9	92	51	4.5	22986	
RS005	2016123100	-32.268	-166.310	1008.5	21.6	90	51	5.9	18582	
RS006	2016123112	-33.824	-163.983	1012.4	20.7	91	90	3.2	29246	
RS007	2017010100	-35.343	-161.605	1016.0	20.3	91	58	8.5	20797	
RS008	2017010106	-36.071	-160.380	1017.1	20.2	86	48	7.1	21961	
RS009	2017010112	-36.807	-159.130	1016.8	19.3	84	61	6.9	20864	
RS010	2017010118	-37.504	-157.821	1016.8	18.8	87	58	8.0	22280	
RS011	2017010200	-38.186	-156.538	1015.1	19.2	81	32	6.9	20785	
RS012	2017010206	-38.882	-155.204	1012.6	18.4	90	26	7.2	20394	RS92
RS013	2017010212	-37.576	-153.732	1009.1	17.6	94	14	8.5	21372	
RS014	2017010218	-40.250	-152.311	1005.8	16.9	96	11	9.3	19666	
RS015	2017010300	-40.934	-150.872	1002.4	15.4	90	358	12.2	24105	
RS016	2017010306	-41.537	-149.377	999.8	16.0	98	353	13.8	18075	
RS017	2017010312	-42.115	-147.839	999.4	15.4	100	345	10.4	16678	
RS018	2017010318	-42.733	-146.302	1002.4	12.5	100	186	11.4	18540	
RS019	2017010400	-43.190	-145.013	1004.1	12.3	100	165	8.6	21521	
RS020	2017010412	-44.149	-142.101	1007.4	11.5	96	171	7.7	20735	
RS021	2017010500	-44.931	-139.159	1011.3	13.0	99	336	5.6	22752	
RS022	2017010512	-45.947	-135.890	1015.1	12.9	99	328	5.6	21786	
RS023	2017010600	-46.748	-132.380	1017.8	12.8	96	326	5.8	22231	
RS024	2017010612	-47.433	-128.840	1018.3	12.2	97	336	5.3	21201	
RS025	2017010700	-48.042	-125.109	1020.0	12.3	93	348	3.5	21294	
RS026	2017010709	-48.367	-122.338	1022.4	11.7	78	32	2.7	20378	
RS027	2017010712	-48.474	-121.398	1022.5	11.0	88	71	2.5	20800	
RS028	2017010800	-48.773	-118.048	1025.3	10.9	86	241	1.7	18227	
RS029	2017010809	-48.964	-115.406	1026.5	9.5	73	173	5.8	23324	
RS030	2017010812	-49.024	-114.639	1025.9	8.9	73	200	6.0	19343	
RS031	2017010900	-49.080	-111.410	1025.0	8.5	77	217	3.2	21872	
RS032	2017010906	-49.097	-109.733	1024.6	8.4	79	206	4.2	21216	
RS033	2017010912	-49.100	-108.011	1022.3	8.8	84	216	5.1	22195	
RS034	2017011000	-49.045	-105.042	1019.1	8.1	87	207	3.2	19971	
RS035	2017011006	-48.969	-103.614	1019.0	8.7	97	149	4.0	18118	
RS036	2017011012	-48.875	-102.260	1017.8	8.2	83	168	3.4	21405	
RS037	2017011100	-48.703	-99.463	1016.2	9.1	76	214	1.2	20638	
RS038	2017011106	-48.542	-98.030	1015.8	9.0	71	227	2.7	21070	RS41
RS039	2017011112	-48.408	-96.661	1014.1	7.6	91	245	5.5	20946	
RS040	2017011200	-48.055	-93.844	1012.5	10.2	79	254	11.2	20429	
RS041	2017011206	-47.846	-92.544	1013.5	9.3	84	218	9.8	21518	
RS042	2017011212	-47.680	-91.152	1014.6	9.9	86	240	10.3	17657	
RS043	2017011300	-47.219	-88.682	1018.3	10.5	81	264	8.9	20881	
RS044	2017011306	-46.952	-87.362	1019.5	10.4	82	263	11.2	21297	
RS045	2017011312	-46.697	-86.093	1019.5	10.8	75	264	10.7	21013	
RS046	2017011400	-45.920	-82.622	1018.5	11.8	75	264	11.2	22353	
RS047	2017011406	-45.496	-81.002	1017.4	11.8	65	259	11.1	19633	
RS048	2017011412	-44.940	-80.049	1016.3	11.7	69	276	8.6	20843	
RS049	2017011418	-44.661	-80.139	1015.3	10.9	86	269	9.1	21309	
RS050	2917011500	-44.542	-80.109	1013.7	11.6	93	295	5.3	21899	
RS051	2017011506	-44.396	-80.021	1011.5	12.6	85	321	9.8	21741	

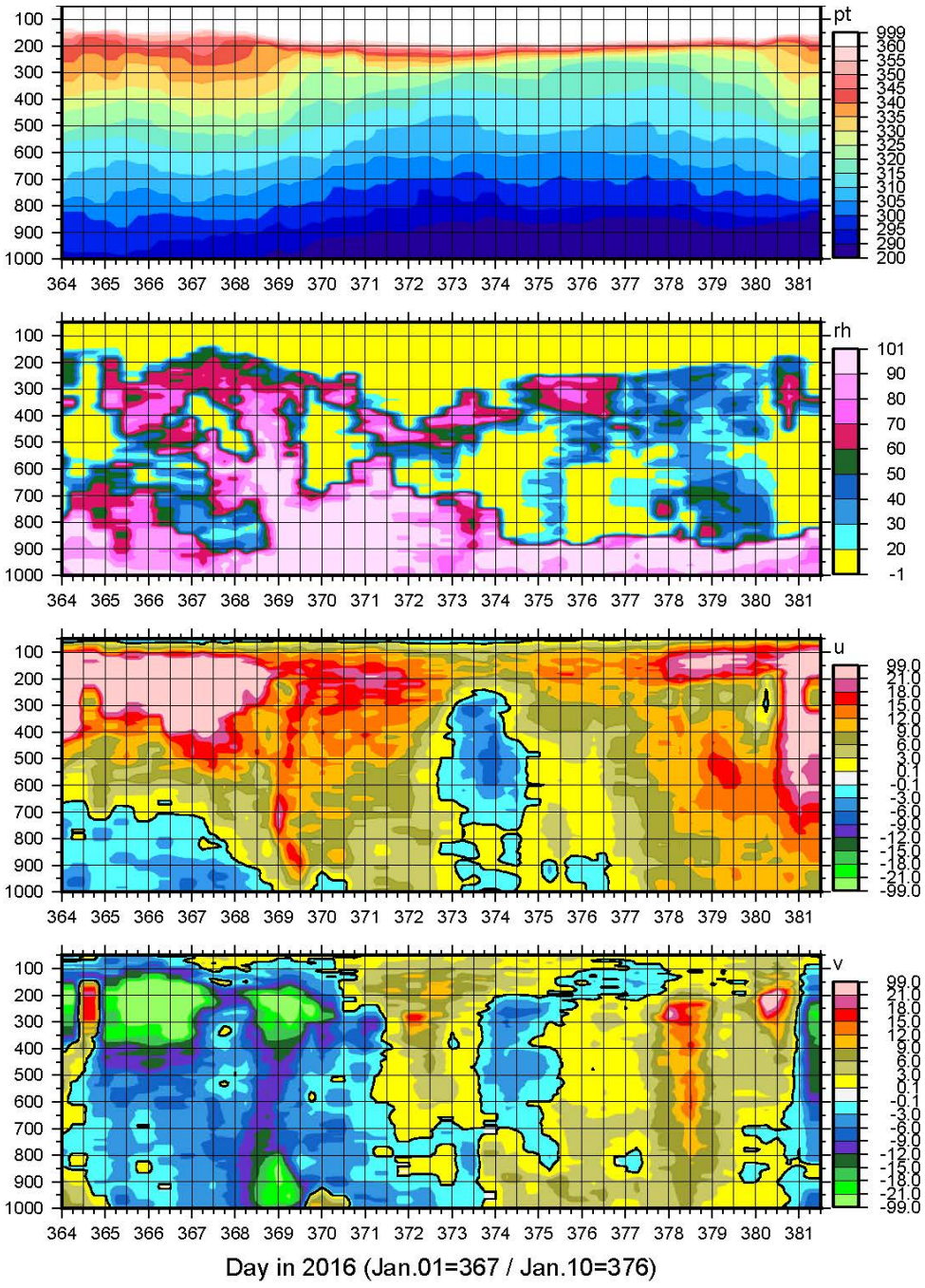

Figure 3.20-1. Time-height (time-pressure) cross section of the obtained data, for (top) potential temperature, (second top) relative humidity, (third) zonal wind, and (bottom) meridional wind, respectively.

4. Station Observation
4.1 Single Channel Seismic Survey

(1) Personnel

Natsue Abe (R&D Center for Ocean Drilling Science, JAMSTEC)

Toshimasa Nasu (Nippon Marine Einterprises,Ink.)

Mitsuteru Kuno (Nippon Marine Einterprises,Ink.)

Satsuki Iijima (Nippon Marine Einterprises,Ink.)

Hiroyuki Hayashi (Nippon Marine Einterprises,Ink.)

(2) Introduction

The SCS reflection data were acquired along 4 lines (L1 ~4), listed below, in two areas with a total length of approximately 240 km (Figures 4.1.1&2; Table 4-1-1).

- Line1 : Start 45-56.33835S, 75-56.36719W - End 46-06.71562S, 76-43.73703W
- Line2 : Start 45-55.04196S, 75-50.95871W - End 45-58.12477S, 76-04.74792W
- Line3 : Start 47-52.64648S, 75-56.24817W – End 47-52.52037S, 76-50.38330W
- Line4_0: Start 47-57.88422S, 75-57.24289W – End 47-57.29004S, 76-01.83151W
- Line4_1: Start 47-57.23190S, 76-02.19543W - ENd47-51.93878S, 76-46.98715W

In all tracks, reflection from the seafloor was clearly recorded. Igneous basement structures were confirmed except beneath steep slope of the ridge-like seamounts and the continental slops. In some places beneath the continental slops, the boundary between the footwall and the hanging wall is likely identified (Lines 3 &4). In the L1&2, half graben structure that was formed during mid-ocean ridge opening are clear reflections were recognized within both sediments and basements. The SCS reflection data across the subduction zone are complex. Further descriptions and investigations will be reported later.

(3) Spec information

The single channel seismic survey equipment and specification is as follows. The image of the single channel seismic system if shown in the Figure 4.1.3. The detail conditions of each lines are listed in the Table 4.1.2.

Streamer

Manufacturer:	S.I.G
Active section length:	65 m
Hydrophone Interval:	1 m
Type of Hydrophone:	S.I.G.16

Hydrophone output:	-90 dB,re 1V/μbar, ±1 dB
Frequency flat from:	10Hz to 1000Hz
Depth sensor:	Yes
Preamplifier gain:	39
Lead in cable length:	135 m
Receiver depth:	9.62 m (Line1), 1.91 m (Line2), 1.75 m (Line3), 1.85 m (Line4_0), 2.19 m (Line4_0)

Source

Manufacturer:	Sercel
Type of airgun:	GI Gun
Volume:	150 cu.in (G:45 cu.in, I:105 cu.in)
Air pressure:	13.5MPa
Source depth:	2 m
Depth sensor:	No
Gun Controller:	Hotshot ver. 3.3000

Air Compressor

Manufacturer:	Service Engineering co.,ltd
Type of machine:	4SA30-A150K
Air supply Capacity:	2.0 m^3/min.

Recording System

Manufacturer:	GEOMETRICS
Type of system:	Geode ver. 11.1.69.0
Recording format:	SEG-D 8058 Rev.1
Recording length:	7,500 msec
Water Delay:	0 msec
Sample rate:	1 msec
High cut filter:	None
Low cut filter:	None
Recording media:	Hard Disk

GPS System

Manufacturer:	Fugro
Type of system:	MultiFix6
DGPS Reference Station:	G2 Reference Station (ASAT)

Navigation System

Manufacturer:	MARIMEX JAPAN
Type of system:	Nav log ver. 2.2.7

Shot Point Geometry

Time mode shooting:	ture mode

Geodetic Parameter

Spheroid:	WGS84
Semi-major Axis:	6,378,137 m
Inverse Flattening:	298.26
Projection:	U.T.M
Zone18	

(4) Data process and Archives

Figure 4-1-4 shows the data processing flow to filtered section. Other details of data acquisition and processing of Single channel seismic survey are attached as below.

Data

Nav_Raw (.csv format): position logging data

SEG-D_Raw (.sgd format): Raw data

SEG-Y_Raw (.sgy): Transform data into SEG-Y from SEG-D_Raw data

SEG-Y_filetr (.seg): Filtering data of SEG-Y

BMP (.BMP format)

Bitmap profile of SEG-Y data for each lines.

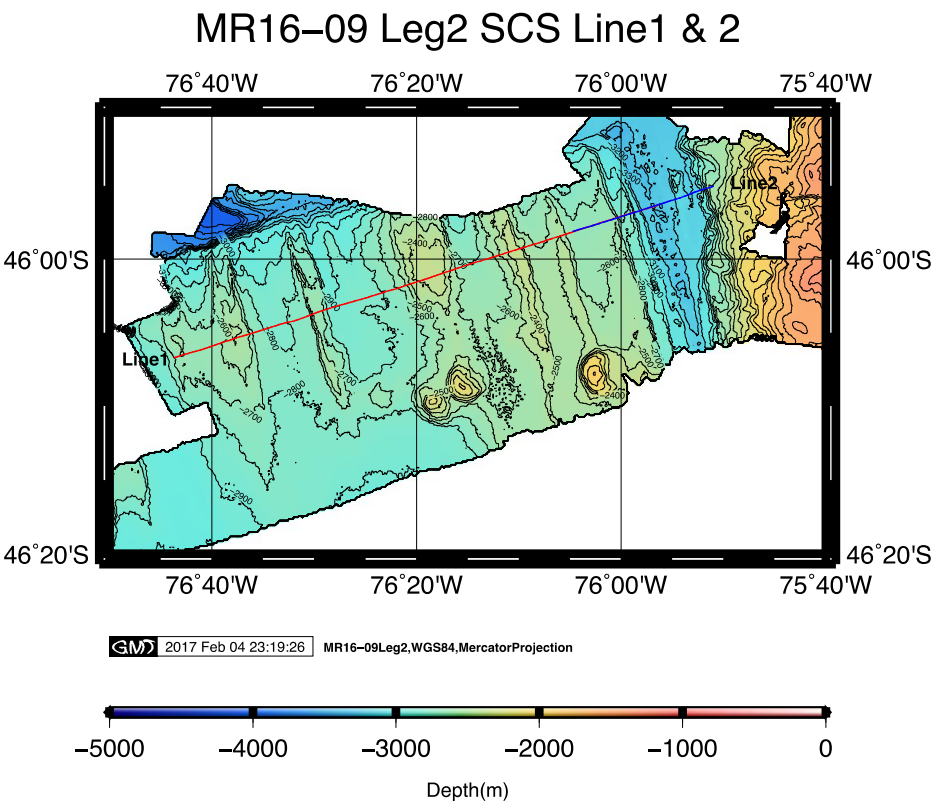

Fig.4-1-1 The location of SCS survey lines 1 and 2.

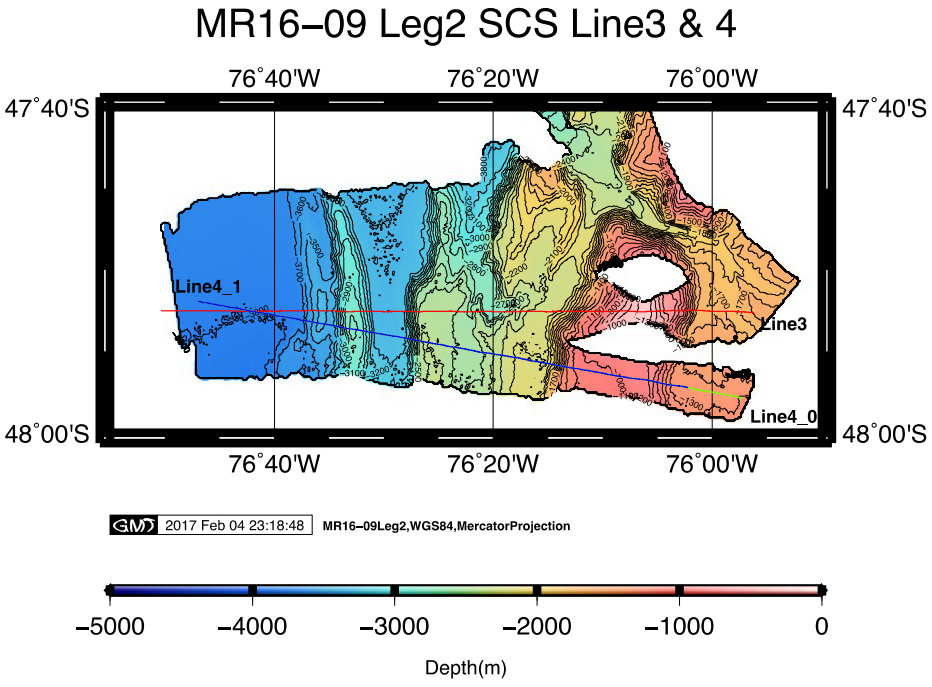

Fig.4-1-2 The location of SCS survey lines 3 and 4.

NME SINGLE CHANNEL SEISMIC SURVEY LINE LIST MR16-09_leg.2

Line No.	Date (UTC)	Time (UTC)	Passing Point	Shot No.	Vessel Position		Length [m]	Direction [deg]	Remarks
					Lat.	Lon.			
Line1	2017/1/23	2:24:43	F.S.P	1001	45-56.33835S	75-56.36719W	64,063.3	251.51	
	2017/1/23	3:05:43	F.G.S.P	1174	45-57.06688S	75-59.90295W			
	2017/1/23	10:54:06	L.G.S.P	3682	46-06.62773S	76-43.32138W			
	2017/1/23	10:58:50	L.S.P	3705	46-06.71562S	76-43.73703W			
Line2	2017/1/25	2:17:12	F.S.P	1001	45-55.04196S	75-50.95871W	18,707.9	251.51	
	2017/1/25	2:17:12	F.G.S.P	1001	45-55.04196S	75-50.95871W			
	2017/1/25	4:57:26	L.G.S.P	1794	45-58.12477S	76-04.74792W			
	2017/1/25	4:57:26	L.S.P	1794	45-58.12477S	76-04.74792W			
Line3_0	2017/1/26	20:23:00	F.S.P	1001	47-52.64648S	75-56.24817W	67,473.6	269.01	SP No.2737 – SP No.2788 = Point 76-28W transit. SP3456(FF3456) is most close to Line4_1.
	2017/1/26	20:23:00	F.G.S.P	1001	47-52.64648S	75-56.24817W			
	2017/1/27	5:58:29	L.G.S.P	3859	47-52.52037S	76-50.38330W			
	2017/1/27	5:58:29	L.S.P	3859	47-52.52037S	76-50.38330W			
Line4_0	2017/1/28	21:24:31	F.S.P	1001	47-57.88422S	75-57.24289W	4,983.2	278.96	
	2017/1/28	21:24:31	F.G.S.P	1001	47-56.75629S	75-57.24289W			
	2017/1/29	22:15:20	L.G.S.P	1253	47-57.37907S	76-01.17737W			
	2017/1/29	22:15:20	L.G.S.P	1253	47-57.37907S	76-01.17737W			
Line4_1	2017/1/28	22:34:36	F.S.P	1001	47-57.23190S	76-02.19543W	56,647.4	278.96	SP3514(FF3514) is most close to Line3.
	2017/1/28	22:34:36	F.G.S.P	1001	47-57.23190S	76-02.19543W			
	2017/1/29	7:59:55	L.G.S.P	3807	47-51.93878S	76-46.98715W			
	2017/1/29	7:59:55	L.S.P	3807	47-51.93878S	76-46.98715W			

Table 4-1-1 Position, length and the azimuth information of each survey lines.

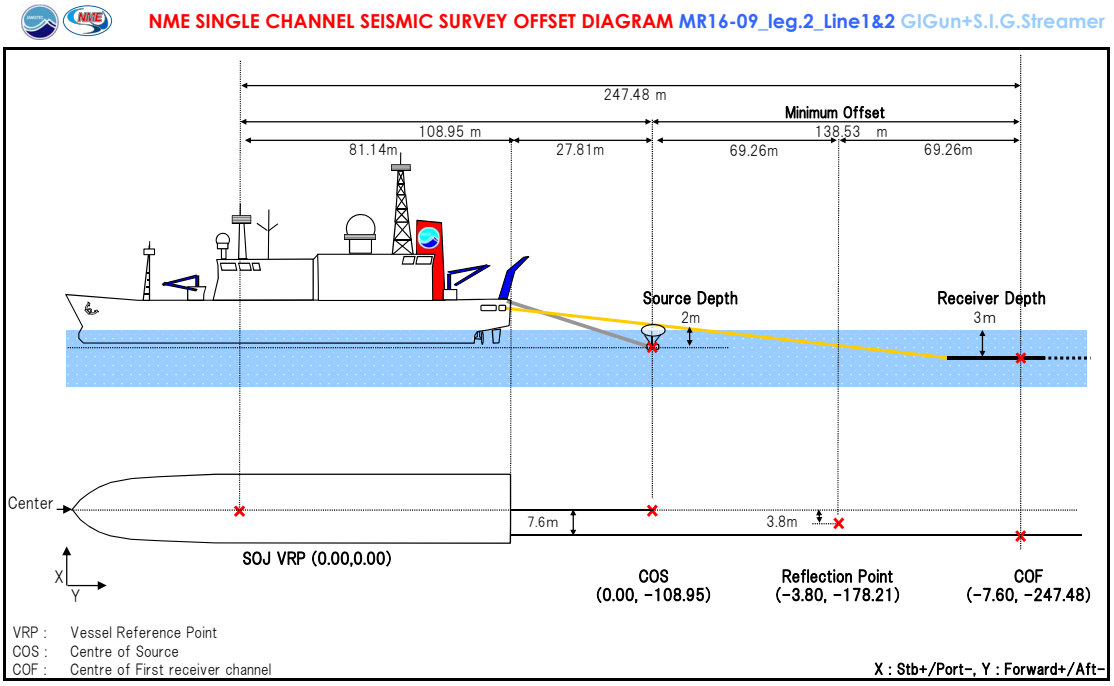

Fig. 4-1-3 Image of the Single Channel Seismic Survey system.

Seismic Data Processing Flow to Filtered Section for MR16-09_Leg2

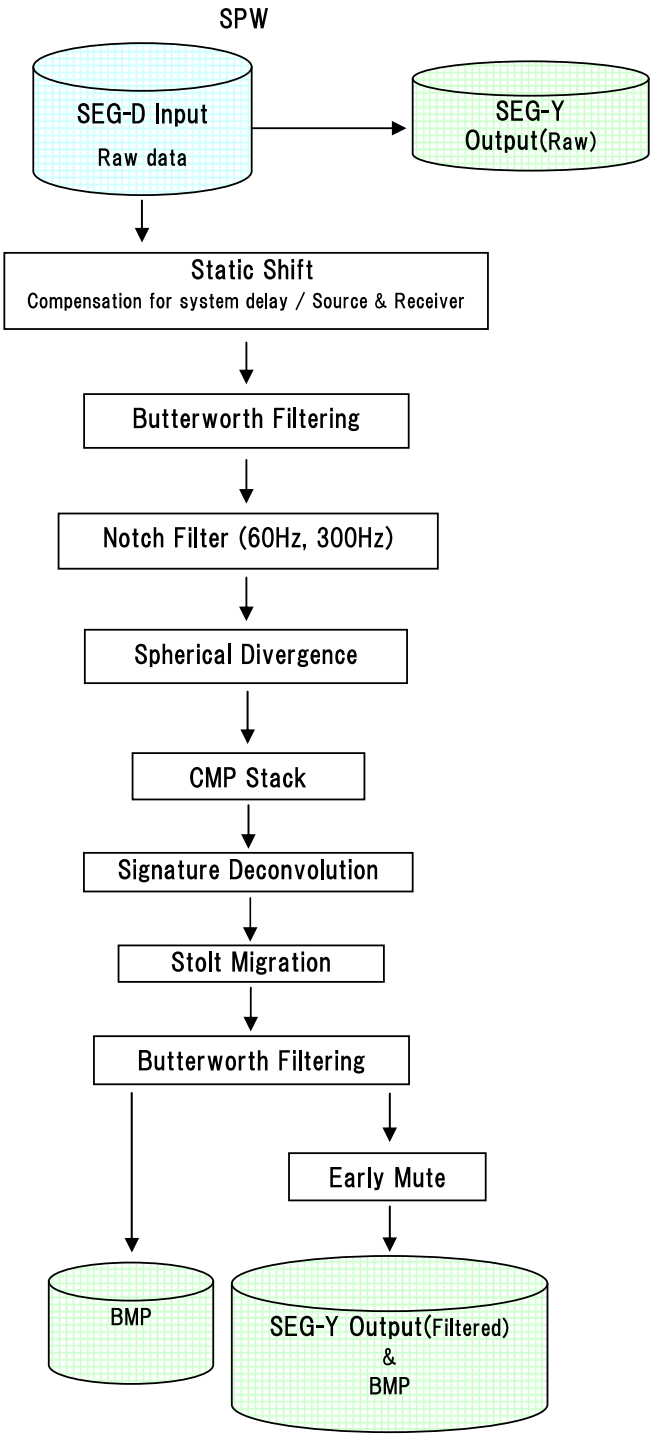

Fig. 4-1-4 Seismic data processing flow to filtered section for MR16-09 Leg 2.

4.2 Sediment Core

4.2.1 Site survey (bathymetry and sediment structure) observations

(1) *Personnel*

Kana Nagashima (JAMSTEC); nagashimak@jamstec.go.jp
Frank Lamy (Alfred Wegener Institute); Frank.Lamy@awi.de
Helge Arz (Ernst-Moritz-Arndt-University Greifswald); helge.arz@io-warnemuende.de
Wataru Tokunaga (NME), Operation Leader; tokunagaw@nme.co.jp
Koichi Inagaki (NME); inagakik@nme.co.jp
Yutaro Murakami (NME); murakamiy@nme.co.jp

(2) *Objective*

To find best location taking the sediment for paleoceanography, site survey was conducted using the Multi-narrow Beam Echo Sounding system (MBES), SEABEAM 3012 (L3 Communications ELAC Nautik GmbH) and Sub-Bottom Profiler (SBP), Bathy 2010 (SyQwest Incorporated) on R/V MIRAI. SBP system collected vertical information of sediments.

(3) *Measured parameters*

System configuration, performance and data acquisition of SEABEAM 3012 and Bathy 2010 systems showed "3.2 Bathymetry (Sea beam, sub-bottom profiler)".

(4) *Preliminary results*

Figures 4.2.1-1 to 4.2.1-5 show survey maps and sub-bottom profiles for Station 02, 03, 08 and 10. Sediment coring was conducted at the stations using multiple piston coring system. Geographic positions of each station were shown in Table 4.2.1-1 below.

(5) *Date archive*

All data are submitted to JAMSTEC Data Management Group (DMG) and is currently under its control and will be opened to public via "R/V MIRAI Data Web Page" in JAMSTEC homepage.

Table 4.2.1-1 Position of each coring station during MR16-09 Leg.2 cruise

Date (UTC) yyyymmdd	Core ID	Station Name	Location	Water Depth (m)	Position		Core Length (cm)
					Latitude (°S)	Longitude (°W)	
2017/1/22	PC01	St.02	Guafo Area	1,535	46-04.2714	75-41.2293	534.5
2017/1/22	MC01	St.02	Guafo Area	1,537	46-04.2885	75-41.2226	-
2017/1/23	PC02	St.03	Off Taitao	2,793	46-04.2316	76-32.0952	1273.0
2017/1/23	MC02	St.03	Off Taitao	2,787	46-04.2249	76-32.0902	-
2017/1/27	PC03	St.08	Off Taitao	3,082	46-24.3180	77-19.4499	1753.0
2017/1/31	PC04	St.10	Off Chile	3,848	50-48.3254	79-07.0752	1695.0
2017/1/31	MC04	St.10	Off Chile	3,851	50-48.3381	79-07.0823	-

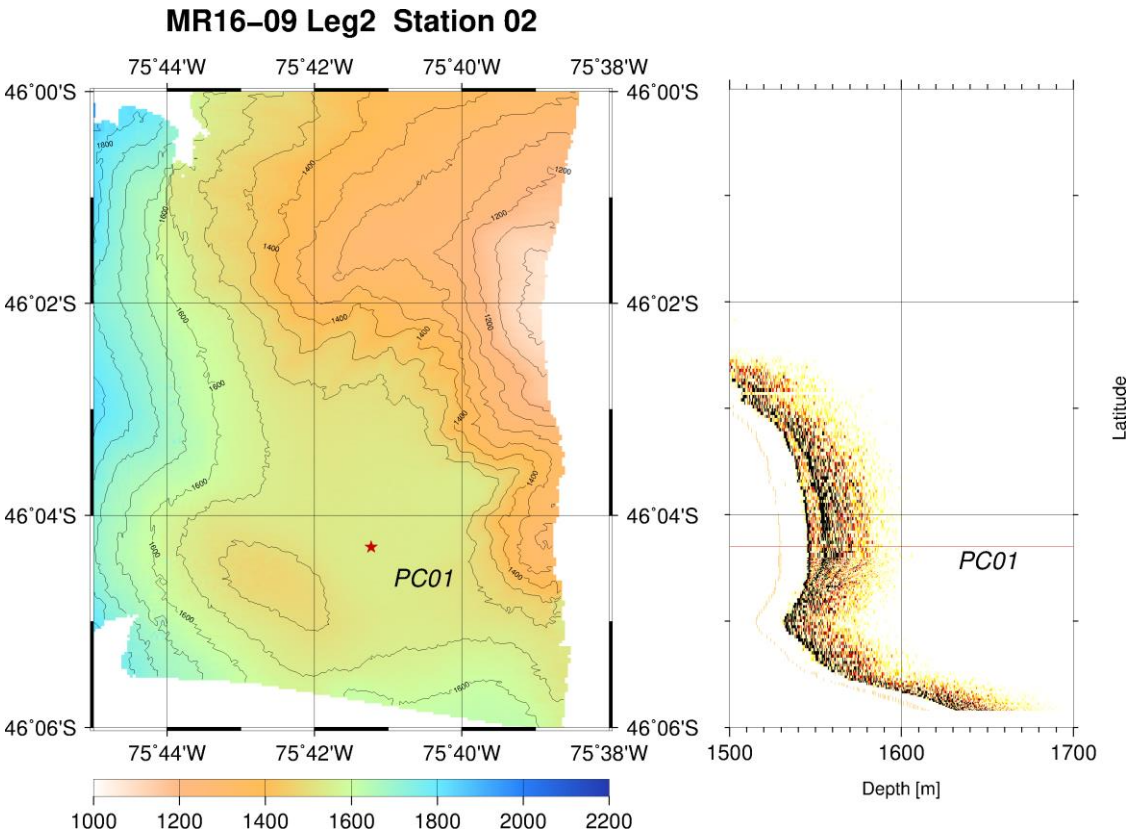

Fig. 4.2.1-1 Bathymetric map (left) and sub-bottom profile (right) around station 02 (coring site of PC01 and MC01).

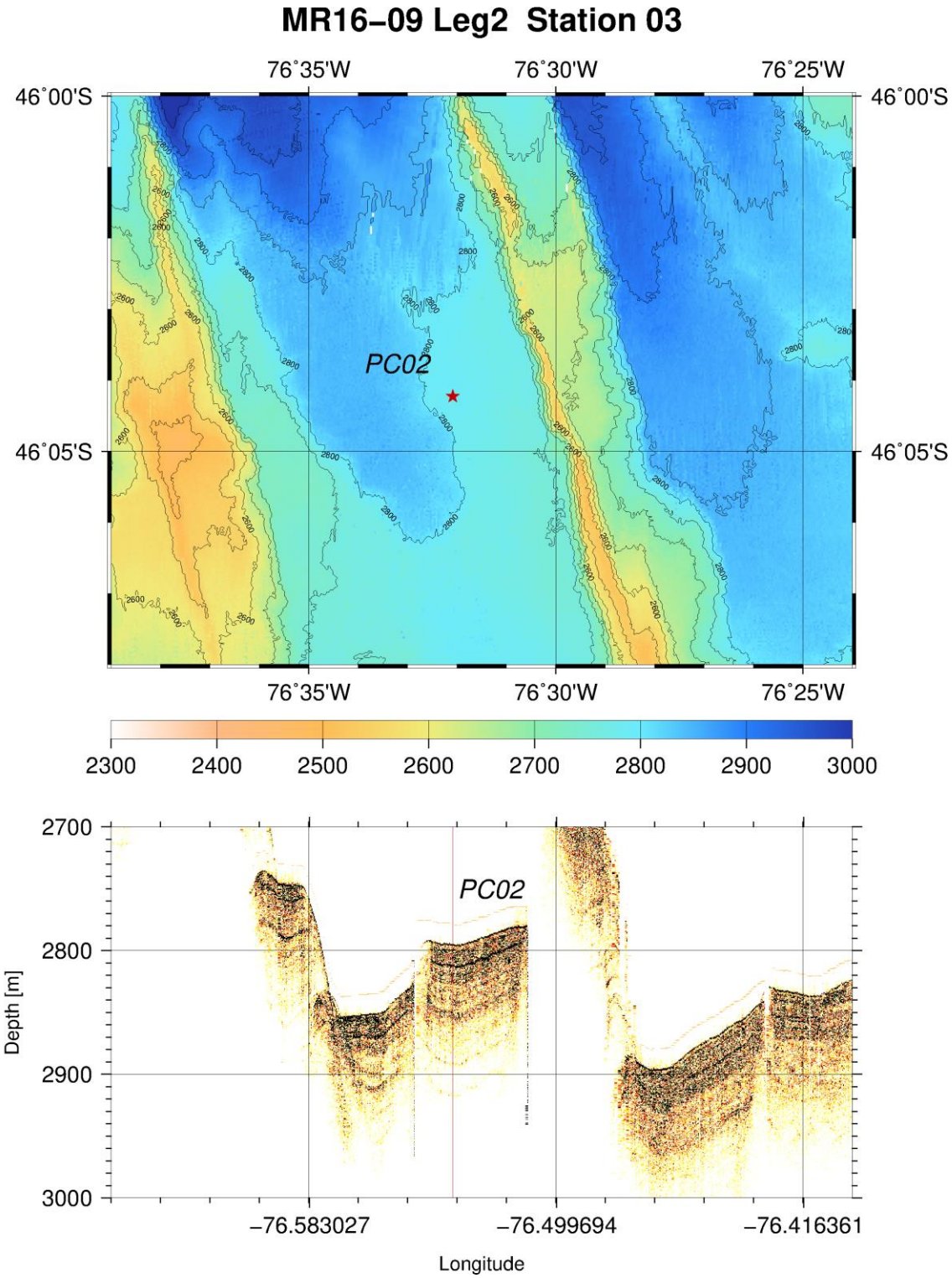

Fig. 4.2.1-2 Bathymetric map (top) and sub-bottom profile (bottom) around station 03 (coring site of PC02 and MC02).

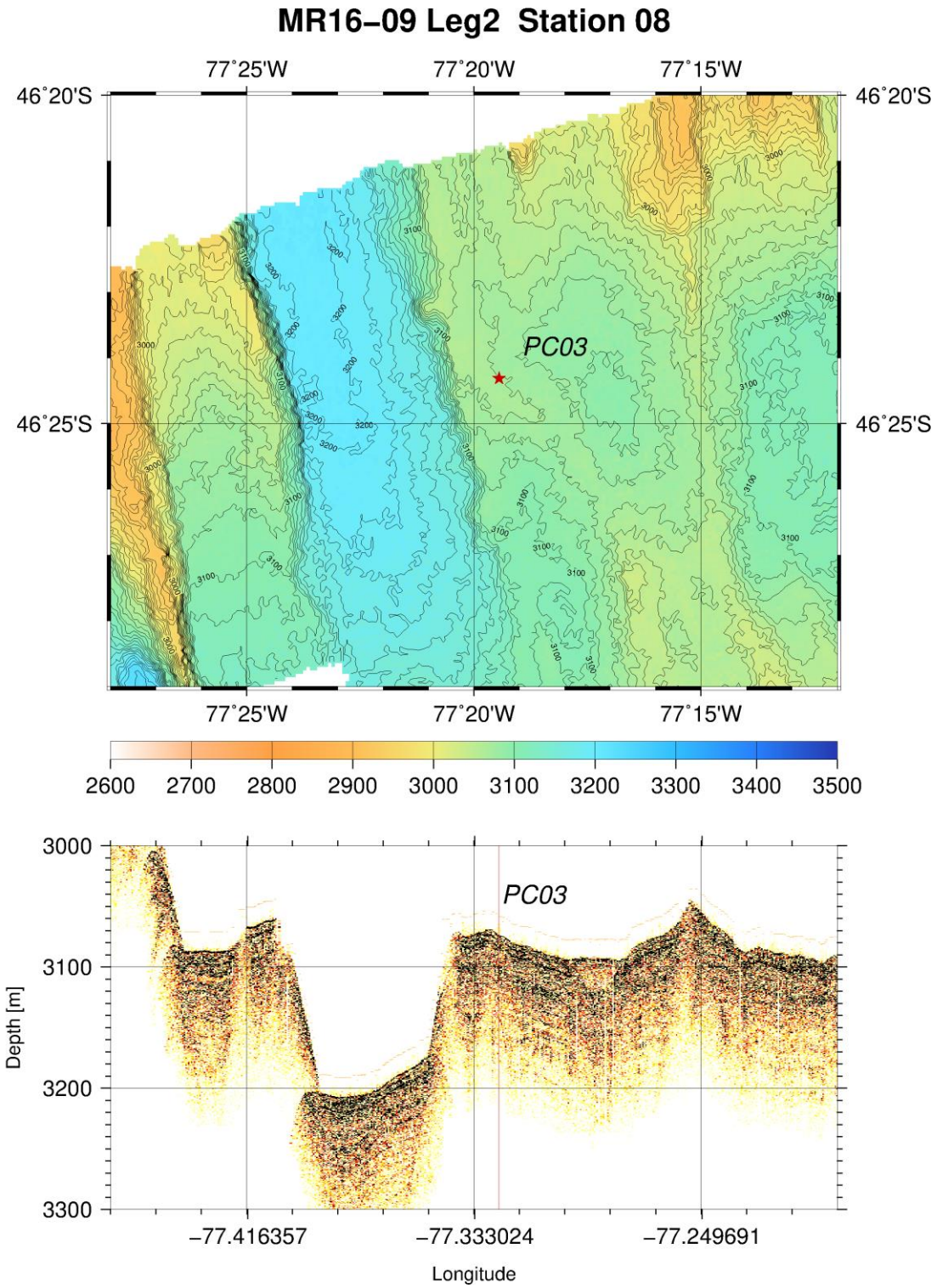

Fig. 4.2.1-3 Bathymetric map (top) and sub-bottom profile (bottom) around station 08 (coring site of PC03).

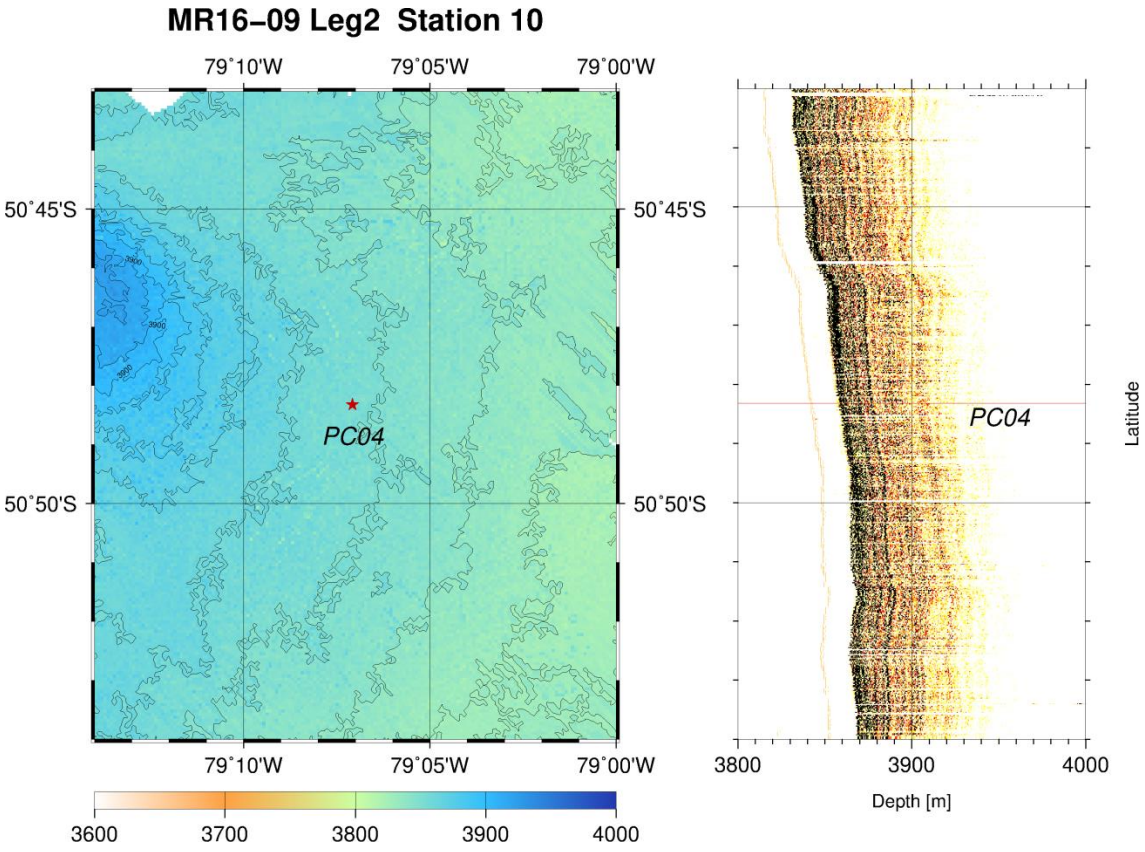

Fig. 4.2.1-4 Bathymetric map (left) and sub-bottom profile (right) around station 10 (coring site of PC04 and MC04).

4.2.2 Piston corer system (PC)

(1) Personnel

Yusuke Sato (Marine Works Japan Co. Ltd); satoy@mwj.co.jp
Ei Hatakeyama (Marine Works Japan Co. Ltd); hatakeyamae@mwj.co.jp
Yohei Katayama (Marine Works Japan Co. Ltd); katayamay@mwj.co.jp

(2) Objective

Collection of sea floor sediment

(3) Instruments and Method

The piston corer system (PC) is composed of the head of the corer, barrels, piston, catcher, bit, trigger and pilot core sampler. The duralumin pipes are used for the barrel. A total of 15 or 20 m-long duralumin pipe is composed of three or four 5 m segments which are combined one another by stainless joint sleeves. We used a 74 mm long type pilot corer for a pilot core sampler. We used inner liners: polycarbonate liner tubes (Inner type). A compass with inclinometer was attached above the weight of the corer to examine performance of the PC. Diagram of PC is shown in the Fig. 4.2.2-1.

In the Inner type piston corer, it pulls out inner tubes only from the duralumin pipes and the sediment can be collected. The inner tubes filled by sediments are cut with the handy cutter every 1 m after taking out from the barrel. The sediment sections are longitudinally cut into working and archive halves by a splitting devise and a stainless wire. After splitting, both cores are putted white pins at interval of 2 cm and orange pins at interval of 10 cm.

Specification of the piston corer system is shown below.

Head of the corer Main unit (Stainless, Lead):
- Weight; 1.3 ton

Barrel (Duralumin):
- Length; 5 m
- Inner diameter; 80 mm
- Outer diameter; 92 mm

Inner tube (Polycarbonate):
- Length; 5 m
- Inner diameter; 74 mm
- Outer diameter; 78 mm

(4) Winch operation

When we started lowering, a speed of wire out was set to be 0.2 m/s., and then gradually increased to the maximum of 1.0 m/s. PC were stopped at a depth about 100 m above the sea floor for 3 minutes to reduce any pendulum motion of the system. After the PC were stabilized, the wire was stored out at a speed of 0.3 m/s, and we carefully watched a tension meter. When the corers touched the bottom, wire tension abruptly decreases by the loss of the corer weight. Immediately after confirmation that the PC hit the bottom, wire out was stopped and rewinding of the wire was started at a dead slow speed (~0.3 m/s.), until the tension gauge indicates that the PC were lifted off the bottom. After leaving the bottom, winch wire was wound in at the maximum speed.

(5) Results

Details of coring positions and core lengths are shown are shown in Table 4.2.1-1.

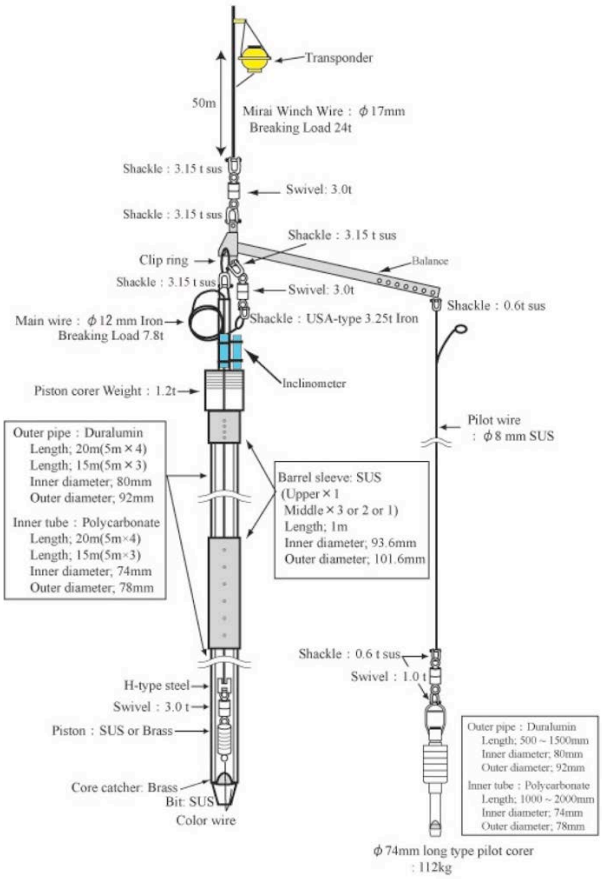

Fig. 4.2.2-1. Diagram of Piston corer system.

4.2.3 Multiple Corer system (MC)

(1) Personnel

Yusuke Sato (Marine Works Japan Co. Ltd); satoy@mwj.co.jp
Ei Hatakeyama (Marine Works Japan Co. Ltd); hatakeyamae@mwj.co.jp
Yohei Katayama (Marine Works Japan Co. Ltd); katayamay@mwj.co.jp

(2) Objective

Collection of surface sediment

(3) Instruments and Methods

Multiple corer (MC) consists of body (620 kg in weight) and eight sub-corer attachments. Acryl pipe and polycarbonate pipe are used for the sediment coring. The pipes are 60 cm in length, and the diameter is 74 mm.

For MC02 and MC04, attached Water sampling system without off line camera and light. Water sampling system attaches four Niskin bottles (8-liter), SBE 39 temperature (pressure optional) recorder and Magnet switch data logger to the body.

(4) Winch Operation

When we starts lowering the MC, a speed of wire out is set to be 0.2 m/s., and then gradually increased to be 1.0 m/s. The MC is stopped at a depth about 50 m above the sea floor for 3 minutes to reduce any pendulum motion of the sampler. After the sampler is stabilized, the wire is stored out at a speed of 0.3 m/s., and we carefully watch a tension meter. When the MC touches the bottom, wire tension leniently decreases by the loss of the sampler weight. After confirmation that the MC touch seafloor, the wire out is stopped then another 3~5 m rewinding. The wire is started at dead slow speed, until the tension gauge indicates that the corer is lifted off the bottom. After leaving the bottom, which wire is wound in at the maximum speed. The MC came back ship deck, sub-corer attachments and Niskin bottles or off line camera were detached from the main body.

(5) Results

Details of coring position are shown in the Table 4. 2. 1-1.

4.2.4 Multi sensor core logger (MSCL)

(1) Personnel:

Kazuma Takahashi (Marine Works Japan Ltd.); takahashik@mwj.co.jp

(2) Objectives

To understand characteristics of sediment samples and to correlate different cores, physical properties, magnetic susceptibility was taken by using the whole round core sections before splitting and the GEOTEC multi-sensor core logger (MSCL).

(3) Measured Parameters

MSCL has sensors of the gamma-ray attenuation (GRA), the P-wave velocity (PWV) and the magnetic susceptibility (MS). Whole-core samples are used for the logger measurements.

(4) Instruments and Methods

Whole-core samples are kept in the laboratory for the night to equalize the sediment temperature with the room temperature. Measurement interval was every 1 cm for all cores (Only PC01 core was measured by 2 cm interval).

GRA is measured a gamma ray source and a detector, which are mounted on the center sensor stand. A narrow beam of gamma ray is emitted by Cesium-137 (137Cs, energies principally at 0.662 MeV). The detector comprises a scintillator (a 2" diameter and 2" thick NaI crystal). The photon of gamma ray is collimated through 5 mm diameter in rotating shutter at the front of the housing of 137Cs. These photons pass through the center of the whole core and are detected the scintillation detector on the other side. The detector comprises a scintillator (a 2" diameter and 2" thick NaI crystal). The calibration of GRA assumes a two-phase system model for sediments, where the two phases are the minerals and the interstitial water. Aluminum has an attenuation coefficient similar to common minerals and is used as the mineral phase standard. Pure water is substituted as the interstitial-water phase standard. The actual standard consists of a telescoping aluminum rob (five elements of varying thickness) mounted in a piece of core liner and filled with pure water. GRA was measured with 10 seconds counting.

PWV is measured by two oil filled the Acoustic Rolling Contact (ARC) transducers, which are mounted on the center sensor stand with the gamma system. These transducers measure the velocity of P-wave through the whole core and the pulse amplitude.

MS is measured by the loop sensor of 100 mm diameter made by the Bartington Instruments Ltd. An oscillator circuit in the sensor produces a low intensity (approx. 80 A/m RMS) non-saturating, alternating magnetic field (0.565 kHz). MS was measured with 1 second. The measured raw data are shown in Fig. 4.2.4-1~4. After the MSCL measurement, whole-core samples are cut into Working and Archive halves by a splitting devise and a nylon line.

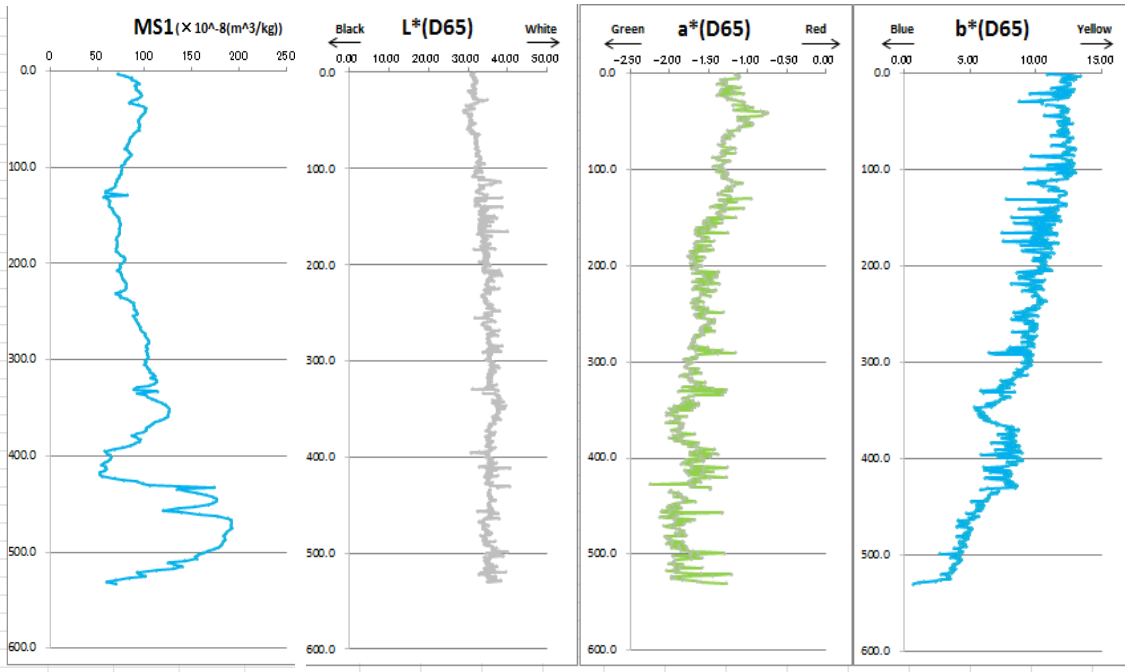

Fig. 4.2.4-1. MS raw data and color data (PC01; Guafo area).

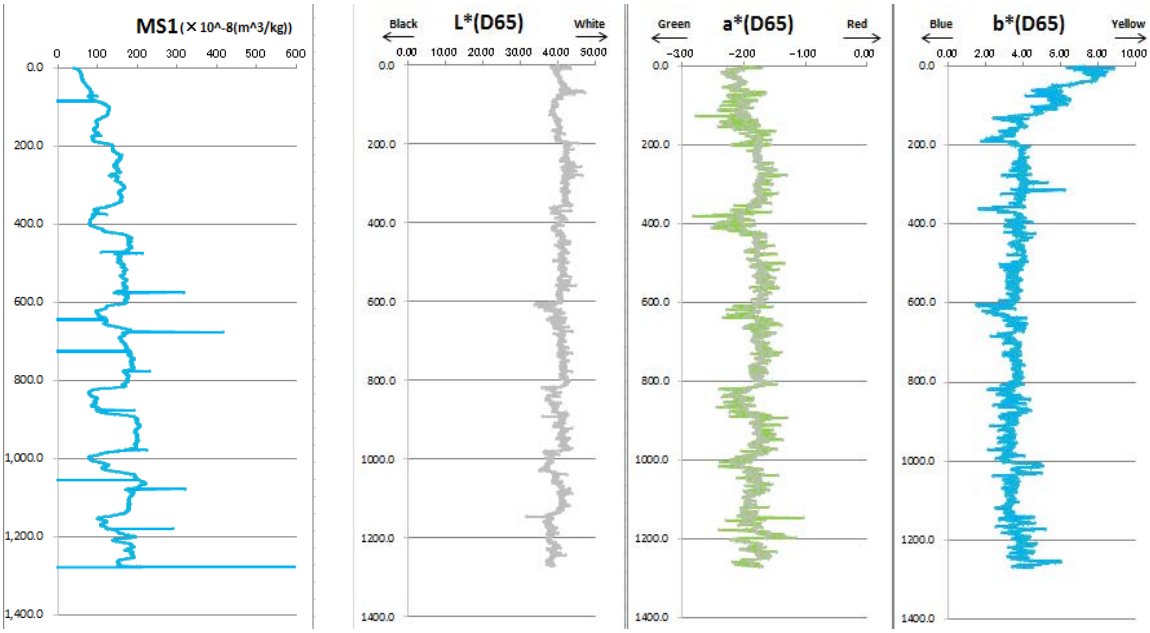

Fig. 4.2.4-2. MS raw data and color data (PC02; Off Taitao).

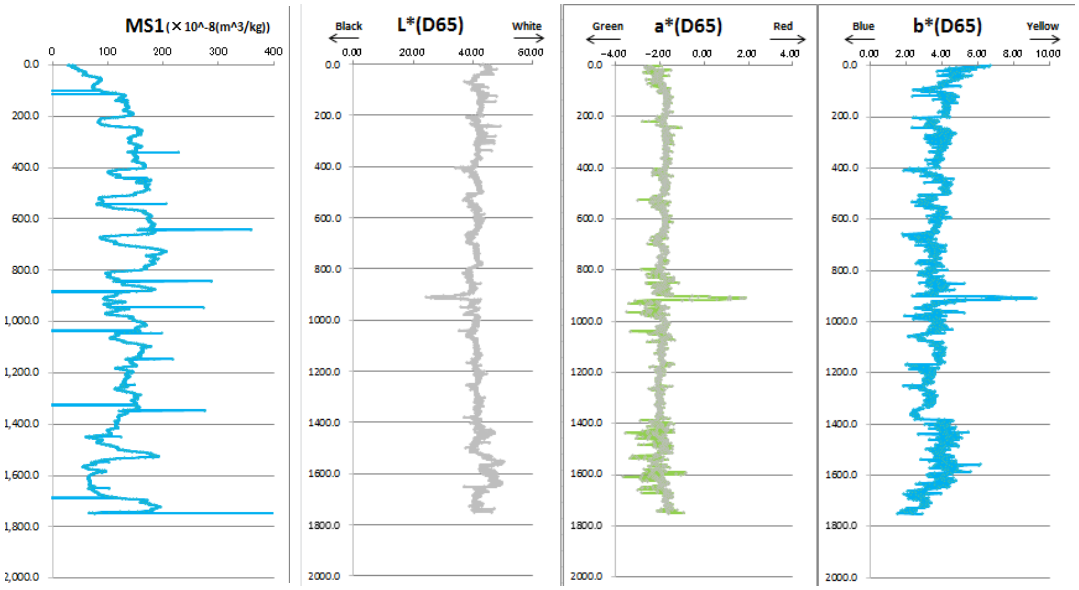

Fig. 4.2.4-3. MS raw data and color data (PC03; Off Taitao).

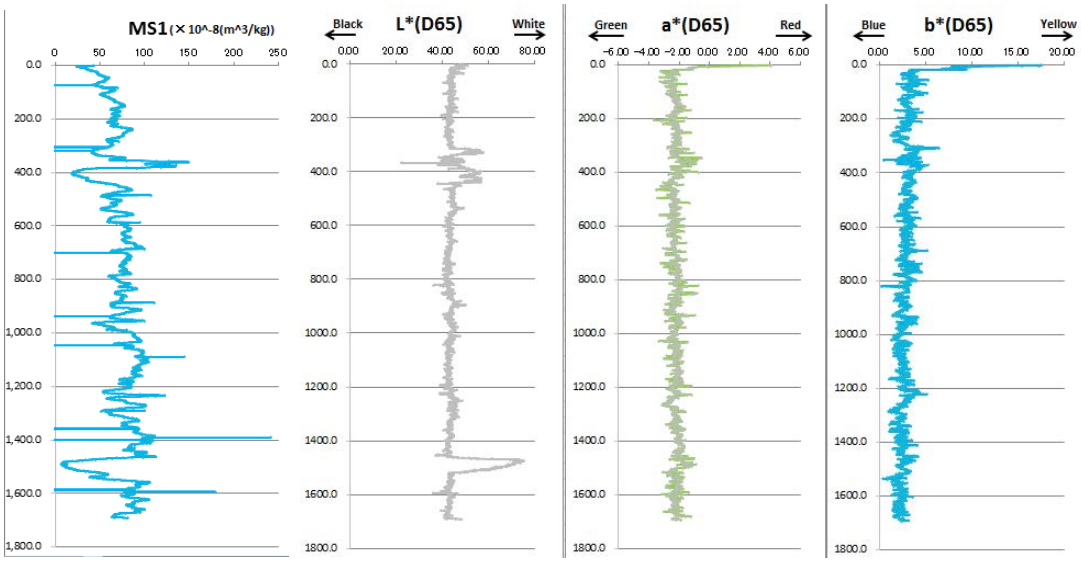

Fig. 4.2.4-4. MS raw data and color data (PC04; Off Chile).

4.2.5 Core color reflectance (CCR)

(1) Personnel:

Yuki Miyajima (Marine Works Japan Ltd.); miyajimay@mwj.co.jp

(2) Objectives

To understand characteristics of sediments such as lithology, redox condition, relative carbonate content, organic matter content and certain inorganic compounds, color reflectance was measured for split half sediments.

(3) Measured Parameters

There are different systems to quantify the color reference for soil and sediment measurements, the most common is the L*a*b* system, also referred to as the CIE (Commision International d'Eclairage) LAB system. It can be visualized as a cylindrical coordinate system in which the axis of the cylinder is the lightness variable L* ranging from 0 % to 100 %, and the radii are the chromaticity variables a* and b*. Variable a* is the green (negative) to red (positive) axis, and variable b* is the blue (negative) to yellow (positive) axis. Spectral data can be used to estimate the abundance of certain components of sediments.

(4) Instruments and Methods

Core color reference was measured by using the Konica Minolta CM-700d reference photo spectrometer using 400 to 700nm in wavelengths. This is a compact and hand-held instrument, and can measure spectral reflectance of sediment surface with a scope of 3 mm diameter. To ensure accuracy, the CM-700d was used with a double-beam feedback system, monitoring the illumination on the specimen at the time of measurement and automatically compensating for any changes in the intensity or spectral distribution of the light.

The CM-700d has a switch that allows the specular component to be include (SCI) or excluded (SCE). We chose setting the switch to SCE. The SCE setting is the recommended mode of operation for sediments in which the light reflected at a certain angle (angle of specular reflection) is trapped and absorbed at the light trap position on the integration sphere.

Calibrations are zero calibration and white calibration before the measurement of core samples. Zero calibration is carried out into the air. White calibration is carried out using the white calibration piece (CM-700d standard accessories) without crystal clear polyethylene wrap.

The color of Archive half core was measured on every 1 cm through crystal clear polyethylene wrap. Measurement parameters are displayed Table 4.2.5-1. The measured raw data are summarized in Fig. 4.2.3-1~4.

Table 4.2.5-1. Measurement parameters.

Instrument	Konica Minolta Photospectrometer CM-700d
Software	Spectra Magic NX CM-S100w Ver.2.51
Illuminant	d/8 (SCE)
Light source	D65
Viewing angle	10 degree
Color system	$L^*a^*b^*$ system

4.2.6 Core photograph

(1) Personnel:

Mika Yamaguchi (Marine Works Japan Ltd.); yamaguchim@mwj.co.jp

(2) Objectives

Photographs were taken to observe sedimentary structures of the cores.

(3) Instruments and methods

Each of Archive half core photographs were taken using a digital camera (Camera body: Nikon D90/ Lens: Nikon AF-NIKKOR 28 mm 1:1.8 D). When using the digital camera, shutter speed was 1/15 ~ 1/40 sec, F-number was 4.5~5.6, sensitivity was ISO 200. File format of raw data is JPEG. Details for settings were included on property of each file.

4.2.7 Visual Core Description

(1) Personnel

Frank Lamy (Alfred Wegener Institute); Frank.Lamy@awi.de
Helge Arz (Ernst-Moritz-Arndt-University Greifswald); helge.arz@io-warnemuende.de

(2) Summary

Visual core description was made on the split surface of the archive half sections. The split surface was scraped using a plastic card to expose fresh surface. Lithological and sedimentological features were described in Fig. 4.2.7-1~5. Primary sediment lithologies were first described directly on the core and later confirmed/ modified by a qualitative and quantitative microscopic examination of representatively taken smear slides . We adopted the IODP-style nomenclature for lithological description (e.g., Mazzullo et al., 1988) with some modifications.

Cores PC01 and PC02 were retrieved close to core locations of the MD159 cruise in 2007 (MD159 – PACHIDERME, IMAGES XV, 2007; cores MD07-3088 and MD07-3119, respectively) with the advantage that Siani et al. (2010) provides a detailed chronostratigraphic framework for core PC01 and the upper part of PC02 based on radiocarbon and tephrochronological data. Onboard GEOTEK measurement of the magnetic susceptibility and GRAPE density were used for a detailed correlation between PC01 and MD07-3088 used for establishing of a preliminary chronostratigraphy. Core PC01 consists in a fairly uniform succession of olive black to grayish olive nannofossil/diatom and silt bearing to silty clay (Fig. 4.2.7-1, 6). Magnetic susceptibility is generally quite low and the correlation to core MD07-3088 (Fig. 4.2.7-6~7) suggests a basal age of 17.5 kyrs BP, thus covering most of the glacial Termination I and the Holocene.

Further offshore, two piston cores of 13 and 17 m were retrieved at 2786 and 3067 m water depth, respectively (Station 03, core PC02 and Station 08, core PC03) from the Chile Rise showing a well-developed stratification in the seismic record. The cores are well comparable and consist of dark olive gray to grey silt- diatom- and occasionally nannofossil-bearing clay to clayey nannofossil ooze with some thin silt and sandy layers that become more frequent in the lower part of the cores and which could be ascribed mainly to turbididic deposits and perhaps also to tephra layers. In core PC03 magnetic susceptibility is low in the upper and the lowermost three meters characterizing sediment with an increased amount of biogenic components. Most of the core, however, consists of glacial clayey sediments with an alternating contribution of coarser grained siliciclastics. At about 9.1 m a prominent 15 cm thick brownisch tephra layer interrupts the normal sedimentation (Fig. 4.2.7-8). The biogenic-rich basal three meters were deposited most probably during the last interglacial Marine Isotope Stage (MIS) 5 and the basal age of the core is suggested to be around 120-130 kyrs BP (Fig. 4.2.7-9).

Core PC04 was cored in 3852 m water depth in the deeper Southeast Pacific south of the Chile Rise at (~50.8°S) ~200 nm off the Chilean coast. Sediment acoustic profiles from this region revealed well-stratified deposits with significantly increased acoustic penetration. With respect to major lithologies, the core is quite different from the shallower continental margin cores further to the northeast. Overlain by a yellowish brown foraminifera and diatom-bearing nannofossil ooze, dark olive to greenish gray clays dominate the sequence. The clay sequence is intercalated with lighter foram-bearing calcareous oozes, the base of which is commonly strongly bioturbated. Calcareous oozes are found at ~3-4, 9-10, ~13, and 14.5-15.5 m. At 14.5-15.5 m the calcareous oozes consist of a compact, stiff, white nannofossil ooze (Fig. 4.2.7-10). The recovered sequence in PC04 is quite similar to those described in cores PS97/112-1 and 114-2 that were recovered during the RV Polarstern cruise PS97 in 2016 about 120 nm offshore Chile 4°

further to the south (55°S) from a comparable water depth of ~3850 m (Expedition PS97 cruise report, 2016). The records of cores PC04 and PS97/114-2 correlate convincingly (Fig. 4.2.7-11). The tentative correlation to the Lisiecki & Rymo (2005) isotope stack and to the Antarctic climate records suggests that the core PC04 reaches back to the Marine Isotope Stage 12 (430 kyrs BP) and has an average sedimentation rate of about 4 cm/kyr. When all PC cores are compiled into one graph, an almost linear relationship between the average sedimentation rate and the distance to the Chilean coast becomes evident. This relationship mainly describes the diminishing influence to the west of the detrital sediment input from the glaciated southernmost Andes (Fig. 4.2.7-12).

References:

Kissel C. and cruise participants (2007): MD159 – PACHIDERME IMAGES XV Cruise report. IPEV, Les rapports de campagnes a` la mer, 83 pp.

Lamy, F. and cruise participants (2016): The Expedition PS97 of the Research Vessel POLARSTERN to the Drake Passage in 2016. Reports on Polar and Marine Research 701, 157 pp. doi:10.2312/BzPM_0701_2016

Mazzullo, J., Meyer, A. and Kidd, R. (1988) New sediment classification scheme for the Ocean Drilling Program. Appendix I, In “Handbook for shipboard sedimentologists” eds. Mazzullo, J. and Graham, A. G., ODP Technical Note, 8, 44-63.

Siani, G., Colin, C., Michel, E., Carel, M., Richter, T., Kissel, C., and Dewilde, F. (2010): Late Glacial to Holocene terrigenous sediment record in the Northern Patagonian margin: Paleoclimate implications, Palaeogeogr. Palaeocl., 297, 26–36.

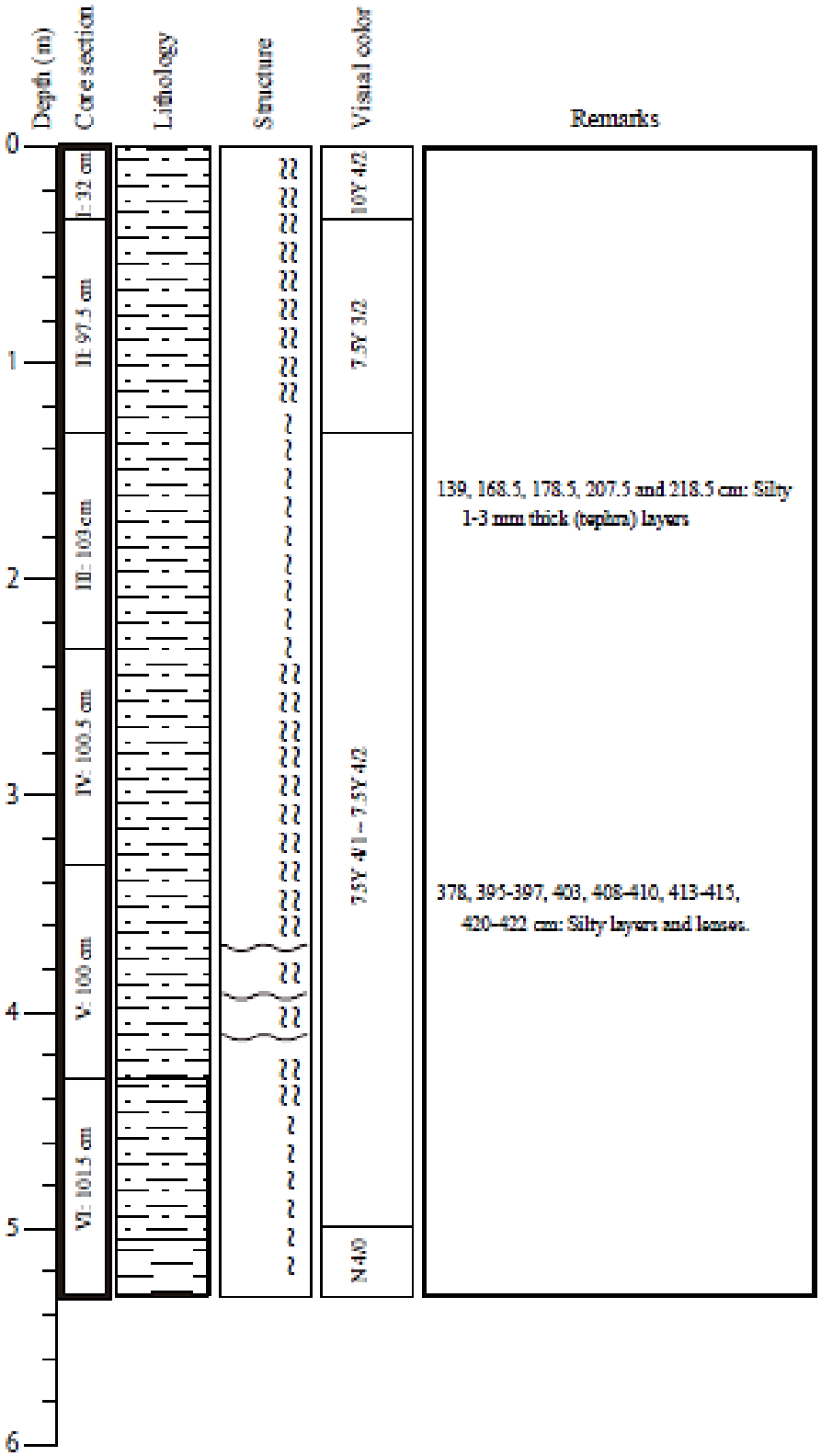

Fig. 4.2.7-1. Visual core description for PC01.

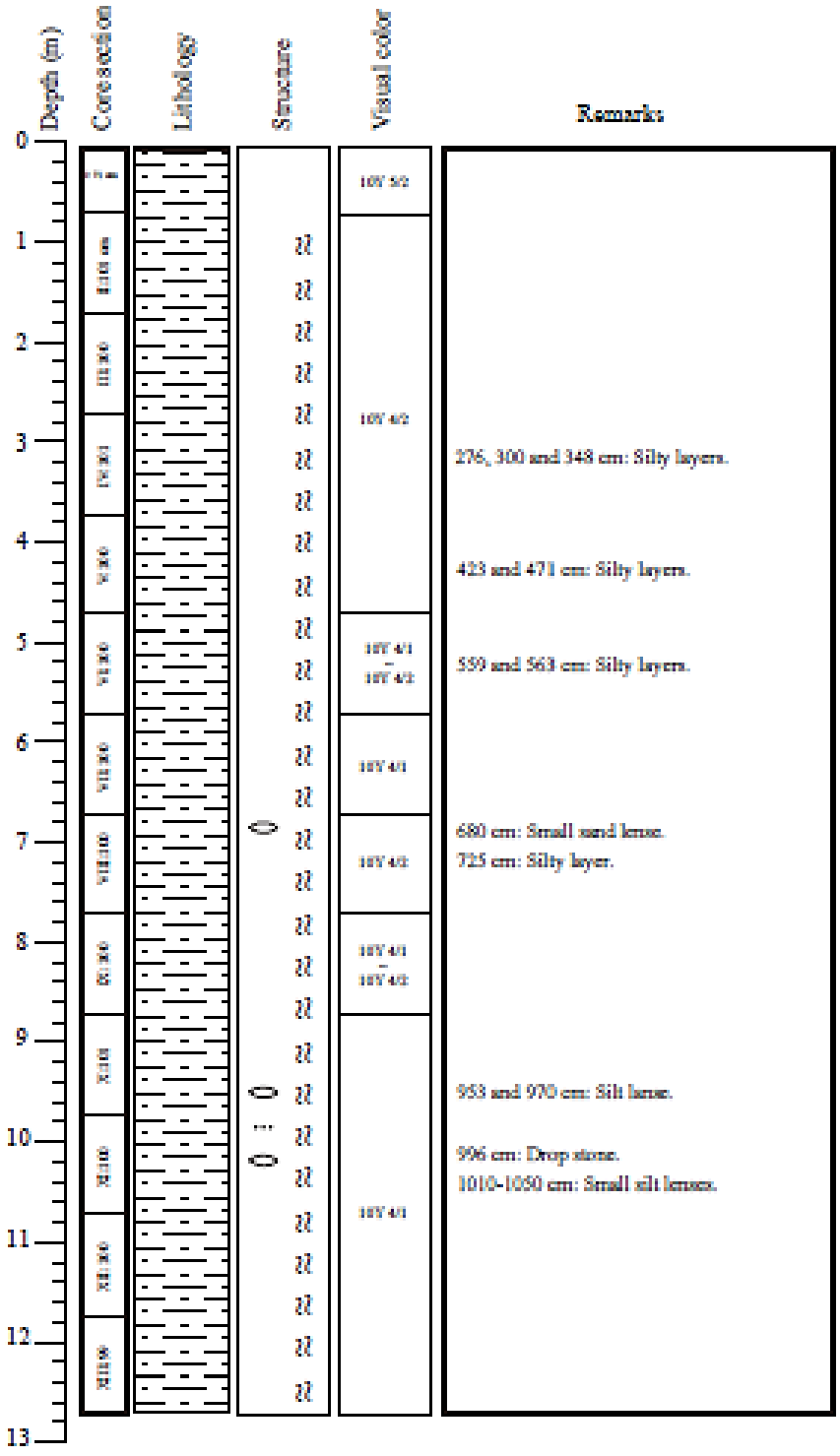

Fig. 4.2.7-2. Visual core description for PC02.

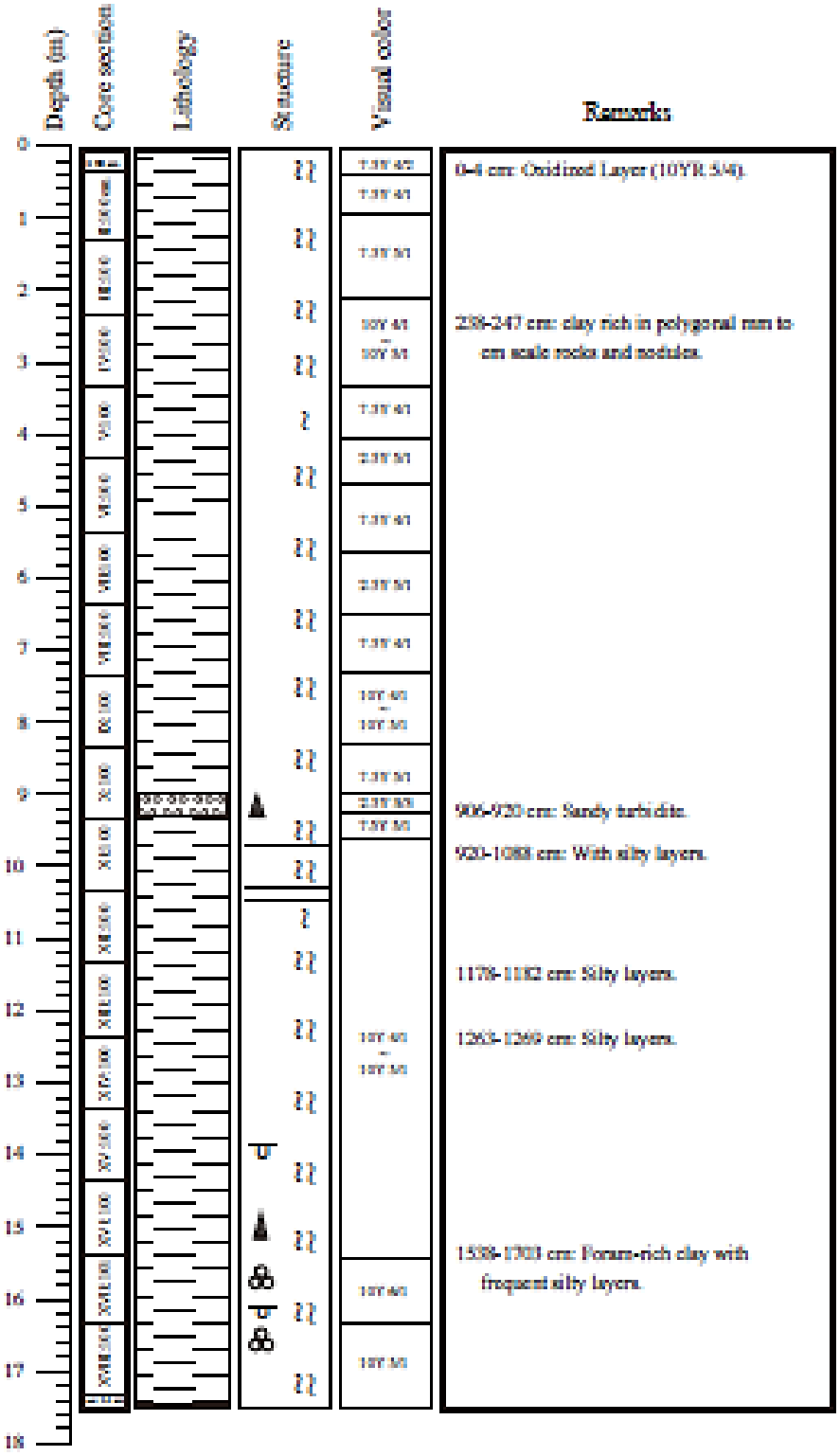

Fig. 4.2.7-3. Visual core description for PC03.

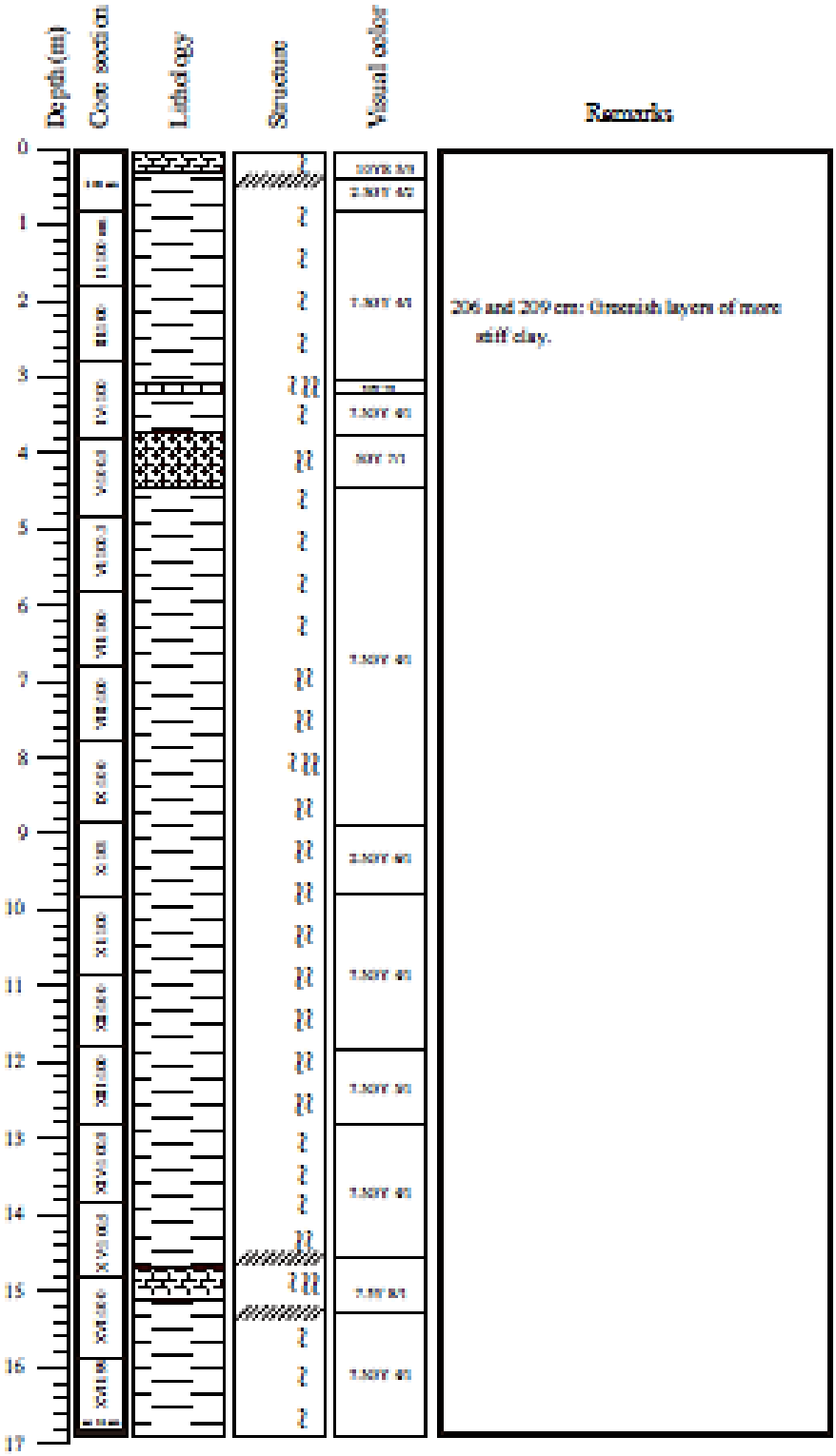

Fig. 4.2.7-4. Visual core description for PC04.

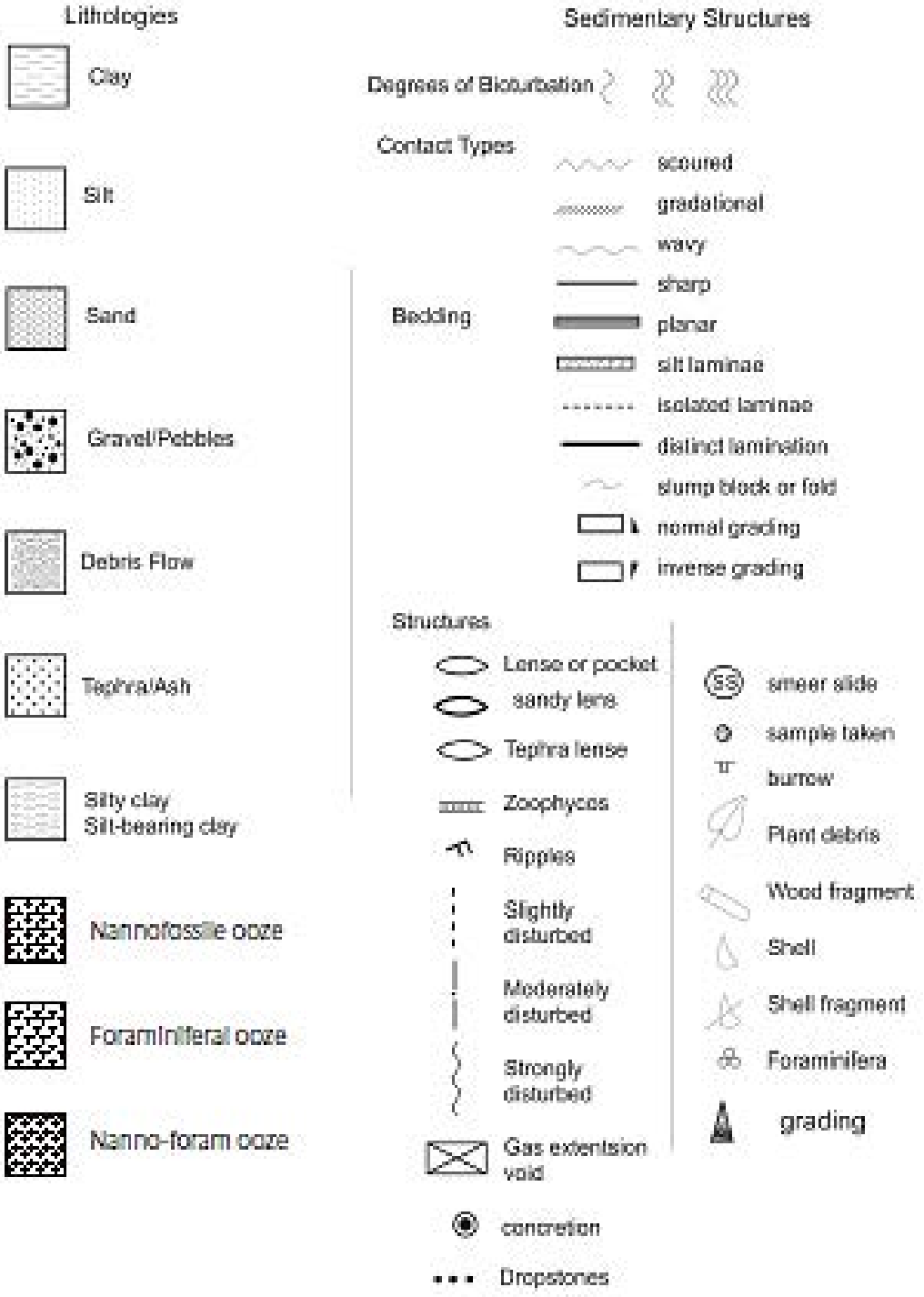

Fig. 4.2.7-5. Legend for core description.

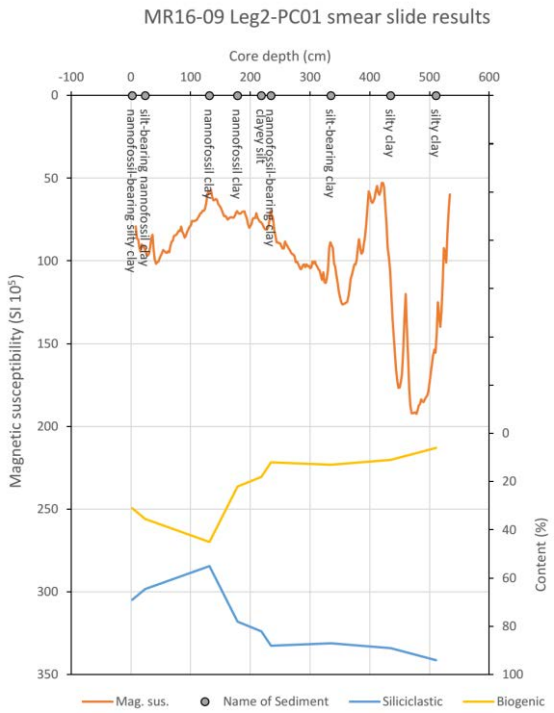

Fig. 4.2.7-6. Graph combining the GEOTEK magnetic susceptibility measurements on core PC01 with the smear slide examinations on the core.

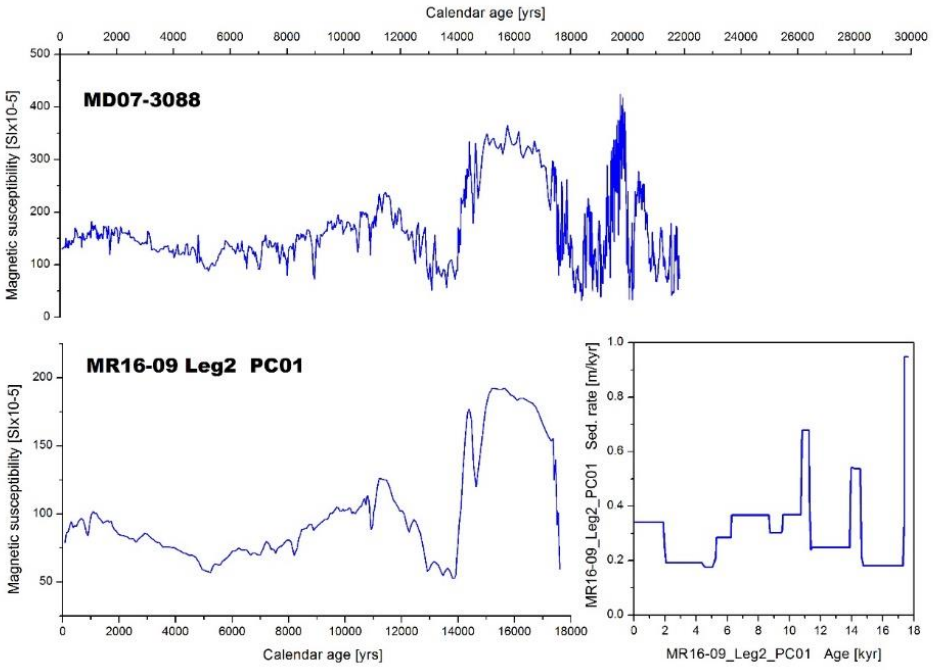

Fig. 4.2.7-7. Correlation of the magnetic susceptibility records of dated core MD07-3088 (Siani et al. 2010) and PC01 with PC01 sedimentation rates.

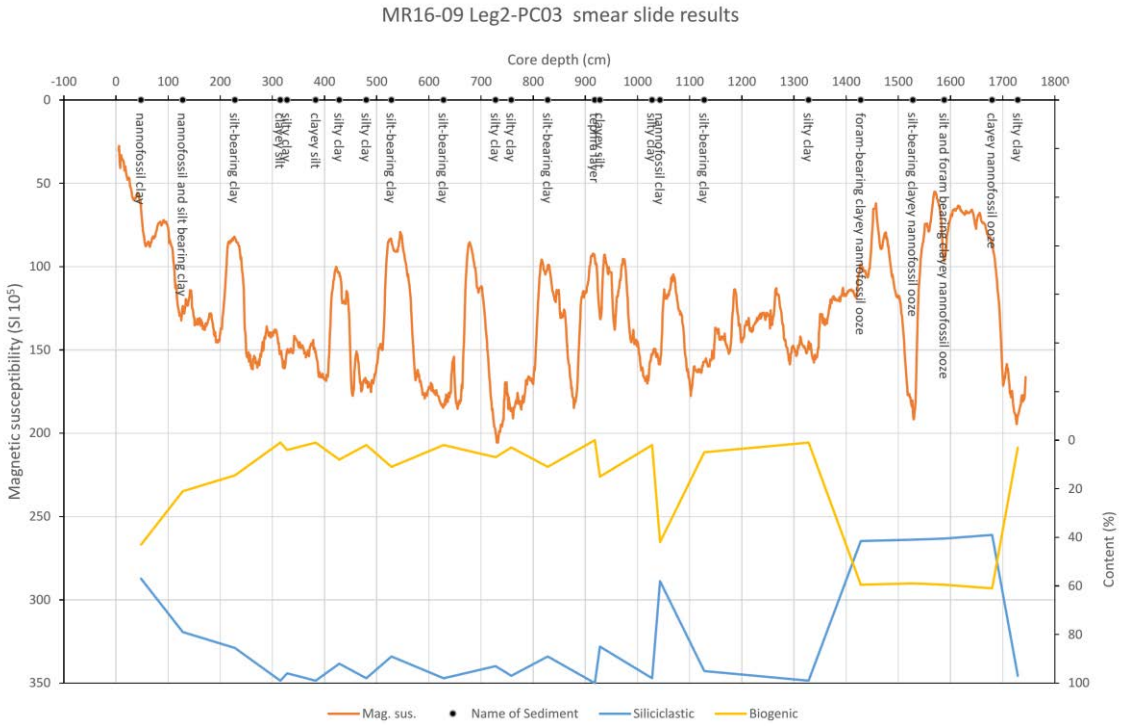

Fig. 4.2.7-8. Graph combining the GEOTEK magnetic susceptibility measurements on core PC03 with the smear slide examinations on the core.

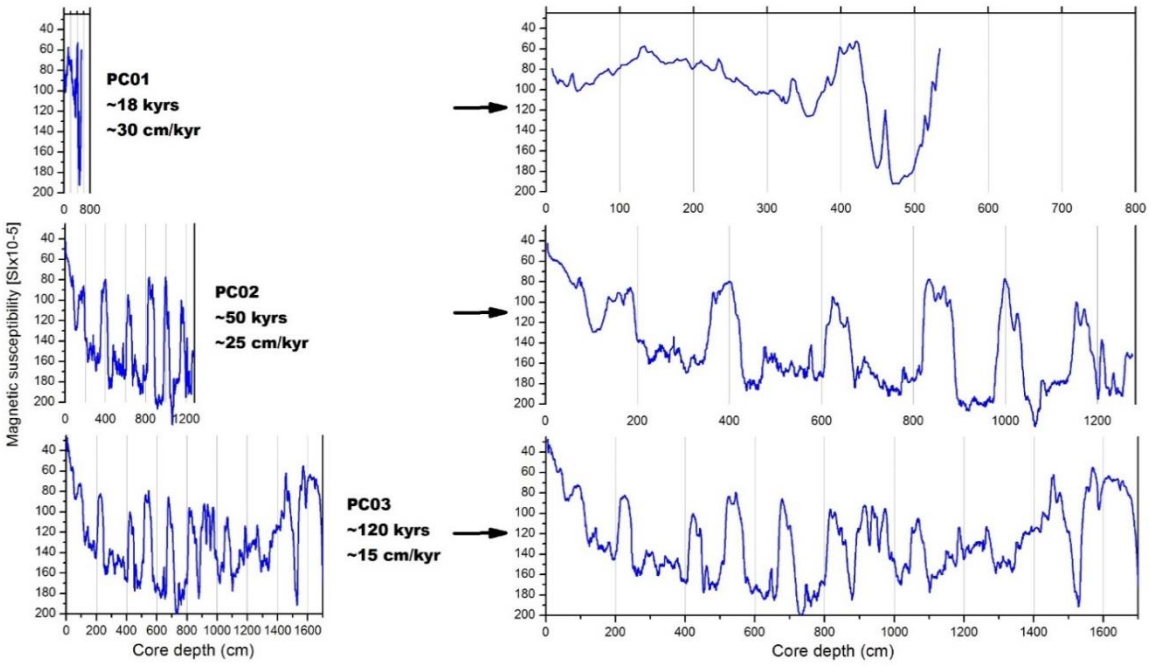

Fig. 4.2.7-9. Correlation of the magnetic susceptibility records of cores PC01, PC02, and PC03 with approximate basal age and average sedimentation rates.

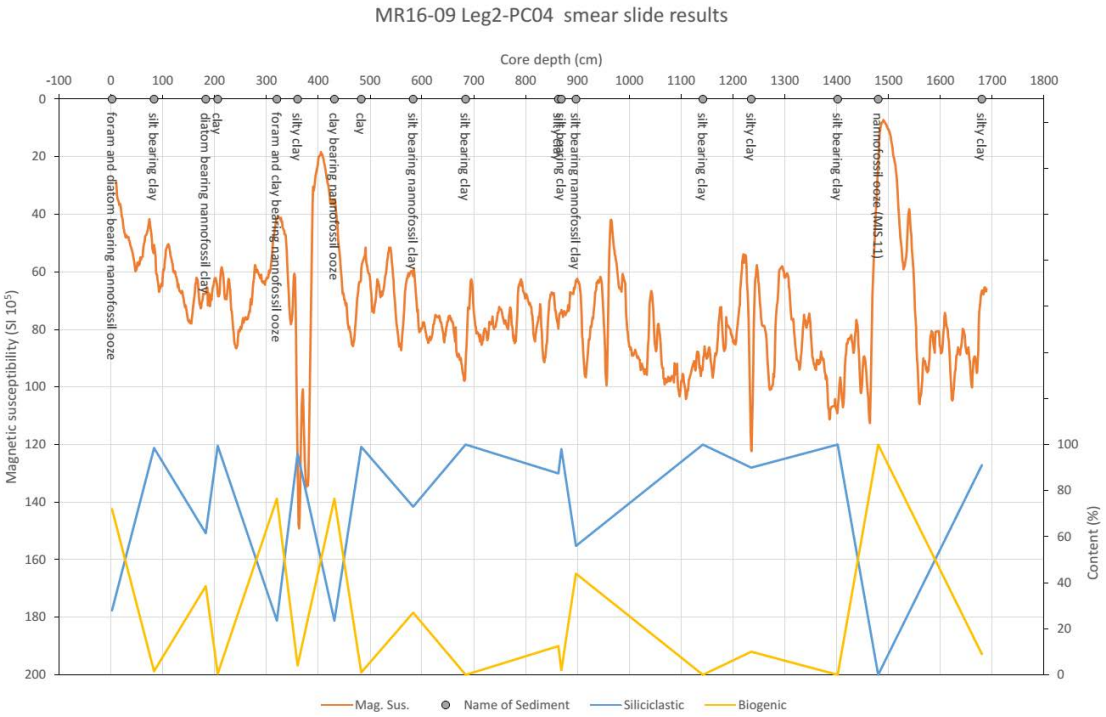

Fig. 4.2.7-10. Graph combining the GEOTEK magnetic susceptibility measurements on core PC04 with the smear slide examinations on the core.

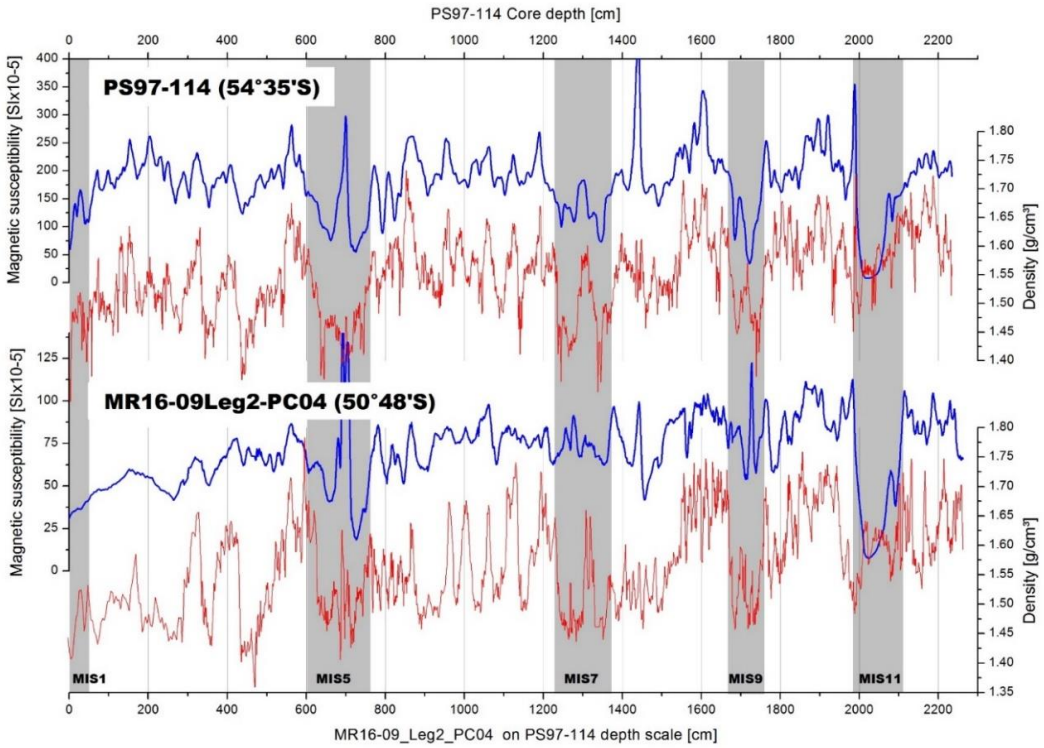

Fig. 4.2.7-11. Correlation of the magnetic susceptibility and GRAPE density data of core PC04 and core PS97/114-2 on a common PS97/114-2 depth scale. Gray bars tentatively indicate the interglacial Marine Isotope Stages 1 to 11.

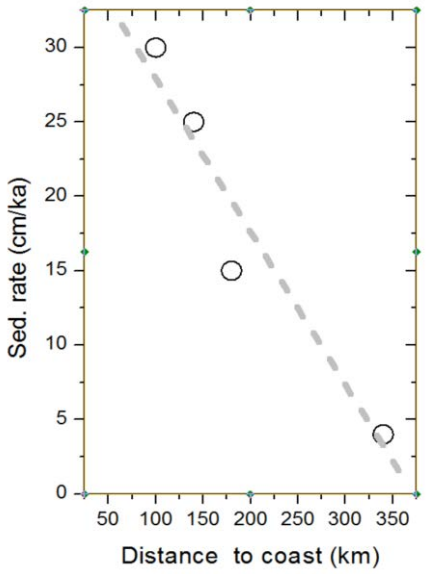

Fig. 4.2.7-12. Close to linear relationship between the average sedimentation rates of cores PC01, PC02, PC03, and PC04 and their distance to the Chilean coast.

4.3 Dredge

4.3.1 Dredge System

(1) Personnel

Yusuke Sato (Marine Works Japan Co. Ltd); satoy@mwj.co.jp
Ei Hatakeyama (Marine Works Japan Co. Ltd); hatakeyamae@mwj.co.jp
Yohei Katayama (Marine Works Japan Co. Ltd); katayamay@mwj.co.jp

(2) Objective

Collection of seafloor rocks and sediments

(3) Instruments and Methods

The dredge sampler system used during MR16-09_Leg2 cruise is shown in Fig.4.1.3-1, showing the configuration of Transponder, Winch wire, Lead wire, Chain, Weight, Pipe dredge, Life wire, Fuse wire and Main Chain-bag Dredge.

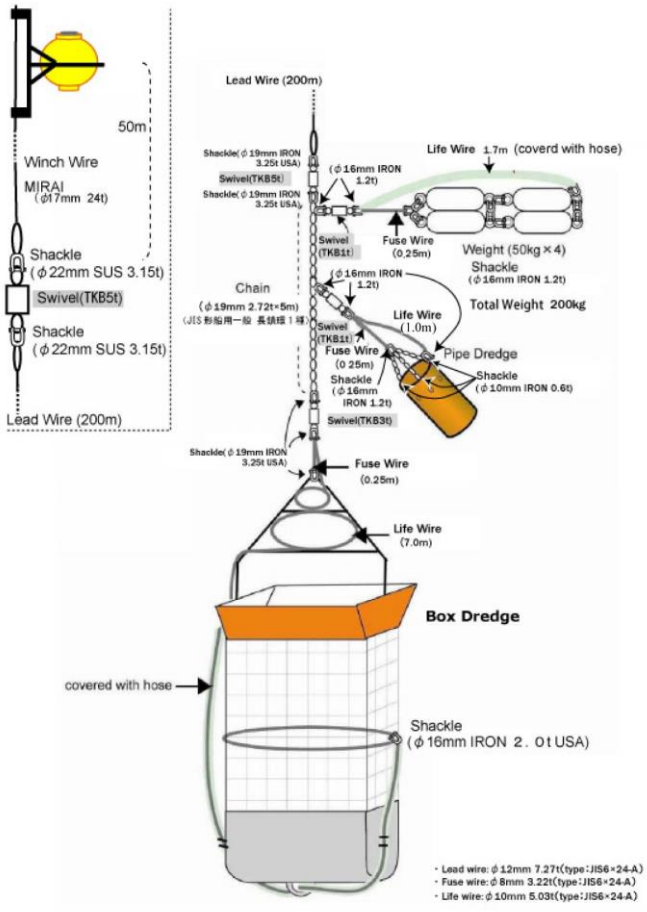

Dredge system with a box-type dredge

Fig. 4.1.3-1. Dredge system with a box-type dredge.

Transponder: Transponder is an equipment that receives acoustic signals and automatically sends out another signal in reply. In this cruise, it is used to make sure the roughly position of the dredge sampler system in water. It was put on the winch wire in two cramps with special housing.

Winch wire: Diameter of winch wire is 17mm. It is 0.983kg weight per one meter in water (i.e. about 983kg for 1,000m in the sea water) and having a 24.2t breaking force.

Lead wire: This wire is prepared for protection against damage to the winch wire, jointed by shackles (3.15t SUS) and a swivel (5t). It is iron wire of 12mm diameter, 200m long and a 7.24t breaking force.

Chain: Chain (19mm diameter, 5m long) is used to stabilize the dredge sampler and was jointed to the lead wire with a swivel (5t) and shackles (ϕ 19).

Weight(50kg per each): The weight is used to assure the dredge sampler is on the bottom as can be observed by the tension meter in the operation room, and linked by shackles (ϕ 16) to the chain together with a swivel (1t), fuse wire (8mm diameter, 0.25m long) and life wire (10mm diameter, 1.7m long).

Pipe dredge: Pipe dredge assumes the function as the backup of the main chain-bag dredge. This is linked as same as the weight. (Life wire is 1m long)

Life wire (chain-bag): End of the life wire (10mm diameter, 7 m long) is connected parallel with fuse wire, and the other end is connected with the middle part of the chain-bag. In the case of fuse wire is broken by a big bite or anchoring, life wire works to prevent the dredge from lost, and keeps the samples in the box type bucket.

Fuse wire: Fuse wire (8mm diameter, 0.25m long) is prepared to release the dredge from big bites that might damage the winch wire. It is jointed to the chain with a swivel (1t or 3t) and shackles in the main chain-bag dredge.

Chain-bag dredge: The square type dredge consists of box type jaw (60*45 cm mouth, 60*27 cm throat), handle (26mm diameter, 85cm long) and steel chain-bag (6 mm diameter, 100cm long) with box type bucket (27*60*50cm) made from stainless steel (5mm thick). The bucket can recover all kinds of sediments on seafloor, it was jointed with shackles to the 0.25 m fuse wire.

About details of wire diameter and breaking force are written in below.

Diameter	Breaking Force
6mm	1.81t
8mm	3.22t
10mm	5.03t
12mm	7.24t

(4) Operation note

Operation of dredging was conducted on the basis of following strategies.

i. *Preparation*

We set the start and end point for dragging of the dredge system on the basis of the contour map.

ii. *The points should be checked before and during deploying the dredge system*

Carefully check on “no loose connections” between the main body, weight, pipe dredge, wires, and chain.

Connect transponder to 50 m of the main wire.

iii. *Approaching to bottom*

Until reach the dredge system to about 100 m depth above the seafloor, the main wire should be rolled out 1.0 m/s.

Keep stopping of wire-out about 3 min, and position and movement of transponder should be

checked.

Wire out restart by the speed of 0.3 m/s until dredge on bottom.

iv. *On bottom*

If we find that the position of transponder is just beneath of stern immediately before the dredge system on bottom, ship should be start to move to the end point in 0.5 knot.

Reach of the dredge system to bottom should be identified on the basis of reduction of tension of the main wire.

The main wire is NOT further rolled out after the dredge system on bottom.

The speed of ship increase to 1.0 knot.

If slight increasing of tension is identified, the speed of ship decrease to 0.5 knot, and several tens of meters (depend on inclinations of slope) of the main wire should be rolled out.

Important point: speed of the dredge system should NOT be more than 1 knot.

In the case of the main wire is rolled in, ship should keep position, and speed of wire is 0.3 m/s.

v. *Off bottom*

We can find out off bottom of the dredge system, if carefully watch the changing of tension of the main wire on the tension meter.

The altitude of 200 or 250 m for transponder is the most important information to identify completely off bottom of the dredge system.

The speed of wire-in should be 0.5 m/s just after off bottom, and increase to 1.0 m/s if altitude of transponder is more than 250 m.

4.3-2. Dredge result

(1) Personnel

Natsue Abe (JAMSTEC)
Shiki Machida (JAMSTEC)
Ryo Anma (Univ. of Tsukuba)
Yuji Orihashi (The Univ. of Tokyo)

(2) Introduction

The Chile Triple Junction (CTJ; Figure 4.3-2-1) is located where subducting spreading centers and accompanying fracture zones of the Chile Ridge system meet with the South American plate. This area is tectonically unique in that the ridge subduction accompanies obduction of an ophiolite nearby (namely, the Taitao ophiolite), providing an excellent opportunity to study the magmatism involved in the ridge subduction processes on land. Our continuous effort toward understanding this magmatism, including the R/V *Mirai* MR08-06 cruise (see Abe, 2009; Harada, 2009), revealed that intensive fore-arc granite magmatism took place during the 6 Ma ridge subduction event (Anma et al., 2009) due to partial melting of the subducting oceanic crust under garnet-free conditions (Kon et al., 2013) to produce I-type granites (Shin et al., 2015), sediments subducted along a fracture zone were incorporated into S-type magmatism in the fore-arc region (Anma and Orihashi, 2013; Shin et al., 2015). Based on these, we planned new dredge sampling for the MR16-09 cruise.

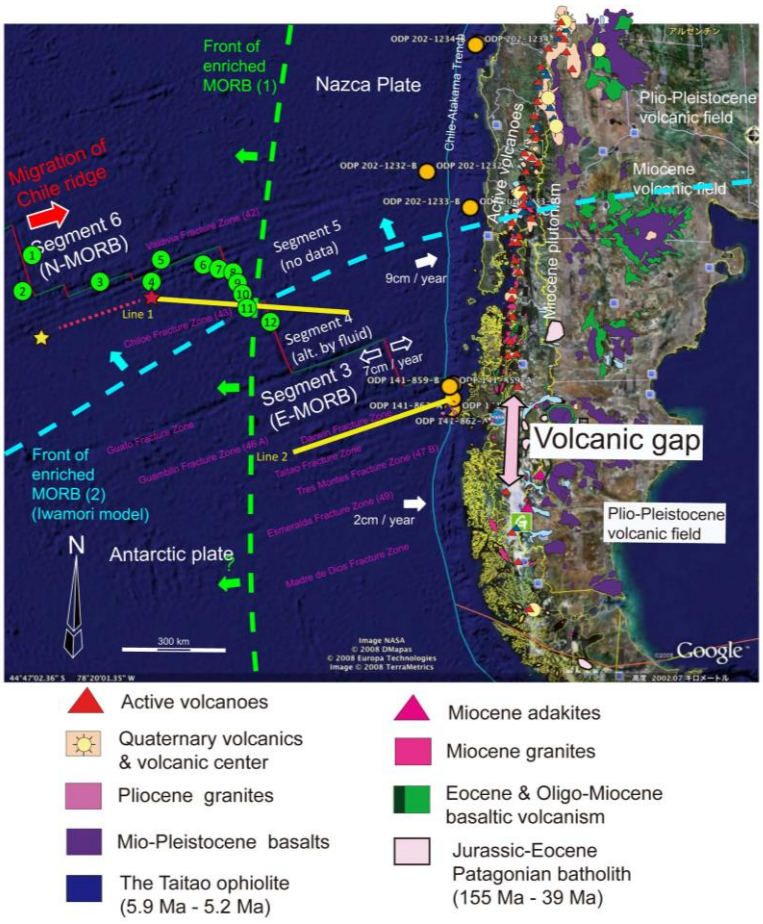

Fig .4-3-2-1. Large area map around survey area.

(3) Objective

The purpose of the dredge sampling in the CTJ area is to collect rock/sediment samples that help to understand solid earth recycling processes occurring/occurred due to subduction of the Chile Ridge system. Target rocks for the dredge operations are 1) igneous rocks distributed in the fore-arc region, 2) MORBs from the Segment 1 of the Chile ridge system and fracture zones, 3) rocks comprising seamounts nearby the subducting Chile Ridge. The dredge in the fore-arc region aims to find unknown igneous activities that are equivalent to the magmatism observed in the Taitao ohiolite-granite complex (Shin et al., 2015). The dredge of MORBs and seamount rocks aims to understand compositions of input materials that subduct and eventually melt to form arc magmas at deeper part of the ridge subduction zone.

(4) Results

Three dredge operations (D11~D13) were performed for the input rocks (MORBs and seamount). The positions of each dredge hauls are listed in the Table 4-3-2-1. D11 to the seamount in the west of Segment 1 recovered pebbles of sub-rounded chert and sandstone, supposedly drop-stones, embedded in mud. Thus, the frank of the seamount was covered by a thick sediment. D12 operation to collect MORB from the Segment 1 was very successful and recovered sum of ~120 kg of basalts partly with quenched glassy rinds. In contrast, D13 to a neighboring mound to the D12 site recovered only few small pieces of volcanic glass (perhaps contamination of D12 dredge) in mud. Furthermore, a dredge operation was planned to collect altered basalts from the fracture zone between Segment 1 and Segment 2 spreading ridges. However, due mostly to wind and current of undesirable direction, this operation was canceled.

Four dredge operations (D14~D17) were performed to find unknown igneous activities in the accretionary complex developed around 47°47'S. We initially planed for dredging nearby the Taitao peninsular for the investigation of the unknown igneous activities, but this attempt was abandoned due to rejection of applied permission for the operation in the Chilean water. As a contingency plan, this area was chosen to find igneous activities due to a ridge subduction event that took place ~14 Ma ago. All dredge operations were successful and we recovered siltstones and sandstones with gravels and conglomerates with different degree of consolidation. The degree of consolidation was measured using a needle penetration tester onboard. The sedimentary rocks from the seaward ridge (D14) were variously consolidated and contain chaotic rocks and various deformation structures including composite foliation and folds developed mainly in mudstones, and calcite veins. Rocks from a landward ridge (D15~17) contain turbidite with various grain size, sedimentary structures, and different degree of consolidation. No calcite vein was observed and deformation texture was less developed comparing to the seaward ridge. These sedimentary rocks will be further examined to understand development of new accretionary prism after the ridge subduction event. A piece of granite was recovered from D16 operation. Further investigation will be made to determine the age of this rock.

(5) References

Abe, N. (2009) MIRAI Cruise Report: MR08-06 Leg1, JAMSTEC Cruise Report, 140 p.

Anma, R., Armstrong, R., Orihashi, Y., Ike, S., Shin, K-C., Kon, Y., Komiya, T., Ota, T., Kagashima, S., Shibuya, T., Yamamoto, S., Veloso, E. E., Fannin, M. and Herve, F. (2009) Are the Taitao granites formed due to subduction of the Chile ridge? Lithos, 113, 246-258.

Anma, R. and Orihashi, Y. (2013) Shallow-depth melt eduction due to ridge subduction: LA-ICPMS U-Pb igneous and detrital zircon ages from the Chile Triple Junction and the Taitao Peninsula, Chilean Patagonia. Geochemical Journal, 47, 149-165.

Harada, N. (2009) MIRAI Cruise Report: MR08-06 Legs. 2 and 3, JAMSTEC Cruise Report, 181 p.

Kon, Y., Komiya, T., Anma, R., Hirata, T., Shibuya, T., Yamamoto, S. and Maruyama, S. (2013) Petrogenesis of the ridge subduction-related granitoids from the Taitao Peninsula, Chile Triple Junction area. Geochemical Journal, 47, 167-183.

Shin, K-C., Anma, R., Nakano, T., Orihashi, Y. and Ike, S. (2015) The Taitao ophiolite-granite complex, Chile: Emplacement of ridge-trench intersection oceanic lithosphere on land and origin of calc-alkaline I-type granites. *Episodes*, 38, 285-299.

Table 4-3-1. Position, depth, tension and hauling time information for each dredge haul during MR16-09 Leg2.

MR16-09 Leg2 Dredge summary

Date (UTC)	Dredge number	Location	On the bottom				Off the bottom				Depth (m)		Tension max. (t)	Survey time
			Lat. (SOQ*)	Lon. (SOQ*)	Lat. (SOJ)	Lon. (SOJ)	Lat. (SOQ*)	Lon. (SOQ*)	Lat. (SOJ)	Lon. (SOJ)	On the bottom	Off the Bottom		
2017/1/23	D11	Off Taitao	46-10.0787S	76-16.3538W	46-10.1219S	76-16.4333W	46-10.0917S	76-17.0023W	46-10.1550S	76-17.2010W	2,574	2,377	2.3	1h10min
2017/1/24	D12	Off Taitao	45-52.4514S	75-58.7050W	45-52-4510S	75-58.8027W	45-52.4599S	75-58.8688W	45-52.4718S	75-59.0717W	3,227	3,307	5.6	32min
2017/1/24	D13	Off Taitao	45-52.6695S	75-59.7638W	45-52.6187S	75-59.7023W	45-52.5500S	75-59.5170W	45-52.4482S	75-59.3372W	3,312	3,281	3.0	40min
2017/1/26	D14	Off Byron	47-46.3587S	76-25.6057W	47-46.3044S	76-25.6099W	47-46.3046S	76-24.8910W	47-46.2416S	76-24.8186W	3,080	2,658	4.3	1h35min
2017/1/26	D15	Off Byron	47-47.5231S	76-02.8022W	47-47.4710S	76-02.8114W	47-47.3277S	76-02.6454W	47-47.2650S	76-02.6813W	1,930	1,755	4.8	1h0min
2017/1/28	D16	Off Byron	47-47.4854S	76-01.8054W	47-47.4266S	76-01.8181W	47-47.2096S	76-01.5343W	47-47.1330S	76-01.5307W	1,831	1,511	2.6	1h11min
2017/1/28	D17	Off Byron	47-47.2193S	76-02.8223W	47-47.1944S	76-02.6611W	47-46.9474S	76-02.5245W	47-46.8179S	76-02.5215W	1,656	1,435	3.0	1h2min

*SOQ = Transponder's position, SOJ = Ship's position

4.4 Biological Sample
Zooplankton: Rationale and Methods for Sample Collection

(1) Personnel:

Prof. Leonardo Castro (COPAS Sur Austral Center, Universidad de Concepción, Chile.

(2) Rationale

During the last years, the use of carbon and nitrogen isotopes has started to be widely utilized to study the structure of the food webs in marine ecosystems. Because enrichment of stable isotopes occurs along the trophic web, stable isotopes such as of carbon (^{13}C) may be used to trace the original carbon source at the base of the web or, as in the case of nitrogen (^{15}N) may be utilized as indicator of the trophic position organisms reaches along the web (Vander Zanden & Rasmussen 1999, Vander Zanden et al. 2001, Bode et al. 2003, 2007; Vargas et al. 2011, Montecinos et al. 2016).

The information available on the marine pelagic community at the Cabo de Hornos Current off the Chilean Patagonia, on its major functional components and the trophic web structure, are very limited. This area, where water masses of different origin (SASW; ESSW, AAIW and EW) (Sievers & Silva 2006, Silva et al. 1997, 1998) converge in a narrow zone both in the horizontal and vertical domain, is expected to contain epi- and mesopelagic organism of diverse origin as well as trophic webs that channelize organic carbon from different sources at different depths. Since some of the micronekton (i.e. myctophid fishes) and mesozooplankton components (i.e. euphausiids) may change their depth of residence during diel vertical migrations or as they develop, changes also in the carbon signature and trophic position of these organisms are also expected to be visualized along the water column.

In the present study, utilizing mesozooplankton samples collected from different depths along the Cabo de Hornos Current, the structure and food web of the epi- and mesopelagic plankton community is assessed by means of stable isotope analyses of the key species zooplankton (and ichthyoplankton) and major functional groups. In principle, differences in the carbon and nitrogen signals ($\delta^{13}C$; $\delta^{15}N$) are expected locally at organisms residing the surface layer according to the influence of major water inputs from the continent (e.g. off the Boca del Guafo, Golfo de Penas; Estuarine Waters). Secondarily, differences are expected also in the vertical plane according to the most common residence layers of the major zooplankton/ichtyoplankton taxa as a result of the influence of the trophic webs associated to the major waters masses present in the area at different depths (SASW; ESSW and AAIW). This information, besides describing for the first time the complex structure of the zooplankton community, will provide insights on the potential importance of the alloctonous material ingress (organic carbon from the continent) to the Cabo de Hornos Current to subsidize the pelagic trophic webs of this Patagonian offshore area.

(3) Methods

Field work. During the MIRAI Cruise MR 16-09 Leg 2, stratified zooplankton samples were collected at 8 bio-oceanographic stations (Table 1). At 7 of these stations, stratified zooplankton samples were collected through oblique tows with a Tucket Trawl net ($1m^2$ mouth opening, 300um mesh, equipped with a GO flowmeter) from 3 (0-50m; 50-400 m; 400-600m) or more strata (up to 6 strata; maximum depth 600m) at day time hours. At an additional station, and due to harsh weather conditions, the stratified oblique sampling was switched to vertical tows with a WP2 net (60 cm mouth diameter, 300um mesh) from 3 depth ranges: 0-50m, 0-400m, 0-600m. On board, the zooplankton samples were splitted and one fraction was preserved in formaline 5% for zooplankton identification and counting, and another was frozen down to -80°C for stable isotope ($\delta^{13}C$; $\delta^{15}N$) analyses.

Table 1. Summary of zooplankton samples collected during the MIRAI Cruise MR 16-09 - Leg 2 along the Cabo de Hornos Current, showing station number, type of net utilized, sampled depth range, and number of subsamples preserved and frozen.

Station	Sampling gear	Sampled Depth Range (m)	Subsamples Formaline 10%	Frozen -80°C	Total subsamples
1	Tucker trawl	0 - 400	1	1	2
		400 - 50	1	1	2
		50 - 0	1	1	2
		0 - 600	1	1	2
		600 - 400	1	1	2
		400 - 0	1	1	2
4	Tucker trawl	0 - 400	1	1	2
		400 - 50	1	1	2
		50 - 0	1	1	2
8	Tucker trawl	0 - 400	1	0	1
		400 - 50	1	1	2
		50 - 0	1	1	2
		0 - 600	1	0	1
		600 - 400	1	1	2
7	Tucker trawl	0 - 400	1	0	1
		400 - 50	1	1	2
		50 - 0	1	1	2
9	Tucker trawl	0 - 400	1	0	1
		400 - 50	1	0	1
		50 - 0	1	0	1
10	Tucker trawl	0 - 400	1	0	1
		400 - 50	1	1	2
		50 - 0	1	1	2
		600 - 400	1	1	2
11B	Tucker trawl	0 - 400	1	1	2
		400 - 50	1	1	2
		50 - 0	1	1	2
		600 - 400	1	1	2
12B	WP2	0 - 600	1	0	1
		0 - 400	1	0	1
		0 - 50	1	0	1
8 stations	7 Tucker + 1 WP2	31 samples	31	21	52

References

Bode, A., Carrera, P., Lens, S., 2003. The pelagic food web in the upwelling ecosystem of Galicia (NW Spain) during spring: natural abundance of stable carbon and nitrogen isotopes. ICES Journal of Marine Science, 60: 11-22.

Bode, A., Alvarez-Ossorio, M.T., Cunha, M.E., Garrido, S., Peleteiro, J.B., Porteiro, C., Valdes, L., Varela, M., 2007. Stable nitrogen isotope studies of the pelagic food web on the Atlantic shelf of the Iberian Peninsula. Progress in Oceanography, 74, 115-131.

Montecinos S., L R. Castro & S Neira. 2016. Stable isotope ($\delta^{13}C$ and $\delta^{15}N$) and trophic position of Patagonian sprat (*Sprattus fuegensis*) from the Northern Chilean Patagonia. Fisheries Research 179 (2016) 139–147.

Sievers H.A. & N Silva. 2006. Masas de agus y circulación en los canales y fiordos australes. En N. Silva y S Palma (Eds),"Avances del conocimiento oceanográfico de las aguas interiores chilenas: Puerto Mont a cabo de Hornos". Comité Oceanográfico Nacional. P Universidad Católica de Valparaíso. Pp. 53-58.

Silva N, C Calvete & H. Sievers. 1997. Características oceanográficas físicas y químicas de canales australes chilenos entre Puerto Montt y Laguna San Rafael (Crucero Cimar-Fiordo l). Ciencia y Tecnología del Mar 20: 23-106

Silva.N, C Calvete & H. Sievers. 1998. Masas de agua y circulación general para algunos canales autrales entre Puerto Montt y Laguna San Rafael, Chile (Crucero CIMAR Fiordo l). Ciencia y Tecnología del Mar 21. 17-48.

Vander Zanden, M.J., Rasmussen, J.B., 1999. Primary consumer delta C-13 and delta N-15 and the trophic position of aquatic consumers. Ecology, 80, 1395-1404.

Vander Zanden, M.J., Rasmussen, J.B., 2001. Variation in delta N-15 and delta C-13 trophic fractionation: Implications for aquatic food web studies. Limnology and Oceanography, 46, 2061-2066.

Vargas, C.A., Martinez, R.A., San Martin, V., Aguayo, M., Silva, N., Torres, R., 2011. Allochthonous subsidies of organic matter across a lake-river-fjord landscape in the Chilean Patagonia: Implications for marine zooplankton in inner fjord areas. Continental Shelf Research, 31, 187-201.

4.5 Suspended Particles

(1) Personnel

Humberto E. Gonzalez and Eduardo Menschel (Universidad Austral de Chile, Valdivia and FONDAP-IDEAL center, Valdivia and Punta Arenas, Chile)

(2) Sampling and scientific motivation

Two types of samples were collected:

1) **Particulate Organic Carbon (POC)**

Methods: From 1.0 to 2.5 Lt of water were filtrated through a pre-combusted glass fiber filters (Whatman GF/F). The filters were stored frozen and at the laboratory were decarbonated (using HCl_2 acid) and dried (at 50ºC overnight). The filter were sent to the University of California at Davis for C and N elemental composition and natural isotopes analysis.

Scientific relevance: The POC constituted an important component of the carbon pool in the ocean and a key component of the carbon biogeochemical cycle (i. e. carbon export to the deep sea). It is a relevant proxy of the food resources available to be channeled through the microbial and particulate food webs in the ocean. In addition, the natural isotope signature can give us insights about the precedence (origin) of this POC.

2) **Microzooplankton (μzoo) composition and abundance**:

Methods: From 7.0 to 12.0 Lt of water were filtrated through a 20 μm nitex sieve and resuspended in a final volume of ca. 300 ml. These samples were preserved with buffered lugol to further analysis at the laboratory.

Scientific relevance: The μzoo are an important component of the heterotrophic functional groups of the plankton, especially in open waters. Some of these groups, such as foraminifers, radiolarians, can be used as paleoceanographic conditions.

Almost no information on POC and μzoo from the deep ocean side of the eastern south Pacific are available. The analysis of these samples would contribute to fill the gap on the knowledge of the quantity and quality of these components.

Station 1 21 Jan. 2017	Position (44º17S 75º36W) Max. Depth = 1928 m	Sampling depth (m)	Filter (Nº)	Water Volume Filtrated for POC (Lt)	Water Volume filtrated for µzoo (Lt)
		0	135	1	10
		10	552	1	7
		25	32	1	7,5
		50	343	1,5	7
		100	79	2	7,5
		700	344	2	7
		1918 (B-10)	252	2	8
Station 4 24 Jan. 2017	Position (46º08S 76º04W) time 00:05 hr, Depth = 2400 m	Sampling depth (m)	Filter (Nº)	Water Volume Filtrated for POC (Lt)	Water Volume filtrated for µzoo (Lt)
		0	307	1	10
		10	30	1	10
		25	162	1	10
		50	166	1,5	10
		100	169	2	10
		300	317	2	10
		700	177	2,5	7
		1918 (B-10)	178	2,5	10

Station 7 28 Jan. 2017	Position (47º47,7S 76º02,6W) time 05:30 hr, Depth = 2000 m	Sampling depth (m)	Filter (Nº)	Water Volume Filtrated for POC (Lt)	Water Volume filtrated for µzoo (Lt)
		0	335	1	11
		10	173	1	11
		25	160	1	11,35
		50	412	1,5	10
		100	251	2	10,2
		300	182	2,5	9,9
		500	181	2,5	9,95
		700	180	2,5	7,1
		1990 (B-10)	179	2,55	9,3

Station 9 29 Jan 2017	Position (48º23,5S 76º28,0W) time 10:00 hr, Depth = 1800 m	Sampling depth (m)	Filter (Nº)	Water Volume Filtrated for POC (Lt)	Water Volume filtrated for µzoo (Lt)
		0	31	1	12,6
		10	167	1	10,85
		25	174	1	10,1
		50	175	1,6	11,3
		100	358	2	10,6
		300	161	2,55	9,9
		500	176	2,6	9
		700	155	2,5	7,6
		1790 (B-10)	329	2,55	10,6
Station 10 31Jan. 2017	Position (50º48,3715S 79º07,096W) time 05:30 hr, Depth = 3851 m	Sampling depth (m)	Filter (Nº)	Water Volume Filtrated for POC (Lt)	Water Volume filtrated for µzoo (Lt)
		0	140	1,5	10,9
		10	328	1	11,1
		25	159	1,5	11,4
		50	60	1,6	10,1
		100	137	2	8,6
		300	138	2,5	11.4
		500	139	2,5	9,1
		700	141	2,5	9,8
		3841 (B-10)	39	2,5	10,15
Station 12B 02 Feb. 2017	Position (54º20,09S 74º38,187W) time 08:00 hr, Depth = 2400 m	Sampling depth (m)	Filter (Nº)	Water Volume Filtrated for POC (Lt)	Water Volume filtrated for µzoo (Lt)
		0	168	1	12,1
		10	20	1	11,1
		25	59	1	7,85
		50	322	1,5	11,1
		100	61	2	10

		300	62	2,7	6,8
		500	63	2,5	10,4
		700	19	2,5	7,65
		2390 (B-10)	18	2,5	9,8

Station 11B 03 Feb. 2017	Position (53º00,08S 75º29,08W) time 01:10 hr, Depth = 1762 m	Sampling depth (m)	Filter (Nº)	Water Volume Filtrated for POC (Lt)	Water Volume filtrated for µzoo (Lt)
		0	142	1	11
		10	146	1	10,5
		25	145	1	10,3
		50	144	2	10,1
		100	64	2	10
		300	89	2,5	10
		500	147	2,5	10,6
		700	34	2,5	7,6
		1752 (B-10)	133	2,5	10

Station 11A 03 Feb. 2017	Position (52º19,0681S 75º56,9148W) time 17:40 hr, Depth = 1880 m	Sampling depth (m)	Filter (Nº)	Water Volume Filtrated for POC (Lt)	Water Volume filtrated for µzoo (Lt)
		0	131	1	11,8
		10	383	1	11,55
		25	37	1	10,5
		50	129	1	10,6
		100	125	2	10,4
		300	134	2,5	10,65
		500	1	2,5	10,95
		700	325	2,5	10,5
		1870 (B-10)	36	2,5	10,45

4.6 Physiological Characteristics of Phytoplankton Assemblages in the Southern Patagonia Pacific Margin Waters

J.L. Iriarte[1] and T. Shiozaki[2]

[1] Centro Investigación Dinámica de Ecosistemas Marinos de Altas Latitudes – IDEAL – Universidad Austral de Chile. COPAS-Sur Austral, Centro de Investigación Oceanográfica en el Pacífico Sur-Oriental (COPAS-Sur Austral), Universidad de Concepción, Chile
[2] Research and Development Center for Global Change, Japan Agency for Marine-Earth Science and Technology – JAMSTEC, Japan

Introduction

High-latitude ecosystems are immersed in environmental regimes that may strongly constrain biological productivity. Rhythms and rates of primary production in these highly seasonal environments depend to a large extent on the timing of nutrient supply and light availability for primary producers. In the fjords and channels of southern Chile, the interaction between oceanic water and freshwater from multiple sources (rivers, surface runoff, snow/glacier melting, precipitation) produces strong vertical and horizontal gradients in salinity, density, inorganic nutrient ratios and light availability. These gradients, and their seasonal and inter-annual changes, may affect both the biomass and composition of phytoplankton assemblages, and ultimately shape the spatial-temporal patterns of carbon fixation, organic matter fluxes, and biogeochemical balances in this region.

Vertical mixing and the exchange of nutrients among the low-salinity, low nutrient and turbid surface layer and the more saline sub-surface layer are the main drivers of spring pulses in primary production and autotrophic biomass. The concentrations of inorganic nutrients show a strongly seasonal signal, with high nitrate and orthophosphate during winter, and lower values during spring, presumably caused by a sharp increase in primary productivity when light availability in near-surface waters increases (Iriarte et al 2007; González et al 2011). Beyond the changes in concentrations of macro and micronutrients, however, changes in freshwater regimes may modify the inorganic chemistry of euphotic-zone waters. In addition, increasing discharges of freshwater from glacier melting and river runoff may alter the acid-base chemistry of near-surface waters, thereby establishing spatial gradients in alkalinity that may in turn determine shifts in phytoplankton composition (e.g. from cyanobacteria/chlorophytes to Diatoms/Dinoflagellates; Chakraborty et al 2011) and productivity (Shi et al 2009). Specifically, combine abiotic factors (e.g. temperature, salinity, Fe, light) may play important role in defining the physiological state of phytoplankton, by inhibitory effects on physiological processes on phytoplankton cells (e.g. respiratory activity). Adaptation mechanisms at cellular level (photosystems I and II, photoprotective pigments) could impact the photochemical efficiency of photosynthesis and thus result in reduced growth rates and photosynthesis efficiency (PS II, F_v/F_m). Basically, our conceptual model would work in the following steps: the presence of high(low) driver (freshwater, wind stress) causes the formation of deep(shallow) mixed layer and pycnocline depth, leading to a rapid water column fluctuation in irradiance (high near surface and low near the pycnocline), which may impinge a great stress on the physiological dynamics of phytoplankton.

The studied area is the large continental shelf of Patagonia (Fig. 1), influenced by freshwater from largest adjacent rivers discharging freshwater. The interplay between freshwater and oceanic water types strongly interact with nutrients supply and may determine the magnitude of phytoplankton biomass and composition. We combine the continuous *in situ* profiling of fluorescence with oceanographic variables in

summer to estimate photosynthetic efficiency, phytoplankton biomass and composition, along with observations of inorganic nutrients, in the continental shelf to address a main question on to what extent the spatial changes in near surface water chemistry may affect phytoplankton community properties in oceanic Patagonian waters.

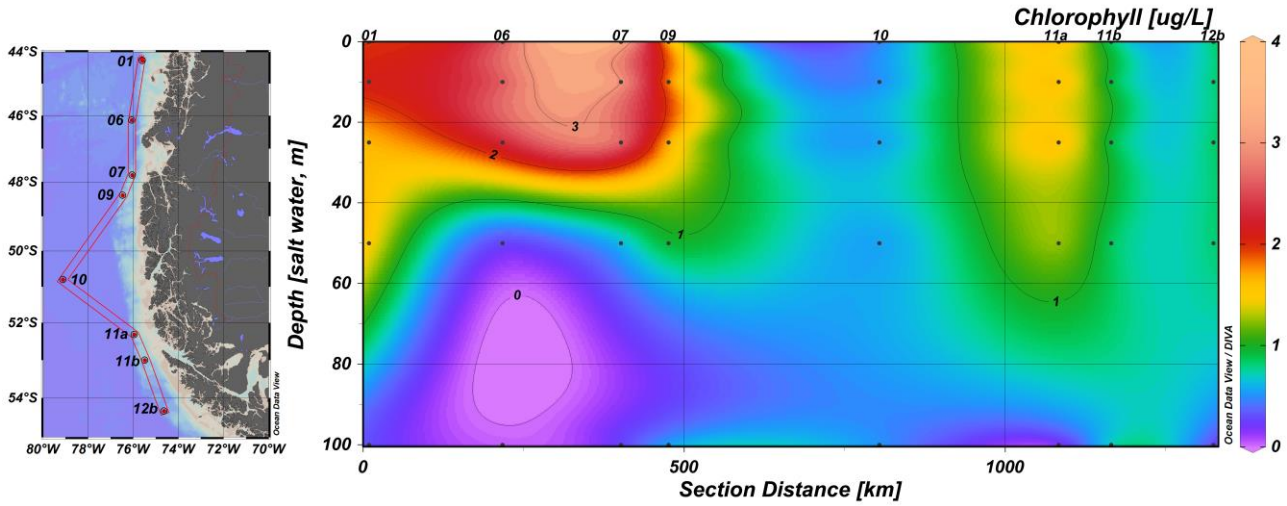

Figure 4.6-1. Autotrophic biomass (as Chlorophyll-*a*, µg L^{-1}) vertical distribution for phytoplankton communities at 8 stations, along the Patagonian shelf, January-February 2017. Depth interval: 0 – 100 m.

Material and Methods

For the first time, we studied physiological features of phytoplankton assemblages in the Patagonian oceanic surface waters using a real-time Fast Repetition Rate Fluorometer (FRRf, Chelsea Technology Group, UK) at 12 stations during austral summer (19 January – 5 February 2017). At each station FRRf equipped with a 20 m cable was deployed in profiling mode with a approximate speed of 0.5 m s^{-1}. With the exception of one station (11B, 21:30 h)), all measurements were done during the daylight between 9:30 to 15:30 h. Fluorescence readings were corrected for background fluorescence signals using filtered seawater previously collected at 10 m depth. All the FRRf deployment were carried out from stern of the vessel. This is essentially a measure of the quantum efficiency of photosystem II and provides an indication of cell health. All these variables and photosynthetic coefficients would give information on the effect of vertical stratification (pycnocline, light, nutricline) on the distribution of $\sigma_{PS\,II}$ during different stations along Patagonia. In addition, it would be expected to find a significant correlation between photosynthetic efficiency fluorescence-based and *in situ* autotrophic biomass (as chlorophyll-a) and primary productivity determined by ^{13}C method in Patagonian waters.

Results and Discussion

Along the shelf transect the highest chlorophyll-a concentrations were observed in the northern area (Sta., 6, 7, 9) at the base of the pycnocline in the upper layer (0 – 25 m) with a mean value of 2.63 μg L^{-1} (range: 1.64 – 3.76 μg L^{-1}) (Fig. 4.6-1). These were associate with the stratified upper part of the water column (< 30 m) and coincided with relatively low salinities (32.75 – 33.35). For the southern stations (Sta., 11, 12), maximum chlorophyll-a values were lower than 1.79 μg L^{-1} (mean: 1.01 μg L^{-1}) in the upper 25 m.

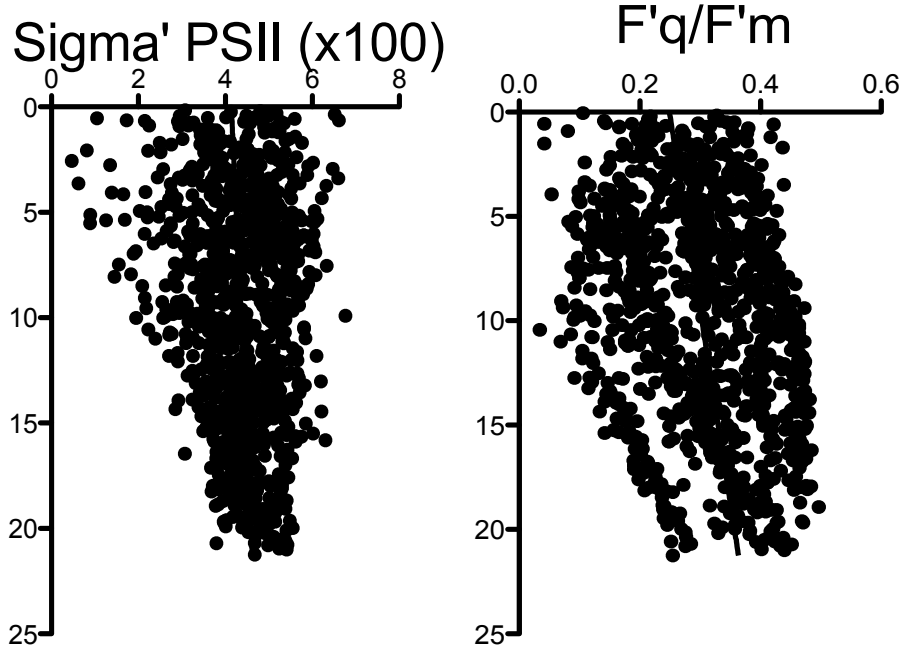

Figure 4.6-2. Vertical distribution of quantum efficiencies of photochemistry in PSII (F'*q*/F'*m*) and functional absorption cross section of photosystem II (σ'_{PSII}: $Å^2$ m^{-2}) for phytoplankton communities under ambient light at 13 stations, along the Patagonian shelf, January-February 2017, were obtained by a Fast Repetition Rate Fluorometer (FRRf). Depth interval: 0.5 – 20 m.

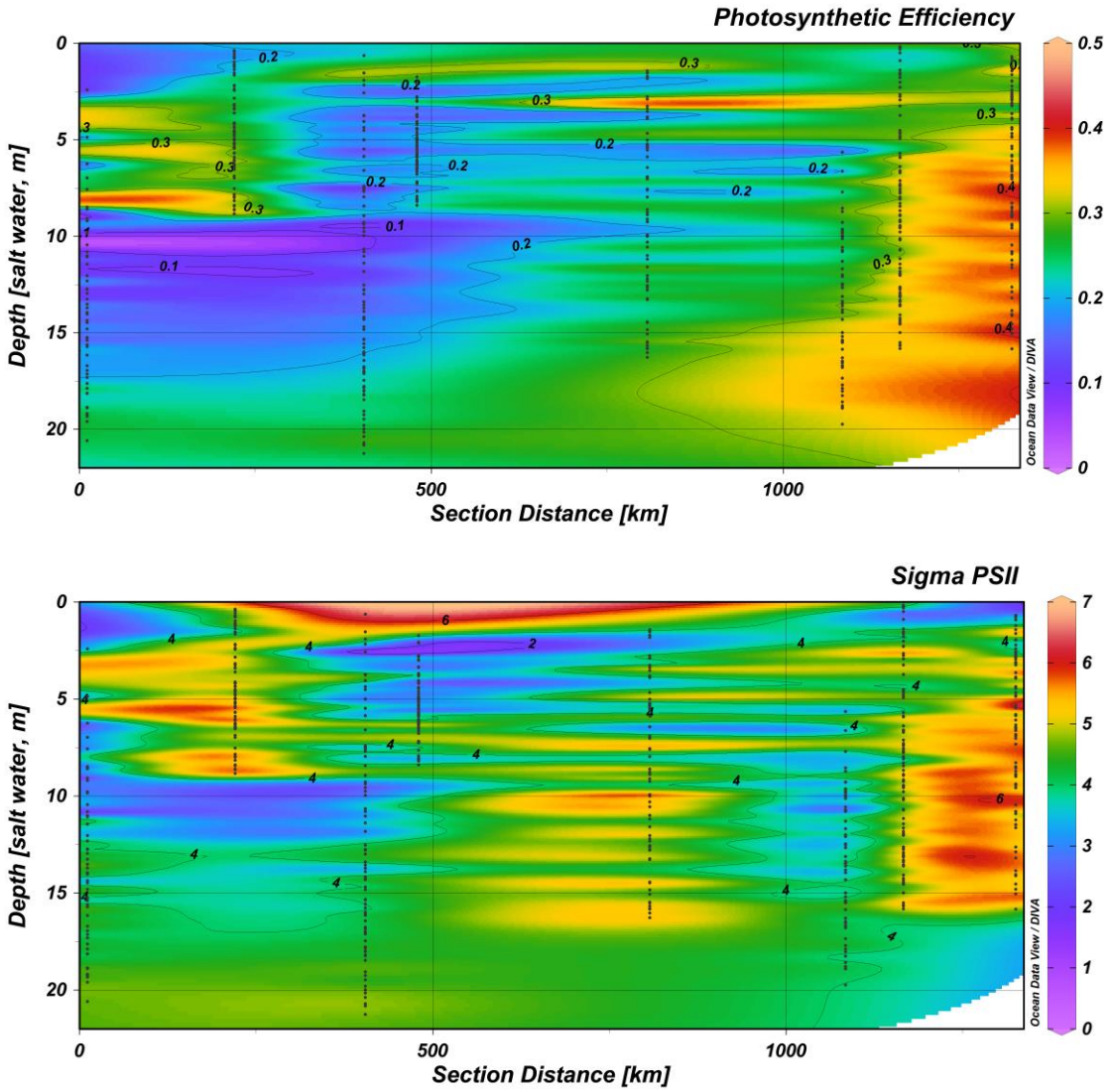

Figure 4.6-3. Horizontal distribution of quantum efficiencies of photochemistry in PSII (F'*q*/F'*m*) and functional absorption cross section of photosystem II (σ'_{PSII}: Å^2 m^{-2}; values*100) for phytoplankton communities under ambient light at 8 stations, along the Patagonian shelf, January-February 2017, were obtained by a Fast Repetition Rate Fluorometer (FRRf). Depth interval: 0.5 – 20 m.

In general, the effective photochemical efficiency of PSII (F'*q*/F'*m*) was low and ranged between 0.081 to 0.497 (median = 0.308, 25% percentile = 0.22, 75% percentile = 0.384), increasing from surface to depth (20 m) at all stations (Y = 0,249 + 0.0054*depth, p = 0.0001, N = 1025) (Fig. 4.6-2). In the northern area (Sta., 2, 6,) F'*q*/F'*m* values increased with depth, attaining values of 0.3 between 5 to 10 m. At southern stations (Sta., 11, 12) 0.3 - 0.45 quantum efficiencies were observed from 5 to 20 m range depth. It seems to be influenced by the low surface salinities, with low values (>0.3) observed in the upper 5 m, while higher than 0.3 quantum efficiency deeper than 5 m were observed at southern stations characterized by deeper mixed layer.

While the functional absorption cross section of photosystem II under ambient light (σ'_{PSII}) showed a homogeneous vertical distribution at most of the stations or slightly increasing with depth (Y = 4.138 + 0.0226*depth, p = 0.0001, N = 1004) (range = 47 – 676 $Å^2$ m^{-2}; median = 442, 25% percentile = 220, 75% percentile = 384) (Fig. 4.6-2) and positive associated to quantum efficiency (Fig. 4.6-3). The preliminary results suggest us that the phytoplankton assemblages were adapted at lower irradiance in the upper 20 m depth. It was interesting to note that at stations 7 and 9, values higher than 500 $Å^2$ m^{-2} functional were observed near surface and well correlated with chorophyll-a biomass.

References

Chakraborty P., T. Acharyya, P.V. Raghunadh Babu & D. Bandhyopadhyay. 2011. Impact of salinity and pH on phytoplankton community in a tropical freshwater system: an investigation with pigment analyses by HPLC. *Journal of Environmental Monitoring*. 13:614-620.

Iriarte J.L., González H.E., Liu K.K., Rivas C. and Valenzuela C. 2007. Spatial and temporal variability of chlorophyll and primary productivity in surface waters of southern Chile (41.5–43°S). *Estuarine Coastal and Shelf Science* 74, 471–480.

González, H.E., Castro, L., Daneri, G., Iriarte, J.L., Silva, N., Vargas, C., Giesecke, R., Sánchez N., 2011. Seasonal plankton variability in Chilean Patagonia fjords: carbon flow through the pelagic food web of the Aysen Fjord and plankton dynamics in the Moraleda Channel basin. *Continental Shelf Research* 31, 225-243.

Shi D., Xu, Y., F.M.M Morel. 2009. Effects of the pH/pCO_2 control method on medium chemistry and phytoplankton growth. *Biogeosciences*, 6:1199-1207

4.7 CTDO$_2$ Measurements

May 14, 2017

(1) Personnel

Hiroshi Uchida (JAMSTEC)
Rei Ito (MWJ)
Sonoka Tanihara (MWJ)
Kenichi Katayama (MWJ)
Shungo Oshitani (MWJ)
Rio Kobayashi (MWJ)
Michinari Sunamura (The University of Tokyo) (CDOM measurement)

(2) Winch arrangements

The CTD package was deployed by using 4.5 Ton Traction Winch System (Dynacon, Inc., Bryan, Texas, USA), which was renewed on the R/V Mirai in April 2014 (e.g. Fukasawa et al., 2004). Primary system components include a complete CTD Traction Winch System with up to 9000 m of 9.53 mm armored cable (Rochester Wire & Cable, LLC, Culpeper, Virginia, USA).

(3) Overview of the equipment

The CTD system was SBE 911plus system (Sea-Bird Electronics, Inc., Bellevue, Washington, USA). The SBE 911plus system controls 36-position SBE 32 Carousel Water Sampler. The Carousel accepts 12-litre Niskin-X water sample bottles (General Oceanics, Inc., Miami, Florida, USA). The SBE 9plus was mounted horizontally in a 36-position carousel frame. SBE's temperature (SBE 3) and conductivity (SBE 4) sensor modules were used with the SBE 9plus underwater unit. The pressure sensor is mounted in the main housing of the underwater unit and is ported to outside through the oil-filled plastic capillary tube. A modular unit of underwater housing pump (SBE 5T) flushes water through sensor tubing at a constant rate independent of the CTD's motion, and pumping rate (3000 rpm) remain nearly constant over the entire input voltage range of 12-18 volts DC. Flow speed of pumped water in standard TC duct is about 2.4 m/s. Two sets of temperature and conductivity modules were used. An SBE's dissolved oxygen sensor (SBE 43) was placed between the primary conductivity sensor and the pump module. Auxiliary sensors, a Deep Ocean Standards Thermometer (SBE 35), an altimeter (PSA-916T; Teledyne Benthos, Inc., North Falmous, Massachusetts, USA), an oxygen optodes (RINKO-III; JFE Advantech Co., Ltd, Kobe Hyogo, Japan), a fluorometers (Seapoint sensors, Inc., Kingston, New Hampshire, USA), a transmissometer (C-Star Transmissometer; WET Labs, Inc., Philomath, Oregon, USA), a turbidity meter (Seapoint Sensors, Inc., Exeter, New Hampshire, USA), a Photosynthetically Active Radiation (PAR) sensor (Satlantic, LP, Halifax, Nova Scotia, Canada), and a colored dissolved organic matter (ECO FL CDOM, WET Labs, Inc., Philomath, Oregon, USA) were also used with the SBE 9plus underwater unit. To minimize rotation of the CTD package, a heavy stainless frame (total weight of the CTD package without sea water in the bottles is about 1000 kg) was used with an aluminum plate (54 × 90 cm).

Summary of the system used in this cruise

36-position Carousel system

Deck unit:

SBE 11plus, S/N 11P54451-0872

Under water unit:

SBE 9plus, S/N 09P21746-0575 (79492)

Temperature sensor:

SBE 3, S/N 031525 (primary)

SBE 3plus, S/N 03P4421 (secondary)

Conductivity sensor:

SBE 4, S/N 042435 (primary)

SBE 4, S/N 041088 (secondary)

Oxygen sensor:

SBE 43, S/N 432471

JFE Advantech RINKO-III, S/N 0024 (foil batch no. 144002A)

Pump:

SBE 5T, S/N 054595 (primary)

SBE 5T, S/N 053293 (secondary)

Altimeter:

PSA-916T, S/N 1157

Deep Ocean Standards Thermometer:

SBE 35, S/N 0045

Fluorometer:

Seapoint Sensors, Inc., S/N 3618 (measurement range: 0-15 μg/L) (Gain: 10X)

Turbidity meter:

Seapoint Sensors, Inc., S/N 14953 (measurement range: 0-500 FTU) (Gain: 5X) for leg 2
(measurement range: 0-25 FTU) (Gain: 100X) for leg 3

Transmissometer:

C-Star, S/N CST-1726DR

PAR:

Satlantic LP, S/N 1025

CDOM:

ECO FL CDOM, S/N FLCDRTD-2014 (measurement range: 0-500 ppb)

Carousel Water Sampler:

SBE 32, S/N 3254451-0826

Water sample bottle:

12-litre Niskin-X model 1010X (no TEFLON coating)

General Oceanics, Inc., Miami, Florida, USA,

(4) Pre-cruise calibration

i. Pressure

The Paroscientific series 4000 Digiquartz high pressure transducer (Model 415K: Paroscientific, Inc.,

Redmond, Washington, USA) uses a quartz crystal resonator whose frequency of oscillation varies with pressure induced stress with 0.01 per million of resolution over the absolute pressure range of 0 to 15000 psia (0 to 10332 dbar). Also, a quartz crystal temperature signal is used to compensate for a wide range of temperature changes at the time of an observation. The pressure sensor has a nominal accuracy of 0.015 % FS (1.5 dbar), typical stability of 0.0015 % FS/month (0.15 dbar/month), and resolution of 0.001 % FS (0.1 dbar). Since the pressure sensor measures the absolute value, it inherently includes atmospheric pressure (about 14.7 psi). SEASOFT subtracts 14.7 psi from computed pressure automatically.

Pre-cruise sensor calibrations for linearization were performed at SBE, Inc. The time drift of the pressure sensor is adjusted by periodic recertification corrections against an electronic dead-weight tester (Model E-DWT-H, S/N 181, Fluke Co, Phoenix, Arizona, USA, Calibrated on 3 April 2016 at Ohte Giken, Inc., Tsukuba, Ibaraki, Japan). The corrections are performed at JAMSTEC, Yokosuka, Kanagawa, Japan by Marine Works Japan Ltd. (MWJ), Yokohama, Kanagawa, Japan, usually once in a year in order to monitor sensor time drift and linearity.

S/N 0575, 13 April 2016

slope = 0.99982448

offset = 2.98685

ii. Temperature (SBE 3)

The temperature sensing element is a glass-coated thermistor bead in a stainless steel tube, providing a pressure-free measurement at depths up to 10500 (6800) m by titanium (aluminum) housing. The SBE 3 thermometer has a nominal accuracy of 1 mK, typical stability of 0.2 mK/month, and resolution of 0.2 mK at 24 samples per second. The premium temperature sensor, SBE 3plus, is a more rigorously tested and calibrated version of standard temperature sensor (SBE 3).

Pre-cruise sensor calibrations were performed at SBE, Inc.

S/N 031525, 7 May 2016

S/N 03P4421, 7 May 2016

iii. Conductivity (SBE 4)

The flow-through conductivity sensing element is a glass tube (cell) with three platinum electrodes to provide in-situ measurements at depths up to 10500 (6800) m by titanium (aluminum) housing. The SBE 4 has a nominal accuracy of 0.0003 S/m, typical stability of 0.0003 S/m/month, and resolution of 0.00004 S/m at 24 samples per second. The conductivity cells have been replaced to newer style cells for deep ocean measurements.

Pre-cruise sensor calibrations were performed at SBE, Inc.

S/N 042435, 12 May 2016

S/N 041088, 12 May 2016

The value of conductivity at salinity of 35, temperature of 15 °C (IPTS-68) and pressure of 0 dbar is 4.2914 S/m.

iv. Oxygen (SBE 43)

The SBE 43 oxygen sensor uses a Clark polarographic element to provide in-situ measurements at depths up to 7000 m. The range for dissolved oxygen is 120 % of surface saturation in all natural waters, nominal accuracy is 2 % of saturation, and typical stability is 2 % per 1000 hours.

Pre-cruise sensor calibration was performed at SBE, Inc.

S/N 432471, 10 May 2016

v. Deep Ocean Standards Thermometer

Deep Ocean Standards Thermometer (SBE 35) is an accurate, ocean-range temperature sensor that can be standardized against Triple Point of Water and Gallium Melt Point cells and is also capable of measuring temperature in the ocean to depths of 6800 m. The SBE 35 was used to calibrate the SBE 3 temperature sensors in situ (Uchida et al., 2007).

Pre-cruise sensor linearization was performed at SBE, Inc.

S/N 0045, 27 September 2002

Then the SBE 35 is certified by measurements in thermodynamic fixed-point cells of the TPW (0.01 °C) and GaMP (29.7646 °C). The slow time drift of the SBE 35 is adjusted by periodic recertification corrections. Pre-cruise sensor calibration was performed at SBE, Inc. Since 2014, fixed-point cells traceable to NIST temperature standards is directly used in the manufacturer's calibration of the SBE 35 (Uchida et al., 2015). Since 2016, pre-cruise sensor calibration was performed at RCGC/JAMSTEC by using fixed-point cells traceable to NMIJ temperature standards.

S/N 0045, 30 June 2016 (slope and offset correction)

Slope = 1.000023

Offset = –0.001053

The time required per sample = 1.1 × NCYCLES + 2.7 seconds. The 1.1 seconds is total time per an acquisition cycle. NCYCLES is the number of acquisition cycles per sample and was set to 4. The 2.7 seconds is required for converting the measured values to temperature and storing average in EEPROM.

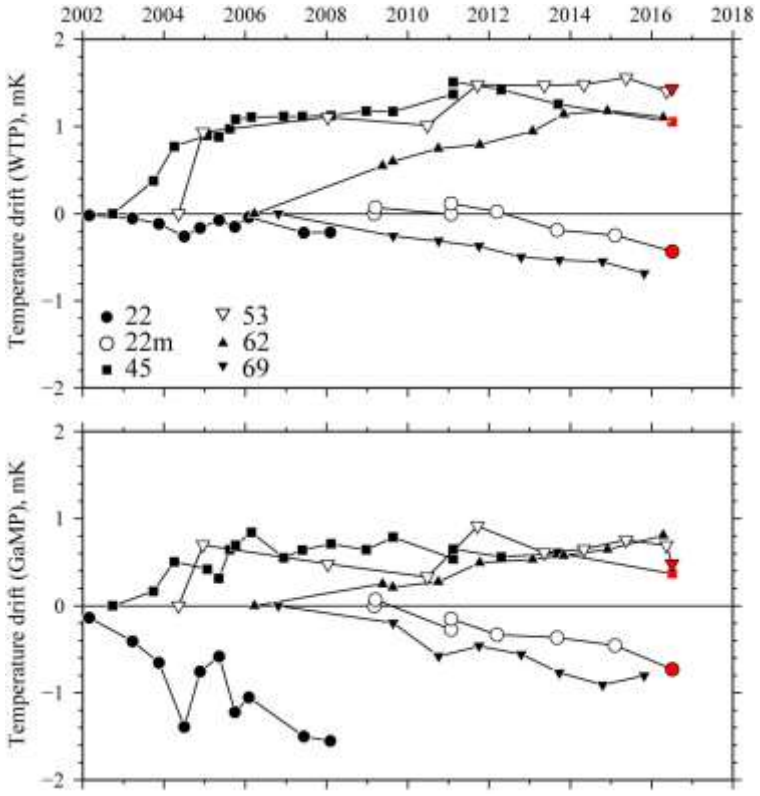

Fig. 4.7.1. Time drifts (temperature offsets relative to the first calibration) of six reference thermometers (SBE 35) based on laboratory calibrations in fixed-point cells. Results performed at JAMSTEC are shown in red marks.

vi. Altimeter

Benthos PSA-916T Sonar Altimeter (Teledyne Benthos, Inc.) determines the distance of the target from the unit by generating a narrow beam acoustic pulse and measuring the travel time for the pulse to bounce back from the target surface. It is rated for operation in water depths up to 10000 m. The PSA-916T uses the nominal speed of sound of 1500 m/s.

vii. Oxygen optode (RINKO)

RINKO (JFE Alec Co., Ltd.) is based on the ability of selected substances to act as dynamic fluorescence quenchers. RINKO model III is designed to use with a CTD system which accept an auxiliary analog sensor, and is designed to operate down to 7000 m.

Data from the RINKO can be corrected for the time-dependent, pressure-induced effect by means of the same method as that developed for the SBE 43 (Edwards et al., 2010). The calibration coefficients, H1 (amplitude of hysteresis correction), H2 (curvature function for hysteresis), and H3 (time constant for hysteresis) were determined empirically as follows.

H1 = 0.0055 (for S/N 0024)

H2 = 5000 dbar

H3 = 2000 seconds

Outputs from RINKO are the raw phase shift data. The RINKO can be calibrated by the modified Stern-Volmer equation slightly modified from a method by Uchida et al. (2010):

$$O_2\ (\mu mol/l) = [(V_0 / V)^E - 1] / K_{sv}$$

where V is voltage, V_0 is voltage in the absence of oxygen, K_{sv} is Stern-Volmer constant. The coefficient E corrects nonlinearity of the Stern-Volmer equation. The V_0 and the K_{sv} are assumed to be functions of temperature as follows.

$$K_{sv} = C_0 + C_1 \times T + C_2 \times T^2$$

$$V_0 = 1 + C_3 \times T$$

$$V = C_4 + C_5 \times V_b$$

where T is CTD temperature (°C) and V_b is raw output (volts). V_0 and V are normalized by the output in the absence of oxygen at 0°C. The oxygen concentration is calculated using accurate temperature data from the CTD temperature sensor instead of temperature data from the RINKO. The pressure-compensated oxygen concentration O_{2c} can be calculated as follows.

$$O_{2c} = O_2\ (1 + C_p p / 1000)$$

where p is CTD pressure (dbar) and C_p is the compensation coefficient. Since the sensing foil of the optode is permeable only to gas and not to water, the optode oxygen must be corrected for salinity. The salinity-compensated oxygen can be calculated by multiplying the factor of the effect of salt on the oxygen solubility (Garcia and Gordon, 1992).

Pre-cruise sensor calibrations were performed at RCGC/JAMSTEC.

S/N 0024, 10 May 2015

viii. Fluorometer

The Seapoint Chlorophyll Fluorometer (Seapoint Sensors, Inc., Kingston, New Hampshire, USA) provides in-situ measurements of chlorophyll-a at depths up to 6000 m. The instrument uses modulated blue LED lamps and a blue excitation filter to excite chlorophyll-a. The fluorescent light emitted by the chlorophyll-a passes through a red emission filter and is detected by a silicon photodiode. The low level signal is then processed using synchronous demodulation circuitry, which generates an output voltage proportional to chlorophyll-a concentration.

ix. Transmissometer

The C-Star Transmissometer (WET Labs, Inc., Philomath, Oregon, USA) measures light transmittance at a single wavelength (650 nm) over a know path (25 cm). In general, losses of light propagating through water can be attributed to two primary causes: scattering and absorption. By projecting a collimated beam of light through the water and placing a focused receiver at a known distance away, one can quantify these losses. The ratio of light gathered by the receiver to the amount originating at the source is known as the beam transmittance. Suspended particles, phytoplankton, bacteria and dissolved organic matter contribute to the losses sensed by the instrument. Thus, the instrument provides information both for an indication of the total concentrations of matter in the water as well as for a value of the water clarity.

Light transmission T_r (in %) and beam attenuation coefficient c_p are calculated from the sensor output (V in volt) as follows.

$$T_r = (c_0 + c_1 V) \times 100$$

$$c_p = -(1 / 0.25) \ln(T_r / 100)$$

Pre-cruise sensor calibration was performed at WET Labs.

S/N CST-1726DR, 26 May 2015

x. Turbidity meter

The Seapoint turbidity meter (Seapoint Sensors, Inc., Kingston, New Hampshire, USA) detects light scattered by particles suspended in water at depths up to 6000 m. The sensor generates an output voltage proportional to turbidity or suspended solids. The unique optical design confines the sensing volume to within 5 cm of the sensor.

xi. PAR

Photosynthetically Active Radiation (PAR) sensors (Satlantic, LP, Halifax, Nova Scotia, Canada) provide highly accurate measurements of PAR (400 – 700 nm) for a wide range of aquatic and terrestrial applications. The ideal spectral response for a PAR sensor is one that gives equal emphasis to all photons between 400 – 700 nm. Satlantic PAR sensors use a high quality filtered silicon photodiode to provide a near equal spectral response across the entire wavelength range of the measurement.

Pre-cruise sensor calibration was performed at Satlantic, LP.

S/N 1025, 6 July 2015

xii. CDOM

The Environmental Characterization Optics (ECO) miniature fluorometer (WET Labs, Inc., Philomath, Oregon, USA) allows the user to measure relative Colored Dissolved Organic Matter (CDOM) concentrations by directly measuring the amount of fluorescence emission in a sample volume of water. The CDOM fluorometer uses an UV LED to provide the excitation source. An interference filter is used to reject the small amount of out-of-band light emitted by the LED. The light from the source enters the water volume at an angle of approximately 55-60 degrees with respect to the end face of the unit. Fluoresced light is received by a detector positioned where the acceptance angle forms a 140-degree intersection with the source beam. An interference filter is used to discriminate against the scattered excitation light.

CDOM (Quinine Dihydrate Equivalent) concentration expressed in ppb can be derived using the equation as follows.

CDOM = Scale Factor * (Output – Dark Counts)

Pre-cruise sensor calibration was performed at WET Labs.

S/N FLCDRTD-2014, 1 September 2015

Dark Counts: 0.025 V

Scale Factor: 106 ppb/V

(5) Data collection and processing

i. Data collection

CTD system was powered on at least 20 minutes in advance of the data acquisition to stabilize the pressure sensor and was powered off at least two minutes after the operation in order to acquire pressure data on the ship's deck.

The package was lowered into the water from the starboard side and held 10 m beneath the surface in order to activate the pump. After the pump was activated, the package was lifted to the surface and lowered at a rate of 1.0 m/s to 200 m (or 300 m when significant wave height was high) then the package was stopped to operate the heave compensator of the crane. The package was lowered again at a rate of 1.2 m/s to the bottom. For the up cast, the package was lifted at a rate of 1.1 m/s except for bottle firing stops. As a rule, the bottle was fired after waiting from the stop for more than 20 seconds and the package was stayed at least 5 seconds for measurement of the SBE 35 at each bottle firing stops. For depths where vertical gradient of water properties were expected to be large (from surface to thermocline), the bottle was exceptionally fired after waiting from the stop for 60 seconds to enhance exchanging the water between inside and outside of the bottle. At 200 m (or 300 m) from the surface, the package was stopped to stop the heave compensator of the crane.

Water samples were collected using a 36-bottle SBE 32 Carousel Water Sampler with 12-litre Niskin-X bottles. Before a cast taken water for CFCs, the bottle frame and Niskin-X bottles were wiped with acetone.

Data acquisition software

SEASAVE-Win32, version 7.23.2

ii. Data collection problems

(a) Miss trip, miss fire, and remarkable leak

Miss trip, miss fire and remarkable leak occurred during the cruise were listed below.

Miss trip	Miss fire	Leak
none	none	007_1 #20 end closure: O-ring of the end closure replaced
		010_1 #21 end closure: O-ring of the end closure replaced
		022_1 #22 end closure: O-ring of the end closure checked
		024_1 #4 end closure: O-ring of the end closure checked

(b) Slight leaks

Slight leaks were observed from the root of stopcocks during drawing of the samples at station leg3_011_1 (#2, #4, #5, #7, #11, #12), leg3_015_1 (#25, #26, #27, #29), leg3_016_1 (#25, #27), leg3_018_1 (#3), and leg3_026_1 (#36). The bottle flags for those bottles were set to 2 since the bottle data (salinity and oxygen) were normal and there was no leak for those bottles at the leak check before the drawing of the samples.

(c) Noise in down cast data

Transmissometer data were noisy at station leg2_006_1 (504~506, 519~521, 820~826, 833~838, 939~947, 968~970, 1063~1067, 1255~1259 dbar), leg2_007_1 (117~118, 1022~1025 dbar), leg2_12B_1 (736~741, 1035~1037 dbar), leg2_11B_1 (131~133 dbar), leg3_009_1 (1071-1076 dbar), leg3_015_1 (821~826 dbar), leg3_016_1 (1497~1541, 1574~1578 dbar), leg3_021_1 (400~527 dbar), leg3_023_1 (992~998 dbar), leg3_024_1 (2248~2253 dbar) and leg3_025_1 (64~65, 473~475 dbar), and the data were removed and linearly interpolated.

iii. Data processing

SEASOFT consists of modular menu driven routines for acquisition, display, processing, and archiving of oceanographic data acquired with SBE equipment. Raw data are acquired from instruments and are stored as unmodified data. The conversion module DATCNV uses instrument configuration and calibration coefficients to create a converted engineering unit data file that is operated on by all SEASOFT post processing modules. The following are the SEASOFT and original software data processing module sequence and specifications used in the reduction of CTD data in this cruise.

Data processing software

SBEDataProcessing-Win32, version 7.23.2

DATCNV converted the raw data to engineering unit data. DATCNV also extracted bottle information where scans were marked with the bottle confirm bit during acquisition. The duration was set to 4.4 seconds, and the offset was set to 0.0 second. The hysteresis correction for the SBE 43 data (voltage) was applied for both profile and bottle information data.

RINKOCOR (original module, version 1.0) corrected the time-dependent, pressure-induced effect (hysteresis) of the RINKO for both profile data.

RINKOCORROS (original module, version 1.0) corrected the time-dependent, pressure-induced effect (hysteresis) of the RINKO for bottle information data by using the hysteresis-corrected profile data.

BOTTLESUM created a summary of the bottle data. The data were averaged over 4.4 seconds.

ALIGNCTD converted the time-sequence of sensor outputs into the pressure sequence to ensure that all calculations were made using measurements from the same parcel of water. For a SBE 9plus CTD with the ducted temperature and conductivity sensors and a 3000-rpm pump, the typical net advance of the conductivity relative to the temperature is 0.073 seconds. So, the SBE 11plus deck unit was set to advance the primary and the secondary conductivity for 1.73 scans (1.75/24 = 0.073 seconds). Oxygen data are also systematically delayed with respect to depth mainly because of the long time constant of the oxygen sensor and of an additional delay from the transit time of water in the pumped plumbing line. This delay was compensated by 5 seconds advancing the SBE 43 oxygen sensor output (voltage) relative to the temperature data. Delay of the RINKO data was also compensated by 1 second advancing sensor output (voltage) relative to the temperature data. Delay of the transmissometer data was also compensated by 2 seconds advancing sensor output (voltage) relative to the temperature data.

WILDEDIT marked extreme outliers in the data files. The first pass of WILDEDIT obtained an accurate estimate of the true standard deviation of the data. The data were read in blocks of 1000 scans. Data greater than 10 standard deviations were flagged. The second pass computed a standard deviation over the same 1000 scans excluding the flagged values. Values greater than 20 standard deviations were marked bad. This process was applied to pressure, temperature, conductivity, and SBE 43 output.

CELLTM used a recursive filter to remove conductivity cell thermal mass effects from the measured

conductivity. Typical values used were thermal anomaly amplitude alpha = 0.03 and the time constant 1/beta = 7.0.

FILTER performed a low pass filter on pressure with a time constant of 0.15 seconds. In order to produce zero phase lag (no time shift) the filter runs forward first then backwards.

WFILTER performed as a median filter to remove spikes in fluorometer, turbidity meter, transmissometer, and CDOM data. A median value was determined by 49 scans of the window. For CDOM data, an additional box-car filter with a window of 361 scans was applied to remove noise.

SECTIONU (original module, version 1.1) selected a time span of data based on scan number in order to reduce a file size. The minimum number was set to be the start time when the CTD package was beneath the sea-surface after activation of the pump. The maximum number was set to be the end time when the depth of the package was 1 dbar below the surface. The minimum and maximum numbers were automatically calculated in the module.

LOOPEDIT marked scans where the CTD was moving less than the minimum velocity of 0.0 m/s (traveling backwards due to ship roll).

DESPIKE (original module, version 1.0) removed spikes of the data. A median and mean absolute deviation was calculated in 1-dbar pressure bins for both down- and up-cast, excluding the flagged values. Values greater than 4 mean absolute deviations from the median were marked bad for each bin. This process was performed 2 times for temperature, conductivity, SBE 43, and RINKO output.

DERIVE was used to compute oxygen (SBE 43).

BINAVG averaged the data into 1-dbar pressure bins. The center value of the first bin was set equal to the bin size. The bin minimum and maximum values are the center value plus and minus half the bin size. Scans with pressures greater than the minimum and less than or equal to the maximum were averaged. Scans were interpolated so that a data record exist every dbar.

BOTTOMCUT (original module, version 0.1) deleted the deepest pressure bin when the averaged scan number of the deepest bin was smaller than the average scan number of the bin just above.

DERIVE was re-used to compute salinity, potential temperature, and density (σ_θ).

SPLIT was used to split data into the down cast and the up cast.

Remaining spikes in the CTD data were manually eliminated from the 1-dbar-averaged data. The data gaps resulting from the elimination were linearly interpolated with a quality flag of 6.

(6) Post-cruise calibration

i. Pressure

The CTD pressure sensor offset in the period of the cruise was estimated from the pressure readings on the ship deck. For best results the Paroscientific sensor was powered on for at least 20 minutes before the operation. In order to get the calibration data for the pre- and post-cast pressure sensor drift, the CTD deck pressure was averaged over first and last one minute, respectively. Then the atmospheric pressure deviation from a standard atmospheric pressure (14.7 psi) was subtracted from the CTD deck pressure to check the pressure sensor time drift. The atmospheric pressure was measured at the captain deck (20 m high from the base line) and sub-sampled one-minute interval as a meteorological data.

Time series of the CTD deck pressure is shown in Figs. 4.7.2 and 4.7.3. The CTD pressure sensor offset was estimated from the deck pressure. Mean of the pre- and the post-casts data over the whole period gave an estimation of the pressure sensor offset (0.66 dbar) from the pre-cruise calibration. The post-cruise correction of the pressure data was carried out by subtracting 0.66 dbar from the pressure data. Figs. 4.7.2 and 4.7.3 show the pressure data after the post-cruise correction.

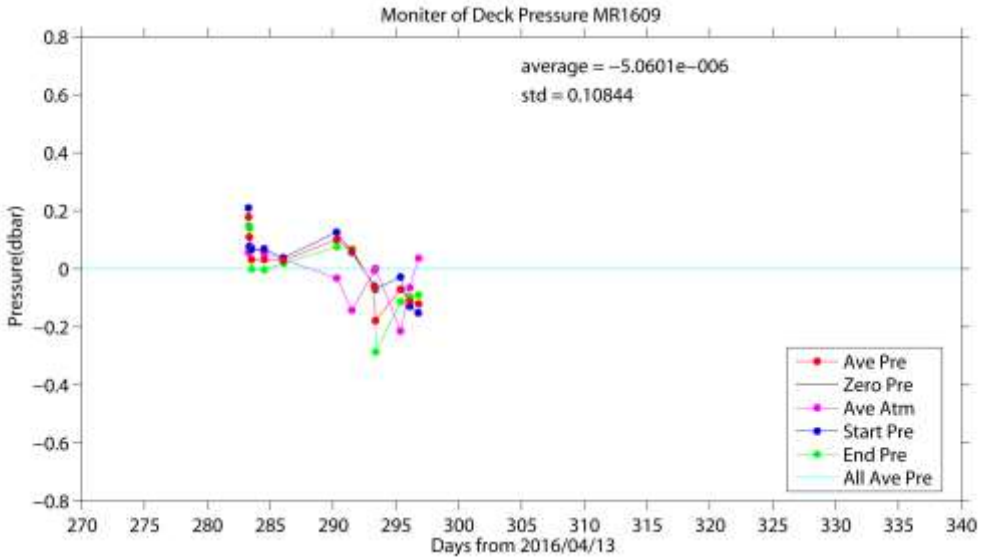

Fig. 4.7.2 Time series of the CTD deck pressure for leg 2. Atmospheric pressure deviation (magenta dots) from a standard atmospheric pressure was subtracted from the CTD deck pressure. Blue and green dots indicate pre- and post-cast deck pressures, respectively. Red dots indicate averages of the pre- and the post-cast deck pressures.

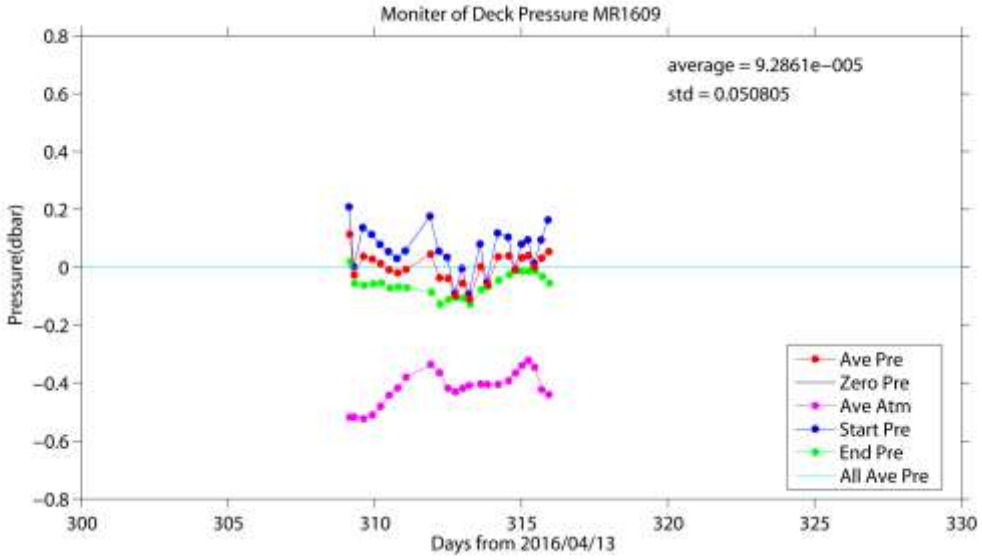

Fig. 4.7.3 Same as Fig. 4.7.2, but for leg 3.

ii. Temperature

The CTD temperature sensors (SBE 3) were calibrated with the SBE 35 under the assumption that discrepancies between SBE 3 and SBE 35 data were due to pressure sensitivity, the viscous heating effect, and time drift of the SBE 3, according to a method by Uchida et al. (2007).

Post-cruise sensor calibration for the SBE 35 will be performed at JAMSTEC in 2017

The CTD temperature was preliminary calibrated as

Calibrated temperature = $T - (c_0 \times P + c_1 \times t + c_2)$

where T is CTD temperature in °C, P is pressure in dbar, t is time in days from pre-cruise calibration date of the CTD temperature and c_0, c_1, and c_2 are calibration coefficients. The coefficients were determined using the data for the depths deeper than 1950 dbar. The coefficient c_1 was set to zero for this cruise.

The primary temperature data were basically used for the post-cruise calibration. The secondary temperature sensor was also calibrated and used instead of the primary temperature data when the data quality of the primary temperature data was bad. The calibration coefficients are listed in Table 4.7.1. The results of the post-cruise calibration for the CTD temperature are summarized in Table 4.7.2 and shown in Figs. 4.7.4 and 4.7.5.

Table 4.7.1 Calibration coefficients for the CTD temperature sensors.

Serial number	c_0 (°C/dbar)	c_1 (°C/day)	c_2 (°C)
031525	–1.713992e–8	0.0	0.00029

Table 4.7.2 Difference between the CTD temperature and the SBE 35 after the post-cruise calibration. Mean and standard deviation (Sdev) are calculated for the data below and above 1950 dbar. Number of data used is also shown.

Serial number	Pressure ≥ 1950 dbar			Pressure < 1950 dbar		
	Number	Mean (mK)	Sdev (mK)	Number	Mean (mK)	Sdev (mK)
031525	326	0.0	0.2	616	–0.3	2.7

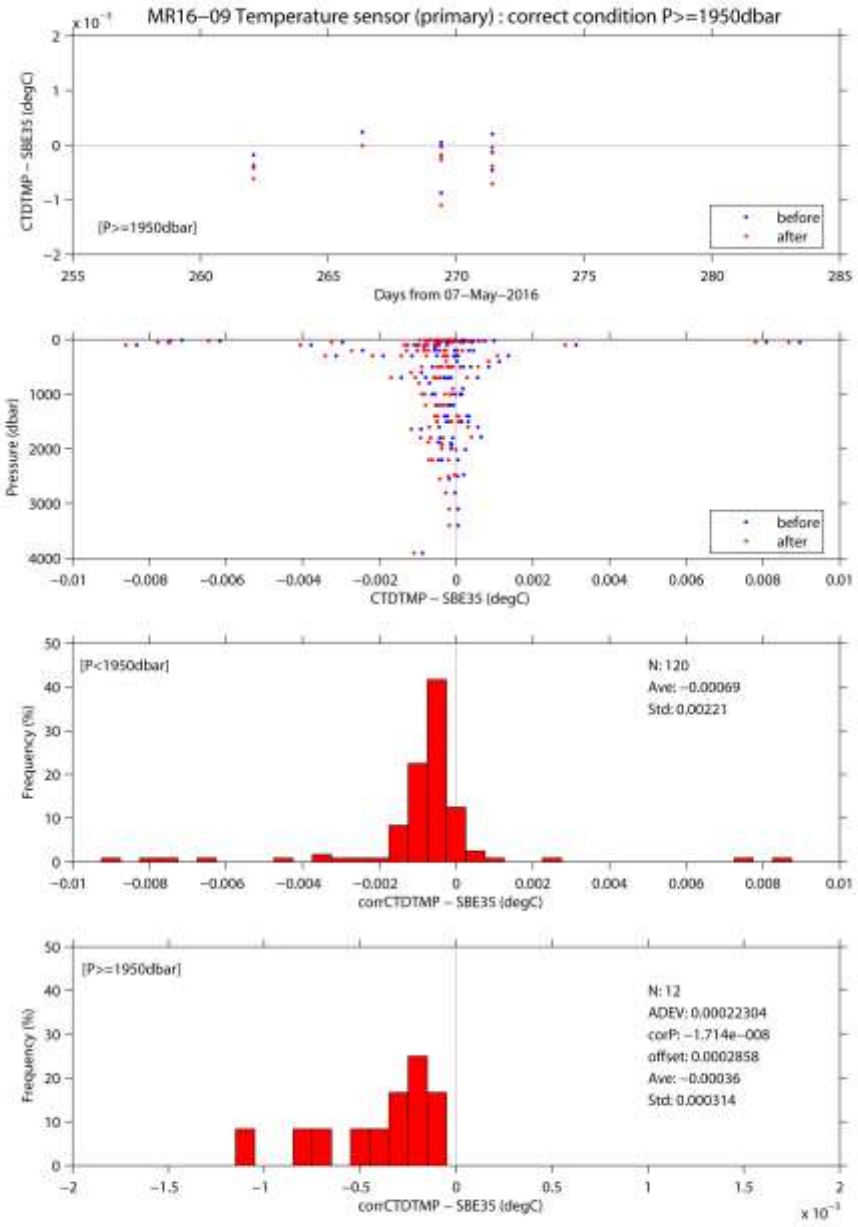

Fig. 4.7.4 Difference between the CTD temperature (primary) and the SBE 35 for leg 2. Blue and red dots indicate before and after the post-cruise calibration using the SBE 35 data, respectively. Lower two panels show histogram of the difference after the calibration.

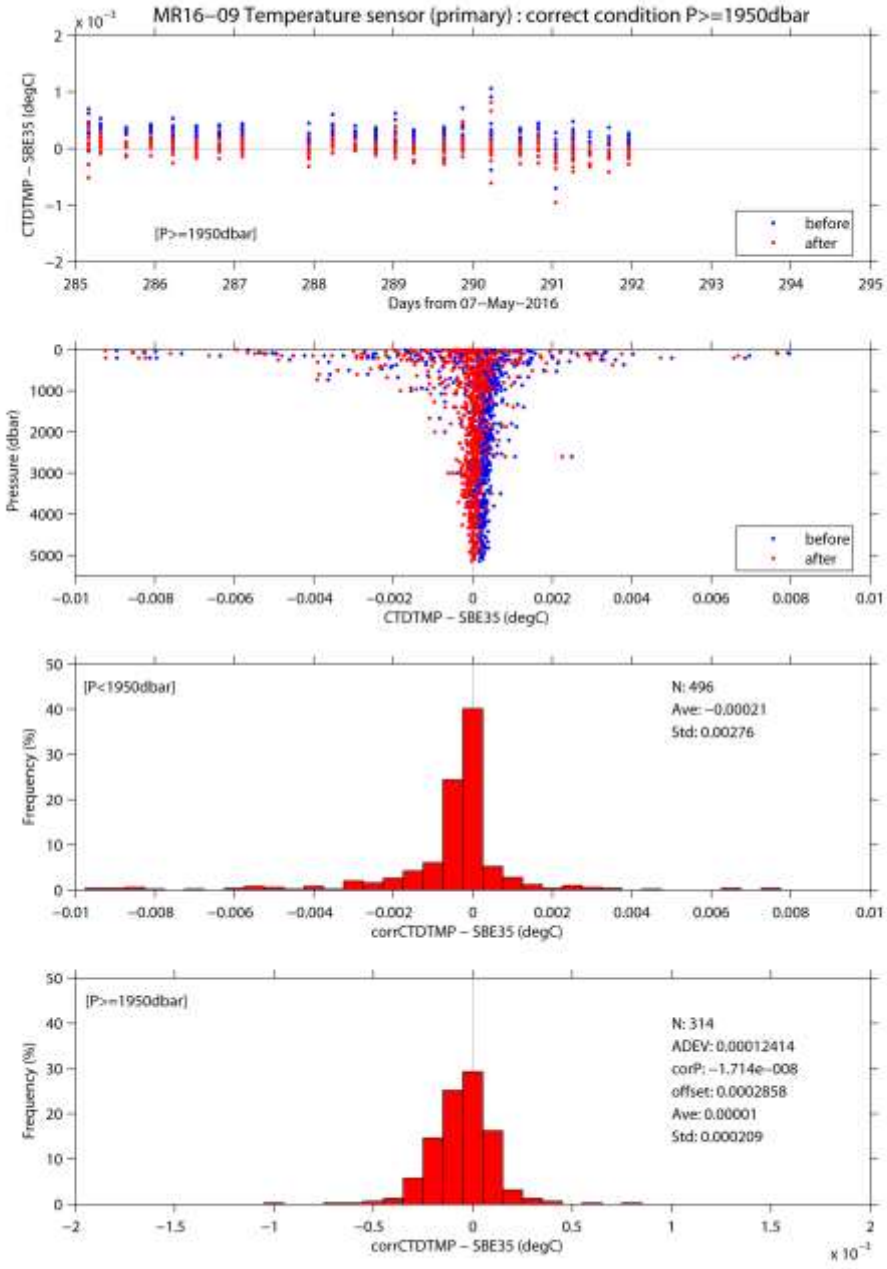

Fig. 4.7.5 Same as Fig. 4.7.4, but for leg 3.

iii. Salinity

The discrepancy between the CTD conductivity and the conductivity calculated from the bottle salinity data with the CTD temperature and pressure data is considered to be a function of conductivity, pressure and time. The CTD conductivity was calibrated as

Calibrated conductivity =

$$C - (c_0 \times C + c_1 \times P + c_2 \times C \times P + c_3 \times P^2 + c_4 \times P^2 \times C + c_5 \times P^2 \times C^2 + c_6)$$

where C is CTD conductivity in S/m, P is pressure in dbar, and c_0, c_1, c_2, c_3, c_4, c_5 and c_6 are calibration coefficients. The best fit sets of coefficients were determined by a least square technique to minimize the deviation from the conductivity calculated from the bottle salinity data.

The primary conductivity data created by the software module ROSSUM were used after the post-cruise calibration for the temperature data. The calibration coefficients are listed in Table 4.7.3. The results of the post-cruise calibration for the CTD salinity are summarized in Table 4.7.4 and shown in Figs 4.7.6 and 4.7.7.

Table 4.7.3 Calibration coefficients for the CTD conductivity sensors.

Coefficient	S/N 042435
c0	7.2645896049e–6
c1	2.9691992467e–7
c2	–7.2958281688e–8
c3	1.9466613572e–10
c4	–1.6842918454e–10
c5	3.3411307753e–11
c6	–9.7770147557e–5

Table 4.7.4 Difference between the CTD salinity and the bottle salinity after the post-cruise calibration. Mean and standard deviation (Sdev) (in 10^{-3}) are calculated for the data below and above 950 dbar. Number of data used is also shown.

Serial number	Pressure ≥ 950 dbar			Pressure < 950 dbar		
	Number	Mean	Sdev	Number	Mean	Sdev
042435	465	–0.1	0.6	390	0.1	3.1

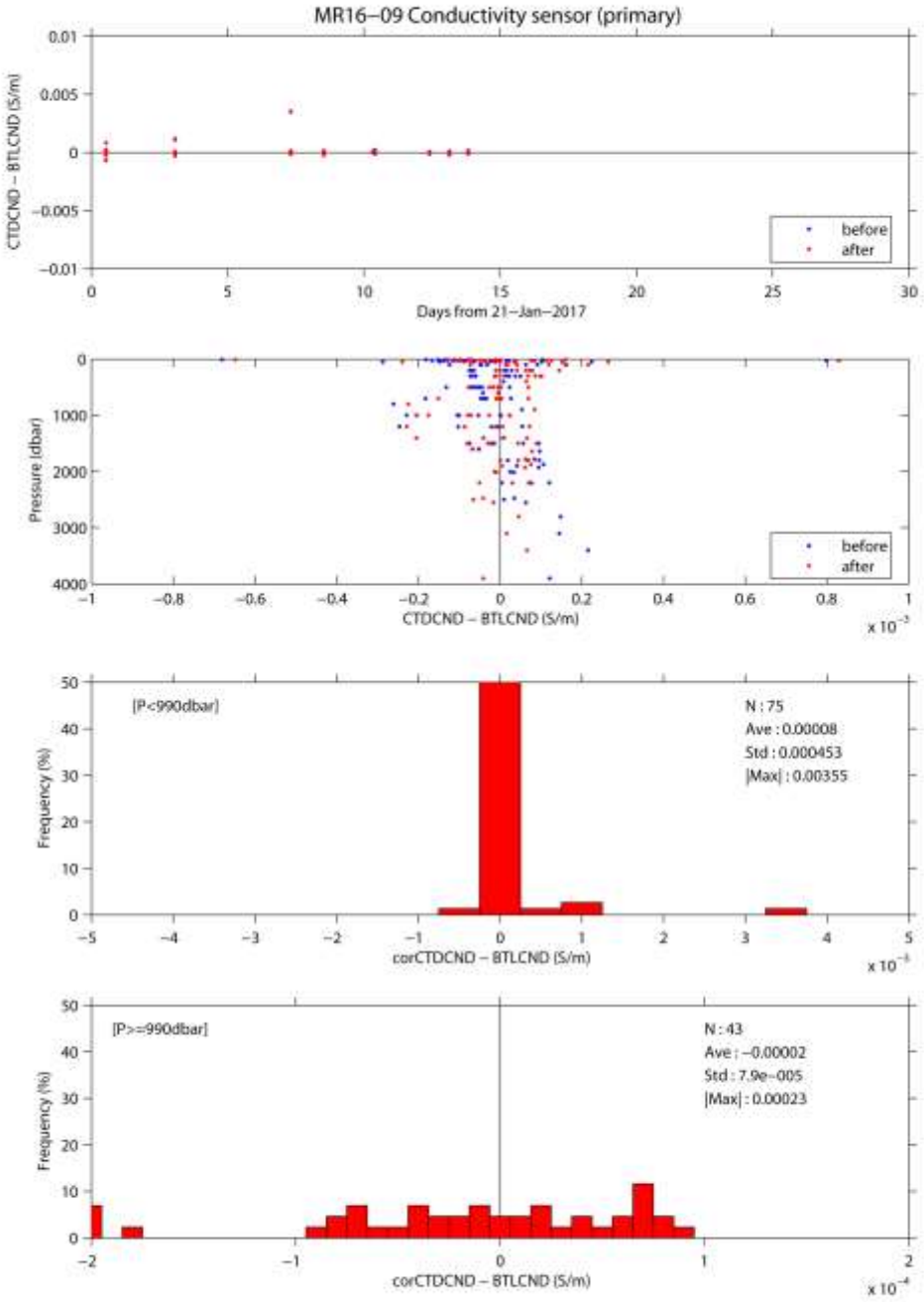

Fig. 4.7.6 Difference between the CTD salinity (primary) and the bottle salinity for leg 2. Blue and red dots indicate before and after the post-cruise calibration, respectively. Lower two panels show histogram of the difference after the calibration.

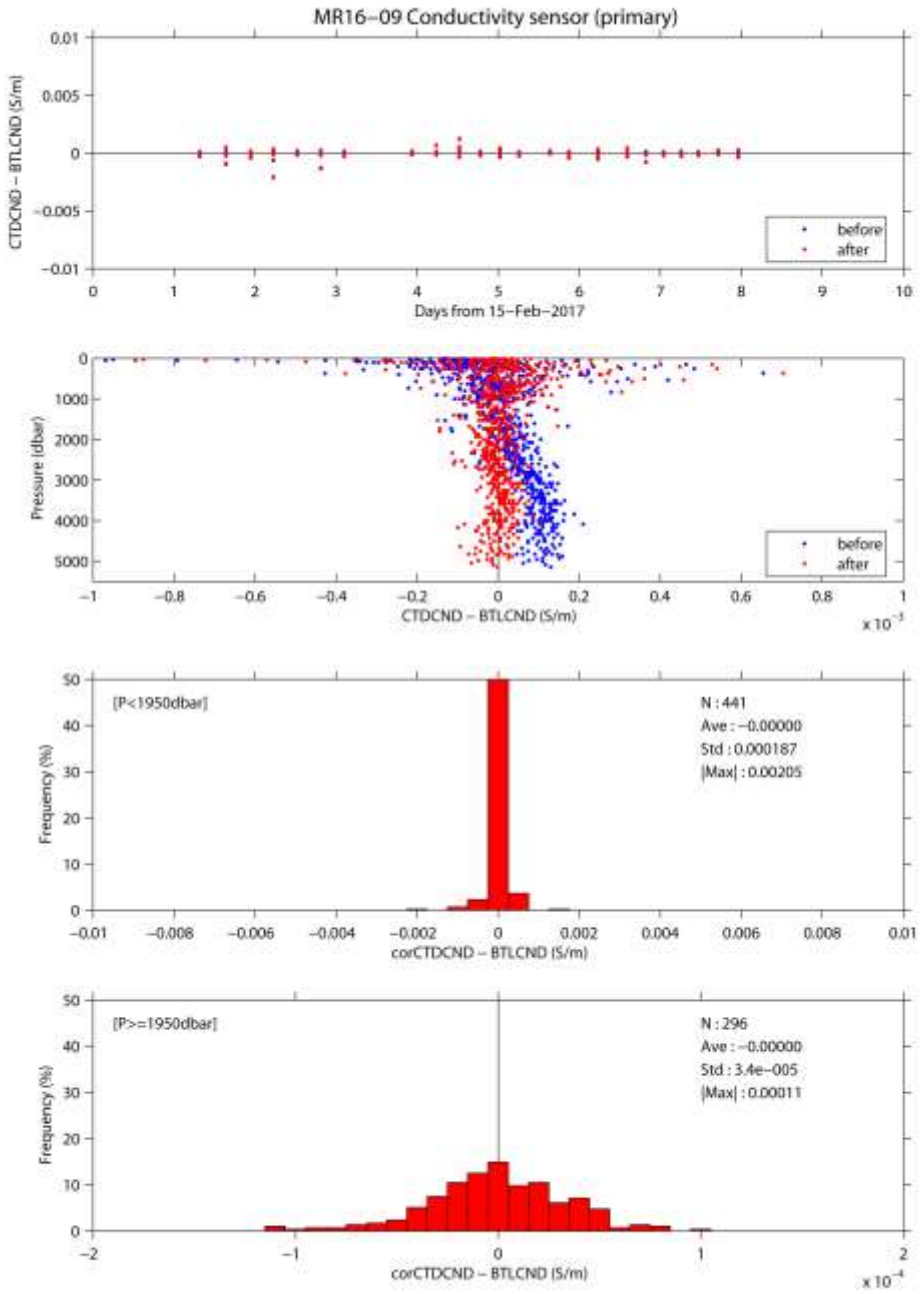

Fig. 4.7.7 Same as Fig. 4.7.6, but for leg 3.

iv. Oxygen

The RINKO oxygen optode (S/N 0024) was calibrated and used as the CTD oxygen data, since the RINKO has a fast time response. The pressure-hysteresis corrected RINKO data was calibrated by the modified Stern-Volmer equation, basically according to a method by Uchida et al. (2010) with slight modification:

$$[O_2]\ (\mu mol/l) = [(V_0 / V)^{1.5} - 1] / K_{sv}$$

and

$$K_{sv} = C_0 + C_1 \times T + C_2 \times T^2$$

$$V_0 = 1 + C_3 \times T$$

$$V = C_4 + C_5 \times V_b + C_6 \times t + C_7 \times t \times V_b$$

where V_b is the RINKO output (voltage), V_0 is voltage in the absence of oxygen, T is temperature in °C, and t is working time (days) integrated from the first CTD cast. Time drift of the RINKO output was corrected. The calibration coefficients were determined by minimizing the sum of absolute deviation with a weight from the bottle oxygen data. The revised quasi-Newton method (DMINF1) was used to determine the sets.

The post-cruise calibrated temperature and salinity data were used for the calibration. The calibration coefficients are listed in Table 4.7.5. The results of the post-cruise calibration for the RINKO oxygen are summarized in Table 4.7.6 and shown in Figs. 4.7.8 and 4.7.9.

Table 4.7.5 Calibration coefficients for the RINKO oxygen sensors.

Coefficient	S/N 0024
c_0	5.942125838095365e–3
c_1	2.112922682529651e–4
c_2	2.453149432631086e–6
c_3	–2.858906729587995e–3
c_4	–3.724762205027561e–2
c_5	0.3277293704143511
c_6	6.221125143791855e–4
c_7	–5.158472610105331e–4
C_p	0.014

Table 4.7.6 Difference between the RINKO oxygen and the bottle ooxygen after the post-cruise calibration. Mean and standard deviation (Sdev) are calculated for the data below and above 950 dbar. Number of data used is also shown.

Serial number	Pressure ≥ 950 dbar			Pressure < 950 dbar		
	Number	Mean [μmol/kg]	Sdev	Number	Mean [μmol/kg]	Sdev
0024	465	0.00	0.27	391	–0.10	0.88

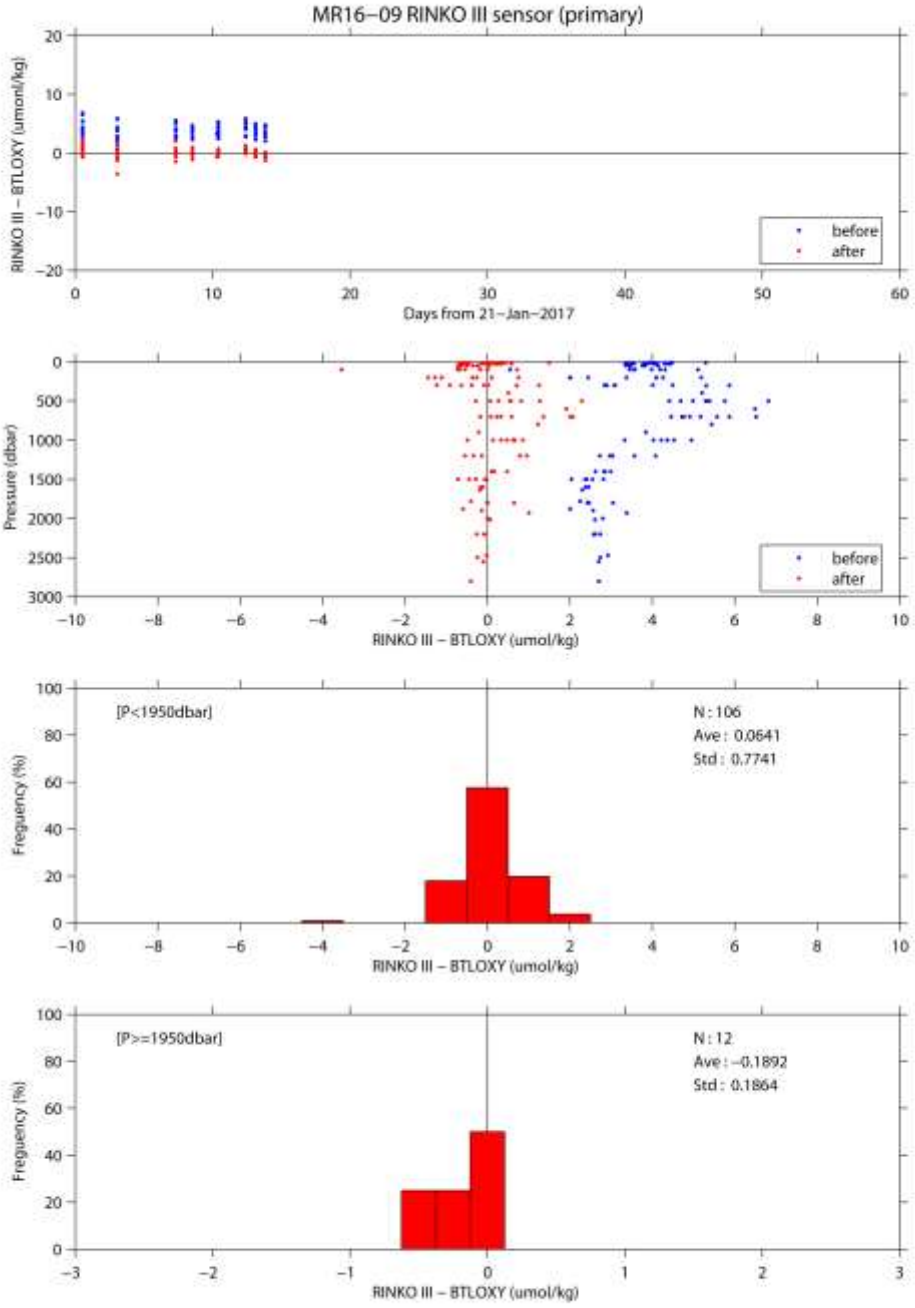

Fig. 4.7.8 Difference between the CTD oxygen and the bottle oxygen for leg 2. Blue and red dots indicate before and after the post-cruise calibration, respectively. Lower two panels show histogram of the difference after the calibration.

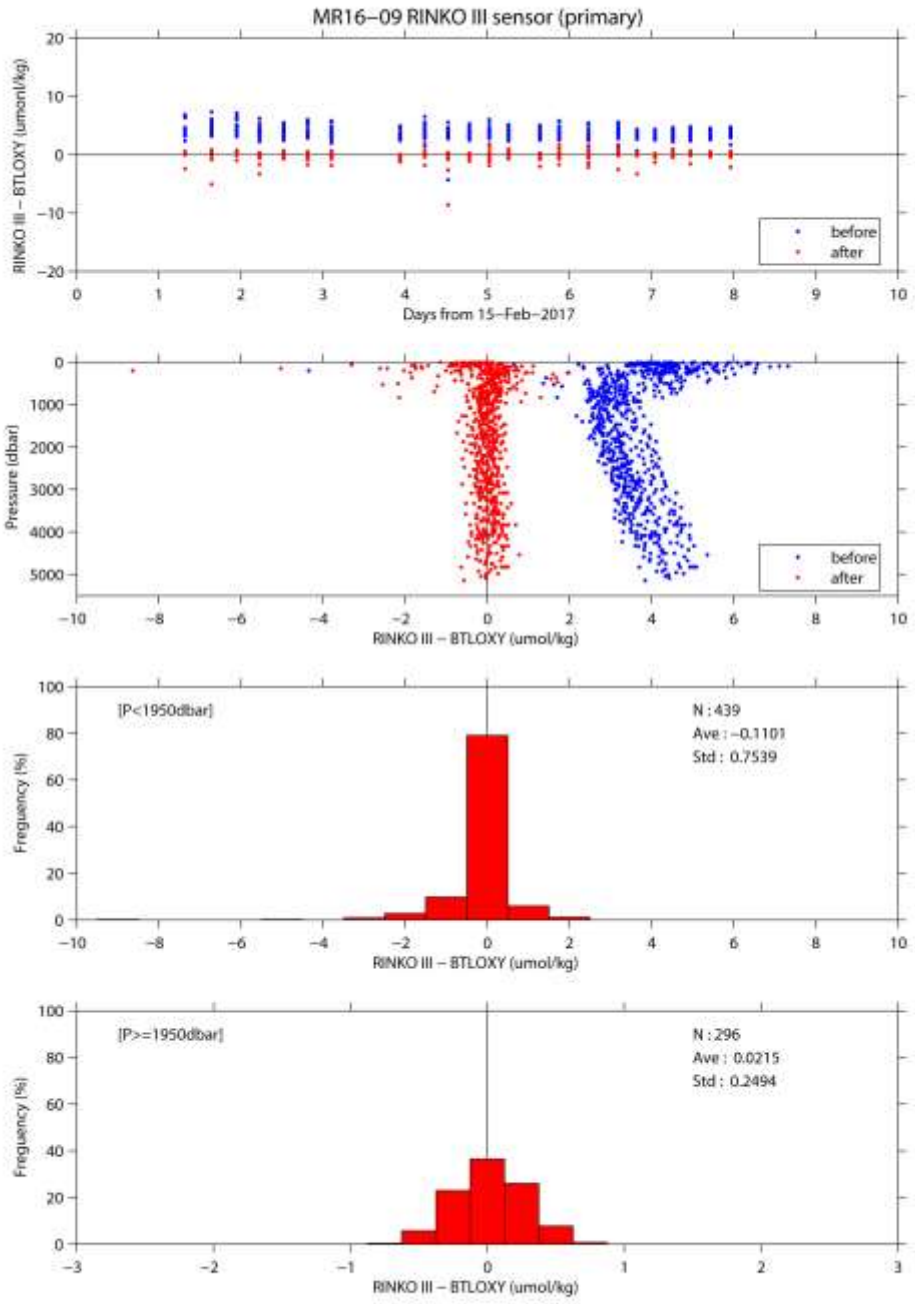

Fig. 4.7.9 Same as Fig. 4.7.8, but for leg 3.

v. Fluorometer

The CTD fluorometer (FLUOR in µg/L) was calibrated by comparing with the bottle sampled chlorophyll-a as

$$FLUORc = c_0 + c_1 \times FLUOR$$

where c_0 and c_1 are calibration coefficients. The CTD fluorometer data is slightly noisy so that the up cast

profile data which was averaged over one decibar agree with the bottle sampled data better than the discrete CTD fluorometer data obtained at bottle-firing stop. Therefore, the CTD fluorometer data at water sampling depths extracted from the up cast profile data were compared with the bottle sampled chlorophyll-a data. The bottle sampled data obtained at dark condition [PAR (Photosynthetically Available Radiation) < 50 μE/(m^2 sec)] were used for the calibration, since sensitivity of the fluorometer to chlorophyll *a* is different at nighttime and daytime (Section 2.4 in Uchida et al., 2015).

Firstly, bias of sensor output ($-c_0/c_1$) was determined from the minimum of the sensor output as 0.022. Then the calibration coefficients were determined under this condition ($-c_0/c_1 = 0.022$) for three groups: station 007 of leg 2, stations of leg 2 except for 007, and stations of leg 3. The calibration coefficients are listed in Table 4.7.7. The results of the post-cruise calibration for the fluorometer are summarized in Table 4.7.8 and shown in Fig. 4.7.10.

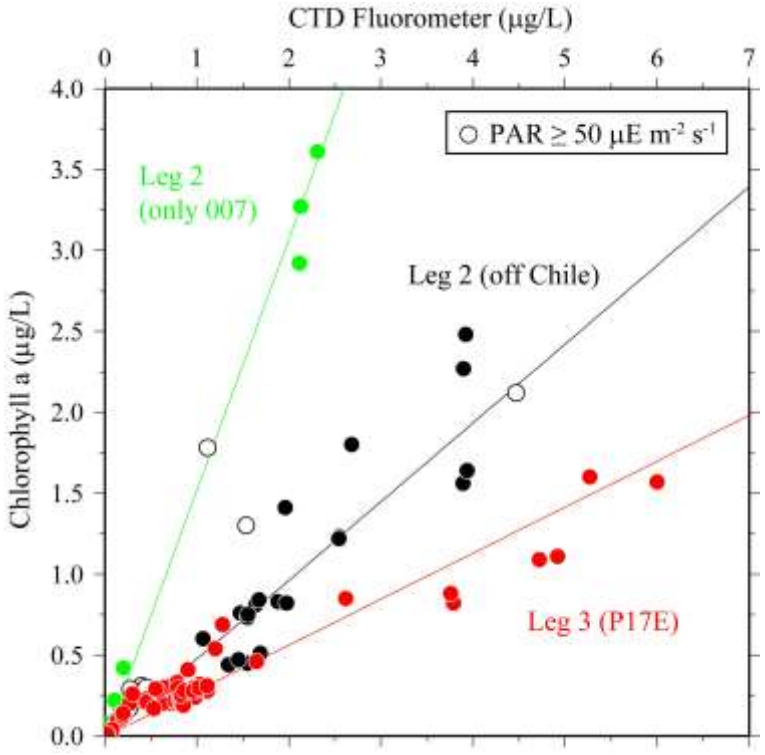

Fig. 4.7.10. Comparison of the CTD fluorometer and the bottle sampled chlorophyll-a. The regression lines are also shown.

Table 4.7.7. Calibration coefficients for the CTD fluorometer.

c_0	c_1	Note
–3.415403161178421e-02	1.552455920202864	for stn. 007 of leg 2
–1.070073772820049e-02	0.4863967142398999	for leg 2 except for stn. 007
–6.244323339035114e-03	0.2839634259958261	for leg 3

Table 4.7.8. Difference between the CTD fluorometer and the bottle chlorophyll-a after the post-cruise calibration. Mean, standard deviation (Sdev), and number of data used are shown. Data obtained at daytime are also used in this calculation.

Number	Mean	Sdev
306	0.00 µg/L	0.12 µg/L

vi. Transmissometer

The transmissometer (T_r in %) is calibrated as

$$T_r = (V - V_d) / (V_r - V_d) \times 100$$

wehre V is the measured signal (voltage), V_d is the dark offset for the instrument, and V_r is the signal for clear water. V_d can be obtained by blocking the light path. V_d and V_{air}, which is the signal for air, were measured on deck before each cast after wiping the optical windows with ethanol. V_d was constant (0.0024) during the cruise. Vr is estimated from the measured maximum signal in the deep ocean at each cast. Since the transmissometer drifted in time (Fig. 4.7.11), Vr is expressed as

$$V_r = c_0 + c_1 \times t + c_2 \times t^2$$

where t is working time (in days) of the transmissometer integrated from the first CTD cast., and c_0, c_1, and c_2 are calibration coefficients.

Maximum signal was extracted for each cast. Data for leg 2 were not used to estimate V_r (open dots in Fig. 4.7.11). The calibration coefficients are listed in Table 4.7.9.

Table 4.7.9 Calibration coefficients for the CTD transmissometer.

Coefficient	
c0	4.749551191426855
c1	–7.943810401172799e–3
c2	9.065035348634040e–4
Vd	0.0024

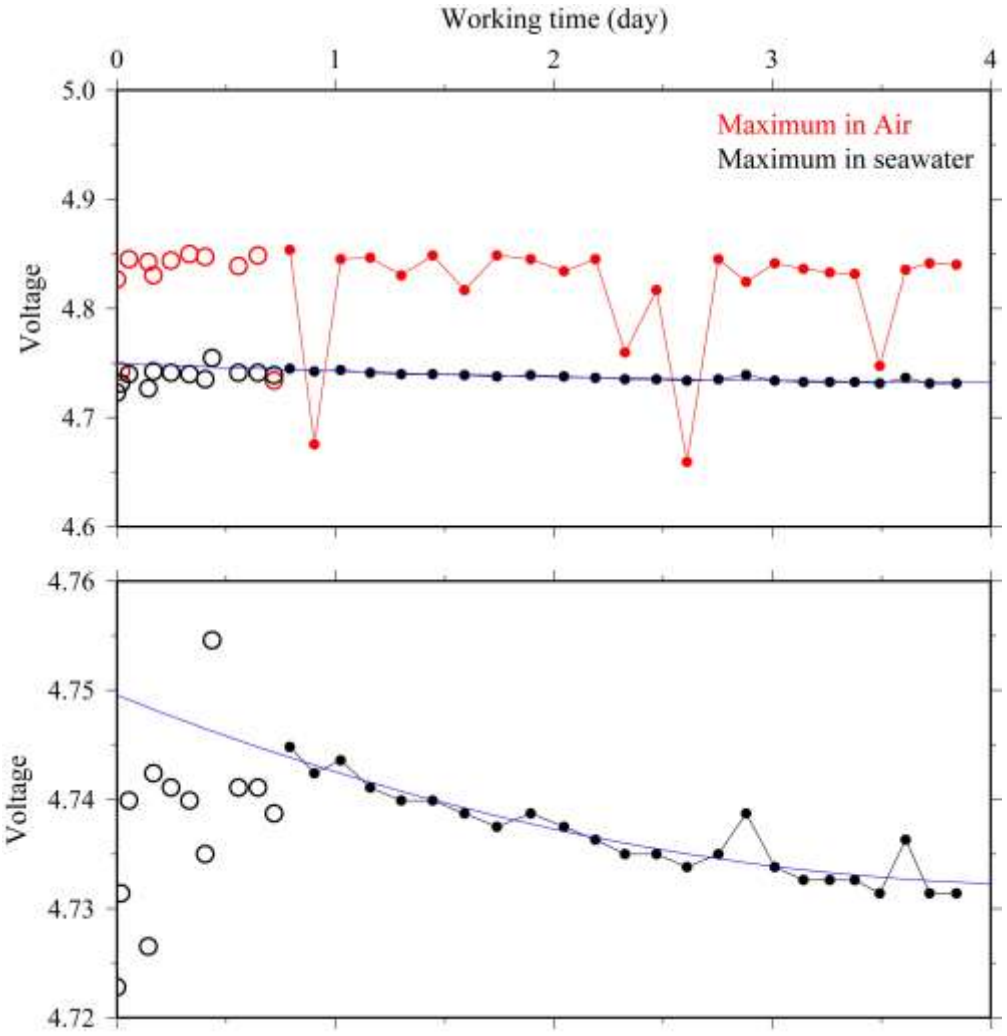

Fig. 4.7.11. Time series of an output signal (voltage) from transmissometer at deep ocean (Vdeep). Data in air are also shown in red dots. The black solid line indicates the modeled signal in the deep clear ocean. Open dots were not used to estimate the final calibration coefficients.

vii. Turbidity meter

Turbidity data obtained in leg 2 were not available, because measurement range of the sensor was inadequate (0-500 FTU) to resolve actual turbidity signal. Post-cruise correction for the turbidity meter data wasn't carried out. The turbidity data are well correlated with beam attenuation coefficient data obtained from transmissometer (Fig. 4.7.12).

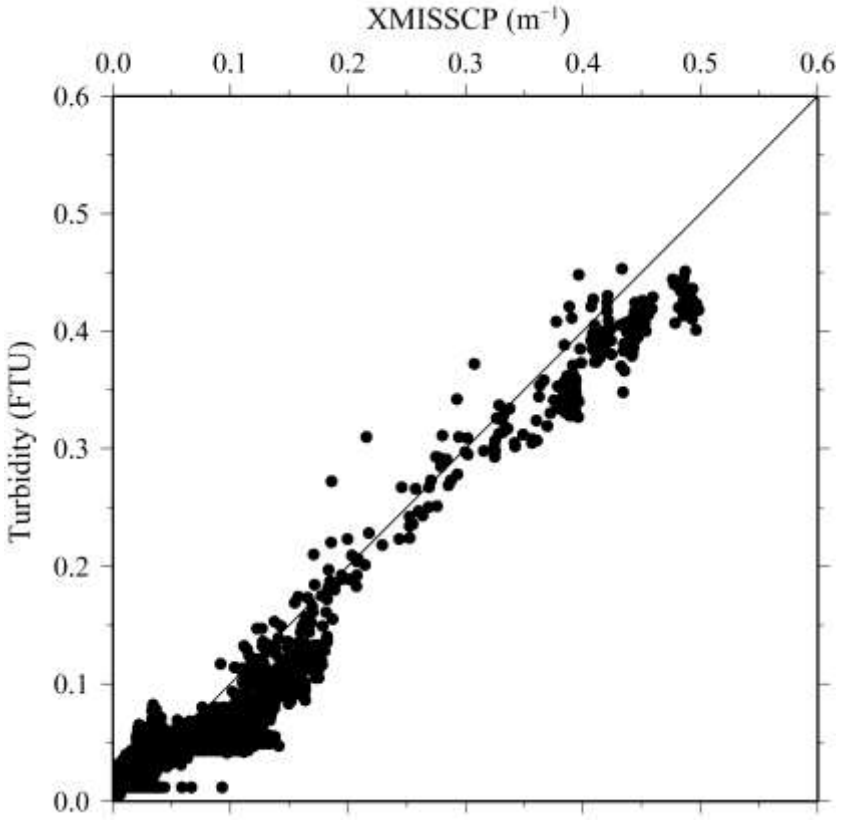

Fig. 4.7.12. Comparison between turbidity data and beam attenuation coefficient data (XMISSCP) from transmissometer.

viii. PAR

The PAR sensor was calibrated with an offset correction. The offset was estimated from the data measured in the deep ocean during the cruise. The corrected data (PARc) is calculated from the raw data (PAR) as follows:

$$PARc\ [\mu E\ m^{-2}\ s^{-1}] = PAR - 0.104.$$

ix. CDOM

Post-cruise correction for the CDOM sensor wasn't carried out. The data were low-pass filtered by a running mean with a window of 15 seconds (about 13 m) in the data processing mentioned above, since the data was noisy. Moreover, CDOM data were flagged as 4 (bad measurement) for depths deeper than about 4000 m due to large shift of the data caused by unknown reason.

(7) References

Edwards, B., D. Murphy, C. Janzen and N. Larson (2010): Calibration, response, and hysteresis in deep-sea dissolved oxygen measurements, *J. Atmos. Oceanic Technol.*, 27, 920–931.

Fukasawa, M., T. Kawano and H. Uchida (2004): Blue Earth Global Expedition collects CTD data aboard Mirai, BEAGLE 2003 conducted using a Dynacon CTD traction winch and motion-compensated crane, *Sea Technology*, 45, 14–18.

García, H. E. and L. I. Gordon (1992): Oxygen solubility in seawater: Better fitting equations. *Limnol. Oceanogr.*, 37 (6), 1307–1312.

Uchida, H., G. C. Johnson, and K. E. McTaggart (2010): CTD oxygen sensor calibration procedures, The GO-SHIP Repeat Hydrography Manual: A collection of expert reports and guidelines, IOCCP Rep., No. 14, ICPO Pub. Ser. No. 134.

Uchida, H., K. Katsumata, and T. Doi (2015): WHP P14S, S04I Revisit Data Book, JASTEC, Yokosuka, 187 pp.

Uchida, H., T. Nakano, J. Tamba, J. V. Widiatmo, K. Yamazawa, S. Ozawa and T. Kawano (2015): Deep ocean temperature measurement with an uncertainty of 0.7 mK, J. Atmos. Oceanic Technol., 32, 2199–2210.

Uchida, H., K. Ohyama, S. Ozawa, and M. Fukasawa (2007): In situ calibration of the Sea-Bird 9plus CTD thermometer, *J. Atmos. Oceanic Technol.*, 24, 1961–1967.

4.8 Bottle Salinity

May 14, 2017

(1) Personnel

Hiroshi Uchida (JAMSTEC)
Sonoka Tanihara (MWJ)
Akira Watanabe (MWJ)

(2) Objectives

Bottle salinities were measured to calibrate CTD salinity data.

(3) Instrument and Method

Salinity measurement was conducted basically based on a method by Kawano (2010).

i. Salinity Sample Collection

The bottles in which the salinity samples were collected and stored were 250 ml brown borosilicate glass bottles with screw caps (PTFE packing). Each bottle was rinsed three times with sample water and was filled to the shoulder of the bottle. The caps were also thoroughly rinsed. Salinity samples were stored more than 24 hours in the same laboratory as the salinity measurement was made.

For the salinity samples for correction of the thermo-salinograph, a polyethylene inner plug was used for the sample bottle to store a few weeks.

ii. Instruments and Methods

Salinity of water samples was measured with a salinometer (Autosal model 8400B; Guildline Instruments Ltd., Ontario, Canada; S/N 62556 for legs 1~3 and S/N 71758 for leg 4), which was modified by adding a peristaltic-type intake pump (Ocean Scientific International Ltd., Hampshire, UK) and two platinum resistance thermometers (Guildline Instruments Ltd., model 9450). One thermometer monitored an ambient temperature and the other monitored a salinometer's bath temperature. The resolution of the thermometers was 0.001 °C. The measurement system was almost same as Aoyama et al. (2002). The salinometer was operated in the air-conditioned laboratory of the ship at a bath temperature of 24 °C.

The ambient temperature varied from approximately 22.3 to 24.3 °C, while the bath temperature was stable and varied within ±0.006 °C. A measure of a double conductivity ratio of a sample was taken as a median of 31 readings. Data collection was started after 10 seconds and it took about 10 seconds to collect 31 readings by a personal computer. Data were sampled for the sixth and seventh filling of the cell. In case where the difference between the double conductivity ratio of these two fillings was smaller than 0.00002, the average value of the two double conductivity ratios was used to calculate the bottle salinity with the algorithm for practical salinity scale, 1978 (UNESCO, 1981). When the difference was greater than or equal to the 0.00003, we measured another additional filling of the cell. In case where the double conductivity ratio of the additional filling did not satisfy the criteria above, we measured other additional fillings of the cell within 10 fillings in total. In case where the number of fillings was 10 and those fillings did not satisfy the criteria above, the median of the double conductivity ratios of five fillings were used to calculate the bottle salinity.

The measurement was conducted about from 2 to 19 hours per day and the cell was cleaned with soap (50 times diluted solution of S-CLEAN WO-23 [Neutral], Sasaki Chemical Co. Ltd., Kyoto, Japan) after the measurement for each day. A total of 1672 water samples for legs 1~3 were measured during the cruise, and a total of 12 water samples for leg 4 were measured after the cruise (5 April, 2017) in a

laboratory at JAMSTEC, Yokosuka.

(4) Results

i. Standard Seawater

Standardization control was set to 702. The value of STANDBY was 5206±0001 and that of ZERO was 0.00000 or ±0.00001. We used IAPSO Standard Seawater batch P159 whose conductivity ratio is 0.99988 (double conductivity ratio is 1.99976) as the standard for salinity measurement. We measured 66 bottles of the Standard Seawater during the cruise and measured three bottles after the cruise for the samples for leg 4. History of double conductivity ratio measurement of the Standard Seawater for legs 1~3 is shown in Fig. 4.8.1.

Time drift of the salinometer was corrected by using the Standard Seawater measurements. Linear time drift of the salinometer was estimated from the Standard Seawater measurement excluding the shifted data (–0.00006 in double conductivity ratio) in the middle of the measurements by using the least square method (thin black line in Fig. 4.8.1). Additional offset (0.00006) correction was applied to the measurement during shift. The average of double conductivity ratio after the corrections was 1.99976 and the standard deviation was 0.00001, which is equivalent to 0.0002 in salinity.

For leg 4, there was no remarkable drift for the Standard Seawater measurements and the average of double conductivity ratio was adjusted to 1.99976 and the standard deviation was 0.00002, which is equivalent to 0.0004 in salinity.

Fig. 4.8.1. History of double conductivity ratio measurement of the Standard Seawater (P159). Horizontal and vertical axes represent date and double conductivity ratio, respectively. Red dots indicate raw data and blue dots indicate corrected data.

ii. Sub-Standard Seawater

We also used sub-standard seawater which was deep-sea water filtered by pore size of 0.45 μm and stored in a 20 liter cubitainer made of polyethylene and stirred for at least 24 hours before measuring. It was measured every 6-8 samples to check the possible sudden drift of the salinometer. During the whole measurements, there was no detectable sudden drift of the salinometer.

iii. Replicate Samples

We took 149 pairs of replicate samples collected from the same Niskin bottle in leg 2 and 3. Histogram of the absolute difference between replicate samples is shown in Fig. 4.8.2. The

root-mean-square for 148 pairs of replicate samples which are acceptable-quality data was 0.0003.

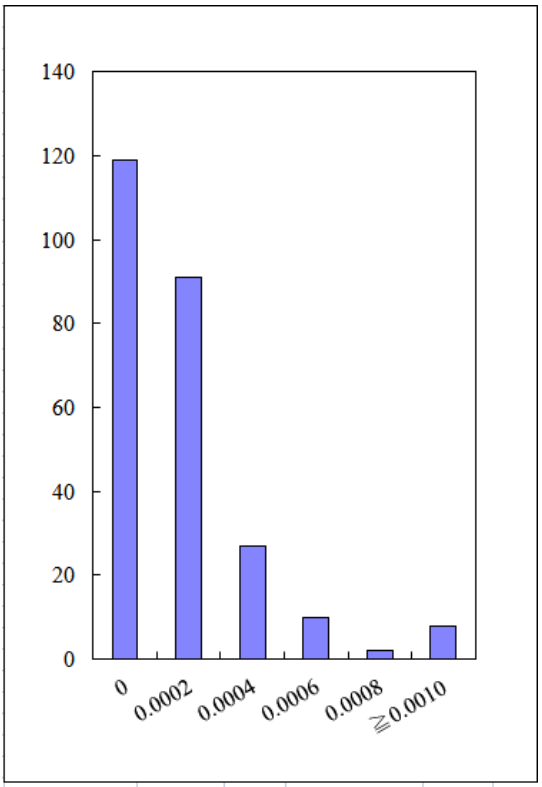

Fig. 4.8.2. Histogram of the absolute difference between replicate samples. Horizontal axis is absolute difference in salinity and vertical axis is frequency.

iv. Duplicate Samples

In this cruise, four to six Niskin bottles were closed at same depth (deeper than 1700 dbar) of station leg3_003_1 (#1, #2, #3, #4, #5), leg3_005_1 (#6, #7, #8, #9, #10), leg3_007_1 (#11, #12, #13, #14), leg3_009_1 (#15, #16, #17, #18, #19), leg3_011_1 (#20, #21, #22, #23, #24), leg3_015_1 (#3, #4, #5, #6, #7, #8 [originally #25, #26, #27, #28, #29, #30]), and leg3_018_1 (#4, #5, #6, #7, #8, #9 [originally #31, #32, #33, #34, #35, #36]) for duplicate samples. The standard deviation for each group was 0.0002 in salinity on average (from 0.0000 to 0.0004) when excluding the result for Niskin bottle #16. For the Niskin bottle #16, salinity measurement was largely deviated (0.0015) from the mean, though oxygen measurement was not deviated (0.02 μmol/kg) from the mean.

(5) References

Aoyama, M., T. Joyce, T. Kawano and Y. Takatsuki (2002): Standard seawater comparison up to P129. Deep-Sea Research, I, Vol. 49, 1103-1114.

Kawano (2010): Salinity. The GO-SHIP Repeat Hydrography Manual: A collection of Expert Reports and Guidelines, IOCCP Report No. 14, ICPO Publication Series No. 134, Version 1.

UNESCO (1981): Tenth report of the Joint Panel on Oceanographic Tables and Standards. UNESCO Tech. Papers in Mar. Sci., 36, 25 pp.

4.9 Oxygen

May 1, 2017

(1) Personnel

Yuichiro Kumamoto [1)], ***Hironori Sato*** [2)], ***Haruka Tamada*** [2)], ***Masanori Enoki*** [2)], ***Misato Kuwahara*** [2)], ***Masahiro Oorui*** [2)], ***Ei Hatakeya*** [2)]

1) Japan Agency for Marine-Earth Science and Technology

2) Marine Works Japan Co. Ltd

(2) Objectives

Dissolved oxygen is one of good tracers for the ocean circulation. Climate models predict a decline in dissolved oxygen concentration and a consequent expansion of oxygen minimum layer under the global warming condition, which results mainly from decreased interior advection and ongoing oxygen consumption by remineralization. The mechanism of the decrease, however, is still unknown. During MR16-09 Leg-2 and Leg-3 cruise, we measured dissolved oxygen concentration from surface to bottom layer at all the hydrocast stations in the South Pacific Ocean and Southern Ocean. Our purpose is to evaluate temporal change in dissolved oxygen concentration in these oceans during the past decades. In addition, dissolved oxygen in surface seawater, which was pumped up from about 4 meter depth, was measured for calibration of oxygen sensors for the surface water during all the legs (Leg-1, 2, 3, and 4).

(3) Reagents

Pickling Reagent I: Manganous chloride solution (3M)

Pickling Reagent II: Sodium hydroxide (8M) / sodium iodide solution (4M)

Sulfuric acid solution (5M)

Sodium thiosulfate (0.025M)

Potassium iodate (0.001667M): National Metrology Institute of Japan (NMIJ), Certified Reference Material (CRM), 3006-a No.045, Mass fraction: 99.973 ± 0.018 % (expanded uncertainty)

CSK standard of potassium iodate: Lot KPG6393, Wako Pure Chemical Industries Ltd., 0.0100N

(4) Instruments

Burette for sodium thiosulfate and potassium iodate;

APB-620 and APB-510 manufactured by Kyoto Electronic Co. Ltd. / 10 cm^3 of titration vessel

Detector;

Automatic photometric titrator, DOT-01X manufactured by Kimoto Electronic Co. Ltd.

(5) Seawater sampling

During the Leg-2 and 3, seawater samples were collected from 12-liter Niskin sample bottles attached

to the CTD-system. During Leg-2, surface seawater was collected using a bucket. The pumped-up surface seawater was collected from a tap on conduit once a day approximately. Seawater for bottle oxygen measurement was transferred to a volume calibrated glass flask (ca. 100 cm^3) through a plastic tube. Three times volume of the flask of seawater was overflowed. Sample temperature was measured during the water sampling using a thermometer. Then two reagent solutions (Reagent I, II) of 1.0 cm^3 each were added immediately into the sample flask and the stopper was inserted carefully into the flask. The sample flask was then shaken vigorously to mix the contents and to disperse the precipitate finely throughout. After the precipitate has settled at least halfway down the flask, the flask was shaken again to disperse the precipitate. The sample flasks containing pickled samples were stored in an air-conditioned laboratory until they were titrated. These procedure is based on a determination method in the WHP Operations Manual (Dickson, 1996).

(6) Sample measurement

At least two hours after the re-shaking, the pickled samples were measured on board. A magnetic stirrer bar and 1 cm^3 sulfuric acid solution were added into the sample flask and stirring began. Samples were titrated by sodium thiosulfate solution whose molarity was determined by potassium iodate solution. Temperature of sodium thiosulfate during titration was recorded by a thermometer. We measured dissolved oxygen concentration using three sets of the titration apparatus system, named DOT-6, DOT-7, and DOT-8. Dissolved oxygen concentration ($\mu mol\ kg^{-1}$) was calculated by the sample temperature during the sampling, salinity, flask volume, and titrated volume of the sodium thiosulfate solution.

(7) Standardization

Concentration of sodium thiosulfate titrant (ca. 0.025M) was determined by potassium iodate solution. The NMIJ-CRM potassium iodate was dried in an oven at 130°C. 1.7835 g potassium iodate weighed out accurately was dissolved in deionized water and diluted to final volume of 5 dm^3 in a calibrated volumetric flask (0.001667M). 10 cm^3 of the standard potassium iodate solution was added to a flask using a volume-calibrated dispenser. Then 90 cm^3 of deionized water, 1 cm^3 of sulfuric acid solution, and 1.0 cm^3 of pickling reagent solution II and I were added into the flask in order. Amount of titrated volume of sodium thiosulfate (usually 5 times measurements average) gave the molarity of the sodium thiosulfate titrant. Table 4.9.1-4 show results of the standardization during this cruise. Coefficient of variation (C.V.) for the standardizations for Leg-1, 2, 3, and 4 were 0.025 ± 0.015 % (standard deviation, n = 5), 0.016 ± 0.005 % (n = 10), 0.018 ± 0.007 % (n = 17), and 0.017 ± 0.006 % (n = 4), respectively.

(8) Determination of the blank

The oxygen in the pickling reagents I (1.0 cm^3) and II (1.0 cm^3) was assumed to be 7.6×10^{-8} mol

(Murray *et al.*, 1968). The blank from the presence of redox species apart from oxygen in the reagents (the pickling reagents I, II, and the sulfuric acid solution) was determined as follows. 1 and 2 cm^3 of the standard potassium iodate solution were added to two flasks respectively. Then 100 cm^3 of deionized water, 1 cm^3 of sulfuric acid solution, and 1.0 cm^3 of pickling reagent solution II and I each were added into the two flasks in order. The blank was determined by difference between the two times of the first (1 cm^3 of KIO_3) titrated volume of the sodium thiosulfate and the second (2 cm^3 of KIO_3) one. The results of 3 times blank determinations were averaged (Table 4.9.1-4).

Table 4.9.1 Standardization (End point, E.P.) and blank determinations (cm^3) during Leg-1.

Date (UTC)	KIO_3 No.	$Na_2S_2O_3$ No.	DOT-8		Samples
			E.P.	blank	
2016/12/28	K1605C01	T1606E	3.966	0.004	TSG01-03
2017/01/01	K1605C02	T1606E	3.964	0.005	TSG04-07
2017/01/05	K1605C03	T1606E	3.964	0.006	TSG08-12
2017/01/09	K1605C04	T1606E	3.963	0.004	TSG13-18

Table 4.9.2 Same as Table 4.9.1 but for Leg-2.

Date (UTC)	KIO_3 No.	$Na_2S_2O_3$ No.	DOT-7		DOT-8		Samples
			E.P.	blank	E.P.	blank	
2017/01/22	K1605D01	T1606F	3.959	0.002	3.965	0.004	Stn.01,06,TSG01-05
2017/01/27	K1605D02	T1606F	3.958	0.003	3.962	0.005	Stn.07,09,10,TSG06-12
2017/02/01	K1605D03	T1606F	3.963	0.007	3.963	0.005	Stn.12B,11A,11B,TSG13-15

Table 4.9.3 Same as Table 4.9.1 but for Leg-3.

Date (UTC)	KIO_3 No.	$Na_2S_2O_3$ No.	DOT-6		DOT-8		Stations
			E.P.	blank	E.P.	blank	
2017/02/11	K1606E01	T1606F	3.966	0.006	3.963	0.003	TSG01-05
2017/02/18	K1606E03	T1606G	3.965	0.007	3.963	0.003	Stn.01-13,15,16,18,TSG06-11
2017/02/21	K1606E05	T1606H	3.965	0.005	3.965	0.004	Stn.20-26,TSG12-13
2017/02/24	K1606E06	T1606H	3.964	0.007	3.965	0.006	TSG14-21

Table 4.9.4 Same as Table 4.9.1 but for Leg-4.

Date (UTC)	KIO_3 No.	$Na_2S_2O_3$ No.	DOT-6		Samples
			E.P.	blank	
2017/03/10	K1606F01	T1606H	3.966	0.005	TSG01-02
2017/03/16	K1606F02	T1606H	3.968	0.007	TSG03-08
2017/03/22	K1606F03	T1606H	3.966	0.004	TSG09-12

(9) Replicate sample measurement

At all the hydrocast stations during Leg-2 and 3, a pair of replicate samples was collected at a few

depths. The standard deviations of the replicate measurement during Leg-2 and 3 were 0.09 (n = 16) and 0.08 μmol kg^{-1} (n = 92), respectively. The difference between the pair of replicate measurement did not depend on the concentration (Fig. 4.9.1).

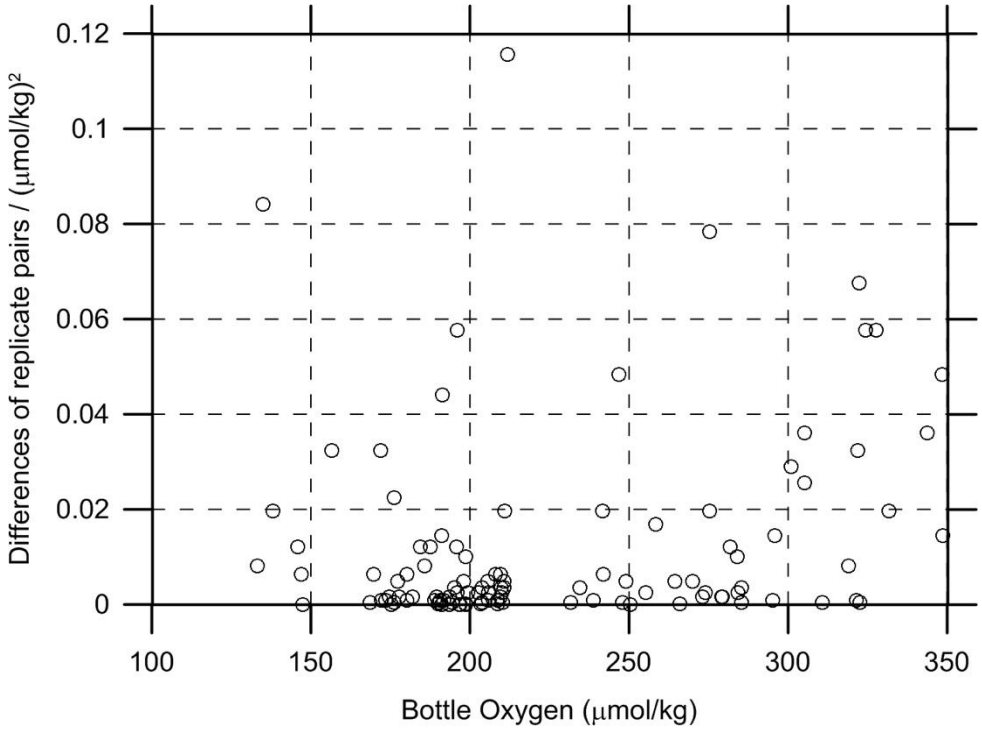

Figure 4.9.1 Oxygen difference between measurements of a replicate pair against oxygen concentration.

(10) Duplicate sample measurement

During Leg-3 duplicate sampling was taken for all the Niskin bottles (36 bottles, Table 4.9.5). The standard deviation of the duplicate measurements were calculated to be 0.09 μmol kg^{-1}, which were equivalent with that of the replicate measurements (0.08 μmol kg^{-1}, see section 9).

(11) CSK standard measurements

The CSK standard is a commercial potassium iodate solution (0.0100 N) for analysis of dissolved oxygen. We titrated the CSK standard solution (Lot KPG6393) against our KIO_3 standards as samples during this cruise (Table 4.9.6). A good agreement among them confirms that there was no systematic shift in our oxygen analyses on board.

Table 4.9.5 Results of duplicate sample measurements.

No.	Leg	Station	Sampling Pres.(db)	Niskin position #	Niskin bottle #	Dissolved oxygen (μmol/kg)
1	3	3	4849	1	X12J01	215.09
				2	X12J02	215.27
				3	X12J03	215.25
				4	X12J04	215.11
				5	X12J05	215.11
2	3	5	4985	6	X12J06	211.20
				7	X12J07	211.16
				8	X12J08	211.10
				9	X12J09	210.85
				10	X12J10	211.16
3	3	7	5099	11	X12J11	203.95
				12	X12J12	203.91
				13	X12J13	203.83
				14	X12J14	203.84
4	3	9	4880	15	X12J15	193.33
				16	X12J16	193.46
				17	X12J17	193.42
				18	X12J18	193.50
				19	X12J19	193.49
5	3	11	4718	20	X12J20	212.81
				21	X12J21	212.66
				22	X12J22	212.69
				23	X12J23	212.66
				24	X12J24	212.63
6	3	15*	4260	3	X12J25	202.81
				4	X12J26	202.96
				5	X12J27	203.01
				6	X12J28	202.96
				7	X12J29	202.96
				8	X12J30	202.92
7	3	18*	4190	4	X12J31	204.90
				5	X12J32	204.91
				6	X12J33	205.11
				7	X12J34	204.83
				8	X12J35	204.92
				9	X12J36	204.83

*At stations 15 and 18 position of Niskin bottle was changed for the duplicate sampling.

Table 4.9.6 Results of the CSK standard (Lot KPG6393) measurements.

Date (UTC)	KIO_3 ID No.	Conc. (N)	error (N)	Conc. (N)	error (N)	Remarks
				DOT-8		
2016/12/28	K1605C01			0.010004	0.000003	Leg-1
2017/01/15	K1605C05			0.010016	0.000005	Leg-1
		DOT-7		DOT-8		
2017/01/22	K1605D01	0.010003	0.000002	0.010001	0.000002	Leg-2
		DOT-6		DOT-8		
2017/02/11	K1606E01	0.010003	0.000004	0.010006	0.000004	Leg-3
		DOT-6				
2017/03/10	K1606F01	0.010009	0.000003			Leg-4

(12) Quality control flag assignment

Quality flag values for oxygen data from Niskin bottles were assigned according to the code defined in Table 4.9 of WHP Office Report WHPO 90-1 Rev.2 section 4.5.2 (Joyce *et al*., 1994). Measurement flags of 2 (good), 3 (questionable), 4 (bad), and 5 (missing) have been assigned (Table 4.9.7). For the choice between 2, 3, or 4, we basically followed a flagging procedure as listed below:

a. Bottle oxygen concentration at the sampling layer was plotted against sampling pressure. Any points not lying on a generally smooth trend were noted.

b. Difference between bottle oxygen and oxygen sensor was then plotted against sampling pressure. If a datum deviated from a group of plots, it was flagged 3.

c. Vertical sections against pressure and potential density were drawn. If a datum was anomalous on the section plots, datum flag was degraded from 2 to 3, or from 3 to 4.

d. If there was problem in the measurement, the datum was flagged 4.

e. If the bottle flag was 4 (did not trip correctly), a datum was flagged 4 (bad). In case of the bottle flag 3 (leaking) or 5 (unknown problem), a datum was flagged based on steps a, b, c, and d.

Quality flag values for oxygen data from pumped-up surface seawater were assigned according to a flagging procedure as listed below:

f. Bottle oxygen data was plotted against that from oxygen sensors. If a datum deviated from a group of plots, it was flagged 3.

g. If there was problem in the measurement, the datum was flagged 4.

Table 4.9.7 Summary of assigned quality control flags.

Flag	Definition	Number*
2	Good	922
3	Questionable	0
4	Bad	0
5	Not report (missing)	0
	Total	922

*Replicate samples (n = 108) were not included.

References

Dickson, A. (1996) Determination of dissolved oxygen in sea water by Winkler titration, in WHPO Pub. 91-1 Rev. 1, November 1994, Woods Hole, Mass., USA.

Joyce, T., and C. Corry, eds., C. Corry, A. Dessier, A. Dickson, T. Joyce, M. Kenny, R. Key, D. Legler, R. Millard, R. Onken, P. Saunders, M. Stalcup (1994) Requirements for WOCE Hydrographic Programme Data Reporting, WHPO Pub. 90-1 Rev. 2, May 1994 Woods Hole, Mass., USA.

Murray, C.N., J.P. Riley, and T.R.S. Wilson (1968) The solubility of oxygen in Winkler reagents used for determination of dissolved oxygen, Deep-Sea Res., 15, 237-238.

4.10 Nutrients

29 March 2017 ver.2.0

(1) Personnel

Michio AOYAMA(JAMSTEC/Fukushima Univ. , Principal Investigator)

LEG 2

Tomomi SONE (Department of Marine & Earth Science, Marine Works Japan Ltd.)

Atsushi ONO (Department of Marine & Earth Science, Marine Works Japan Ltd.)

LEG 3

Tomomi SONE (Department of Marine & Earth Science, Marine Works Japan Ltd.)

Shinichiro YOKOGAWA (Department of Marine & Earth Science, Marine Works Japan Ltd.)

Yoshiko ISHIKAWA (Department of Marine & Earth Science, Marine Works Japan Ltd.)

Yoshiaki SATO (Department of Marine & Earth Science, Marine Works Japan Ltd.)

(2) Objectives

The objectives of nutrients analyses during the R/V Mirai MR1609 cruise, cruise in Chilean coastal area (Leg2) and GO-SHIP P17E repeat cruise in 2017, in the South Pacific Ocean (Leg3) are as follows;

Leg2

- Understand the progress in ocean acidification Chilean coastal area and marine organism's responses in the modern ocean and reconstruction of the past climate change recorded in sediments.
- Investigate marine biodiversity and relationship with changes in surrounding environment.

Leg3

- Describe the present status of nutrients concentration with excellent comparability.
- The determinants are nitrate, nitrite, silicate, phosphate and ammonium.
- Study the temporal and spatial variation of nutrients concentration based on a part of the previous high quality experiments data of WOCE previous P17E cruises in 1992.
- Study of temporal and spatial variation of nitrate: phosphate ratio, so called Redfield ratio.
- Obtain more accurate estimation of total amount of nitrate, silicate, phosphate and ammonium in the interested area.
- Provide more accurate nutrients data for physical oceanographers to use as tracers of water mass movement.

(3) Summary of nutrients analysis

We made 8 QuAAtro 2-HR runs for the samples collected by 9 casts at 8 stations in Leg2 and 23 runs for the samples collected by 23 casts at 23 stations in Leg3. The total amount of layers of the

seawater sample reached to 270 in Leg2 and 1460 in Leg3. We made duplicate measurement at all layers at all stations. We made basically duplicate measurement. The station locations for nutrients measurement is shown in Figure 4.10.1, Figure 4.10.2, Table 4.10.1 and Table 4.10.2.

We also measured the samples as listed below. 99 pore water samples, 6 sea samples collected from just above the sea bottom, 24 salinity standard samples and 36 underway samples.

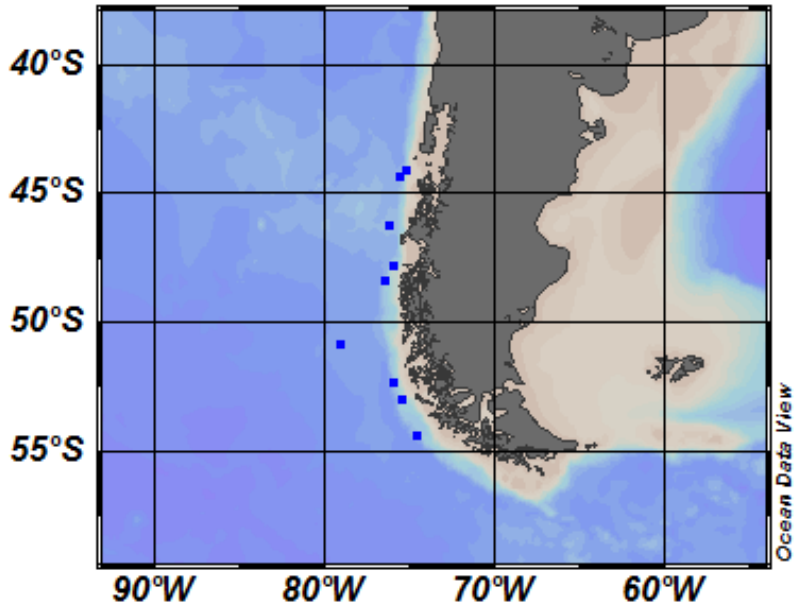

Figure 4.10.1 Sampling positions of nutrients sample in MR1609Leg2.

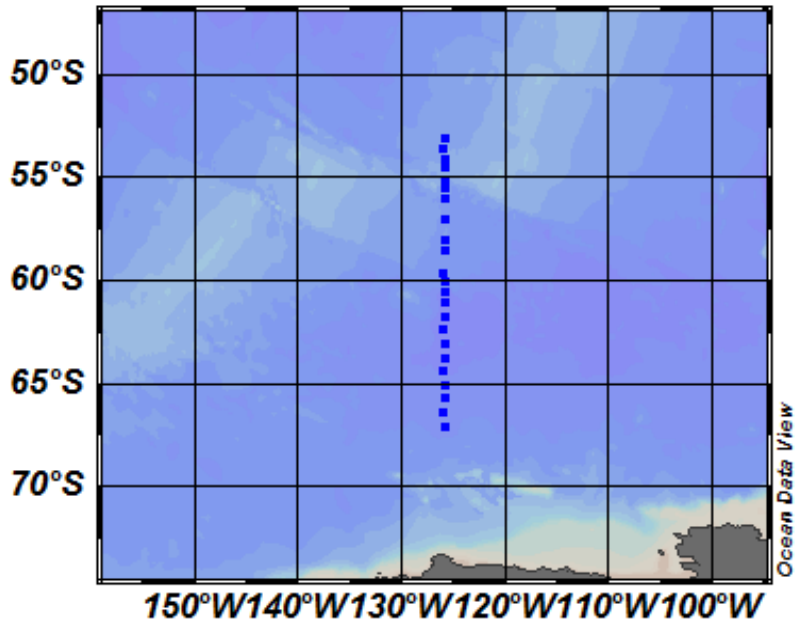

Figure 4.10.2 Sampling positions of nutrients sample in MR1609Leg3.

Table 4.10.1 List of stations of MR1609Leg2

Station	Cast	Station serial	Date (UTC)	Position*		Depth (dbar)
			(mmddyy)	Latitude	Longitude	
001	1	1	012117	44-17.72S	75-35.53W	1,920
006	1	2	012417	46-10.81S	76-17.64W	2,522
007	1	3	012817	47-47.96S	76-01.99W	1,992
009	1	4	012917	48-23.16S	76-28.09W	1,639
010	1	5	013117	50-48.41S	79-06.80W	3,852
010	2	5	013117	50-48.46S	79-07.15W	3,852
012B	1	6	020217	54-20.20S	74-38.03W	2,462
011B	1	7	020317	53-00.08S	75-29.35W	1,767
011A	1	8	020317	52-19.08S	75-56.71W	1,822

Table 4.10.2 List of stations of MR1609Leg3

Station	Cast	Station serial	Date (UTC)	Position*		Depth (dbar)
			(mmddyy)	Latitude	Longitude	
001	2		021617	66-59.99S	125-58.58W	3,709
002	1		021617	66-21.56S	126-03.77W	4,470
003	1		021617	65-39.45S	125-57.43W	4,745
004	1		021717	65-01.00S	125-57.59W	4,866
005	1		021717	64-20.81S	126-01.84W	4,891
006	1		021717	63-41.01S	125-59.57W	4,955
007	1		021817	63-01.25S	125-59.78W	4,994
008	1		021817	62-20.12S	126-06.64W	5,047
009	1		021917	61-39.83S	125-59.62W	4,833
010	1		021917	60-58.71S	126-00.43W	4,590
011	1		021917	60-28.63S	125-58.51W	4,833
012	1		022017	60-00.83S	125-58.53W	4,634
013	1		022017	59-36.44S	126-03.24W	4,637
015	1		022017	58-29.95S	125-59.05W	4,209
016	1		022017	58-00.63S	125-59.75W	4,274
018	1		022117	57-01.00S	125-59.23W	4,168
020	1		022117	56-00.65S	125-57.34W	4,169
021	1		022117	55-30.21S	125-58.63W	3,502
022	1		022217	55-01.09S	125-58.60W	3,654
023	1		022217	54-28.36S	125-59.12W	3,629
024	1		022217	54-00.38S	125-58.60W	3,586
025	1		022217	53-30.49S	126-01.35W	3,742
026	1		022217	53-00.73S	126-00.05W	4,229

(4) Instrument and Method

(4.1) Analytical detail using QuAAtro 2-HR systems (BL-Tech)

We applied two units of QuAAtro in this cruise. Unit 1 and Unit 2 were put for R/V Mirai equipment. Configurations of all units are completely same for five parameters, Nitrate, Nitrite, Silicate, Phosphate, and Ammonium.

Nitrate + nitrite and nitrite were analyzed according to the modification method of Grasshoff (1970). The sample nitrate was reduced to nitrite in a cadmium tube inside of which was coated with metallic copper. The sample streamed with its equivalent nitrite was treated with an acidic, sulfanilamide reagent and the nitrite forms nitrous acid which reacted with the sulfanilamide to produce a diazonium ion. N-1-Naphthylethylene-diamine added to the sample stream then coupled with the diazonium ion to produce a red, azo dye. With reduction of the nitrate to nitrite, both nitrate and nitrite reacted and were measured; without reduction, only nitrite reacted. Thus, for the nitrite analysis, no reduction was performed and the alkaline buffer was not necessary. Nitrate was computed by difference.

The silicate method was analogous to that described for phosphate. The method used was essentially that of Grasshoff et al. (1983), wherein silicomolybdic acid was first formed from the silicate in the sample and added molybdic acid; then the silicomolybdic acid was reduced to silicomolybdous acid, or "molybdenum blue" using ascorbic acid as the reductant. The analytical methods of the nutrients, nitrate, nitrite, silicate and phosphate, during this cruise were same as the methods used in (Kawano et al. 2009).

The phosphate analysis was a modification of the procedure of Murphy and Riley (1962). Molybdic acid was added to the seawater sample to form phosphomolybdic acid which was in turn reduced to phosphomolybdous acid using L-ascorbic acid as the reductant.

The details of modification of analytical methods for four parameters, Nitrate, Nitrite, Silicate and Phosphate, used in this cruise are also compatible with the methods described in nutrients section in GO-SHIP repeat hydrography manual (Hydes et al., 2010), while an analytical method of ammonium is compatible with Determination of ammonia in seawater using a vaporization membrane permeability method (Kimura, 2000). The flow diagrams and reagents for each parameter are shown in Figures 4.10.3 to 4.10.7.

(4.2) Nitrate Reagents

Imidazole (buffer), 0.06 M (0.4 % w/v)

Dissolve 4 g imidazole, $C_3H_4N_2$, in 1000 mL DIW, add 2 mL concentrated HCl. After mixing, 1 mL Triton^{TM} X-100 (50 % solution in ethanol) is added.

Sulfanilamide, 0.06 M (1 % w/v) in 1.2 M HCl

Dissolve 10 g sulfanilamide, 4-$NH_2C_6H_4SO_3H$, in 900 mL of DIW, add 100 ml concentrated HCl. After mixing, 2 mL Triton^{TM} X-100 (50 %f solution in ethanol) is added.

N-1-Napthylethylene-diamine dihydrochloride, 0.004 M (0.1 %f w/v)

Dissolve 1 g NEDA, $C_{10}H_7NHCH_2CH_2NH_2$•2HCl, in 1000 mL of DIW and add 10 mL concentrated HCl. After mixing, 1 mL Triton™ X-100 (50 %f solution in ethanol) is added.

Stored in a dark bottle.

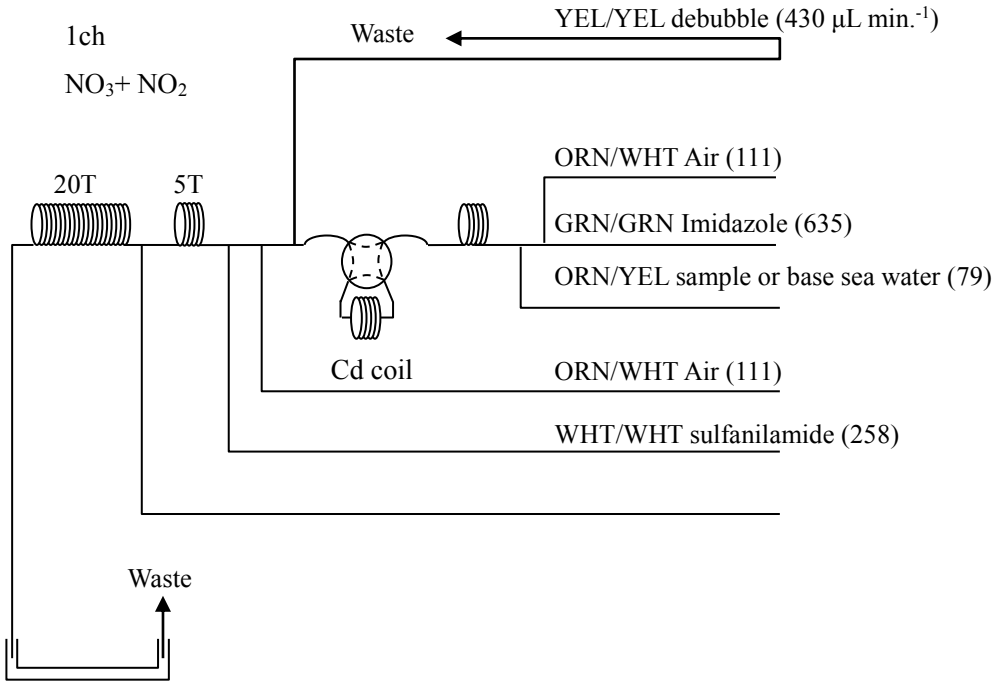

1.0 mm I.D. × 10.0 mm

LED 545 nm

Figure 4.10.3 NO3+NO2 (1ch) Flow diagram

(4.3) Nitrite Reagents

Sulfanilamide, 0.06 M (1% w/v) in 1.2 M HCl

Dissolve 10 g sulfanilamide, 4-$NH_2C_6H_4SO_3H$, in 900 mL of DIW, add 100 mL concentrated HCl. After mixing, 2 mL Triton™ X-100 (50% solution in ethanol) is added.

N-1-Napthylethylene-diamine dihydrochloride, 0.004 M (0.1% w/v)

Dissolve 1 g NEDA, $C_{10}H_7NHCH_2CH_2NH_2$•2HCl, in 1000 mL of DIW and add 10 mL concentrated HCl. After mixing, 1 mL Triton™ X-100 (50% solution in ethanol) is added. This reagent was stored in a dark bottle.

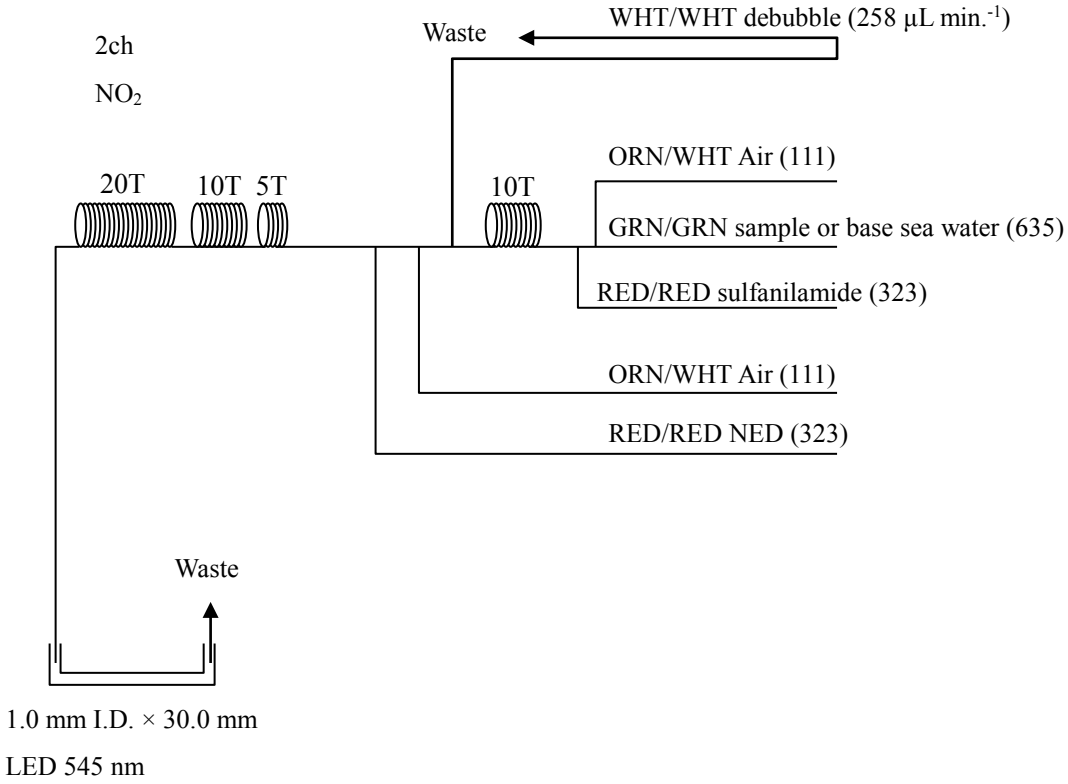

Figure 4.10.4 NO_2 (2ch.) Flow diagram.

(4.4) Silicate Reagents

Molybdic acid, 0.06 M (2% w/v)

Dissolve 15 g disodium Molybdate(VI) dihydrate, $Na_2MoO_4 \cdot 2H_2O$, in 980 mL DIW, add 8 mL concentrated H_2SO_4. After mixing, 20 mL sodium dodecyl sulphate (15% solution in water) is added.

Oxalic acid, 0.6 M (5% w/v)

Dissolve 50 g oxalic acid anhydrous, HOOC: COOH, in 950 mL of DIW.

Ascorbic acid, 0.01 M (3% w/v)

Dissolve 2.5g L(+)-ascorbic acid, $C_6H_8O_6$, in 100 mL of DIW. This reagent was freshly prepared at every day.

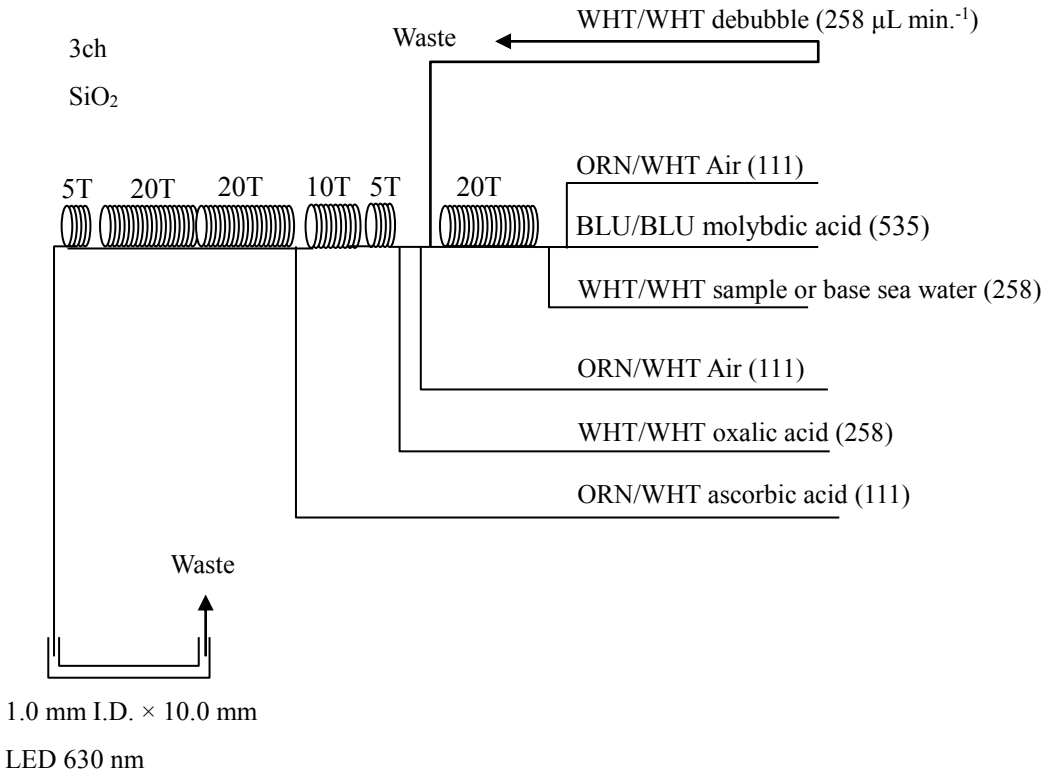

Figure 4.10.5 SiO_2 (3ch.) Flow diagram.

(4.5) Phosphate Reagents

Stock molybdate solution, 0.03 M (0.8% w/v)

Dissolve 8 g disodium molybdate(VI) dihydrate, $Na_2MoO_4 \cdot 2H_2O$, and 0.17 g antimony potassium tartrate, $C_8H_4K_2O_{12}Sb_2 \cdot 3H_2O$, in 950 mL of DIW and added 50 ml concentrated H_2SO_4.

Mixed Reagent

Dissolve 1.2 g L(+)-ascorbic acid, $C_6H_8O_6$, in 150 mL of stock molybdate solution. After mixing, 3 mL sodium dodecyl sulphate (15% solution in water) was added. This reagent was freshly prepared before every measurement.

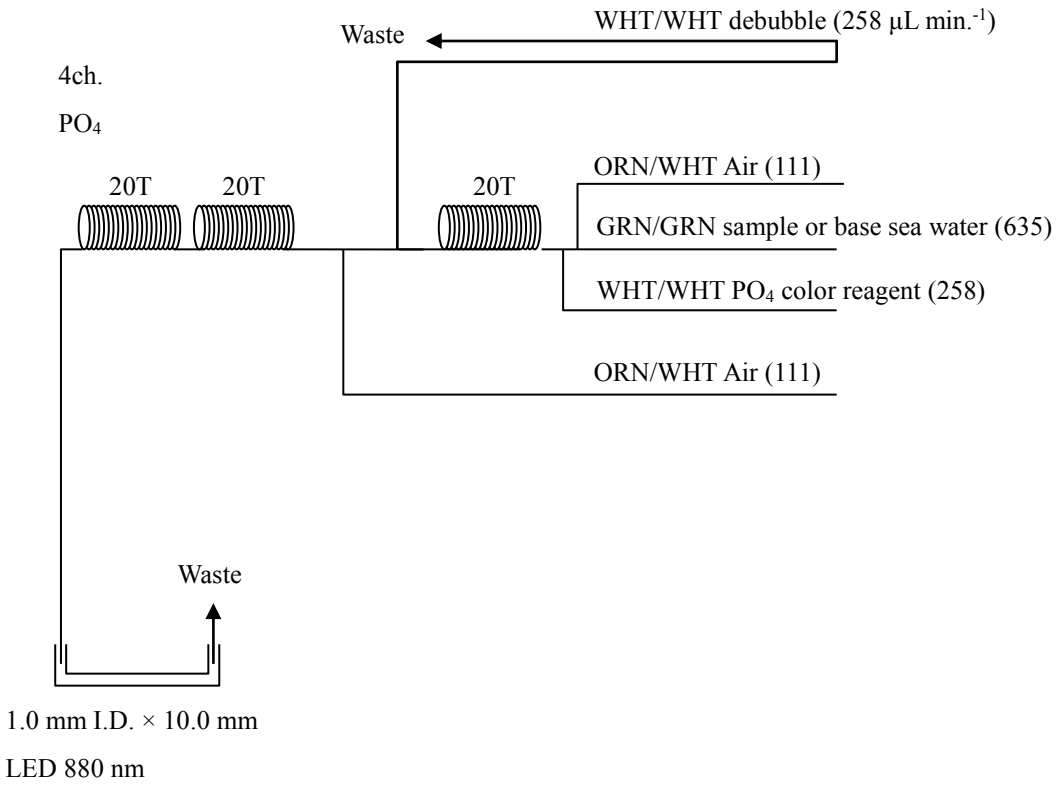

Figure 4.10.6 PO_4 (4ch.) Flow diagram.

(4.6) Ammonium Reagents

EDTA

Dissolve 41 g EDTA (ethylenediaminetetraacetatic acid tetrasodium salt), $C_{10}H_{12}N_2O_8Na_4 \bullet 4H_2O$, and 2 g boric acid, H_3BO_3, in 200 mL of DIW. After mixing, 1 mL Triton™ X-100 (30% solution in DIW) is added. This reagent is prepared at a week about.

NaOH

Dissolve 5 g sodium hydroxide, NaOH, and 16 g EDTA in 100 mL of DIW. This reagent is prepared at a week about.

Stock Nitroprusside

Dissolve 0.25 g sodium pentacyanonitrosylferrate(II), $Na_2[Fe(CN)_5NO]$, in 100 mL of DIW and add 0.2 mL 1N H_2SO_4. Stored in a dark bottle and prepared at a month about.

Nitroprusside solution

Mixed 4 mL stock nitroprusside and 5 mL 1N H_2SO_4 in 500 mL of DIW. After mixing, 2 mL Triton™ X-100 (30% solution in DIW) is added. This reagent is stored in a dark bottle and prepared at every 2 or

3 days.

Alkaline phenol

Dissolve 10 g phenol, C_6H_5OH, 5 g sodium hydroxide and citric acid, $C_6H_8O_7$, in 200 mL DIW. Stored in a dark bottle and prepared at a week about.

NaClO solution

Mix 3 mL sodium hypochlorite solution, NaClO, in 47 mL DIW. Stored in a dark bottle and fleshly prepared before every measurement. This reagent is prepared 0.3% available chlorine.

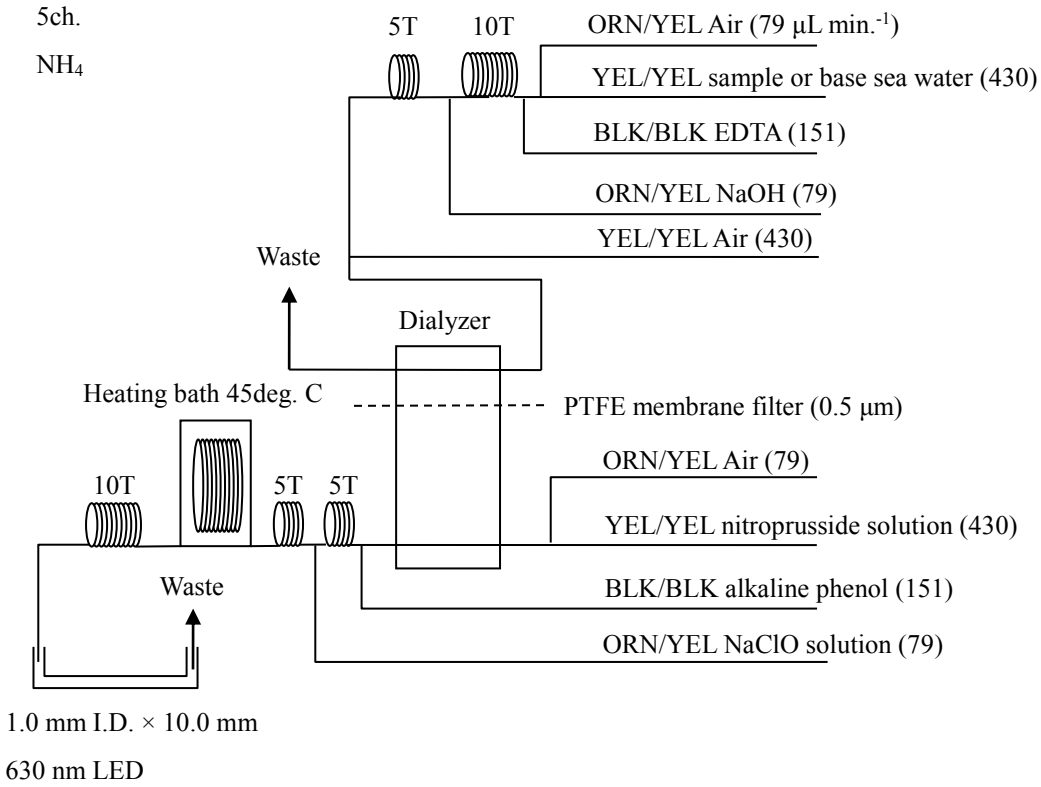

Figure 4.10.7 NH_4 (5ch.) Flow diagram.

(4.7) Sampling procedures

Sampling of nutrients followed that oxygen, salinity and trace gases. Samples were drawn into two of virgin 10 mL polyacrylates vials without sample drawing tubes. These were rinsed three times before filling and then vials were capped immediately after the drawing. The vials were put into water bath adjusted to ambient temperature, 22 ± 1 deg. C, in about 30 minutes before use to stabilize the temperature of samples in MR1609.

No transfer was made and the vials were set an auto sampler tray directly. Samples were analyzed

after collection basically within 24 hours in principal.

(4.8) Data processing

Raw data from QuAAtro 2-HR was treated as follows:

- Checked baseline shift.
- Checked the shape of each peak and positions of peak values taken, and then changed the positions of peak values taken if necessary.
- Carry-over correction and baseline drift correction were applied to peak heights of each samples followed by sensitivity correction.
- Baseline correction and sensitivity correction were done basically using liner regression.
- Loaded pressure and salinity from CTD data to calculate density of seawater. In case of bucket sample, we generally used bottle salinity from AUTOSAL.
- Calibration curves to get nutrients concentration were assumed second order equations.

(5) Certified Reference Material of nutrients in seawater

KANSO CRMs (Lot: BY, CD, CA, BW, CC, CB, BZ) were used to ensure the comparability and traceability of nutrient measurements during this cruise. The details of CRMs are shown below.

Production

KANSO CRMs are certified reference material (CRM) for inorganic nutrients in seawater. These were produced by KANSO Co.,Ltd. This certified reference material has been produced using autoclaved natural seawater on the basis of quality control system under IS0 Guide 34 (JIS Q 0034).
KANSO Co.,Ltd. has been accredited under the Accreditation System of National Institute of Technology and Evaluation (ASNITE) as a CRM producer since 2011. (Accreditation No.: ASNITE 0052 R)

Property value assignment

The certified values are arithmetic means of the results of 30 bottles from each batch (measured in duplicates) analysed by KANSO Co.,Ltd. and Japan Agency for Marine-Earth Science and Technology (JAMSTEC) using the colorimetric method (continuous flow analysis, CFA, method). The salinity of calibration solutions were adjusted to the salinity of this CRM ±0.5 psu.

Metrological Traceability

Each certified value of nitrate, nitrite, and phosphate of KANSO CRMs were calibrated versus one of Japan Calibration Service System (JCSS) standard solutions for each nitrate ions, nitrite ions, and phosphate ions. JCSS standard solutions are calibrated versus the secondary solution of JCSS for each of these ions. The secondary solution of JCSS is calibrated versus the specified primary solution produced

by Chemicals Evaluation and Research Institute (CERI), Japan. CERI specified primary solutionsare calibrated versus the National Metrology Institute of Japan (NMIJ) primary standards solution of nitrate ions, nitrite ions and phosphate ions, respectively.
For a certified value of silicate of KANSO CRM was determined by one of Merck KGaA silicon standard solution 1000 mg/L Si traceable to National Institute of Standards and Technology (NIST) SRM of silicon standard solution (SRM3150).

The certified values of nitrate, nitrite, and phosphate of KASNO CRM are thus traceable to the International System of Units (SI) through an unbroken chain of calibrations, JCSS, CERI and NMIJ solutions as stated above, each having stated uncertainties. The certified values of silicate of KANSO CRM are traceable to the International System of Units (SI) through an unbroken chain of calibrations, Merck KGaA and NIST SRM3150 solutions, each having stated uncertainties.

As stated in the certificate of NMIJ CRMs each certified value of dissolved silica, nitrate ions, and nitrite ions was determined by more than one method using one of NIST (National Institute of Standards and Technology) SRM of silicon standard solution and NMIJ primary standards solution of nitrate ions and nitrite ions. The concentration of phosphate ions as stated information value in the certificate was determined NMIJ primary standards solution of phosphate ions. Those values in the certificate of NMIJ CRMs are traceable to the International System of Units (SI).

One of analytical methods used for certification of NMIJ CRM for nitrate ions, nitrite ions, phosphate ions and dissolved silica was colorimetric method (continuous mode and batch one). The colorimetric method is same as the analytical method (continuous mode only) used for certification of KANSO CRM. For certification of dissolved silica, exclusion chromatography/isotope dilution-inductively coupled plasma mass spectrometry and Ion exclusion chromatography with post-column detection were used. For certification of nitrate ions, Ion chromatography by direct analysis and Ion chromatography after halogen-ion separation were used. For certification of nitrite ions, Ion chromatography by direct analysis was used.

NMIJ CRMs were analysed at the time of certification process for CRM and the results were confirmed within expanded uncertainty stated in the certificate of NMIJ CRMs.

(5.1) CRMs for this cruise

5 lot of CRMs were used as calibration standards together with the C-6. These bottles were stored at a room in the ship, REAGENT STORE, where the temperature was maintained around 20- 24 deg. C. The concentrations for CRM lots BY, CD, CA, BW, CB, BZ, and CC are shown in Table 4.10.3.

Table 4.10.3 Certified concentration and uncertainty (k=2) of CRMs.

unit: μmol kg^{-1}

Lot	Nitrate	Nitrite	Silicate	Phosphate	Ammonia*
BY	**0.02 ± 0.02**	**0.02 ± 0.01**	**1.76 ± 0.06**	**0.039 ± 0.010**	**0.89**
CD	**5.50 ± 0.05**	**0.02 ± 0.01**	**13.93 ± 0.10**	**0.446 ± 0.008**	**1.11**
CA	**19.66 ± 0.15**	**0.06 ± 0.01**	**36.58 ± 0.22**	**1.407 ± 0.014**	**0.67**
BW	**24.59 ± 0.20**	**0.07 ± 0.01**	**60.01 ± 0.42**	**1.541 ± 0.014**	**0.93**
CB	**35.79 ± 0.27**	**0.12 ± 0.01**	**109.2 ± 0.62**	**2.520 ± 0.022**	**0.77**
BZ	**43.35 ± 0.33**	**0.22 ± 0.01**	**161.0 ± 0.93**	**3.056 ± 0.033**	**0.43**
CC	**30.88 ± 0.24**	**0.12 ± 0.01**	**86.16 ± 0.48**	**2.080 ± 0.019**	**1.05**

*For ammonia values are references

(6) Nutrients standards

(6.1) Volumetric laboratory ware of in-house standards

All volumetric glass ware and polymethylpentene (PMP) ware used were gravimetrically calibrated. Plastic volumetric flasks were gravimetrically calibrated at the temperature of use within 3 K.

Volumetric flasks

Volumetric flasks of Class quality (Class A) are used because their nominal tolerances are 0.05 % or less over the size ranges likely to be used in this work. Class A flasks are made of borosilicate glass, and the standard solutions were transferred to plastic bottles as quickly as possible after they are made up to volume and well mixed in order to prevent excessive dissolution of silicate from the glass. PMP volumetric flasks were gravimetrically calibrated and used only within 3 K of the calibration temperature.

The computation of volume contained by glass flasks at various temperatures other than the calibration temperatures were done by using the coefficient of linear expansion of borosilicate crown glass.

Because of their larger temperature coefficients of cubical expansion and lack of tables constructed for these materials, the plastic volumetric flasks were gravimetrically calibrated over the temperature range of intended use and used at the temperature of calibration within 3 K. The weights obtained in the calibration weightings were corrected for the density of water and air buoyancy.

Pipettes and pipettors

All pipettes were gravimetrically calibrated in order to verify and improve upon the nominal tolerance.

(6.2) Reagents, general considerations

Specifications

For nitrate standard, "potassium nitrate 99.995 suprapur®" provided by Merck, Lot. B0771365211, CAS No.: 7757-91-1, was used.

For nitrite standard solution, we used "nitrous acid iron standard solution (NO_2^- 1000) provided by Wako, Lot ECF5432 (Leg2) and ECP4122 (Leg3), Code. No. 140-06451." This standard solution was certified by Wako using Ion chromatograph method. Calibration result is 999 mg L^{-1} at 20 degree Celsius. Expanded uncertainty of calibration (k=2) is 0.7 % for the calibration result.

For phosphate standard, "potassium dihydrogen phosphate anhydrous 99.995 suprapur®" provided by Merck, Lot. B1144508528, CAS No.: 7778-77-0, was used.

For the silicate standard, we use "Silicon standard solution SiO_2 in NaOH 0.5 mol/l CertiPUR®" provided by Merck, CAS No.: 1310-73-2, of which lot number is HC54715536 are used. The silicate concentration is certified by NIST-SRM3150 with the uncertainty of 0.7 %. HC54715536 is certified as 1005 mg L^{-1}.

For ammonia standard, "ammonium Chloride" provided by NMIJ. We used NMIJ CRM 3011-a. The purity of this standard was greater than 99.9 %. Expanded uncertainty of calibration (k=2) is 0.065 %.

Treatment of silicate standard due to high alkalinity

Since the silicon standard solution Merck CertiPUR® is in NaOH 0.5 mol/l, we need to dilute and neutralize to avoid make precipitation of $MgOH_2$ etc. When we make B standard, silicon standard solution is diluted by factor 12 with pure water and neutralized by HCl 1.0 mol L^{-1} to be about 7. After that B standard solution is used to prepare C standards.

Ultra pure water

Ultra pure water (MilliQ water) freshly drawn was used for preparation of reagents, standard solutions and for measurement of reagent and system blanks.

Low-Nutrient Seawater (LNSW)

Surface water having low nutrient concentration was taken and filtered using 0.20 μm pore capsule cartridge filter at MR1505 cruise on January, 2016. This water is stored in 20 liter cubitainer with paper box.

LNSW concentrations were assigned in August 2016 during MR1606 cruise.

(6.3) Concentrations of nutrient for A, B and C standards

Concentrations of nutrients for A, B, C and D standards are set as shown in Table 4.10.4 and Table 4.10.6. The C standard is prepared according recipes as shown in Table 4.10.5. and Table 4.10.7. All

volumetric laboratory tools were calibrated prior the cruise as stated in chapter (6.1). Then the actual concentration of nutrients in each fresh standard was calculated based on the ambient, solution temperature and determined factors of volumetric laboratory wares.

The calibration curves for each run were obtained using 6 levels, C-1, C-2, C-3, C-4, C-5 and C-6. C-1, C-2, C-3, C-4 and C-5 were the certified reference material of nutrients in seawater (hereafter CRM) and C-6 was in-house standard.

Table 4.10.4 Nominal concentrations of nutrients for A, B and C standards in Leg2.

	A	B	D	C-1	C-2	C-3	C-4	C-5	C-6	C-7	C-8
NO_3(μM)	22500	900	900	BY	CD	BW	CC	CB	45	-	-
NO_2(μM)	21800	26	875	BY	CD	BW	CC	CB	1.0	-	-
SiO_2(μM)	35800	2860		BY	CD	BW	CC	CB	144	-	-
PO_4(μM)	3000	60		BY	CD	BW	CC	CB	3.0	-	-
NH_4(μM)	4000	200		-	-	-	-	-	6.0	2.0	0

Table 4.10.5 Working calibration standard recipes in Leg2.

C std.	B-1 std.	B-2 std.	B-3 std
C-6	25 mL	20 mL	15 mL
C-7	-	-	5 mL
C-8	-	-	0 mL

Table 4.10.6 Nominal concentrations of nutrients for A, B and C standards in Leg3.

	A	B	D	C-1	C-2	C-3	C-4	C-5	C-6	C-7	C-8
NO_3(μM)	22500	900	900	BY	CD	CA	BW	BZ	36	-	-
NO_2(μM)	21800	26	875	BY	CD	CA	BW	BZ	1.0	-	-
SiO_2(μM)	35800	2860		BY	CD	CA	BW	BZ	115	-	-
PO_4(μM)	3000	60		BY	CD	CA	BW	BZ	2.4	-	-
NH_4(μM)	4000	200		-	-	-	-	-	6.0	2.0	0

Table 4.10.7 Working calibration standard recipes in Leg3.

C std.	B-1 std.	B-2 std.	B-3 std
C-6	20 mL	20 mL	15 mL
C-7	-	-	5 mL
C-8	-	-	0 mL

B-1 std.: Mixture of nitrate, silicate and phosphate

B-2 std.: Nitrite

B-3 std: Ammonium

(6.4) Renewal of in-house standard solutions.

In-house standard solutions as stated in paragraph (5) were renewed as shown in Table 4.10.8 (a) to (c).

Table 4.10.8(a) Timing of renewal of in-house standards.

NO_3, NO_2, SiO_2, PO_4, NH_4	Renewal
A-1 std. (NO_3)	maximum a month
A-2 std. (NO_2)	commercial prepared solution
A-3 std. (SiO_2)	commercial prepared solution
A-4 std. (PO_4)	maximum a month
A-5 std. (NH_4)	maximum a month
B-1 std. (mixture of A-1, A-3 and A-4 std.)	maximum 8 days
B-2 std. (dilute D-2 std.)	maximum 8 days
B-3 std. (dilute A-5 std.)	maximum 8 days

Table 4.10.8(b) Timing of renewal of in-house standards.

Working standards	Renewal
C-6 std. (mixture of B-1, B-2 and B-3 std.) C-7 std. (dilute B-3 std.) C-8 (LNSW)	every 24 hours

Table 4.10.8(c) Timing of renewal of in-house standards for reduction estimation.

Reduction estimation	Renewal
D-1 std. (900 µM NO_3)	maximum 8 days
D-2 std. (875 µM NO_2)	maximum 8 days
36 µM NO_3	when C Std. renewed
35 µM NO_2	when C Std. renewed

(7) Quality control

(7.1) Precision of nutrients analyses during this cruise

Precision of nutrients analyses during this cruise was evaluated based on the 7 to 11 measurements, which are measured every 8 to 13 samples, during a run at the concentration of C-6 std. Summary of precisions are shown as Table 4.10.9, Table 4.10.10 and Figures 4.10.8 to 4.10.13, the precisions for each parameter are generally good considering the analytical precisions during the R/V Mirai cruses conducted in 2009 - 2015. Analytical precisions in Leg2 were 0.15% for nitrate, 0.13% for phosphate and 0.07% for silicate in terms of median of precision, respectively. Analytical precisions in Leg3 were 0.18% for nitrate, 0.15% for phosphate and 0.12% for silicate in terms of median of precision, respectively.

Table 4.10.9 Summary of precision based on the replicate analyses for unit 1 in Leg2.

	Nitrate CV%	Nitrite CV%	Silicate CV%	Phosphate CV %	Ammonium CV %
Median	**0.15**	**0.13**	**0.07**	**0.14**	**0.24**
Mean	**0.15**	**0.13**	**0.07**	**0.13**	**0.27**
Maximum	**0.26**	**0.26**	**0.17**	**0.19**	**0.40**
Minimum	**0.06**	**0.04**	**0.03**	**0.08**	**0.16**
N	**8**	**8**	**8**	**8**	**8**

Table 4.10.10 Summary of precision based on the replicate analyses for all unit in Leg3.

	Nitrate CV%	Nitrite CV%	Silicate CV%	Phosphate CV %	Ammonium CV %
Median	**0.17**	**0.21**	**0.12**	**0.14**	**0.25**
Mean	**0.18**	**0.25**	**0.12**	**0.15**	**0.28**
Maximum	**0.42**	**0.56**	**0.25**	**0.27**	**0.51**
Minimum	**0.07**	**0.10**	**0.04**	**0.06**	**0.09**
N	**23**	**23**	**23**	**23**	**23**

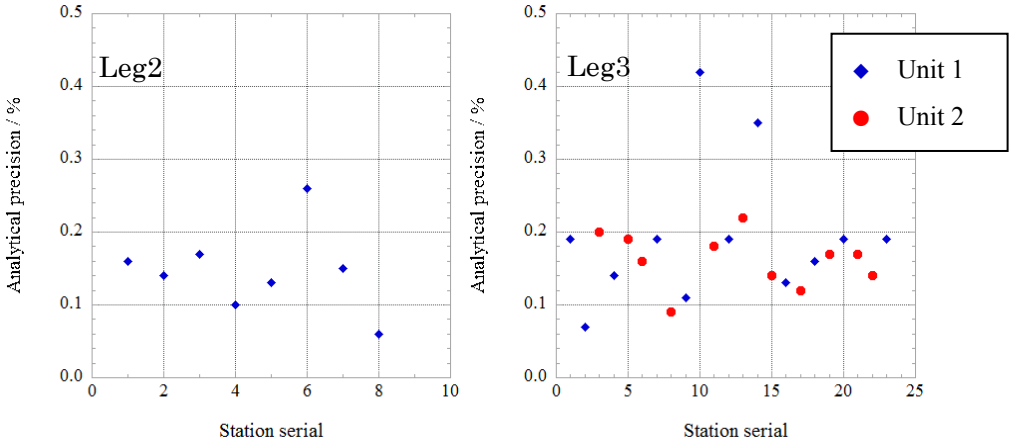

Figure 4.10.8 Time series of precision of nitrate in MR1609Leg2 and Leg3.

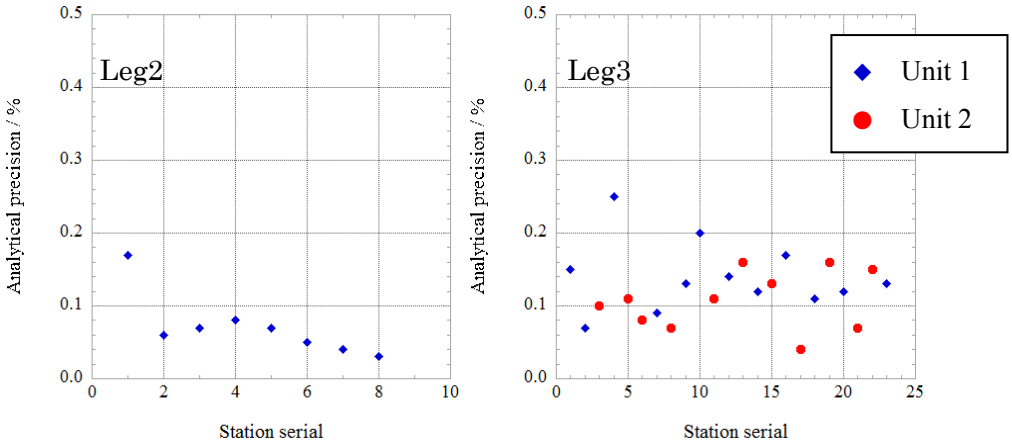

Figure 4.10.9 Time series of precision of silicate in MR1609Leg2 and Leg3

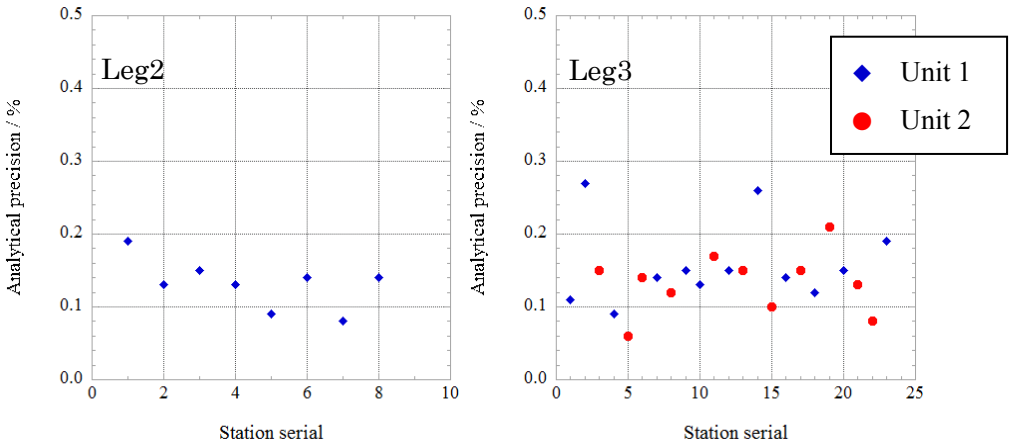

Figure 4.10.10 Time series of precision of phosphate in MR1609Leg2 and Leg3.

(7.2) CRM lot. CC measurement during this cruise

CRM lot. CC was measured every run to monitor the comparability among runs. The results of lot. BV during this cruise are shown as Figures 4.10.11 to 4.10.16. Error bars represent analytical precision in Figures 4.10.8 to 4.10.13.

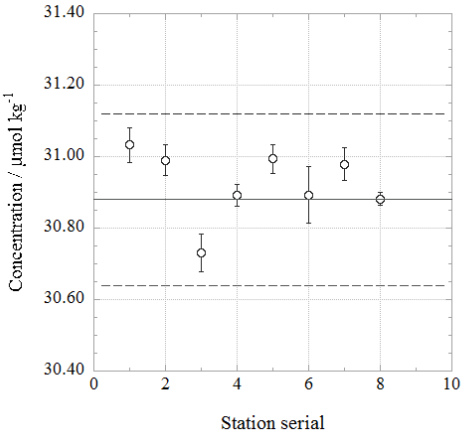

Figure 4.10.11 Time series of CRM-CC of nitrate in MR1609Leg2.
Solid line : certified value, broken line : uncertainty of certified value (*k*=2)

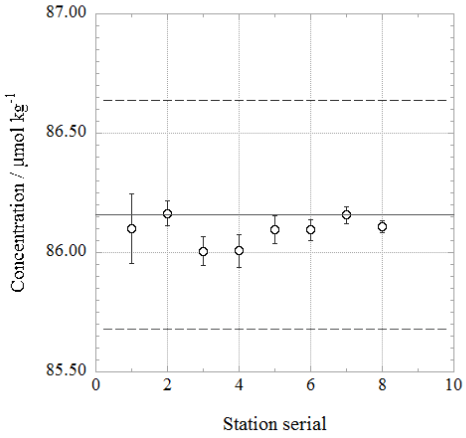

Figure 4.10.12 Time series of CRM-CC of silicate in MR1609Leg2.
Solid line : certified value, broken line : uncertainty of certified value (*k*=2)

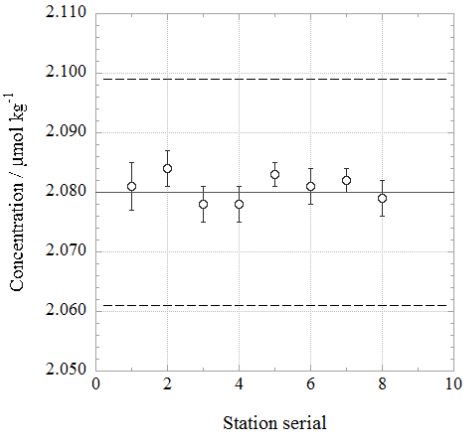

Figure 4.10.13 Time series of CRM-CC of phosphate in MR1609Leg2.
Solid line : certified value, broken line : uncertainty of certified value (*k*=2)

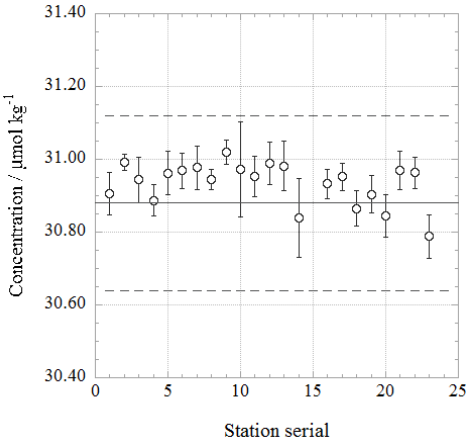

Figure 4.10.14 Time series of CRM-CC of nitrate in MR1609Leg3.
Solid line : certified value, broken line : uncertainty of certified value (*k*=2)

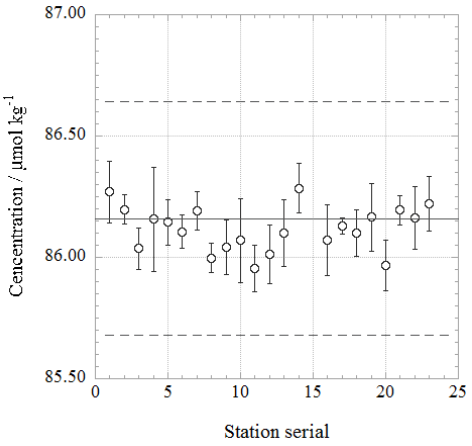

Figure 4.10.15 Time series of CRM-CC of silicate in MR1609Leg3.
Solid line : certified value, broken line : uncertainty of certified value (*k*=2)

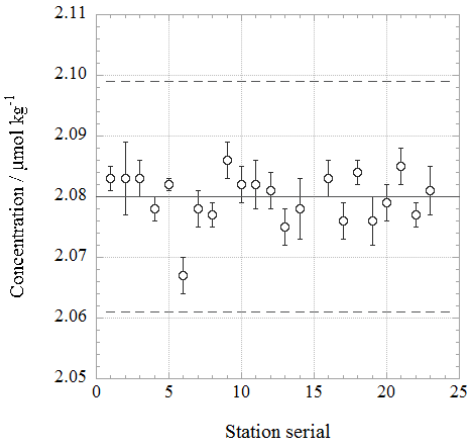

Figure 4.10.16 Time series of CRM-CC of phosphate in MR1609Leg3.
Solid line : certified value, broken line : uncertainty of certified value (*k*=2)

(7.3) Carryover

We can also summarize the magnitudes of carryover throughout the cruise. These are small enough within acceptable levels as shown in Table 4.10.11, Table 4.10.12 and Figures 4.10.17 to 4.10.19. The carryover in silicate and phosphate had a bias by equipments. It was 0.09% and 0.14%, mean value, at Unit 2. The other hand, it was 0.17% and 0.29 %, mean value, at Unit 1.

Table 4.10.11 Summary of carry over throughout Leg2.

	Nitrate CV%	Nitrite CV%	Silicate CV%	Phosphate CV %	Ammonium CV %
Median	0.19	0.16	0.20	0.16	0.66
Mean	0.19	0.16	0.20	0.16	0.63
Maximum	0.22	0.35	0.22	0.19	0.95
Minimum	0.15	0.00	0.18	0.12	0.19
N	8	8	8	8	8

Table 4.10.12 Summary of carry over throughout Leg3.

	Nitrate CV%	Nitrite CV%	Silicate CV%	Phosphate CV %	Ammonium CV %
Median	0.18	0.14	0.11	0.17	0.77
Mean	0.18	0.15	0.13	0.22	0.74
Maximum	0.26	0.48	0.24	0.43	1.34
Minimum	0.11	0.00	0.00	0.04	0.14
N	23	23	23	23	23

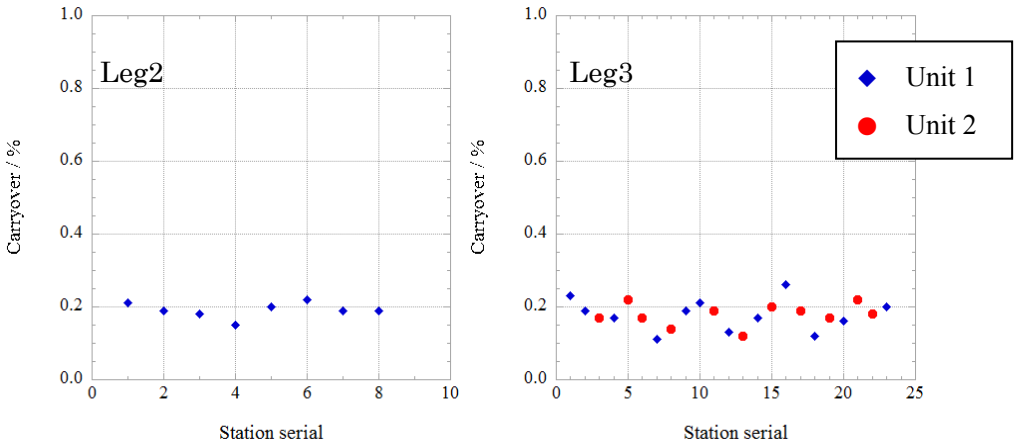

Figure 4.10.17 Time series of carryover of nitrate in MR1609Leg2 and Leg3.

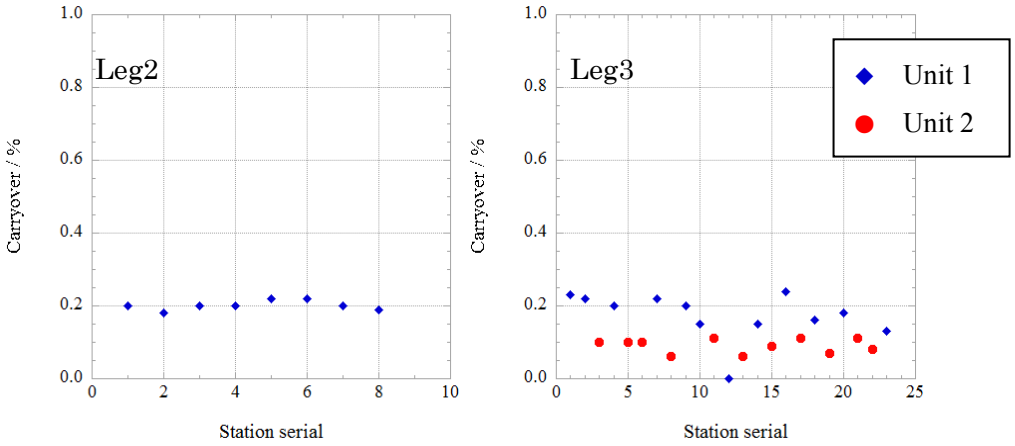

Figure 4.10.18 Time series of carryover of silicate in MR1609Leg2 and Leg3.

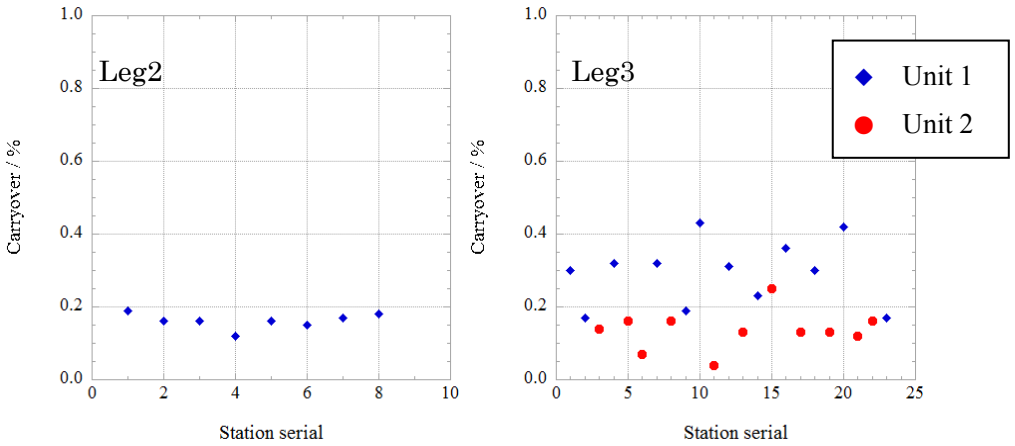

Figure 4.10.19 Time series of carryover of phosphate in MR1609Leg2 and Leg3.

(7.4) Estimation of uncertainty of phosphate, nitrate and silicate concentrations

We estimate the uncertainty of measurement of nutrient by merging data from both Leg2 and Leg3 because the numbers of the run in each leg were small, 8 runs and 23 runs, respectively.

Empirical equations, eq. (1), (2), and (3) to estimate uncertainty of measurement of phosphate, nitrate and silicate are used based on measurements of 31 sets of CRMs during this cruise. Empirical equations, eq. (4), (5) are used to estimate uncertainty of measurement of nitrite and ammonium based on duplicate measurements of the samples. These empirical equations and graphic presentation of equations are as follows, respectively.

Phosphate Concentration Cp in μmol kg^{-1}:

Uncertainty of measurement of phosphate (%) =

$0.051 + 0.256 * (1 / Cp)$ --- (1)

where Cp is phosphate concentration of sample.

Nitrate Concentration Cno_3 in µmol kg^{-1}:

Uncertainty of measurement of nitrate (%) =

$0.13 + 1.46 * (1 / Cno_3)$ --- (2)

where Cno_3 is nitrate concentration of sample.

Silicate Concentration Cs in µmol kg^{-1}:

Uncertainty of measurement of silicate (%) =

$0.08 + 2.19 * (1 / Cs)$ --- (3)

where Cs is silicate concentration of sample.

Nitrite Concentration Cno_2 in µmol kg^{-1}:

Uncertainty of measurement of nitrite (%) =

$-0.23 + 0.25 * (1 / Cno_2) - 0.000014 * (1 / Cno_2) * (1 / Cno_2)$ --- (4)

where Ca is ammonium concentration of sample.

Ammonium Concentration Ca in µmol kg^{-1}:

Uncertainty of measurement of ammonium (%) =

$0.58 + 1.50 * (1 / Ca) - 0.00046 * (1 / Ca) * (1 / Ca)$ --- (5)

where Ca is ammonium concentration of sample.

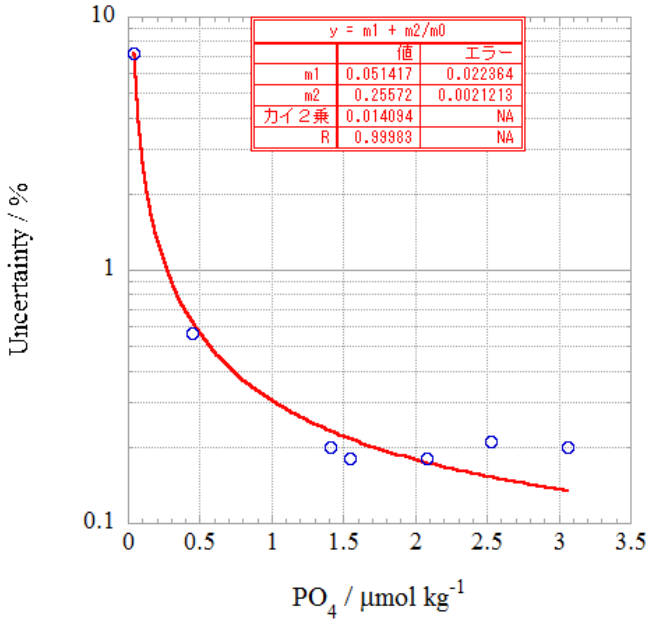

Figure 4.10.20 Estimation of uncertainty for phosphate in MR1609.

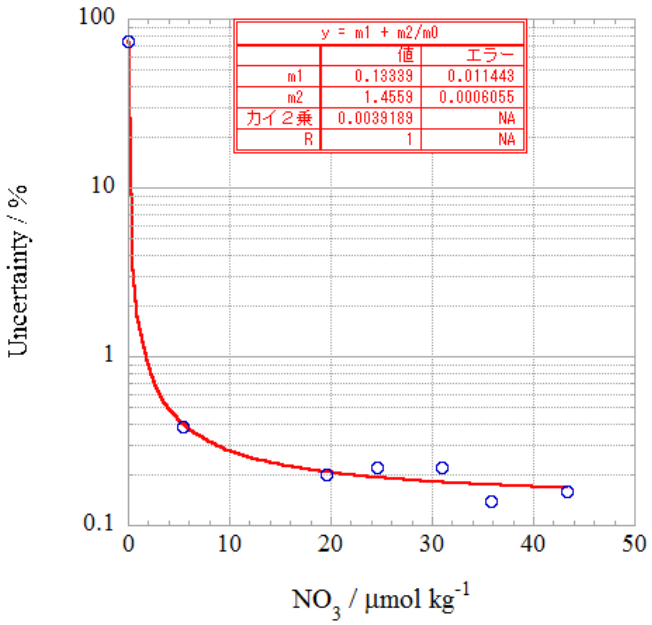

Figure 4.10.21 Estimation of uncertainty for nitrate in MR1609.

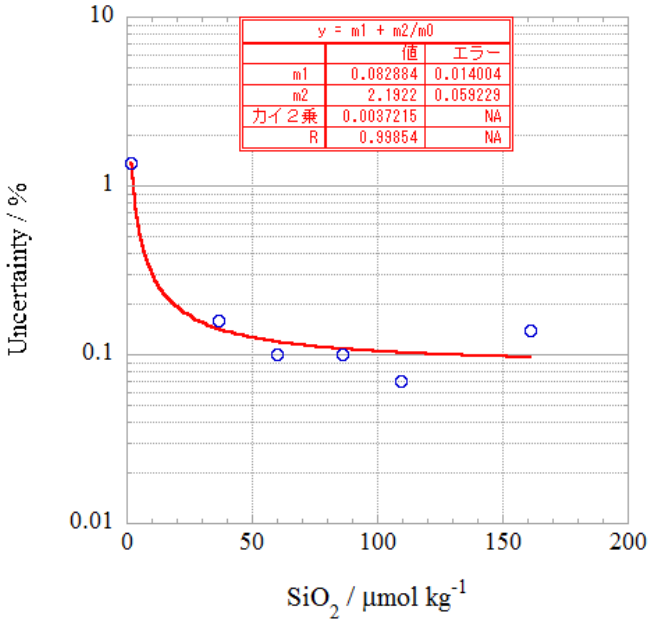

Figure 4.10.22 Estimation of uncertainty for silicate in MR1609.

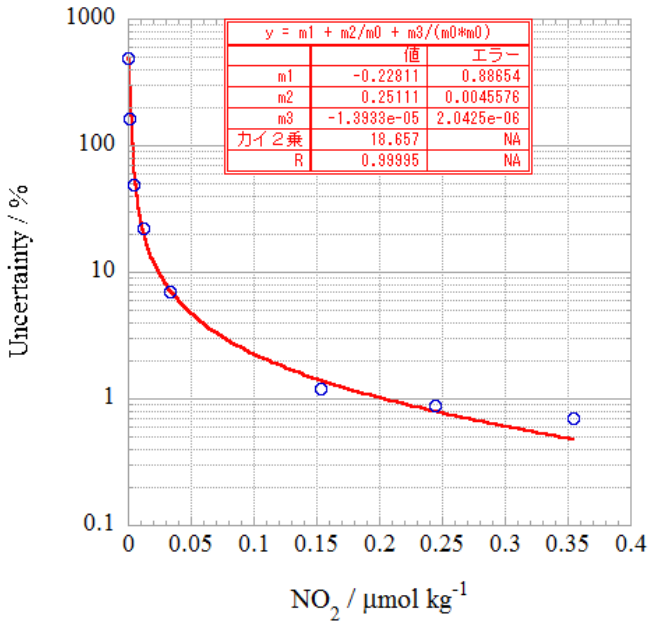

Figure 4.10.23 Estimation of uncertainty for nitrite in MR1609.

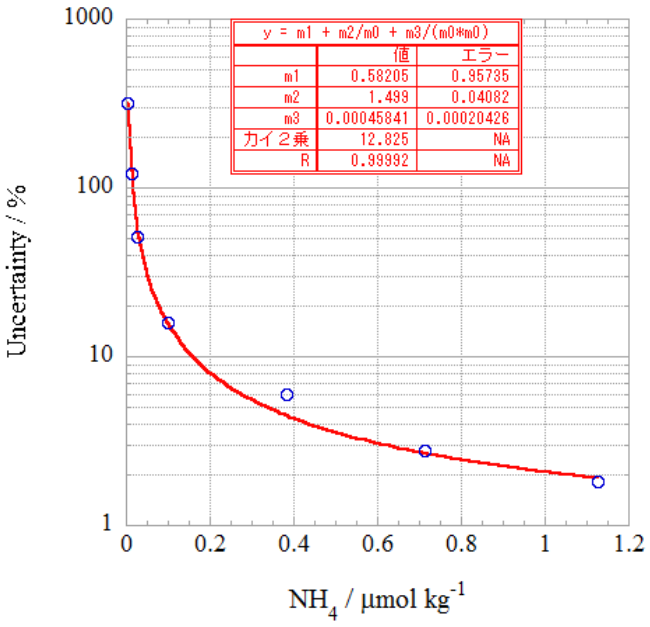

Figure 4.10.24 Estimation of uncertainty for ammonium in MR1609.

(8) Problems / improvements occurred and solutions

(8.1) Centrifuged samples

When we found the value of transparency of the sample was less than 100% or doubtful for the particles in the sample, we carried out centrifuging for the samples by using the centrifuge (type : CN-820, AZONE). The centrifuged sample list for nutrients is shown in Table 4.10.13 and Table 4.10.14.

Table 4.10.13 Centrifugation sample list of MR1609Leg2

Station	Cast	Bottle	Depth(dbar)	Trans(%)
6	1	0	0	-
		32	10.6	86.591
		35	25.7	86.667
		29	25.7	86.612
10	2	0	0	-
		34	10.8	96.177
		33	25.6	96.200
		32	51	96.283
12	B	35	27	95.235
		30	26.6	95.270
		27	50.4	95.305
		24	102	99.468

11	B	0	0	-
		32	11.4	96.237
		35	25.8	96.217
		29	26.1	96.247
		26	50.7	96.273
11	A	0	0	-
		32	11	92.910
		29	25.1	92.765
		26	50	95.334
		23	101.4	99.720

Table4.10.14 Centrifugation sample list of MR1609Leg3

Station	Cast	Bottle	Depth(dbar)	Trans(%)
2	1	0	0	-
		36	11.2	89.205
		2	21.2	89.464
		35	51.6	95.998
		34	99.8	99.994
3	1	0	0	-
		36	12.6	90.649
		35	50.8	91.419
		34	101	99.875
4	1	0	0	-
		36	11.8	92.014
		2	31.3	92.152
		35	51.4	95.637
		34	101.5	99.606
5	1	0	0	-
		36	10.6	96.588
		35	50.6	96.441
		34	100.2	99.501
		33	150.9	99.992
6	1	0	0	-
		36	10.1	96.804
		35	50.6	96.816
		2	69.9	97.251
		34	102.4	98.945
		33	150.9	99.946
7	1	0	0	-
		36	11.7	96.804
		35	51.7	96.844
		34	101.2	99.672

		33	150.8	99.858
8	1	0	0	-
		36	11.2	97.279
		35	50.3	97.292
		2	67.6	98.584
		34	101.8	99.388
		33	151.6	99.699
9	1	0	0	-
		36	12	97.035
		35	52.1	97.04
		34	101.5	99.548
		33	151.6	99.773
10	1	0	0	-
		36	10.2	97.433
		35	52	97.424
		2	67.3	97.449
		34	102.3	99.107
		33	150.3	99.836
11	1	0	0	-
		36	10.5	97.242
		35	51.3	97.503
		34	102	99.117
		33	152.4	99.578
		32	201.6	99.885
		31	250.9	99.997
12	1	0	0	-
		36	11.4	98.067
		35	52.5	98.286
		2	80.4	98.402
		34	101.7	99.367
		33	150.6	99.908
13	1	0	0	-
		36	11.9	97.178
		2	31.7	97.077
		35	52.2	97.258
		34	101.7	98.83
		33	150.8	99.519
15	1	0	0	-
		36	10	97.758
		35	50.3	97.774
		2	75.9	97.812
		34	100.5	98.683

		33	152.1	99.706
		32	200.4	99.956
16	1	0	0	-
		36	12.1	98.011
		35	53	98.083
		2	77.3	98.242
		34	104.1	99.211
18	1	0	0	-
		36	11.5	98.226
		35	51	98.232
		2	82.5	98.503
		34	101.6	99.776
20	1	0	0	-
		36	10.7	98.364
		35	51.2	98.386
		2	86	98.525
		34	101.9	99.12
		33	151.6	99.875
21	1	0	0	-
		36	11.2	97.343
		35	50.7	97.489
		2	66.5	97.987
		34	101.9	99.987
22	1	0	0	-
		36	11.3	97.419
		35	51.3	97.556
		34	101.8	99.961
23	1	0	0	-
		36	11.8	97.86
		2	32.5	97.804
		35	51.9	97.875
		34	101.2	98.583
24	1	0	0	-
		36	10.8	97.95
		2	30.9	97.937
		35	50.2	98.013
		34	100.2	98.279
25	1	0	0	-
		36	10.9	97.569
		2	21.4	97.588
		35	52.1	97.62
		34	102	99.851

		0	0	-
		36	11	97.177
26	1	35	51	97.28
		2	75.9	97.536
		34	100.8	99.342

(8.2) Bad peak shape at NO3+NO2 channel

We found that peak shape at NO3+NO2 channel became bad in the middle of run for stn. 10 and stn. 11 in Leg3. The bad peak shape was probably due to clogging of Cd coil. We speculated that at stations 1, 2 and 4, the chlorophyll concentration exceeded 1 micro g l^{-1} and transparency of samples were around 90 %, then the magnitude of centrifugation of these samples might not enough and a part of the particles remains. The cause of the damage of the Cd coil might come from the remained particles.

We analysed again all samples of stn. 10 and stn. 11. We accepted NO3 data of first run for all samples except for 10_1_9 that both primary and secondary peak shape was bad at the first run. NO_3 data of second run was accepted for 10_1_9.

We should re-examine the condition of centrifugation of such samples of which chlorophyll contents is high and transparency is low.

(9) Data archive

All data will be submitted to JAMSTEC Data Management Office (DMO) and is currently under its control.

References

Aminot, A. and Kerouel, R. 1991. Autoclaved seawater as a reference material for the determination of nitrate and phosphate in seawater. Anal. Chim. Acta, 248: 277-283.

Aminot, A. and Kirkwood, D.S. 1995. Report on the results of the fifth ICES intercomparison exercise for nutrients in sea water, ICES coop. Res. Rep. Ser., 213.

Aminot, A. and Kerouel, R. 1995. Reference material for nutrients in seawater: stability of nitrate, nitrite, ammonia and phosphate in autoclaved samples. Mar. Chem., 49: 221-232.

Aoyama M., and Joyce T.M. 1996, WHP property comparisons from crossing lines in North Pacific. In Abstracts, 1996 WOCE Pacific Workshop, Newport Beach, California.

Aoyama, M., 2006: 2003 Intercomparison Exercise for Reference Material for Nutrients in Seawater in a Seawater Matrix, Technical Reports of the Meteorological Research Institute No.50, 91pp, Tsukuba, Japan.

Aoyama, M., Susan B., Minhan, D., Hideshi, D., Louis, I. G., Kasai, H., Roger, K., Nurit, K., Doug, M., Murata, A., Nagai, N., Ogawa, H., Ota, H., Saito, H., Saito, K., Shimizu, T., Takano, H., Tsuda, A., Yokouchi, K., and Agnes, Y. 2007. Recent Comparability of Oceanographic Nutrients Data: Results of a 2003 Intercomparison Exercise Using Reference Materials. Analytical Sciences, 23: 1151-1154.

Aoyama M., J. Barwell-Clarke, S. Becker, M. Blum, Braga E. S., S. C. Coverly,E. Czobik, I. Dahllof, M. H. Dai, G. O. Donnell, C. Engelke, G. C. Gong, Gi-Hoon Hong, D. J. Hydes, M. M. Jin, H. Kasai, R. Kerouel, Y. Kiyomono, M. Knockaert, N. Kress, K. A. Krogslund, M. Kumagai, S. Leterme, Yarong Li, S. Masuda, T. Miyao, T. Moutin, A. Murata, N. Nagai, G.Nausch, M. K. Ngirchechol, A. Nybakk, H. Ogawa, J. van Ooijen, H. Ota, J. M. Pan, C. Payne, O. Pierre-Duplessix, M. Pujo-Pay, T. Raabe, K. Saito, K. Sato, C. Schmidt, M. Schuett, T. M. Shammon, J. Sun, T. Tanhua, L. White, E.M.S. Woodward, P. Worsfold, P. Yeats, T. Yoshimura, A.Youenou, J. Z. Zhang, 2008: 2006 Intercomparison Exercise for Reference Material for Nutrients in Seawater in a Seawater Matrix, Technical Reports of the Meteorological Research Institute No. 58, 104pp.

Aoyama, M., Nishino, S., Nishijima, K., Matsushita, J., Takano, A., Sato, K., 2010a. Nutrients, In: R/V Mirai Cruise Report MR10-05. JAMSTEC, Yokosuka, pp. 103-122.

Aoyama, M., Matsushita, J., Takano, A., 2010b. Nutrients, In: MR10-06 preliminary cruise report. JAMSTEC, Yokosuka, pp. 69-83

Gouretski, V.V. and Jancke, K. 2001. Systematic errors as the cause for an apparent deep water property variability: global analysis of the WOCE and historical hydrographic data・REVIEW ARTICLE, Progress In Oceanography, 48: Issue 4, 337-402.

Grasshoff, K., Ehrhardt, M., Kremling K. et al. 1983. Methods of seawater anylysis. 2nd rev. Weinheim: Verlag Chemie, Germany, West.

Hydes, D.J., Aoyama, M., Aminot, A., Bakker, K., Becker, S., Coverly, S., Daniel, A., Dickson, A.G., Grosso, O., Kerouel, R., Ooijen, J. van, Sato, K., Tanhua, T., Woodward, E.M.S., Zhang, J.Z., 2010. Determination of Dissolved Nutrients (N, P, Si) in Seawater with High Precision and Inter-Comparability Using Gas-Segmented Continuous Flow Analysers, In: GO-SHIP Repeat Hydrography Manual: A Collection of Expert Reports and Guidelines. IOCCP Report No. 14, ICPO Publication Series No 134.

Joyce, T. and Corry, C. 1994. Requirements for WOCE hydrographic programmed data reporting. WHPO Publication, 90-1, Revision 2, WOCE Report No. 67/91.

Kawano, T., Uchida, H. and Doi, T. WHP P01, P14 REVISIT DATA BOOK, (Ryoin Co., Ltd., Yokohama, 2009).

Kimura, 2000. Determination of ammonia in seawater using a vaporization membrane permeability method. 7th auto analyzer Study Group, 39-41.

Kirkwood, D.S. 1992. Stability of solutions of nutrient salts during storage. Mar. Chem., 38 : 151-164.

Kirkwood, D.S. Aminot, A. and Perttila, M. 1991. Report on the results of the ICES fourth intercomparison exercise for nutrients in sea water. ICES coop. Res. Rep. Ser., 174.

Mordy, C.W., Aoyama, M., Gordon, L.I., Johnson, G.C., Key, R.M., Ross, A.A., Jennings, J.C. and Wilson. J. 2000. Deep water comparison studies of the Pacific WOCE nutrient data set. Eos Trans-American Geophysical Union. 80 (supplement), OS43.

Murphy, J., and Riley, J.P. 1962. Analyticachim. Acta 27, 31-36.

Sato, K., Aoyama, M., Becker, S., 2010. CRM as Calibration Standard Solution to Keep Comparability for Several Cruises in the World Ocean in 2000s. In: Aoyama, M., Dickson, A.G., Hydes, D.J., Murata, A., Oh, J.R., Roose, P., Woodward, E.M.S., (Eds.), Comparability of nutrients in the world's ocean. Tsukuba, JAPAN: MOTHER TANK, pp 43-56.

Uchida, H. &Fukasawa, M. WHP P6, A10, I3/I4 REVISIT DATA BOOK Blue Earth Global Expedition 2003 1, 2, (Aiwa Printing Co., Ltd., Tokyo, 2005).

4.11 Density

March 4, 2017

(1) Personnel

Hiroshi Uchida (JAMSTEC)

Takuhei Shiozaki (JAMSTEC)

(2) Objectives

The objective of this study is to collect absolute salinity (also called "density salinity") data, and to evaluate an algorithm to estimate absolute salinity provided along with TEOS-10 (the International Thermodynamic Equation of Seawater 2010) (IOC et al., 2010).

(3) Materials and methods

Seawater densities were measured during the cruise with an oscillation-type density meter (DMA 5000M, serial no. 80570578, Anton-Paar GmbH, Graz, Austria) with a sample changer (Xsample 122, serial no. 80548492, Anton-Paar GmbH). The sample changer was used to load samples automatically from up to ninety-six 12-mL glass vials.

The water samples were collected in 100-mL aluminum bottles (Mini Bottle Can, Daiwa Can Company, Japan). The bottles were stored at room temperature (~23 ºC) upside down usually for 12 to 24 hours to make the temperature of the sample equal to the room temperature. The water sample was filled in a 12-mL glass vial and the glass vial was sealed with Parafilm M (Pechiney Plastic Packaging, Inc., Menasha, Wisconsin, USA) immediately after filling. Densities of the samples were measured at 20 ºC by the density meter two times for each bottle and averaged to estimate the density. When the difference between the two measurements was greater than 0.002 kg/m^3, additional measurements were conducted until two samples satisfying the above criteria were obtained.

Time drift of the density meter was monitored by periodically measuring the density of ultra-pure water (Milli-Q water, Millipore, Billerica, Massachusetts, USA) prepared from Yokosuka (Japan) tap water in October 2012. The true density at 20 ºC of the Milli-Q water was estimated to be 998.2042 kg m^{-3} from the isotopic composition (δD = –8.76 ‰, δ^{18}O = –56.86 ‰) and International Association for the Properties of Water and Steam (IAPWS)-95 standard. An offset correction was applied to the measured density by using the Milli-Q water measurements ($\rho_{\text{Milli-Q}}$) with a slight modification of the density dependency (Uchida et al., 2011). The offset (ρ_{offset}) of the measured density (ρ) was reevaluated for the serial no. 80570578 in November 2014 as follows:

$$\rho_{\text{offset}} = (\rho_{\text{Milli-Q}} - 998.2042) - (\rho - 998.2042) \times 0.000411 \text{ [kg m}^{-3}\text{]}.$$

The offset correction was verified by measuring Reference Material for Density in Seawater (prototype Dn-RM1 and PRE18) developing with Marine Works Japan, Ltd., Kanagawa, Japan, and produced by Kanso Technos Co., Ltd., Osaka, Japan, along with the Milli-Q water.

Density salinity can be back calculated from measured density and temperature (20 ºC) with TEOS-10.

(4) Results

Results of density measurements of the Reference Material for Density in Seawater (Dn-RM1 and

PRE18) were shown in Table 4.11.1.

A total of 37 pairs of replicate samples were measured. The root-mean square of the absolute difference of replicate samples was 0.0015 g/kg.

The measured density salinity anomalies (δS_A) are shown in Fig. 4.11.1. The measured δS_A were slightly smaller than calculated δS_A from Pawlowicz et al. (2011) which exploits the correlation between δS_A and nutrient concentrations and carbonate system parameters based on mathematical investigation using a model relating composition, conductivity and density of arbitrary seawaters.

(5) References

IOC, SCOR and IAPSO (2010): The international thermodynamic equation of seawater – 2010: Calculation and use of thermodynamic properties. Intergovernmental Oceanographic Commission, Manuals and Guides No. 56, United Nations Educational, Scientific and Cultural Organization (English), 196 pp.

Pawlowicz, R., D. G. Wright and F. J. Millero (2011): The effects of biogeochemical processes on ocean conductivity/salinity/density relationships and the characterization of real seawater. *Ocean Science*, 7, 363–387.

Uchida, H., T. Kawano, M. Aoyama and A. Murata (2011): Absolute salinity measurements of standard seawaters for conductivity and nutrients. *La mer*, 49, 237–244.

Table 4.11.1. Result of density measurements of the Reference Material for Density in Seawater (prototype Dn-RM1 and PRE18). Number in parentheses shows number of measurements.

Date	Stations	Mean density of Dn-RM1 (kg/m^3)	Mean density of PRE18 (kg/m^3)
2017/02/10-11	all of leg 2	1024.2627 (3)	1024.2223 (18)
2017/02/17-19	1,2,4	1024.2632 (3)	1024.2244 (12)
2017/02/20-21	6,8,12	1024.2628 (3)	1024.2226 (15)
2017/02/24-26	16,20,22,23,24,26	1024.2612 (3)	1024.2211 (13)
			1024.2205 (8)
	Average:	1024.2624 ± 0.0011	1024.2222 ± 0.0017

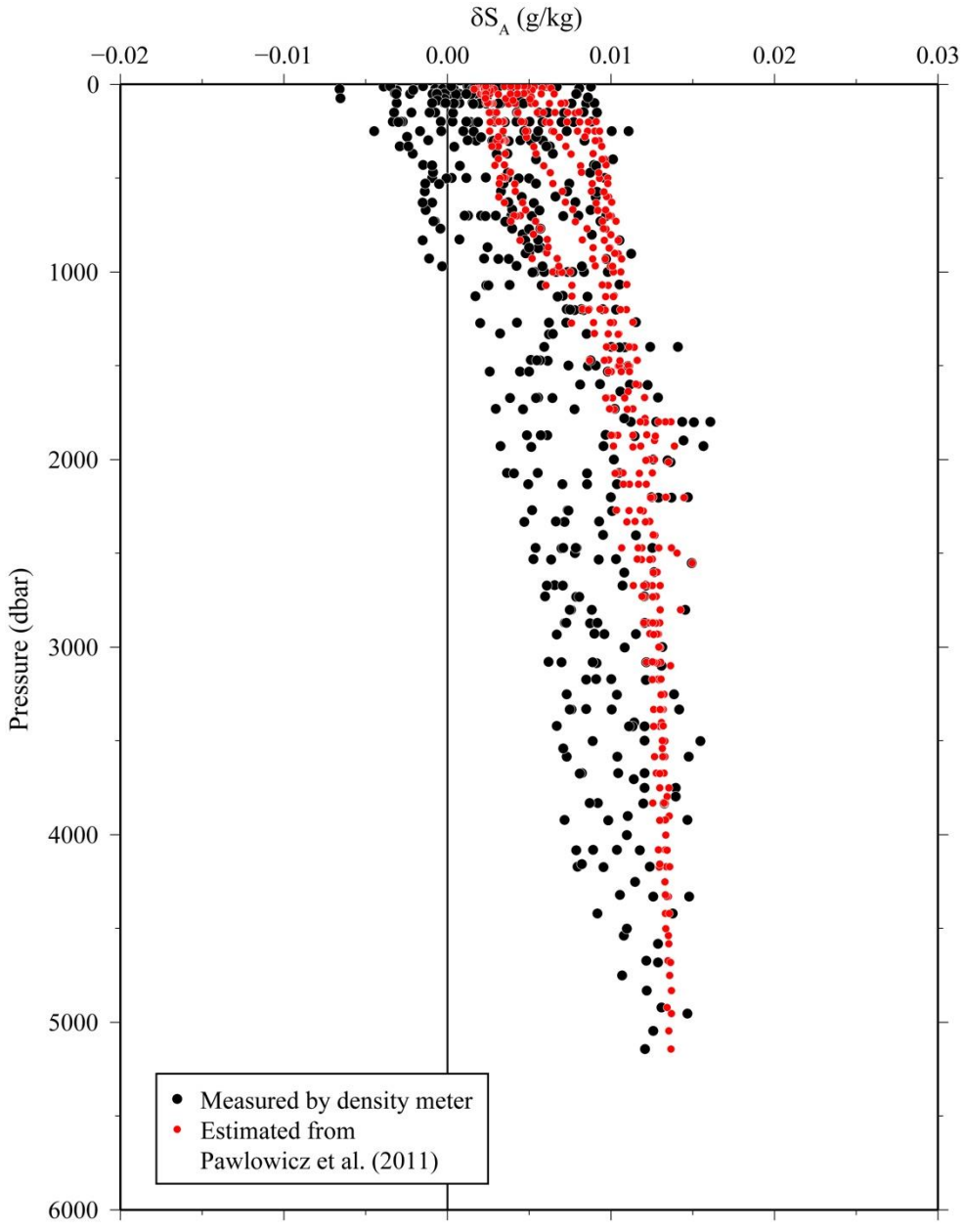

Figure 4.11.1. Vertical distribution of density salinity anomaly measured by the density meter. Absolute Salinity anomaly estimated from nutrients and carbonate parameters (Pawlowicz et al., 2011) are also shown for comparison.

4.12 Carbon items

(1) Personnel

Akihiko Murata (JAMSTEC)

Tomonori Watai (MWJ)

Atsushi Ono (MWJ)

Emi Deguchi (MWJ)

Nagisa Fujiki (MWJ)

(2) Objectives

Concentrations of CO_2 in the atmosphere are now increasing at a rate of about 2.0 ppmv y^{-1} owing to human activities such as burning of fossil fuels, deforestation, and cement production. It is an urgent task to estimate as accurately as possible the absorption capacity of the oceans against the increased atmospheric CO_2, and to clarify the mechanism of the CO_2 absorption, because the magnitude of the anticipated global warming depends on the levels of CO_2 in the atmosphere, and because the ocean currently absorbs 1/3 of the 6 Gt of carbon emitted into the atmosphere each year by human activities.
The South Pacific is one of the regions where uncertainty of uptake of anthropogenic CO_2 is large. In this cruise, therefore, we intended to quantify how much anthropogenic CO_2 was absorbed in the ocean interior of the South Pacific. For the purpose, we measured CO_2-system parameters such as dissolved inorganic carbon (C_T), and total alkalinity (A_T) in the Chilean coastal area and along the WHP line (P17E).

(3) Apparatus

i. C_T

Measurement of C_T was made with automated TCO_2 analyzer (Nippon ANS, Inc., Japan). The system comprises of a seawater dispensing system, a CO_2 extraction system and a coulometer (Model 3000, Nippon ANS, Inc., Japan). Specification of the system is as follows:

The seawater dispensing system has an auto-sampler (6 ports), which dispenses seawater from a 300 ml borosilicate glass bottle into a pipette of about 15 ml volume by PC control. The pipette is kept at 20 °C by a water jacket, in which water from a water bath set at 20 °C is circulated. CO_2 dissolved in a seawater sample is extracted in a stripping chamber of the CO_2 extraction system by adding phosphoric acid (~ 10 % v/v) of about 2 ml. The stripping chamber is approx. 25 cm long and has a fine frit at the bottom. The acid is added to the stripping chamber from the bottom of the chamber by pressurizing an acid bottle for a given time to push out the right amount of acid. The pressurizing is made with nitrogen gas (99.9999 %). After the acid is transferred to the stripping chamber, a seawater sample kept in a pipette is introduced to the stripping chamber by the same method as in adding an acid.

The seawater reacted with phosphoric acid is stripped of CO_2 by bubbling the nitrogen gas through a fine frit at the bottom of the stripping chamber. The CO_2 stripped in the chamber is carried by the nitrogen gas (flow rates is 140 ml min^{-1}) to the coulometer through a dehydrating module. The module consists of two electric dehumidifiers (kept at ~4 °C) and a chemical desiccant ($Mg(ClO_4)_2$).

The measurement sequence such as system blank (phosphoric acid blank), 1.5 % CO_2 gas in a nitrogen base, sea water samples (6) is programmed to repeat. The measurement of 1.5 % CO_2 gas is made to monitor response of coulometer solutions purchased from UIC, Inc.

ii. A_T

Measurement of A_T was made based on spectrophotometry with a single acid addition procedure using a custom-made system (Nippon ANS, Inc., Japan). The system comprises of a water dispensing unit, an auto-syringe (Hamilton) for hydrochloric acid, a spectrophotometer (TM-UV/VIS C10082CAH, Hamamatsu Photonics, Japan), and a light source (Mikropack, Germany), which are automatically controlled by a PC. The water dispensing unit has a water-jacketed pipette (42.3525 mL at 25°C) and a titration cell, which is also controlled at 25°C.

A seawater of approx. 42 ml is transferred from a sample bottle (DURAN® glass bottle, 100 ml) into the pipette by pressurizing the sample bottle (nitrogen gas), and is introduced into the titration cell. The seawater is used to rinse the titration cell. Then, Milli-Q water is introduced into the titration cell, also for rinse. A seawater of approx. 42 ml is weighted again by the pipette, and is transferred into the titration cell. Then, for seawater blank, absorbances are measured at three wavelengths (730, 616 and 444 nm). After the measurement, an acid titrant, which is a mixture of approx. 0.049992 M HCl at 25°C in 0.65 M NaCl and 38 μM bromocresol green (BCG) is added into the titration cell. The volume of the acid titrant is changed between 1.970 mL and 2.100 mL according to estimated values of A_T. The seawater + acid titrant solution is stirred for over 9 minutes with bubbling by nitrogen gas in the titration cell. Then, absorbances at the three wavelengths are measured.

Calculation of A_T is made by the following equation:

$$A_T = (-[H^+]_T V_{SA} + M_A V_A) / V_S,$$

where M_A is the molarity of the acid titrant added to the seawater sample, $[H^+]_T$ is the total excess hydrogen ion concentration in the seawater, and V_S, V_A and V_{SA} are the initial seawater volume, the added acid titrant volume, and the combined seawater plus acid titrant volume, respectively. $[H^+]_T$ is calculated from the measured absorbances based on the following equation (Yao and Byrne, 1998):

$$pH_T = -\log[H^+]_T = 4.2699 + 0.002578(35 - S) + \log((R - 0.00131)/(2.3148 - 0.1299R)) - \log(1 - 0.001005S),$$

where S is the sample salinity, and R is the absorbance ratio calculated as:

$$R = (A_{616} - A_{730})/(A_{444} - A_{730}),$$

where A_i is the absorbance at wavelength i nm.

(4) Results

Cross sections of C_T, and A_T along WOCE P14E line are illustrated in Figs. 4.12.1 and 4.12.2, respectively.

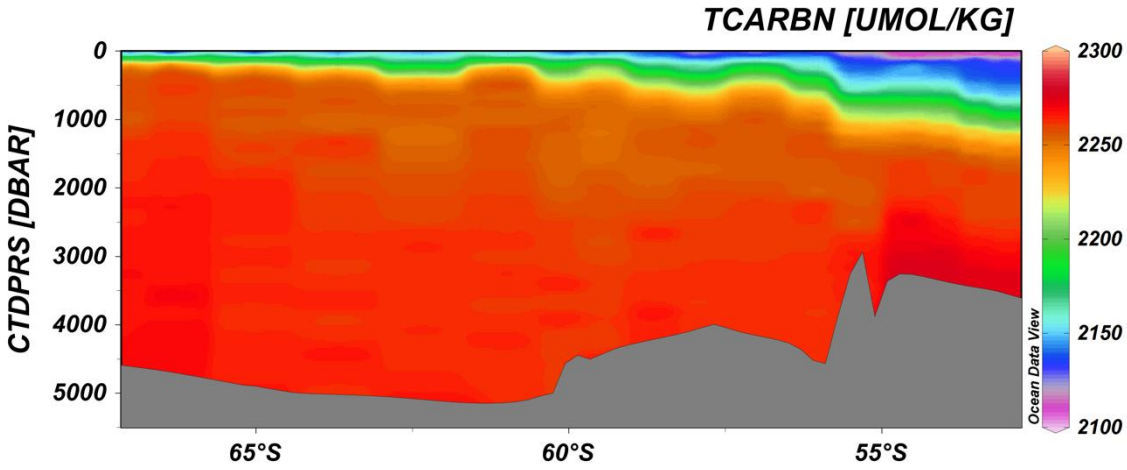

Fig. 4.12.1. Distributions of C_T along the P14E section.

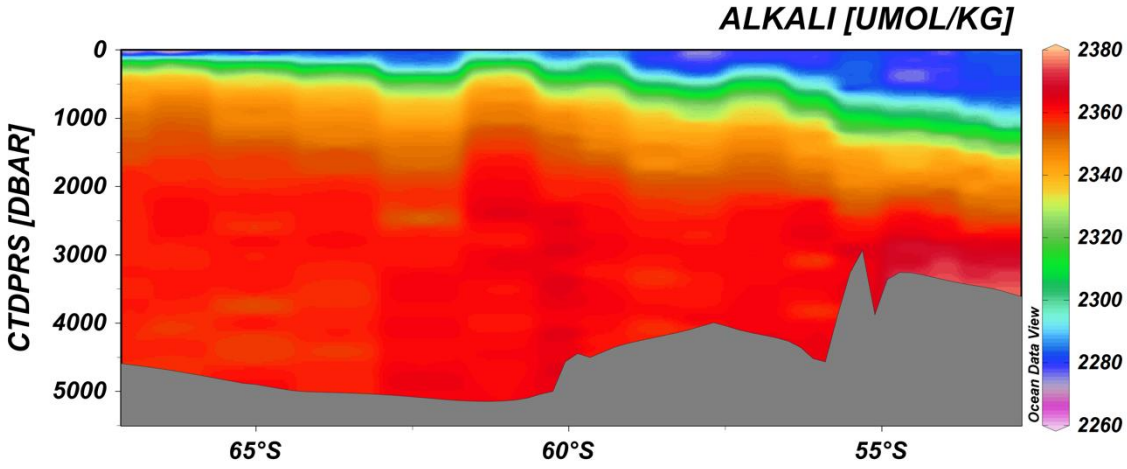

Fig. 4.12.2. Distributions of A_T along the P14E section.

Reference

Clayton T.D. and R.H. Byrne (1993) Spectrophotometric seawater pH measurements: total hydrogen ion concentrtaion scale calibration of m-cresol purple and at-sea results. Deep-Sea Research 40, 2115-2129.

4.13 Geochemistry and Microbiology: Nitrogen and Carbon Cycles

(1) Personnel

Chisato Yoshikawa (JAMSTEC)

Osamu Yoshida (Rakuno Gakuen University)

Kanta Chida (Rakuno Gakuen University)

Noriko Iwamatsu (Rakuno Gakuen University)

Minami Koya (Rakuno Gakuen University)

Akiko Makabe (JAMSTEC)

(2) Introduction

Knowledge about oceanic nitrogen and carbon cycles has been dramatically changed in this decade. In nitrogen cycle, major ammonia oxidizers were believed to be a few lineages of Proteobacteria, but it has been revealed that archaeal ammonia oxidizers (AOA) shared more than 10% of microbial population in dark ocean, and nitrous oxide production is necessary for the growth of AOA. In addition, significant contribution of heterotrophic nitrogen fixation and anaerobic ammonia oxidizers are also been found in the oceanic nitrogen cycle. On the other hand, in carbon cycle, microbial life in dark ocean below mesopelagic water (corresponding to 200-1000 m depth range) is thought to be primarily supported by sinking organic carbons from surface waters. However, it has been recently revealed that the deep-sea biogeochemical cycles are more complex than previously expected, and the dark carbon fixation coupled with nitrification and sulfur- and hydrogen-oxidations is also recognized as another significant organic carbon source in dark ocean (Francis et al. 2007; Alonso-Sáez et al. 2010; Swan et al. 2011; Anantharaman et al. 2013; Herndl and Reinthalar 2013).

The marine nitrogen cycle in surface waters is known to control biological activity in the ocean, because inorganic forms of nitrogen such as nitrate are indispensable nutrients for phytoplankton. Following the primary production, organic nitrogen compounds are metabolized into ammonium and low molecular organic nitrogen compounds that are substrates for nitrification and/or nitrogen source of microbes. Among the components of marine nitrogen cycle, Nitrous Oxide (N_2O) is recognized as significant anthropogenic greenhouse gas and a stratospheric ozone destroyer. The estimation of global N_2O flux from ocean to the atmosphere is 3.8 $TgNyr^{-1}$ and the estimation varies greatly, from 1.8 to 5.8 $TgNyr^{-1}$ (IPCC, 2013). This is because previous models had estimated N_2O concentration from oxygen concentration indirectly. In fact, marine N_2O production processes are very complicated; hydroxylamine oxidation during nitrification, nitrite reduction during nitrifier denitrification and nitrite reduction during denitrification produce N_2O and N_2O deduction during denitrification consumes N_2O (Dore et al. 1998; Knowles et al. 1981; Rysgaard et al. 1993; Svensson 1998; Ueda et al. 1993). In addition, currently, previously unknown systems in nitrification in AOA have been reported. One is the N_2O production with

unknown pathway using NO as one of the substrate (Santoro et al. 2011; Stieglmeier et al. 2014), and the other is ammonia oxidation via urea degradation in AOA has also been reported (Alonso-Sáez et al. 2010). Therefore marine N_2O production processes are poorly understood quantitatively. N_2O isotopomers (oxygen isotope ratio ($\delta^{18}O$), difference in abundance of $^{14}N^{15}N^{16}O$ and $^{15}N^{14}N^{16}O$ (SP), and average nitrogen isotope ratio ($\delta^{15}N$)) are useful tracers to distinguish these processes and had revealed N_2O production processes in various ocean environments (e.g., Yoshida and Toyoda, 2000), but we need to improve the model with novel findings in the marine nitrogen cycle.

To reduce the uncertainties in global N_2O budget a marine N_2O model constrained by isotope dataset was developed and applied to the western North Pacific (Yoshikawa et al., 2016). In this study we conducted water sampling for isotope analysis of N_2O and related substances (NO_3^-, phytoplankton and Chlorophyll-a). By using the results of isotope analysis we will apply the model to the Chilean Coastal Sea and the Southern Ocean and estimate the sea to air N_2O flux there. Moreover, we examine both inorganic and organic carbon uptake activity associated with AOA during and after the cruise, and identify genetic markers for each process of nitrogen cycle by molecular biology techniques.

The atmospheric concentrations of the greenhouse gases methane (CH_4) have increased since 1750 due to human activity. In 2011 the concentrations of CH_4 was 1803 ppb exceeded the pre-industrial levels by about 150% (IPCC 2013). In order to understand the current global CH_4 cycle, it is necessary to quantify its sources and sinks. At present, there remain large uncertainties in the estimated CH_4 fluxes from sources to sinks. The ocean's source strength for atmospheric CH_4 should be examined in more detail, even though it might be a relatively minor source, previously reported to be 0.005 to 3% of the total input to the atmosphere (Cicerone and Oremland 1988; Bange et al. 1994; Lelieveld et al. 1998).

To estimate an accurate amount of the CH_4 exchange from the ocean to the atmosphere, it is necessary to explore widely and vertically. Distribution of dissolved CH_4 in surface waters from diverse locations in the world ocean is often reported as a characteristic subsurface maximum representing a supersaturation of several folds (Yoshida et al. 2004; 2011). Although the origin of the subsurface CH_4 maximum is not clear, some suggestions include advection and/or diffusion from local anoxic environment nearby sources in shelf sediments, and in situ production by methanogenic bacteria, presumably in association with suspended particulate materials (Karl and Tilbrook 1994; Katz et al. 1999). These bacteria are thought to probable live in the anaerobic microenvironments supplied by organic particles or guts of zooplankton (Alldredge and Cohen 1987). So, this study investigates in detail profile of CH_4 concentration in the water column in the Chilean Coastal Sea and the Southern Ocean to clarify CH_4 dynamics and estimate the flux of CH_4 to the atmosphere.

(3) Materials and methods

Seawater samples are taken by CTD-CAROUSEL system attached Niskin samplers of 12 L

at 36 layers and surface layer taken by plastic bucket at hydrographic stations as shown in Table 1 for Leg 2 and Table 2 for Leg 3.

Table 1. Parameters and hydrographic station names for Leg 2.

Parameters	Hydrographic Station Numbers
1. $\delta^{15}N$ of NO_3	1, 6, 7, 9, 10c1, 10c2, 11A, 11B, 12B
2. $\delta^{15}N$ of Chlorophyll *a*	1, 6, 7, 9, 10c1, 10c2, 11B, 12B
3. $\delta^{15}N$ of Phytoplankton	1, 6, 7, 9, 10c1, 10c2, 11B, 12B
4. $\delta^{15}N$ of N_2O and $\delta^{13}C$ of CH_4	1, 6, 7, 9, 10c1, 10c2, 11B, 12B
6. CH_4 and N_2O concentrations	1, 6, 7, 9, 10c1, 10c2, 11B, 12B

Table 2. Parameters and hydrographic station names for Leg 3.

Parameters	Hydrographic Station Numbers (P17E)
1. $\delta^{15}N$ of NO_3	1, 4, 8, 10, 13, 15, 18, 21, 23
2. $\delta^{15}N$ of N_2O and $\delta^{13}C$ of CH_4	1, 4, 8, 10, 11, 12, 13, 15, 18, 20, 21, 22, 23
3. CH_4 and N_2O concentrations	1, 4, 8, 10, 11, 12, 13, 15, 18, 20, 21, 22, 23

Isotopic analyses for N_2O, methane, NO_3^-, chlorophyll a and phytoplankton

Sample for N_2O isotopomer analysis was transferred to 100 ml glass vials from the Niskin sampler without headspace. After an approximately two-fold volume overflow, 100μL of saturated $HgCl_2$ solution were added. The vials were sealed with butyl rubbers and aluminum caps and stored in dark at 4°C until analysis. The $\delta^{15}N$, $\delta^{18}O$ and SP values and concentrations of N_2O in seawater will be determined by slightly modified version of GC-IRMS described in detail in Yamagishi et al. (2007).

Water samples for $\delta^{13}C$-CH_4 analysis were transferred to 100 mL glass vials from the Niskin sampler without headspace. After an approximately two-fold volume overflow, 100μL of saturated $HgCl_2$ solution were added. The vials were sealed with butyl rubbers and aluminum caps and stored in dark at 4°C until analysis. The $\delta^{13}C$ value of Methane will be measured using isotope ratio mass spectrometry using a method of Tsunogai et al. (1998 and 2000).

Sample for nitrate isotope analysis was collected into a 50 ml syringe equipped with a DISMIC® filter (pore size: 0.45 μm) and filtered immediately after sampling. These samples were removed nitrite with sulfamic acid using the method of Granger and Sigman (2009) and preserved at -23°C until chemical analysis. The $\delta^{15}N$ and $\delta^{18}O$ values of NO_3^- will be measured using the "bacterial" method of Sigman et al., (2001) in which N_2O converted from nitrate is analyzed using GasBench/ PreCon/IRMS.

Sample for chlorophyll isotope analysis was collected into a 20L polypropylene tanks. The samples were filtered under reduced pressure and collected on two-three pre-combusted Whatman GF-75 filters. The filters were double up and wrapped in aluminum foil and stored at -23°C until analysis. Chlorophyll pigments will be extracted and split into each pigments by HPLS. The $\delta^{15}N$ values of Chlorophyll pigments will be measured by using EA-IRMS at JAMSTEC.

Sample for phytoplankton isotope analysis was collected into a 20L polypropylene tanks. The samples were condensed using an ultrafiltration system. The condensed water was put into cryotubes and were frozen with liquid nitrogen. The thawed samples will be sorted to each phytoplankton spices by using a cell sorter. The $\delta^{15}N$ values of phytoplankton will be measured by using EA-IRMS at JAMSTEC.

Nitrous oxide and methane concentration measurements

Sample for N_2O and CH_4 concentration analyses were carefully subsampled into 30 mL glass vials to avoid air contamination for analyses of N_2O and CH_4 concentration. The seawater samples were poisoned by 20 μL (30 mL vials) of mercuric chloride solution (Tilbrook and Karl 1995; Watanabe et al. 1995), and were closed with rubber-aluminum and plastic caps. These were stored in a dark and cool place until we got to land, where we conducted gas chromatographic analyses of N_2O and CH_4 concentration at the laboratory.

The measurement system consists of a purge and trap unit, a desiccant unit, rotary valves, gas chromatograph equipped with a electron capture detector for concentration of N_2O and a flame ionization detector for concentration of CH_4, and data acquisition units. The entire volume of seawater in each glass vial was processed all at once to avoid contamination and loss of N_2O and CH_4. Precision obtained from replicate determinations of N_2O and CH_4 concentration was estimated to be better than 5% for the usual concentration in seawater.

Prokaryotic uptakes of organic and inorganic carbon measurements

See “Prokaryotic activity measurements” in the chapter “Vertical profiles of aquatic microbial abundance, activity and diversity in the eastern Indian Ocean”.

Genetic markers of geochemical processes

Microbial cells in water samples were filtrated on cellulose acetate filter (0.2μm) and stored at -80˚C. Environmental DNA or RNA will be extracted from the filtrated cells and used for molecular analyses (e.g. clone analysis and quantitative PCR) to investigate the microbial components related to nitrification, nitrogen fixation and methanogenesis.

(4) Expected results

In the surface layer, N_2O concentration of water affects the sea-air flux directly (Dore et al. 1998). However the pathway of N_2O production in surface layer is still unresolved. In the surface layer, N_2O is predominantly produced by nitrification, but also by nitrifer-denitrification and denitrification if oxygen concentration is low in the water mass or particles (Maribeb and Laura, 2004). The observed concentrations and isotopomer ratios of N_2O together with those values of substrates for N_2O (NO_3^-, phytoplankton and Chlorophyll-a) will reveal the pathway of N_2O production in the surface layer and will improve the marine N_2O isotopomer model. Moreover, the horizontal isotope dataset will help to apply the model to the Chilean Coastal Sea and the Southern Ocean.

Subsurface maximum concentrations of CH_4 (>3 nmol kg^{-1}) were expected to be observed in the Indian Ocean. A commonly-encountered distribution in the upper ocean with a CH4 peak within the pycnocline (e.g., Ward et al. 1987; Owens et al. 1991; Watanabe et al. 1995; Yoshida et al. 2011). Karl and Tilbrook (1994) suggested the suboxic conditions would further aid the development of microenvironments within particles in which CH_4 could be produced. The organic particles are accumulated in the pycnocline, and CH_4 is produced in the micro reducing environment by methanogenic bacteria. Moreover, in situ microbial CH_4 production in the guts of zooplankton can be expected (e.g., Owens et al. 1991; de Angelis and Lee 1994; Oudot et al. 2002; Sasakawa et al. 2008). Watanabe et al. (1995) pointed out that the diffusive flux of CH_4 from subsurface maxima to air-sea interface is sufficient to account for its emission flux to the atmosphere. In the mixed layer above its boundary, the CH_4 is formed and discharged to the atmosphere in part, in the below its boundary, CH_4 diffused to the bottom vertically. By using concentration and isotopic composition of CH_4 and hydrographic parameters for vertical water samples, it is possible to clarify its dynamics such as production and/or consumption in the water column.

References

Alldredge AA, Cohen Y (1987) Can microscale chemical patches persist in the sea? Microelectrode study of marine snow, fecal pellets. Science, 235:689-691

Alonso-Sáez L, Galand PE, Casamayor EO, Pedrós-Alió C, Bertilsson S (2010) High bicarbonate assimilation in the dark by Arctic bacteria. ISME J, 174:1581–90

Anantharaman K, Breier JA, Sheik CS, Dick GJ (2013) Evidence for hydrogen oxidation and metabolic plasticity in widespread deep-sea sulfur-oxidizing bacteria. Proceedings of the National Academy of Sciences, 110:330–335

Bange, HW, Bartell UH, Rapsomanikis S, Andreae MO (1994) Methane in the Baltic and the North seas and a reassessment of the marine emissions of methane. Global Biogeochemical Cycles, 8:465–480

Cicerone RJ, Oremland RS (1988) Biogeochemical aspects of atmospheric methane, Global Biogeochemical Cycles, 2:299–327

de Angelis MA, Lee C (1994) Methane production during zooplankton grazing on marine phytoplankton. Limnology and Oceanography, 39:1298-1308

Dore JE, Popp BN, Karl DM, Sansone FJ (1998) A large source of atmospheric nitrous oxide from subtropical North Pacific surface water. Nature, 396:63-66

Francis CA, Beman JM, Kuypers MM (2007) New processes and players in the nitrogen cycle: the microbial ecology of anaerobic and archaeal ammonia oxidation. ISME J 1: 19–27

Granger J, Sigman DM (2009) Removal of nitrite with sulfamic acid for nitrate N and O isotope analysis with the denitrifier method. Rapid Communications in Mass Spectrometry, 23:3753-3762

Herndl GJ, Reinthaler T (2013) Microbial control of the dark end of the biological pump. Nature

Geoscience, 6:718–724

IPCC Working group I (2013): Climate change 2013: The physical science basis. IPCC The 5th Assessment report, http://www.ipcc.ch/report/ar5/wg1/.

Karl DM, Tilbrook BD (1994) Production and transport of methane in oceanic particulate organic matter. Nature, 368:732–734

Katz ME, Pak DK, Dickkens GR, Miller KG (1999) The source and fate of massive carbon input during the latest Paleocene thermal maximum. Scince, 286:1531–1533

Knowles R, Lean DRS, Chan YK (1981) Nitrous oxide concentrations in lakes: variations with depth and time. Limnology and Oceanography, 26:855-866

Lelieveld J, Crutzen PJ, Dentener FJ (1998) Changing concentration, lifetime and climate forcing of atmospheric methane. Tellus Series B, 50:128–150

Maribeb CG, Laura F (2004) N_2O cycling at the core of the oxygen minimum zone off northern Chile. Marine Ecology Progress Series, 280:1-11

Oudot C, Jean-Baptiste P, Fourre E, Mormiche Guevel C, Ternon JF-, Corre PL (2002) Transatlantic equatorial distribution of nitrous oxide and methane. Deep-Sea Research Part I, 49:1175–1193

Owens NJP, Law CS, Mantoura RFC, Burkill PH, Llewellyn CA(1991) Methane flux to the atmosphere from the Arabian Sea. Nature, 354:293–296

Rysgaard S, Risgaard-Petersen N, Nielsen LP, Revsbech NP (1993) Nitrification and denitrification in lake and estuarine sediments measured by the ^{15}N dilution technique and isotope pairing. Applied and Environmental Microbiology, 59:2093-2098

Sasakawa M, Tsunogai U, Kameyama S, Nakagawa F, Nojiri Y, Tsuda A (2008) Carbon isotopic characterization for the origin of excess methane in subsurface seawater. Journal of Geophysical Research, 113:C03012, doi: 10.1029/2007JC004217

Santoro AE, Buchwald C, McIlvin MR, Casciotti KL (2011) Isotopic signature of N_2O produced by marine ammonia-oxidizing Archaea. Science, 333:1282-1285

Sigman DM, Casciotti KL, Andreani M, Barford C, Galanter M, Boehlke JK (2001) A bacterial method for the nitrogen isotopic analysis of nitrate in seawater and freshwater. Analytical Chemistry, 73:4145-4153

Stieglmeier M, Mooshammer M, Kitzler B, Wanek W, Zechmeister-Boltenstern S, Richter A, Schleper C (2014) Aerobic nitrous oxide production through N-nitrosating hybrid formation in ammonia-oxidizing archaea. ISME J, 8:1135-1146

Swan BK, Martinez-Garcia M, Preston CM, Sczyrba A, Woyke T, Lamy, D, Reinthaler T, Poulton NJ, Masland ED, Gomez ML, Sieracki ME, DeLong EF, Herndl GJ, Stepanauskas R (2011) Potential for chemolithoautotrophy among ubiquitous bacteria lineages in the dark ocean. Science, 333:1296-1300

Svensson JM (1998) Emission of N_2O, nitrification and denitrification in a eutrophic lake sediment

bioturbated by Chironomus plumosus. Aquatic Microbial Ecology, 14:289-299

Tilbrook BD, Karl DM (1995) Methane sources, distributions and sinks from California coastal waters to the oligotrophic North Pacific gyre. Marine Chemistry, 49:51–64

Tsunogai U, Ishibashi J, Wakita H, Gamo T (1998) Methane-rich plumes in the Suruga Trough (Japan) and their carbon isotopic characterization. Earth and Planetary Science Letters, 160:97-105

Tsunogai U, Yoshida N, Ishibashi J, Gamo T (2000) Carbon isotopic distribution of methane in deep-sea hydrothermal plume, Myojin Knoll Caldera, Izu-Bonin arc: Implications for microbial methane oxidation in the oceans and applications to heat flux estimation. Geochimca et Cosmochimca Acta, 64:2439-2452

Ueda S, Ogura N, Yoshinari T (1993) Accumulation of nitrous oxide in aerobic ground water. Water Research, 27:1787-1792

Ward BB, Kilpatrick KA, Novelli PC, Scranton MI (1987) Methane oxidation and methane fluxes in the ocean surface layer and deep anoxic waters. Nature, 327:226–229

Watanabe S, Higashitani N, Tsurushima N, Tsunogai S (1995) Methane in the western North Pacific. Journal of Oceanography, 51:39–60

Yamagishi H, Westley MB, Popp BN, Toyoda S, Yoshida N, Watanabe S, Koba K, Yamanaka Y (2007) Role of nitrification and denitrification on the nitrous oxide cycle in the eastern tropical North Pacific and Gulf of California. J. Geophys. Res. Biogeosciences, doi:10.1029/2006JG000227

Yoshida N, Toyoda S (2000) Constraining the atmospheric N_2O budget from intramolecular site preference in N_2O isotopomers. Nature, 405:330-334

Yoshida O, Inoue HY, Watanabe S, Noriki S, Wakatsuchi M (2004) Methane in the western part of the Sea of Okhotsk in 1998-2000. Journal of Geophysical Research, doi:10.1029/2003JC001910

Yoshida O, Inoue HY, Watanabe S, Suzuki K, Noriki S (2011) Dissolved methane distribution in the South Pacific and the Pacific Ocean in austral summer. Journal of Geophysical. Research, doi:10.1029/2009JC006089

Yoshikawa C, Abe H, Aita MN, Breider F, Kuzunuki K, Ogawa NO, Suga H, Ohkouchi N, Danielache SO, Wakita M, Honda MC, Toyoda S, Yoshida N (2016) Insights into the production processes of nitrous oxide in the western north Pacific by using a marine ecosystem isotopomer model. Journal of Oceanography, 72, 491–508

4.14 Vertical Profiles of Microbial Abundance, Activity and Diversity

(1) Personnel

Taichi Yokokawa (JAMSTEC)

Michinari Sunamura (The University of Tokyo)

Takuro Nunoura (JAMSTEC)

(2) Introduction

Prokaryotes (Bacteria and Archaea) play a major role in marine biogeochemical fluxes. Biogeochemical transformation rates and functional diversity of microbes are representative major topics in marine microbial ecology. However, the link between prokaryotes properties and biogeochemistry in the meso- and bathypelagic layers has not been explained systematically despite of the recent studies that highlight the role of microbes in the cycling of organic and inorganic matter. (Herndl and Reinthaler 2013; Yokokawa et al. 2013; Nunoura et al. 2015). Moreover, microbial diversity and biogeography in meso- and bathypelagic ocean and its relationship with upper layers and deep-water circulation have also not been well studied.

The objectives of this study, which analyze the water columns from sea surface to just above the bottom of Southern Ocean, were 1) to determine the abundance of microbes; 2) to study the heterotrophic production of prokaryotes; 3) to assess the community composition of prokaryotes; 4) to know microbial diversity through water columns along the latitudinal transect.

(3) Methods

Microbial abundance

Samples for microbial abundances (prokaryotes, eukaryotes and viruses) were collected in every routine cast and depth. Samples were fixed with glutaraldehyde (final concentration 1%) and/or mixed with Glycerol-EDTA, and frozen at -80°C. The abundance and relative size of microbes and viruses will be measured by a flow cytometry in both The University of Tokyo (Sunamura) and JAMSTEC (Yokokawa) after nucleic acid staining with SYBR-Green I.

For the correction of flow cytometry data and morphological analysis of microbial cells, microbial cells in seawater were filtered and collected on polycarbonate membrane after formalin fixation. The filter samples were frozen at -80°C. The samples will be observed by fluorescent microscope at The University of Tokyo (Sunamura). Samples for fluorescent microscopy is collected at stn.1, 10 and 23.

Microbial activity measurements

Heterotrophic microbial production and microbial respiration were determined based on

^{3}H-leucine incorporation rate and CTC-formazan reduction rate. ^{3}H-leucine incorporation rate was determined as a proxy for heterotrophic or mixotrophic prokaryotic production. Triplicate subsamples (1.5 mL) dispensed into screw-capped centrifuge tubes amended with 10 nmol L^{-1} (final concentration) of [^{3}H]-leucine (NET1166, PerkinElmer) and incubated at in situ temperature (± 2°C) in the dark. One trichloroacetic acid (TCA) killed blank was prepared for each sample. Incubation periods were 1 hour and 24 hours for the upper (0 – 250 m) and deeper (300 – bottom) water layers, respectively. After the incubation, proteins were TCA (final conc. 5%) extracted twice by centrifugation (15000 rpm, 10 min, Kubota 3615-sigma), followed by the extraction with ice-cold 80% ethanol.

The samples will be radioassayed with a liquid scintillation counter using Ultima-GOLD (Packard) as scintillation cocktail. Quenching is corrected by external standard channel ratio. The disintegrations per minute (DPM) of the TCA-killed blank is subtracted from the average DPM of the samples, and the resulting DPM is converted into leucine incorporation rates.

Tetrazolium salts are reduced by electron transport chain and produce formazan dye. Respiration microbial cell numbers and fluorescent intensities were determined based on the fluorescent CTC formazan. A 760µl of seawater was added in a 1.5ml protein low bind tube with a CTC tetrazolium salts (final conc. 5mM), Phenazine methoxy sulfate (final conc. 25µM), KCN (final conc. 1mM), Gly-TE. The tubes were incubated at in situ temperature (± 2°C) in the dark. Duplicate 150µl of the incubated sample was subsampled into 96 well plate and frozen at -80°C to stop incubation at the incubation period of 2h, 8h, and 24h. Densities and fluorescent intensity of total microbial cells and CTC formazan produced cells will be measured by a flow cytometer (Attune / CytoFlex) after nucleic stain by SYBR Green I.

Samples for leucine incorporation activity measurements and CTC reduction rates measurements were taken at stations 1, 4, 10, 13, 18, 21, 22 and 23 in the routine casts.

Microbial diversity

Microbial cells in water samples were filtrated on cellulose acetate filter (0.2µm) and stored at -80˚C. Environmental DNA or RNA will be extracted from the filtrated cells and used for 16S/18S rRNA gene tag sequencing using MiSeq, quantitative PCR for genes for 16S rRNA, and/or metatranscriptomics. Moreover, selected water samples were mixed with glycerol-EDTA and stored at -80˚C for single cell genomic analyses. Samples for microbial diversity were taken at stations 1, 4, 10, 13, 18, 21, 22 and 23 in the routine casts.

References

Herndl GJ, Reinthaler T (2013) Microbial control of the dark end of the biological pump. Nature geoscience, 6:718-724

Yokokawa T, Yang Y, Motegi C, Nagata T (2013) Large-scale geographical variation in prokaryotic

abundance and production in meso- and bathypelagic zones of the central Pacific and Southern Ocean. Limnology and Oceanography, 58:61-73

Nunoura T, Takaki Y, Hirai M, Shimamura S, Makabe A, Koide O, Kikuchi T, Miyazaki J, Koba K, Yoshida N, Sunamura M, Takai K (2015) Hadal biosphere: Insight into the microbial ecosystem in the deepest ocean on Earth. Proceedings of the Natioanl Academy of Sciences 112:1230-1236

4.15 Chlorophyll *a*

(1) Personnel

Kosei Sasaoka (JAMSTEC) (Leg 3)

Takuhei Shiozaki (JAMSTEC) (Leg 2)

Hironori Sato (MWJ) (Leg 1)

Masanori Enoki (MWJ) (Leg 3)

Misato Kuwahara (MWJ) (Leg 3)

Haruka Tamada (MWJ) (Leg 3)

Ei Hatakeyama (MWJ) (Leg 3)

(2) Objectives

Chlorophyll *a* is one of the most convenient indicators of phytoplankton stock, and has been used extensively for the estimation of phytoplankton abundance in various aquatic environments. In this study, we investigated horizontal and vertical distribution of phytoplankton around the Chilean coast (Leg 2) and along the P17E section (Leg 3) in the Southern Ocean. The chlorophyll *a* data is also utilized for calibration of fluorometers, which were installed in the surface water monitoring and CTD profiler system.

(3) Instrument and Method

Seawater samples were collected in 280 mL (Leg 2) and 500 mL (Leg 3) brown Nalgene bottles without head-space, and samples from the surface (0 m) were collected using a bucket. The whole samples were gently filtrated by low vacuum pressure (<0.02 MPa) through Whatman GF/F filter (diameter 25 mm) in the dark room. Whole volume of each sampling bottle was precisely measured in advance. After filtration, phytoplankton pigments were immediately extracted in 7 ml of N,N-dimethylformamide (DMF), and samples were stored at –20°C under the dark condition to extract chlorophyll *a* more than 24 hours. Chlorophyll *a* concentrations were measured by the Turner fluorometer (10-AU-005, TURNER DESIGNS), which was previously calibrated against a pure chlorophyll *a* (Sigma-Aldrich Co., LLC) (Figure 4.15.1). To estimate the chlorophyll *a* concentrations, we applied to the fluorometric "Non-acidification method" (Welschmeyer, 1994).

(4) Results

Vertical profiles of chlorophyll *a* concentrations around the Chilean coast (Leg 2) and along the P17E section (Leg 3) during the cruise are shown in Figure 4.15.2 and Figure 4.15.3, respectively. Cross section of chlorophyll *a* concentrations along the P17E line (Leg 3) is shown in Figure 4.15.4. To estimate the measurement precision, 34-pairs of replicate samples were obtained from hydrographic

casts (Leg 3). All pairs of the replicate samples were collected in 500 ml bottles. Although the absolute values of the difference between 34-pairs replicate samples were 0- 0.07 μg/L, those standard deviations were approximately 0.013.

(5) Reference

Welschmeyer, N. A. (1994): Fluorometric analysis of chlorophyll a in the presence of chlorophyll b and pheopigments. Limnor. Oceanogr., 39, 1985-1992.

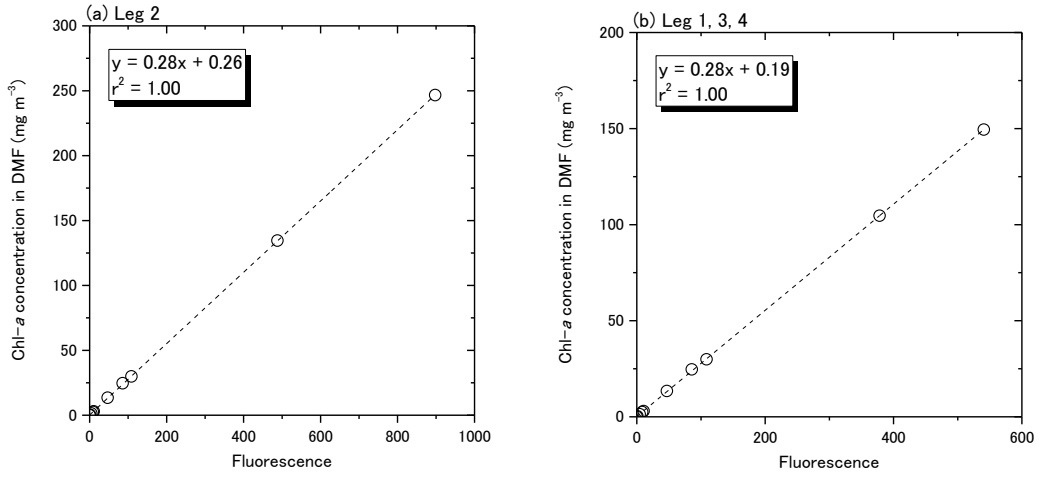

Figure 4.15.1 Relationships between pure chlorophyll *a* concentrations and fluorescence light intensity ((a) Leg 2, (b) Leg 1, 3, 4)

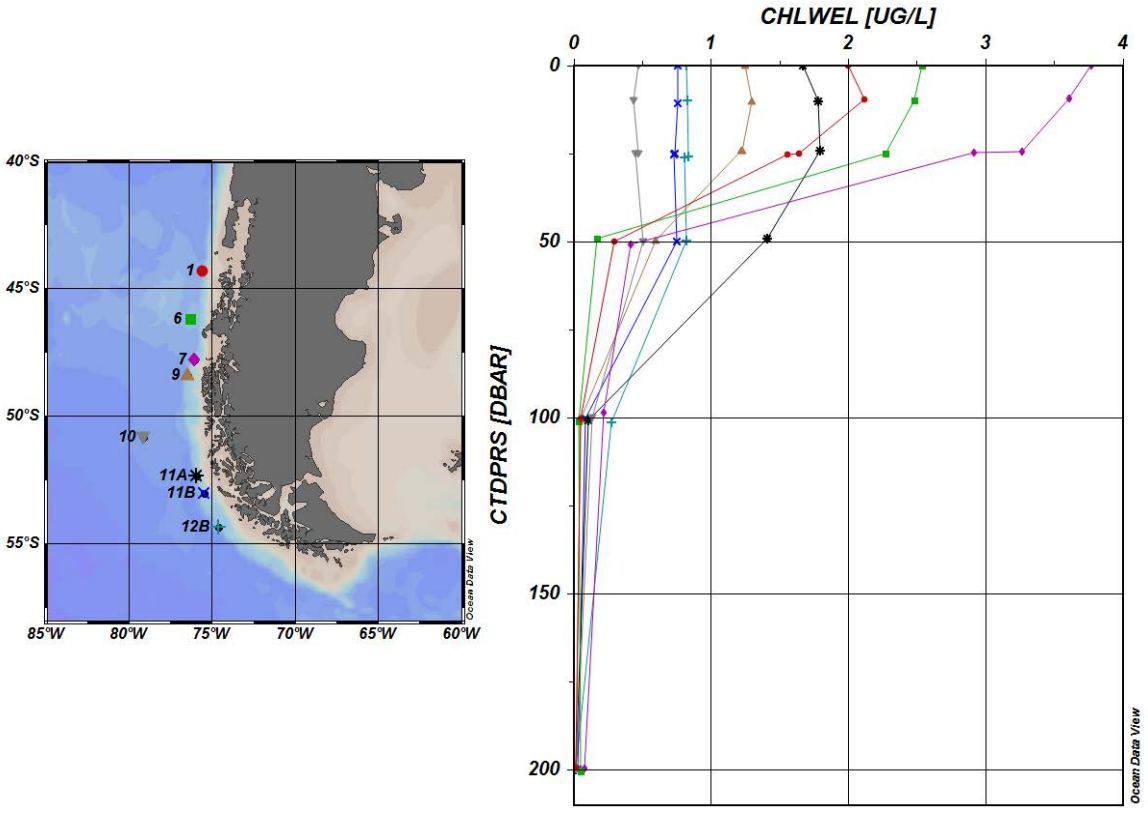

Figure 4.15.2 Vertical profiles of chlorophyll *a* concentrations around the Chilean coast

(Leg 2) obtained from hydrographic casts.

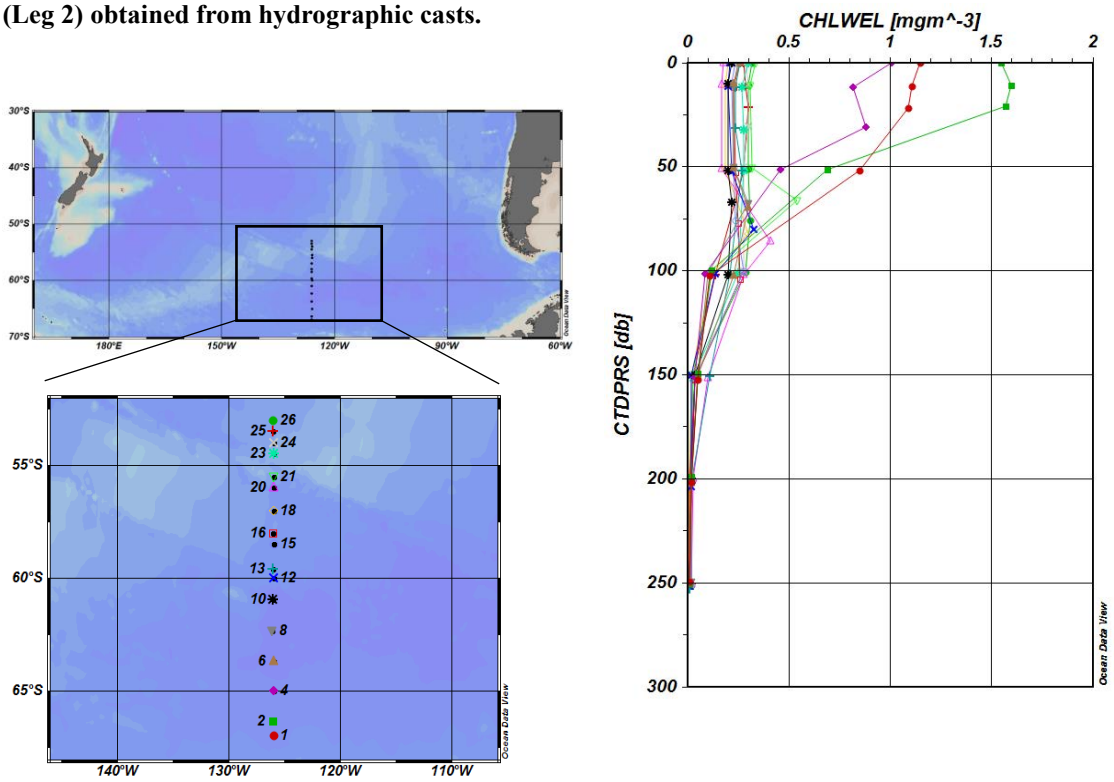

Figure 4.15.3 Vertical profiles of chlorophyll *a* concentrations along the P17E section (Leg 3) obtained from hydrographic casts.

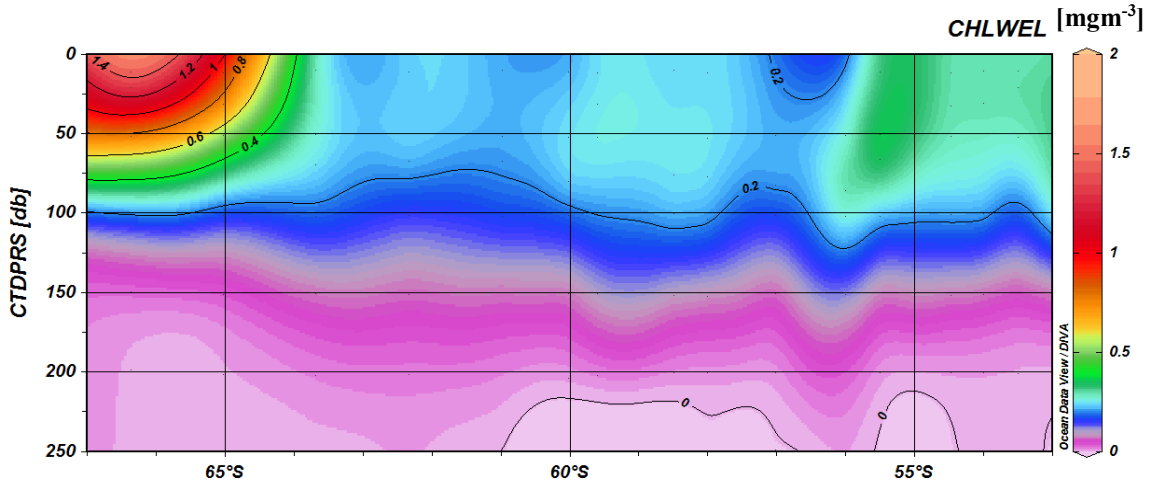

Figure 4.15.4 Cross section of chlorophyll *a* concentrations along the P17E-line (Leg 3) obtained from hydrographic casts.

4.16 Nitrogen Fixation

(1) Personnel

Takuhei Shiozaki (JAMSTEC) -PI

(2) Objectives

Biological nitrogen fixation by specialized prokaryotic microorganisms (diazotrophs) converts dinitrogen gas into ammonia, and is a major source of reactive nitrogen in the ocean. Knowing the distribution and magnitude of oceanic nitrogen fixation, and what controls the biogeography of diazotrophs, is therefore essential for understanding the marine nitrogen cycle. Nitrogen fixation has historically been mainly measured for in the tropical and subtropical oligotrophic ocean regions where diazotrophs were expected to occur under the warm oligotrophic condition. However, recent studies show that nitrogen fixation also occurs in colder and/or nutrient-rich waters such as Arctic Ocean, temperate coastal water, river plumes, coastal upwelling regions, and nutrient-rich aphotic waters. Since such environments have only rarely been surveyed for nitrogen fixation in the past, the global nitrogen inputs by diazotrophs could potentially be much higher than previously thought. Here I examined nitrogen fixation from the surface to the bottom in the temperate Chilean coastal region.

(3) Instruments and methods

Water samples from the subsurface were collected in Niskin-X bottles, and samples from the surface (0 m) were collected using a bucket. Nitrogen fixation was determined by the $^{15}N_2$ gas bubble method (Montoya et al., 1996, Appl. Environ. Microbiol. 62, 986-993), combined with a primary production assay using the ^{15}N-^{13}C dual inlet technique. Seawater samples were transferred into acid-cleaned 1–4.5 L polycarbonate bottles. ^{13}C-labeled sodium bicarbonate (99 atom% ^{13}C; Cambridge Isotope Laboratories, Inc., Andover, MA, USA) was added to the bottles at a final tracer concentration of 200 μmol L^{-1} before sealing it with a thermoplastic elastomer cap. Then, using a gas-tight syringe, 1–5 ml of $^{15}N_2$ gas (99.8 atom% 15N; Shoko) was added to each bottle. The samples collected from the surface and 25 m were incubated in an on-deck incubator cooling by surface seawater and the samples from the aphotic zone were incubated in a thermostatic incubator under dark condition. The incubations were terminated by gentle vacuum filtration of the seawater samples through a precombusted GF/F filter after 24 h. Samples collected for estimating the initial ^{15}N and ^{13}C enrichment of particulate organic matter were filtered immediately at the beginning of the incubation. The filters were kept frozen (-20 °C) for on-shore analysis.

(4) Data archives

These data obtained in this cruise will be submitted to the Data Management Group of JAMSTEC

when ready.

4.17 Absorption coefficients of particulate matter and colored dissolved organic matter (CDOM)

(1) Personnel

Kosei Sasaoka (JAMSTEC) (Leg 3)

(2) Objectives

Absorption coefficients of particulate matter (phytoplankton and non-phytoplankton particles, defined as 'detritus') and colored dissolved organic matter (CDOM) play an important role in determining the optical properties of seawater. In particular, light absorption by phytoplankton is a fundamental process of photosynthesis, and their chlorophyll *a* (Chl-*a*) specific coefficient, a^*_{ph}, can be essential factors for bio-optical models to estimate primary productivities. Absorption coefficients of CDOM are also important parameters to validate and develop the bio-optical algorithms for ocean color sensors, because the absorbance spectrum of CDOM overlaps that of Chl-*a*. The global colored detrital and dissolved materials (CDOM) distribution appears regulated by a coupling of biological, photochemical, and physical oceanographic processes all acting on a local scale, and greater than 50% of blue light absorption is controlled by CDOM (Siegel et al., 2002). Additionally, some investigators have reported that CDOM emerges as a unique tracer for diagnosing changes in biogeochemistry and the overturning circulation, similar to dissolved oxygen (e.g., Nelson et al., 2010). The objectives of this study are to understand the North-South variability of light absorption by phytoplankton and CDOM along the P17E section in the Southern Ocean.

(3) Methods

Seawater samples for absorption coefficient of total particulate matter ($a_p(\lambda)$) were performed using Niskin bottles and a bucket above 100m depth at 7 stations along the P17E section (Fig.4.17-1, Table 4.17-1). Samples were collected in 3000ml dark bottles and filtered (500 - 3000 ml) through 25-mm What-man GF/F glass-fiber filters under a gentle vacuum (< 0.013 MPa) on board in the dark room. After filtration, the optical density of total particulate matter on filter ($OD_{fp}(\lambda)$) between 350 and 750 nm at a rate of 1.0 nm was immediately measured by an UV-VIS recording spectrophotometer (UV-2400, Shimadzu Co.), and absorption coefficient was determined from the OD according to the quantitative filter technique (QFT) (Mitchell, 1990). A blank filter with filtered seawater was used as reference. All spectra were normalized to 0.0 at 750nm to minimize difference between sample and reference filter. To determine the optical density of non-pigment detrital particles ($OD_{fd}(\lambda)$), the filters were then soaked in methanol for a few hours and rinsed with filtered seawater to extract and remove the pigments (Kishino et al., 1985), and its absorption coefficient was measured again by UV-2400. These measured optical densities on filters ($OD_{fp}(\lambda)$ and $OD_{fd}(\lambda)$) were converted to optical densities in suspensions ($OD_{sp}(\lambda)$ and $OD_{sd}(\lambda)$) using the pathlength amplification factor of Cleveland and Weidemann (1993) as follows:

$$OD_{sp}(\lambda) = 0.378\ OD_{fp}(\lambda) + 0.523\ OD_{fp}(\lambda)^2 \text{ and}$$
$$OD_{sd}(\lambda) = 0.378\ OD_{fd}(\lambda) + 0.523\ OD_{fd}(\lambda)^2.$$

The absorption coefficient of total particles ($a_p(\lambda)$ (m^{-1})) and non-pigment detrital particles ($a_d(\lambda)$ (m^{-1})) are computed from the corrected optical densities ($OD_s(\lambda)$):

$a_p(\lambda) = 2.303 \times OD_{sp}(\lambda) / L$ (L = V / S), and

$a_d(\lambda) = 2.303 \times OD_{sd}(\lambda) / L$ (L = V / S),

Where S is the clearance area of the filter (m^2) and V is the volume filtered (m^3). Absorption coefficient of phytoplankton ($a_{ph}(\lambda)$) was obtained by subtracting $a_d(\lambda)$ from $a_p(\lambda)$ as follows:

$$a_{ph}(\lambda) = a_p(\lambda) - a_d(\lambda).$$

Finally, we calculated chl-*a* normalized specific absorption spectra (a^*_{ph}) to divide a_{ph} by chl-*a* concentrations obtained from same hydrographic casts.

Seawater samples for absorption coefficient of CDOM ($a_y(\lambda)$) were collected in 250ml bottles using Niskin bottles and a bucket from surface to bottom (Fig. 4.17-1, Table 4.17-1). CDOM samples were filtered using 0.2 μm Nuclepore polycarbonate filters on board. Optical densities of the CDOM ($OD_y(\lambda)$) in this filtered seawater were recorded against UV-2600 in the range from 300 to 800 nm using 10-cm pathlength glass cells. Milli-Q water was used as a base line. A blank (Milli-Q water versus Milli-Q water) was subtracted from each wavelength of the spectrum. The absorption coefficient of CDOM ($a_y(\lambda)$ (m^{-1})) was calculated from measured optical densities ($OD_y(\lambda)$) as follows:

$a_y(\lambda) = 2.303 \times OD_y(\lambda) / L$ (L is the cuvette path-length (m)).

(4) Preliminary results

Chl-*a* normalized specific absorption spectra (a^*_{ph}) were shown in Fig.4.17-2. Vertical profiles and cross section of CDOM (as absorption coefficient at 325 nm, unit = m^{-1}) along the P17E section were shown in Fig. 4.17-3 and Fig.4.17-4.

(5) References

Cleveland, J.S. and Weidemann, A.D., 1993, Quantifying absorption by aquatic particles: a multiple scattering correction for glass fiber filters, Limnology and Oceanography, 38, 1321-1327.

Kishino, M., Takahashi, M., Okami, N. and Ichimura, S., 1985, Estimation of the spectral absorption coefficients of phytoplankton in the sea, Bulletin of Marine Science, 37, 634-642.

Mitchell, B.G., 1990, Algorithms for determining the absorption coefficient of aquatic particulates using the quantitative filter technique (QFT), Ocean Optics X, SPIE 1302, 137-148.

Nelson, N. B., D. A. Siegel, C. A. Carlson, and C. M. Swan, 2010, Tracing global biogeochemical cycles and meridional overturning circulation using chromophoric dissolved organic matter, Geophys. Res. Lett., 37, L03610, doi:10.1029/2009GL042325.

Siegel, D.A., Maritorena, S., Nelson, N.B., Hansell, D.A., Lorenzi-Kayser, M., 2002, Global distribution and dynamics of colored dissolved and detrital organic materials. J. Geophys. Res., 107, C12, 3228, doi:10.1029/2001JC000965.

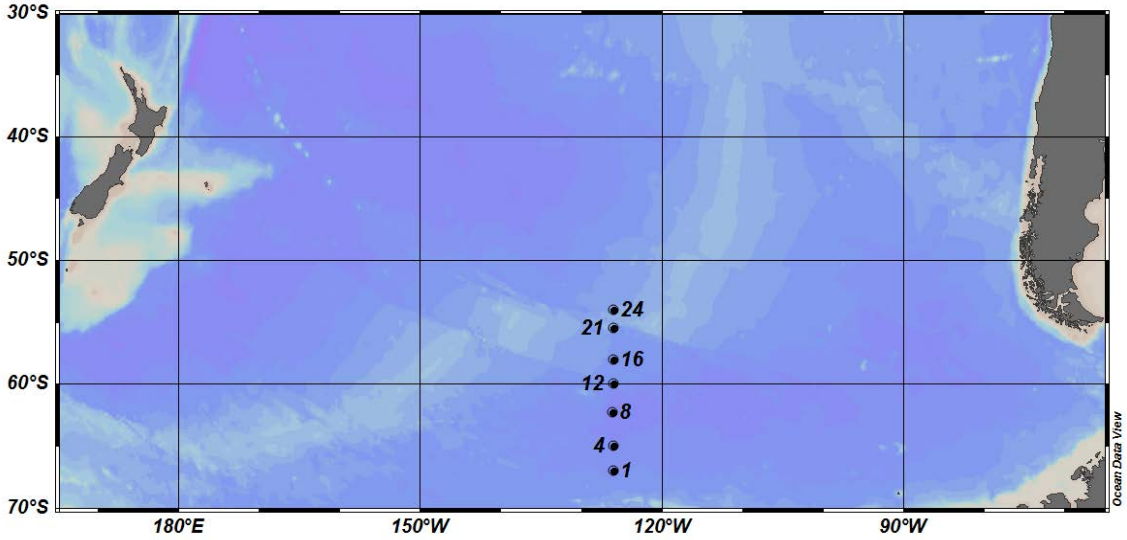

Fig. 4.17-1 Location of 7-sampling stations for absorption coefficients of phytoplankton and CDOM along the P17E section in the Southern Ocean during MR16-09 (Leg 3).

Table 4.17-1 List of sampling stations for absorption coefficients of phytoplankton (Ap) and CDOM during MR16-09 (Leg 3).

Station	Date (UTC)	Time (UTC)	Latitude		Longitude		Sampling type	Cast No.	Sampling depth (db)	
									Particle absorbance	CDOM absorbance
1	02/16/2017	7:39	67.00	S	125.98	W	CTD + Bucket	2	0, Chlmax(20), 10, 50, 100	3797, Chlmax(20), 3000, 1000, 800, 600, 400, 200, 100, 50, 10, 0
4	02/17/2017	5:28	65.02	S	125.96	W	CTD + Bucket	1	0, Chlmax(30), 10, 50, 100	4953, Chlmax(30), 3000, 1000, 800, 600, 400, 200, 100, 50, 10, 0
8	02/18/2017	22:29	62.34	S	126.11	W	CTD + Bucket	1	0, Chlmax(65), 10, 50, 100	5143, Chlmax(65), 3080, 1070, 830, 630, 430, 200, 100, 50, 10, 0
12	02/20/2017	0:36	60.01	S	125.98	W	CTD + Bucket	1	0, Chlmax(80), 10, 50, 100	4683, Chlmax(80), 2930, 970, 770, 570, 370, 200, 100, 50, 10, 0
16	02/20/2017	20:58	58.01	S	126.00	W	CTD + Bucket	1	0, Chlmax(75), 10, 50, 100	4321, Chlmax(75), 2930, 970, 770, 570, 370, 200, 100, 50, 10, 0
21	02/21/2017	19:47	55.50	S	125.98	W	CTD + Bucket	1	0, Chlmax(65), 10, 50, 100	3576, Chlmax(65), 2930, 970, 770, 570, 370, 200, 100, 50, 10, 0
24	02/22/2017	11:19	54.01	S	125.98	W	CTD + Bucket	1	0, Chlmax(30), 10, 50, 100	3541, Chlmax(30), 2930, 970, 770, 570, 370, 200, 100, 50, 10, 0

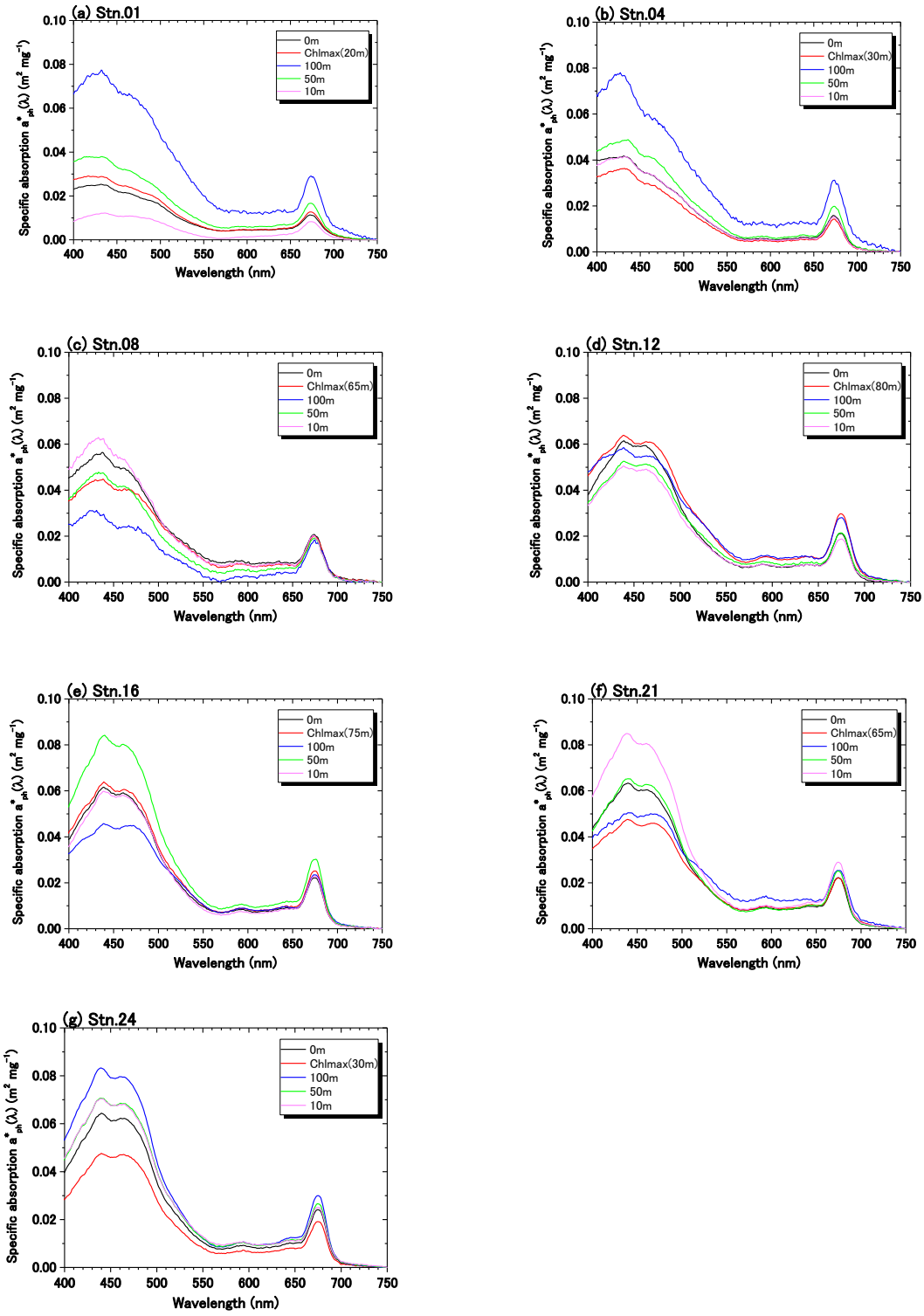

Fig.4.17-2 Chlorophyll-specific phytoplankton absorption coefficient spectra ($a^*_{ph}(\lambda)$) at 400-750 nm. All spectra were normalized to 0.0 at 750nm.

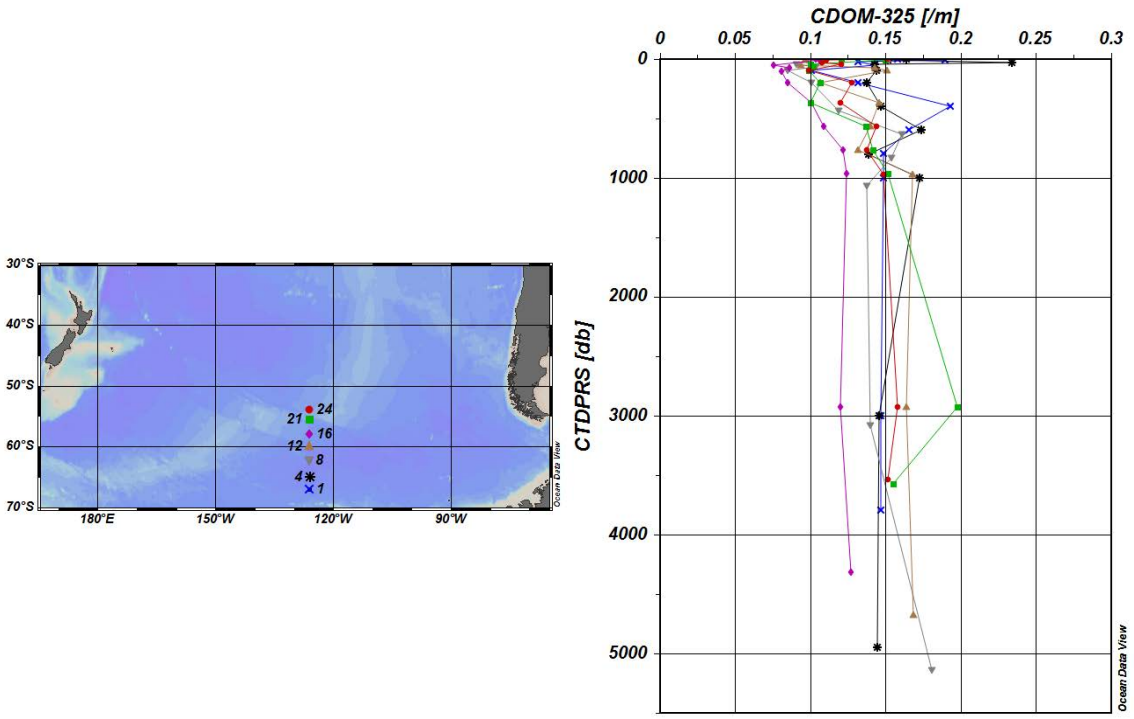

Fig.4.17-3 Vertical profiles of CDOM (as absorption coefficient at 325 nm, unit = m^{-1}) at 7-stations along the P17E section.

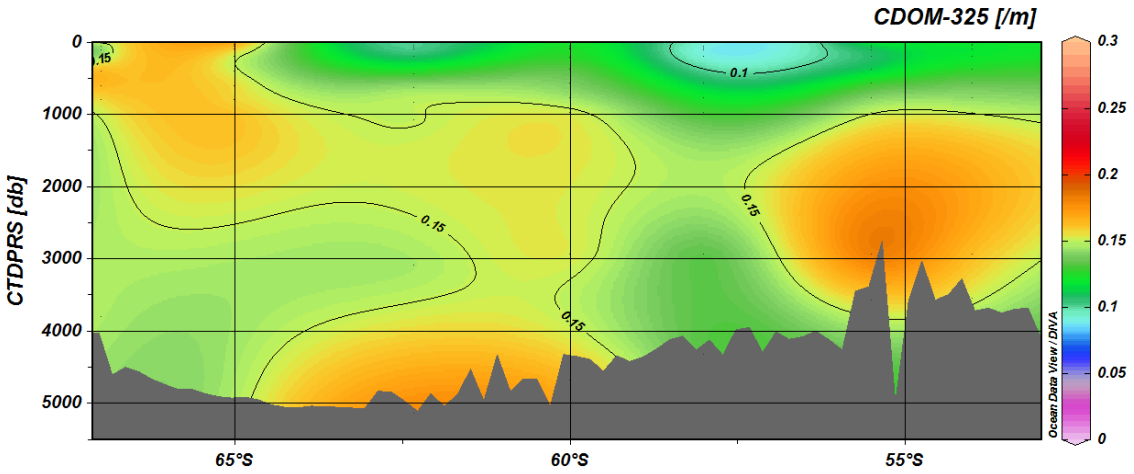

Fig.4.17-4 Contours showing distribution of CDOM (as absorption coefficient at 325 nm, unit = m^{-1}) along the P17E section.

4.18 Calcium

(1) Personnel

Etsuro Ono (JAMSTEC)

(2) Objectives

Calcium is one of the major dissolved components in the sea water. Many corals and marine organisms consume calcium to produce calcium carbonate ($CaCO_3$) as their shells and skeletons.

According to the recent IPCC report, ocean acidification is progressing, because about 30% of the anthropogenic carbon dioxide has been absorbed into the ocean. Ocean acidification is characterized by an increase of H^+ (i.e., a decrease of pH) and a concurrent decrease of carbonate ion concentration (CO_3^{2-}). The decrease of CO_3^{2-} promotes dissolution of $CaCO_3$, which is unfavorable to marine calcifying organisms.

In this cruise, to evaluate dissolution and precipitation of calcium carbonate, we measured directly the concentration of calcium in the sea water in a subantarctic region of the Southern Pacific Ocean and the Antarctic Ocean.

(3) Instruments

The analysis system consisted of a modified Dissolved Oxygen Titrator (DOT-01: Kimoto Electronic Co. Ltd.) which had a band-pass filter centered at 620 nm, a xenon light source, a photodiode detectors, and Auto-Burette system with control unit (Kimoto Electronic Co. Ltd.).

(4) Sampling and analytical methods

The samples from niskin sampler were collected to 60ml of HDPE bottles from niskins. After sampling, the samples were stored at a cool and dark place for about 7days before measurement.

The measurement method of calcium was based on a photometric method suggested by Culkin and Cox (1966).

The reagents and the procedure of the measurement in this cruise were as follows:

- Reagents

  Titrant : 0.02 mol/l EGTA (Ethylene Glycol Tetraacetic Acid)

  Buffer : Mixture solution of 0.4 mol/l NH_4Cl and 0.4 mol/l NH_3

  Indicator : 4mmol/l Zincon® solution

  Zinc source : Mixuture solution of 8mmol/l $ZnSO_4$ and 8mmol/l EGTA

- Pretreatment of sea samples

  10ml of seawater was transferred into a tall beaker by a volumetric pipet.

  A stirrer tip was put into the sample.

1ml of buffer solution was added to keep the solution at pH 9.5.

1ml of Zincon indicator was added which stained the sample red.

1ml of Zinc source was added which turned the sample blue.

Mille-Q water was added such that the overall solution was approx. 80ml.

(When measuring the acidic standard solution, the solution was neutralized by the solution of sodium hydroxide (NaOH) before buffer solution was added.)

(5) Preparation of standard solution

The in-house Ca-standard was prepared for determination of the concentration of EGTA titrant. The concentration of the standard solution was 10mmol/l, which was calculated by the gravimetric method. For preparation of the standard solution, pure $CaCO_3$ produced by NMIJ (CRM 3013-a) was used as Ca-source.

Pure $CaCO_3$ was in advance dried in an oven at 110℃ for 2 hours and accurately weighed at 1.0009g, then 50ml of 0.5M HCl solution was added to $CaCO_3$ until $CaCO_3$ was dissolved completely and degas CO_2 from the solution. After bubbles in the degassing solution calmed down, the solution was transferred to a 1000ml volumetric flask, with pure water added until 1000ml, and the weight of the whole solution was measured. The acidity of the standard solution was about pH=2.0.

The density of the Ca-standard solution was necessary to calculate the concentration of the standard solution. The method is described in Section 4.11 (Density).

(6) Calibration of EGTA titrant

In this cruise, two standard solutions were measured for monitoring the concentration of titrant. One is the in-house Ca-standard and the other is 1000mg/ L Calcium Standard Solution produced by Wako Pure Chemical Industries, Ltd. Volume of the standard solution for the monitoring measurement was 10ml for the in-house Ca-standard and 4ml for the Wako standard, so that calcium level was close to that of the sea samples.

Figure 4.18.1 shows the end point values (ml) of titration and their trends. The end point values tend to decrease. Also, the trend of the value in the in-house Ca-standard measurement is similar to that in the Wako standard. Thus, it's assumed that the concentration of EGTA titrant was increasing during the sample measurements because of evaporation of solvent caused by the headspace in the bottle of titrant. The variation of the concentration was not negligible, because the magnitude of that was more than 0.1% c.v. Therefore, the calibration of EGTA titrant was carried out by fitting a linear function calculated from the in-house Ca-standard.

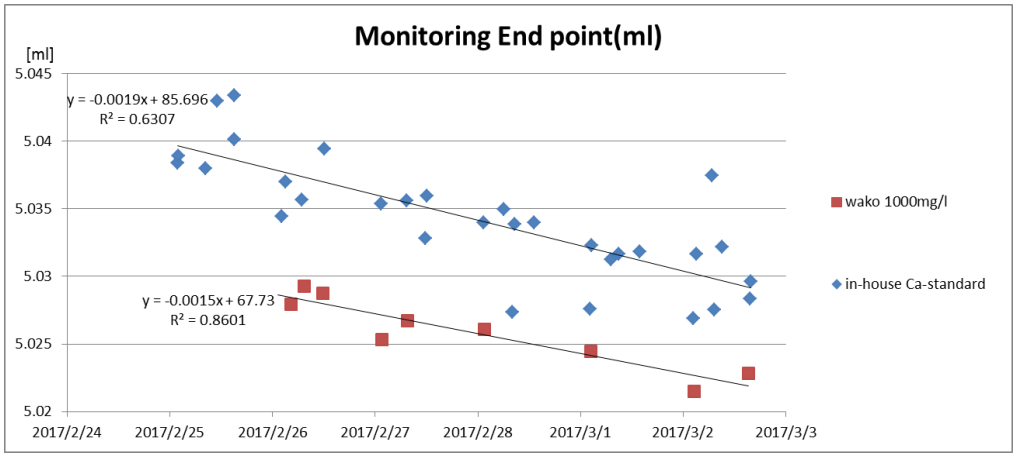

Fig. 4.18.1 Plots of the end point of standard measurements.

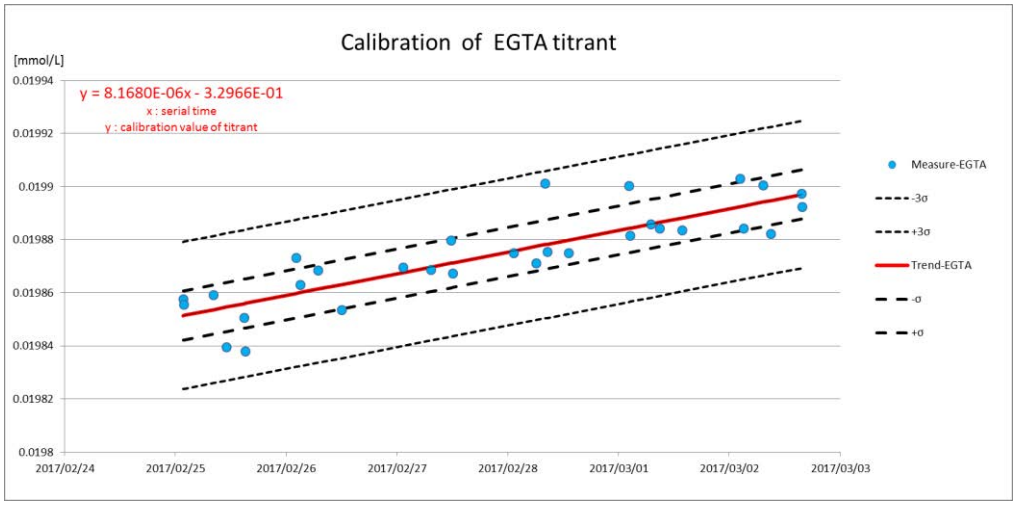

Fig. 4.18.2 Plots and calibration line for EGTA titrant.

(7) Interference to titrations by magnesium

A previous work (Culkin and Cox, 1966) points out that magnesium (Mg) and strontium (Sr) cause positive bias to the titrated volume of Ca because of their interference with the reaction between EGTA and Ca; the bias caused by Mg was 0.729% and by Sr was 0.388%.

Also, in our preparation before the cruise, when Ca-standard with Mg source in same proportion as sea water was measured, it was suggested that the end point of that was increased by 0.745% as compared with the sample without Mg. This result agreed with the previous work.

Although Mg interferes the titration of Ca in this titrating condition, no correction was given to the data submitted in this cruise.

Table 4.18.1 Results of interference by Mg

	Average end point [ml]	2σ	N
No Mg	5.1136	0.0076	9
Add Mg	5.1517	0.0046	9

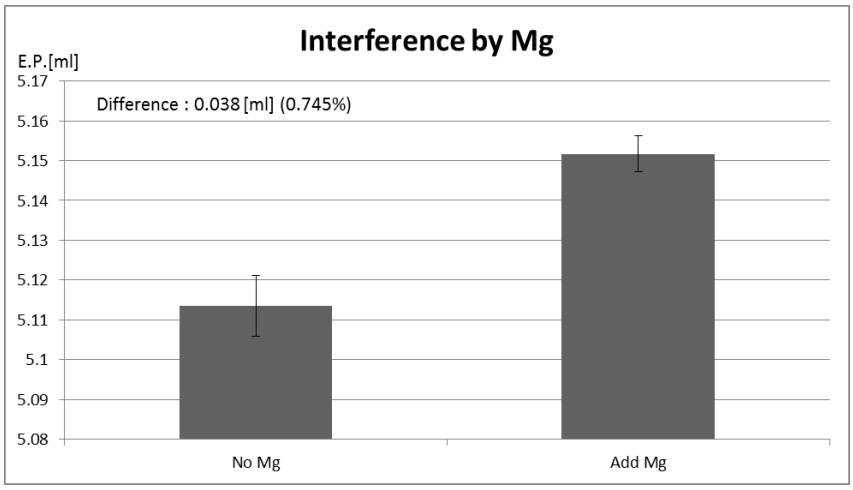

Fig. 4.18.3 Comparison of the end point for Ca-standard added Mg and not containing Mg.

(8) Performance

The replicate samples were collected from 2 layers at each station to examine repeatability. The precision of replicate samples was estimated at 0.0052 mmol kg^{-1} (n=20 pairs). We used the SOP23 method to estimate the repeatability.

There were no major troubles with the analysis during the cruise.

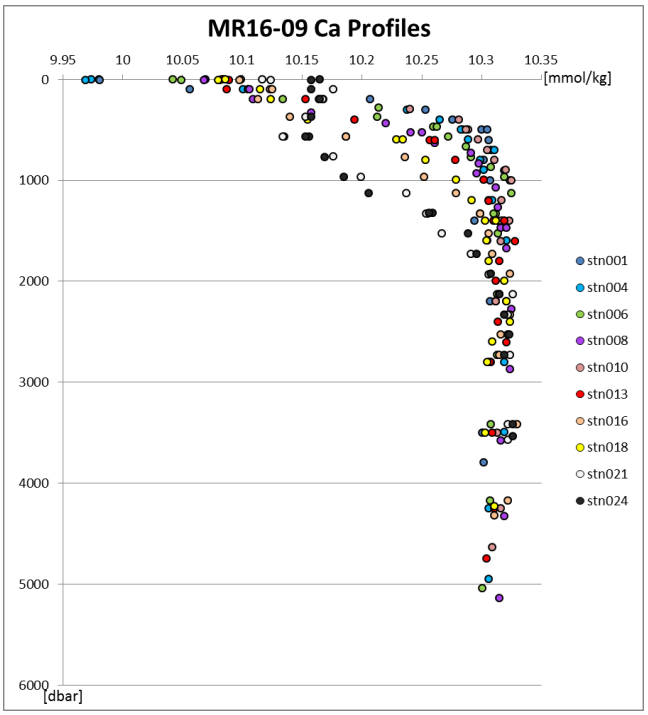

Fig. 4.18.4 Vertical profiles of calcium.

References

F. Culkin, and R. A. Cox (1966) Sodium, potassium, magnesium, calcium and strontium in sea water. Deep-Sea Res., 13, 789-804.

4.19 Dissolved organic matter and the associated parameters

(1) Personnel

Masahito Shigemitsu	(JAMSTEC): Principal investigator
Taichi Yokokawa	(JAMSTEC)
Masahide Wakita	(JAMSTEC)
Akihiko Murata	(JAMSTEC)

(2) Objectives

Dissolved organic matter (DOM) in the ocean can be affected by advection and mixing and DOM has relatively refractory fractions which resist biological degradation. Such characteristics of DOM play some important roles in the ocean biogeochemistry: 1) DOM contributes to the biological pump, which makes the dissolved organic carbon (DOC) in the ocean one of the major carbon reservoirs in the Earth, and 2) Dissolved organic nitrogen (DON) and dissolved organic phosphorus (DOP) can be carried away from the regions where those are produced, making DON and DOP the potential nutrients in the oligotrophic ocean.

In this cruise, we aim to gain insights into the behavior of DOC in the Southern Ocean which is considered to be a key region for the oceanic carbon cycles, and clarify the spatial variations in ratio of DOC:DON:DOP to get some information about the importance of DON and DOP as potential nutrients.

(3) Material and methods

i. DOC and DON

Seawater samples were obtained from Niskin bottles on a CTD-rosette system. Each sample taken in the upper 250 m was filtered using a pre-combusted (450℃ for 4 hours) Whatman 47-mm GF/F filter. The filtration was carried out by connecting a spigot of the Niskin bottle through silicone tube to an inline plastic filter holder. Filtrates were collected in acid-washed 60 mL High Density Polyethylene (HDPE) bottles in duplicates, and were immediately stored frozen until analysis. Other samples taken below 250 m were unfiltered and stored in the same way.

In the analysis after this cruise, the frozen samples are thawed at room temperature, and acidified to pH < 2 with 50% HCl followed by being bubbled to remove dissolved inorganic carbon (DIC) from the samples. Then, the concentrations of DOC and total dissolved nitrogen (TDN) are measured with a total organic carbon analyzer equipped with a chemiluminescence detector unit (Shimadzu, Japan).

Concentration of DON is calculated by subtracting the sum of dissolved inorganic nitrogen (nitrate, nitrite and ammonium) from the measured TDN. The measurement procedure of dissolved inorganic nitrogen is found somewhere in this cruise report.

ii. Surface DOC, DON and DOP

Sea-surface waters (5 m depth) were collected in the sea surface monitoring laboratory once a day along the cruise track except for the Chilean and New Zealand EEZs. The seawater samples were filtered in the similar way to the above. DOC and TDN concentrations for the samples are measured in the same way as stated above, and DON concentration is also calculated as stated above. Soluble reactive phosphorus (SRP) concentration is measured manually by the molymbdenum blue method (Parsons et al., 1984), and concentration of total dissolved phosphorus (TDP) is determined by the method after persulfate oxidation (Menzel and Corwin, 1965). DOP is calculated as difference between TDP and SRP.

iii. Rates of DOC production and DIC fixation

Seawater samples for measurements of rates of DOC production and DIC fixation were obtained at depths. The measurement procedure is basically based on the method of Teira et al. (2003). At each depth at each station, three samples of 30 ml were inoculated with 1480 kBq of $NaH^{14}CO_3$ followed by the incubations in an on-deck incubator. Incubation was stopped by adding 20% glutaraldehyde, and the seawater samples were filtered through 0.2μm cellulose filters. Filter samples are exposed to concentrated HCl fumes and filtrates are bubbled with N_2 gas after addition of 50% HCl. Then, scintillation cocktail is added to filter and filtrate samples, and the radioactivity of them is measured by a liquid scintillation counter. Triplicate blank tests for 0.2μm-filtered seawater were carried out in the same way as the samples.

(4) Data archives

The data of each DOM and the associated parameters obtained in this cruise will be submitted to the Data Management Group of JAMSTEC, and will be open to the public via “Data Research System for Whole Cruise Information in JAMSTEC (DARWIN)” in JAMSTEC web site.

(5) References

Parsons, T.R., Y. Maita, C.M. Lalli (1984), A Manual for Chemical and Biological Methods for Seawater Analysis. Pergamon, Oxford.

Menzel, D.W., and N. Corwin (1965), The measurement of total phosphorus in seawater based on the liberation of organically bound fractions by persulfate oxidation, Limnol. Oceanogr., 10, 280–282.

Teira, E., M.J. Pazo, M. Quevedo, M.V. Fuentes, F.X. Niell, and E. Fernandez (2003), Rates of dissolved organic carbon production and bacterial activity in the eastern North Atlantic Subtropical Gyre during summer, Mar. Ecol. Prog. Ser., 249, 53-67.

4.20 Carbon isotopes

March 3, 2017

(1) Personnel

Yuichiro Kumamoto

Japan Agency for Marine-Earth Science and Technology

(2) Objective

In order to investigate the water circulation and carbon cycle in the eastern Indian Ocean, seawaters for measurements of carbon-14 (radiocarbon) and carbon-13 (stable carbon) of total dissolved inorganic carbon (TDIC) were collected by the hydrocasts from surface to near bottom.

(3) Sample collection

The sampling stations and number of samples are summarized in Table 4.20.1. All samples for carbon isotope ratios (total 254 samples) were collected at 8 stations using 12-liter Niskin-X bottles. The seawater sample was siphoned into a 250 cm^3 glass bottle with enough seawater to fill the glass bottle 2 times. Immediately after sampling, 10 cm^3 of seawater was removed from the bottle and poisoned by 0.1 cm^3 μl of saturated $HgCl_2$ solution. Then the bottle was sealed by a glass stopper with Apiezon grease M and stored in a cool and dark space on board.

(4) Sample preparation and measurements

In our laboratory, dissolved inorganic carbon in the seawater samples will be stripped cryogenically and split into three aliquots: radiocarbon measurement (about 200 μmol), carbon-13 measurement (about 100 μmol), and archive (about 200 μmol). The extracted CO_2 gas for radiocarbon will be then converted to graphite catalytically on iron powder with pure hydrogen gas. The carbon-13 of the extracted CO_2 gas will be measured using Finnigan MAT253 mass spectrometer. The carbon-14 in the graphite sample will be measured by Accelerator Mass Spectrometry (AMS).

Table 4.20.1 Sampling stations and number of samples for carbon isotope ratios.

Station	Lat. (S)	Long. (W)	Sampling Date (UTC)	Number of samples	Number of replicate samples	Max. Pressure (dbar)
01	67-00.00	125-58.56	2017/02/16	28	2	3797
06	63-41.01	125-59.58	2017/02/17	33	2	5045
10	60-58.71	126-04.20	2017/02/19	31	2	4635
13	59-36.44	126-03.24	2017/02/20	31	2	4749
16	58-00.63	125-59.76	2017/02/20	30	2	4321
20	56-00.65	125-57.36	2017/02/21	29	2	4157
23	54-28.36	125-59.10	2017/02/22	27	2	3676
26	53-00.73	126-00.06	2017/02/22	29	2	4341
			Total	238	16	

4.21 Stable Isotopes of Water

February 28, 2017

(1) Personnel

Hiroshi Uchida (JAMSTEC)

Katsuro Katsumata (JAMSTEC)

(2) Objectives

The objective of this study is to collect stable isotopes of water to use as a tracer of ocean circulation.

(3) Materials and methods

The hydrogen (H) and oxygen (O) isotopic ratio of seawater are defined as follows:

$\delta D\ [‰] = 1000\ \{(D/H)_{sample}/(D/H)_{VSMOW} - 1\}$

$\delta^{18}O\ [‰] = 1000\ \{(^{18}O/^{16}O)_{sample}/(^{18}O/^{16}O)_{VSMOW} - 1\}$

where D is deuterium and VSMOW is Vienna Standard Mean Ocean Water. The isotopic ratios of VSMOW water are defined as follows:

$(D/H)_{VSMOW} = 155.76 \pm 0.1$ ppm

$(^{18}O/^{16}O)_{VSMOW} = 2005.20 \pm 0.43$ ppm.

The isotopic ratios will be measured in a laboratory in the Japan Agency for Marine-Earth Science and Technology, Yokosuka, Japan, after the cruise with a Cavity Ring-Down Spectroscopy (CRDS, L112-i, Picarro Inc., Santa Clare, CA, USA).

The water samples were collected in 10-mL borosilicate glass bottles (Butyl rubber stopper with aluminum cap, Maruemu Co., Osaka, Japan). The collected samples are storing at room temperature. A total of 587 samples was collected including 34 pairs of replicate samples.

4.22 Beryllium Isotopes

March 3, 2017

(1) Personnel

Yuichiro Kumamoto

Japan Agency for Marine-Earth Science and Technology

(2) Objective

^{10}Be (half-life 1.36 x 10^6 y) is produced in the atmosphere by cosmic rays. Its production rate is dependent on latitude, altitude and time, because the intensity of the cosmic rays is not homogeneous. The radionuclide is transported by aerosols, and moved from the stratosphere to the surface soil and surface ocean via the troposphere. Rates of production and precipitation of ^{10}Be were calculated by Lal and Peters (1964), but their calculation has not been confirmed experimentally. The purpose of this study is to reveal a depth profile of ^{7}Be and ^{10}Be in the Antarctic Ocean.

(3) Sample collection

Total 18 of seawater sample (40L or 20L) for beryllium isotopes were collected at Station 1 (67.002°S/125.983°W, 16 Feb. 2017). The seawaters were sampled vertically using 12-liter Niskin-X bottles from the surface to the bottom of the water column. The seawater sample was collected into a 20-L plastic container and after two time washing.

(4) Sample preparation and measurements

To recover beryllium isotopes from large volume (40L or 20L) seawater samples, 2 mg of Be carrier, 2g of Fe carrier and 20ml of conc. HCl are added. After three hours or more later, 20ml of conc. NH_4OH are added to the solution to co-precipitate $Be(OH)_2$ and $Fe(OH)_3$. Precipitates of $Be(OH)_2$ and $Fe(OH)_3$ are dissolved by conc. HCl, then concentrated and adjusted to 9M HCl solutions by adding conc. HCl for isopropyl ether extraction. Extraction procedure is repeated three times to remove Fe. The purification for Accelerator Mass Spectrometry (AMS) measurement uses a cation exchange column. For ^{9}Be measurements, 250 ml of filtered seawater samples are separately stored in polypropylene bottles. ^{9}Be is measured using a ICP- MS. ^{7}Be and ^{10}Be are measured using AMS at MALT, Univ. of Tokyo.

4.23 Lowered Acoustic Doppler Current Profiler

(1) Personnel

Shinya Kouketsu (JAMSTEC) (principal investigator)
Hiroshi Uchida (JAMSTEC)
Katsurou Katsumata (JAMSTEC)

(2) Overview of the equipment

An acoustic Doppler current profiler (ADCP) was integrated with the CTD/RMS package. The lowered ADCP (LADCP), Workhorse Monitor WHM300 (Teledyne RD Instruments, San Diego, California, USA), which has 4 downward facing transducers with 20-degree beam angles, rated to 6000 m. The LADCP makes direct current measurements at the depth of the CTD, thus providing a full profile of velocity. The LADCP was powered during the CTD casts by a 48 volts battery pack. The LADCP unit was set for recording internally prior to each cast. After each cast the internally stored observed data was uploaded to the computer on-board. By combining the measured velocity of the sea water and bottom with respect to the instrument, and shipboard navigation data during the CTD cast, the absolute velocity profile can be obtained (e.g. Visbeck, 2002).

The instrument used in this cruise was as follows.

Teledyne RD Instruments, WHM300
S/N 20754 (downward looking), S/N 18324 (upward looking)

(3) Data collection

In this cruise, data were collected with the following configuration.

Bin size: 4.0 m
Number of bins: 25
Pings per ensemble: 1
Ping interval: 1.0 sec

Reference

Visbeck, M. (2002): Deep velocity profiling using Lowered Acoustic Doppler Current Profilers: Bottom track and inverse solutions. *J. Atmos. Oceanic Technol.*, **19**, 794-807.

4.24 Micro Rider

(1) Personnel

Shinya Kouketsu ***(JAMSTEC)***

Hiroshi Uchida ***(JAMSTEC)***

Katsurou Katsumata (JAMSTEC)

(2) Objective

Microstructure observations to evaluate vertical mixing.

(3) Instruments and method

Micro structure observations were carried out by micro-Rider 6000 (MR6000; Rockland Scientific International Inc.), which is mounted CTD rosette and is powered from SBE 9plus. We mounted two FP07 thermistors to obtain the high-frequency changes in temperature. We sometimes replaced the probes during this cruise to compare sensitivities between the probes. The high-frequency pressure and acceleration profiles are also obtained by the sensors in MR6000. The low-frequency profiles of temperature are archived in the MR6000 from the cables connected with SBE-3 sensor on the CTD system. We download the profile data from the MR6000 a cast. After the cruise, we plan to examine the methods of the correction and measurement quality evaluation with the comparison among the micro temperature with CTD rosette, those with free fall instruments, and free fall micro shear structure observations.

(4) Micro-Temperature measurement history

- Sensor socket 1: T1320
- Sensor socket 2: T1337 (St. 1-2), T1338 (St. 3-4), T1339 (St. 5-13) and T1341 (St. 14-26)

4.25 Sound Velocity

May 10, 2017

(1) Personnel

Hiroshi Uchida (JAMSTEC) (Principal investigator)

Rei Ito (MWJ) (Legs 2 and 3)

Sonoka Tanihara (MWJ) (Leg 2)

Kenichi Katayama (MWJ) (Leg 3)

Shungo Oshitani (MWJ) (Leg 3)

Rio Kobayashi (MWJ) (Leg 3)

(2) Objectives

The objective of this study is to estimate Absolute Salinity (also called "density salinity") from sound velocity data with temperature and pressure data from CTD, and to evaluate an algorithm to estimate absolute salinity provided along with TEOS-10 (the International Thermodynamic Equation of Seawater 2010) (IOC et al., 2010).

(3) Materials and methods

Sound velocity profiles were measured at the CTD casts by using a velocimeter (MiniSVP, serial no. 49618, Valeport Ltd., Devon, United Kingdom). The sound velocity sensing elements are a ceramic transducer (signal sound pulse of 2.5 MHz frequency), a signal reflector, and spacer rods to control the sound path length (10 cm), providing a measurement at depths up to 6000 m. The velocimeter was attached to the CTD frame and level of the sound path of the velocimeter was same as that of the CTD temperature sensor, just next to the primary temperature sensor. Although temperature and pressure data were also measured by the velocimeter, only sound velocity data measured at a sampling rate of 8 Hz were combined with the CTD temperature and pressure data measured at a sampling rate of 24 Hz to estimate Absolute Salinity.

The sound velocity data were obtained at all CTD casts in legs 2 and 3. The sound velocity data were roughly combined with the CTD data to match the time going into and coming out of the sea water, and the combined data were interpolated at a sub-sampling rate of 16 Hz. Time difference between the sound velocity data and the CTD data were more strictly adjusted to minimize spikes of salinity data back calculated from the sound velocity, pressure and temperature data as follows. Standard deviations of difference between the back calculated salinity data and their low-pass filtered data by a running mean with a window of 161 scans (10 seconds) were calculated for a segment from 20 to 70 dbar of the down cast by advancing the sound velocity data against the CTD data from –6 scans to +6 scans at one scan intervals, and the advanced scan to minimize the standard deviation was estimated. These

calculations were repeated for a segment at 50 dbar intervals from 20 dbar to 570 dbar, and a median of the estimated advanced scans was calculated as the best estimate of the advanced scan.

The estimated Absolute Salinity (S_v) were calibrated in situ referred to the Absolute Salinity measured by a density meter for water samples. The corrected Absolute Salinity were estimated as

Corrected Absolute Salinity =

$$(c_0 + c_1 \times Sv + c_2 \times T + c_3 \times P + c_4 \times Sv^2 + c_5 \times P^2 + c_6 \times T^2 + c_7 \times Sv \times P + c_8 \times Sv \times T) \times (1 + c_9 \times P)$$

where T is CTD temperature in °C, P is pressure in dbar, and $c_0 \sim c_8$ are calibration coefficients. The best fit sets of coefficients were determined by a least square technique to minimize the deviation from the Absolute Salinity measured by the density meter, except for the coefficient c_9 which was subjectively determined in advance.

The post-cruise calibrated temperature and salinity data were used for the calibration. The calibration coefficients are listed in Table 4.25.1. The results of the post-cruise calibration for the Absolute Salinity estimated from the sound velocity data are summarized in Table 4.25.2 and shown in Fig. 4.25.1. Vertical profiles of the corrected Absolute Salinity were shown in Fig. 4.25.2.

Table 4.25.1 Calibration coefficients for Absolute Salinity estimated from the sound velocity data.

Coefficient	S/N 49618
c_0	26.70938514122043
c_1	–0.5416586809715309
c_2	–0.1354291356712744
c_3	1.401399009550316e–3
c_4	2.245731443302312e–2
c_5	5.894712917405537e–8
c_6	1.067486700100993e–3
c_7	–9.109068401397720e–5
c_8	3.551854573705933e–3
c_9	5.17e–5

Table 4.25.2 Difference between the corrected Absolute Salinity estimated from the sound velocity data and the Absolute Salinity measured by the density meter after the post-cruise calibration. Mean and standard deviation (Sdev) are calculated for the data below and above 950 dbar. Number of data used is also shown.

Serial number	Pressure ≥ 950 dbar			Pressure < 950 dbar		
	Number	Mean [g/kg]	Sdev	Number	Mean [g/kg]	Sdev
49618	227	0.0000	0.0238	227	0.0000	0.0036

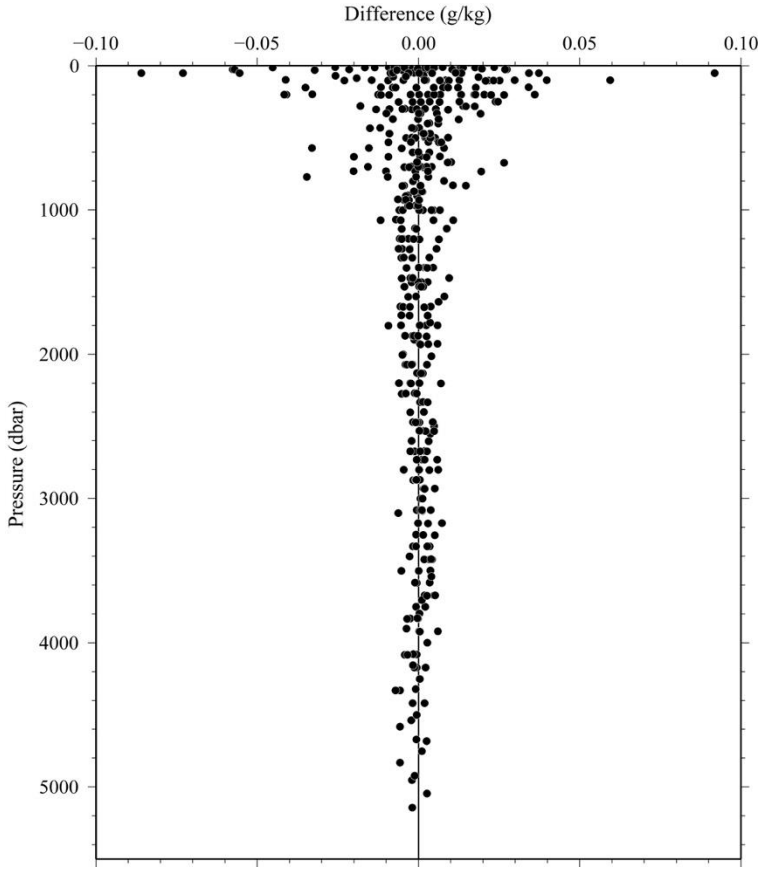

Fig. 4.25.1. Vertical distribution of differences between Absolute Salinity estimated from sound velocity data and Absolute Salinity estimated from the density meter for legs 2 and 3.

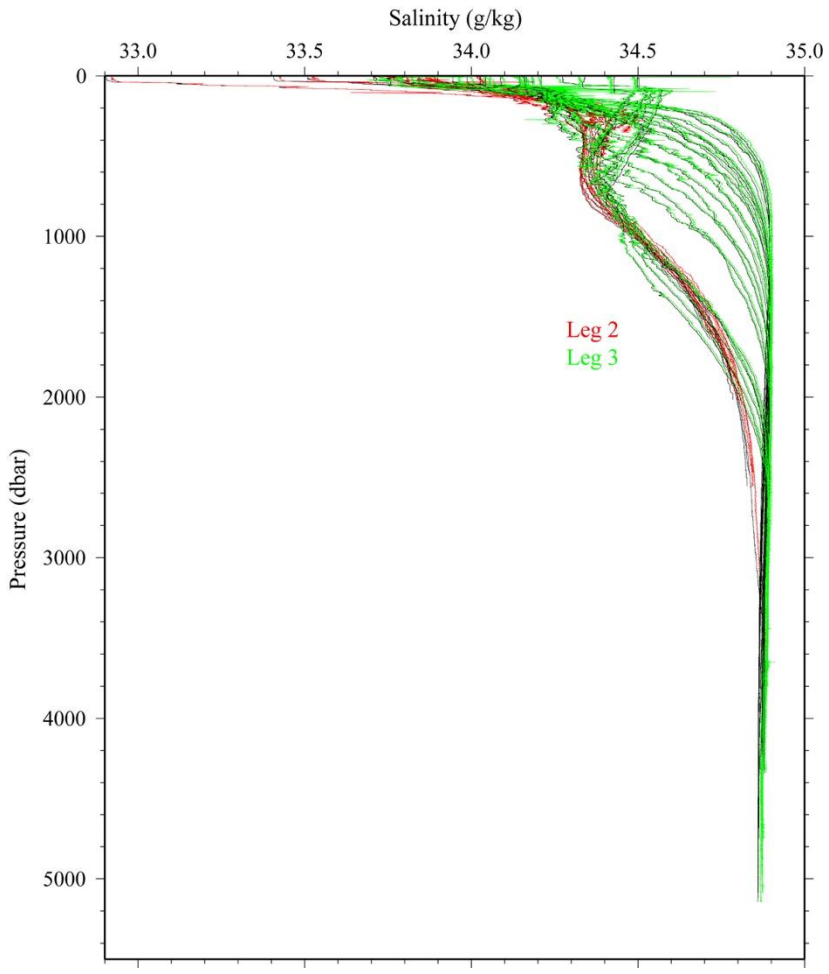

Fig. 4.25.2. Vertical profiles of Absolute Salinity estimated from sound velocity data. Black lines indicate Reference-Composition Salinity derived from CTD salinity data.

(4) Reference

IOC, SCOR and IAPSO (2010): The international thermodynamic equation of seawater – 2010: Calculation and use of thermodynamic properties. Intergovernmental Oceanographic Commission, Manuals and Guides No. 56, United Nations Educational, Scientific and Cultural Organization (English), 196 pp.

4.26 pH, POC, and HPLC sampling for SOCCOM project

(1) Personnel

K. Katsumata, K. Sasaoka (JAMSTEC), E. Boss (University of Maine), A. Dickson, S. Becker, L. Talley (Scripps Institution of Oceanography), R. Key (Princeton University)

(2) Objectives

SOCCOM (Southern Ocean Carbon and Climate Observations and Modeling) is a project funded by NSF, NOAA, and NASA. The primary goal is to better understand the role of Southern Ocean in climate change and biogeochemistry with special emphasis on carbon flux and inventory. The main observational tool is a newly developed Argo-type float additionally equipped with biogeochemical sensors. The long term plan is to deploy approximately 200 floats in the Southern Ocean from 2014 to 2020. As a JAMSTEC contribution towards this project, we deployed five floats during the P17E reoccupation in the southeastern Pacific. It is essential that the float deployment be accompanied with high-quality bottle data for calibrating the float sensors. GO-SHIP cruises strives for state-of-the-art accuracy and precision and are consequently an ideal platform for this purpose. In this section, we describe the bottle sampling accompanying the float deployments. The float deployments are described in Section 5.2.

(3) Stations and depths

At five stations (2, 4, 8, 18, and 24) water samples were collected from Niskin bottles mounted in a Rosette sampler. Samples for pH were collected from all Niskins shallower than 2000 dbar, but not from the surface bucket sampling. Duplicate samplings were collected at two depths. Samples for HPLC and POC were collected from the Niskins near the chlorophyll maximum (when exists) or at a depth between the two bottles near the surface (usually 50 dbar and 100 dbar), when no obvious chlorophyll maximum was found. We monitored the fluorescence during CTD downcast to identify the chlorophyll maximum. Another set of samples was collected from the surface bucket sampling. Chlorophyll maximum sampling was duplicated.

(4) pH

The sampling method followed the instructions in Talley *et al.* (2017). Water samples were collected immediately after dissolved oxygen and CFCs. A Tygon tube designated solely for pH sampling was used to avoid possible contamination with other samples (DOC, in particular). After filling a bottle following a 20 second overflow, 16 mL of sampled sea water were removed by syringe and 120 μL of saturated mercuric chloride was added with an Eppendorf pipette. The bottles were then sealed and the contents mixed by inverting the bottle more than five times. The bottles were kept at about 5 °C

until 27th March 2017 when they were unloaded at Hachinohe port. The bottles were then air-freighted to Scripps Institution, San Diego for analysis.

(5) HPLC and POC

Samples were collected in brown Nalgene bottles using a silicone tube from Niskin bottles or a bucket. HPLC and POC were usually the last items to sample. Before collection, the Nalgene bottles and bucket were rinsed 3 times. After sampling, the sea water was immediately filtered in a dark room. One to three liters of sea water, depending on water clarity, were filtered and the volumes recorded. The filters were kept in a deep freezer at −80 °C. The samples were transferred to a dry shipper cooled with liquid nitrogen on 27th March 2017 at Hachinohe. They were subsequently air-freighted to Scripps Institution, San Diego for analysis.

References

Talley, L.D., S. Becker, R. Key, A. Dickson, E. Boss, C. Sakamoto, 2017, SOCCOM BGC floats shipboard calibration data requirement, version 8 January 2017, available online at https://soccom.princeton.edu/content/manuals

4.27 Chlorofluorocarbons and Sulfur hexafluoride

Ken'ichi Sasaki[1)], Hironori Sato[2)], Hiroshi Hoshino [2)], and Masahiro Orui [2)]

1) Mutsu Institute for Oceanography, Japan Agency for Marine Earth Science and Technology

2) Marine Works Japan Ltd.

1 Objectives

Chlorofluorocarbons (CFCs) and sulfur hexafluoride (SF_6) are man-made stable gases. These atmospheric gases can slightly dissolve in sea surface water by air-sea gas exchange and then are spread into the ocean interior. So dissolved these gases could be used as chemical tracers for the ocean circulation. We measured concentrations of three chemical species of CFCs, CFC-11 (CCl_3F), CFC-12 (CCl_2F_2), and CFC-113 ($C_2Cl_3F_3$), and SF_6 in seawater on board, and made simultaneous analysis of dissolved nitrous oxide (N_2O) for a certain number of seawater samples on the trial base.

2 Apparatus

We use three measurement systems. One of them is CFCs analyzing system. Other two are SF_6/CFCs simultaneous analyzing system. Trial analysis of N_2O was made on latter systems. Both systems are based on purging and trapping gas chromatography.

Table 4-27-1 Instruments

SF_6/CFCs (&N2O) simultaneous analyzing system	
Gas Chromatograph:	GC-14B (Shimadzu Ltd.)
Detector 1:	ECD-14 (Shimadzu Ltd.)
Detector 2:	ECD-14 (Shimadzu Ltd.)
Analytical Column:	
Pre-column 1:	Silica Plot capillary column [i.d.: 0.53 mm, length: 6 m, film thickness: 6 μm]
Pre-column 2:	Molesive 5A Plot capillary column [i.d.: 0.53 mm, length: 5 m, film thickness: 15 μm]
Main column 1:	Connected two capillary columns (Pola Bond-Q [i.d.: 0.53mm, length: 9 m, film thickness: 10μm] followed by Silica Plot [i.d.: 0.53mm, length: 18 m, film thickness: 6μm])
Main column 2:	Connected two capillary columns (Molesive 5A Plot [i.d.: 0.53 mm, length: 3 m, film thickness: 15 μm] followed by Pola Bond-Q [i.d.: 0.53mm, length: 9 m, film thickness: 10μm])
Purging & trapping:	Developed in JAMSTEC. Cold trap columns are 30 cm length stainless

	steel tubing packed the section of 5cm with 80/100 mesh Porapak Q and followed by the section of 5cm of 100/120 mesh Carboxen 1000. Outer diameters of the main and focus trap columns are 1/8" and 1/16", respectively.
CFCs analyzing system	
Gas Chromatograph:	GC-14B (Shimadzu Ltd.)
Detector:	ECD-14 (Shimadzu Ltd.)
Analytical Column:	
Pre-column:	Silica Plot capillary column [i.d.: 0.53mm, length: 6 m, film thickness: 6μm]
Main column:	Connected two capillary columns (Pola Bond-Q [i.d.: 0.53mm, length: 9 m, film thickness: 10μm] followed by Silica Plot [i.d.: 0.53mm, length: 18 m, film thickness: 6μm])
Purging & trapping:	Developed in JAMSTEC. Cold trap columns are 1/16" SUS tubing packed the section of 5cm with 100/120 mesh Porapak T.

3 Procedures

3.1 Sampling

Seawater sub-samples were collected from 12 liter Niskin bottles to 450 ml of glass bottles developed in JAMSTEC. The glass bottles were filled by CFC free gas (pure nitrogen gas) before sampling. Two times of the bottle volume of seawater sample were overflowed. The seawater samples were kept in a thermostatic water bath at 7ºC. The samples were taken to determination as soon as possible after sampling (usually within 12 hours).

In order to confirm CFC/SF_6 concentrations of standard gases and their stabilities and also to check saturation levels in sea surface water, mixing ratios in background air were periodically analyzed. Air samples were continuously led into laboratory by air pump. The end of 10 mm OD Dekaron tubing was put on a head of the compass deck and another end was connected onto the air pump in the laboratory. The tubing was relayed by a T-type union which had a small stop cock. Air sample was collected from the flowing air into a 200ml glass cylinder attached on the cock.

3.2 Analysis

SF_6/CFCs /N_2O simultaneous analyzing system

Constant volume of sample water (200 ml) is taken into a sample loop. The sample is send into

stripping chamber and dissolved SF_6, CFCs and N_2O are de-gassed by N_2 gas purging for 8 minutes. The gas sample is dried by magnesium perchlorate desiccant and concentrated on a main trap column cooled down to -80 ºC. Stripping efficiencies are frequently confirmed by re-stripping of surface layer samples and more than 99 % of dissolved SF_6 and CFCs and ~95 % of N_2O are extracted on the first purge. Following purging & trapping, the main trap column is isolated and electrically heated to 180 ºC. After 1 minute, the desorbed gases are sent onto focus trap cooled down to -80 ºC for 30 seconds. Gaseous sample on the focus trap are desorbed by same manner of the main trap, and lead onto the pre-column 1 (PC 1). Sample gases are roughly separated on the PC 1. Eluting SF_6, CFCs and N_2O onto pre-column 2 (PC 2), PC1 is connected onto cleaning line and high boiling point compounds are flushed by counter flow of pure nitrogen gas. SF_6 and CFCs are quickly eluted from PC 2 onto main-column 1 (MC 1) and N_2O is retained on PC 2. Then PC 2 is connected back-flush carrier gas line and N_2O is sent onto main-column 2 (MC 2). SF_6 and CFCs are further separated on MC 1 and detected by ECD 1. N_2O sent onto MC 2 is detected by ECD 2.

CFCs analyzing system

Constant volume of sample water (50 ml) is taken into a sample loop. The sample is send into stripping chamber and dissolved CFCs are de-gassed by N_2 gas purging for 8 minutes. The gas sample is dried by magnesium perchlorate desiccant and concentrated on a trap column cooled down to -50 ºC. Stripping efficiencies are frequently confirmed by re-stripping of surface layer samples and more than 99.5 % of dissolved CFCs are extracted on the first purge. Following purging & trapping, the trap column is isolated and electrically heated to 140 ºC. The desorbed gases are lead into the pre-column. Sample gases are roughly separated in the pre-column. When CFC-113 eluted from pre-column onto main column, the pre-column is connected onto another line and flushed by counter flow of pure nitrogen gas. CFCs send on MC 1 are further separated and detected by ECD.

Nitrogen gases used in these systems was filtered by gas purifier column packed with Molecular Sieve 13X (MS-13X).

Table 4-27-2 Analytical conditions

SF_6/CFCs(/N_2O) simultaneous analyses	
Temperature	
Analytical Column:	95 ºC
Detector (ECD):	300 ºC
Trap column:	-80 ºC (at adsorbing) & 170 ºC (at desorbing)
Mass flow rate of nitrogen gas (99.99995%)	

Carrier gas 1: 10 ml/min
Carrier gas 2: 10 ml/min
Detector make-up gas 1: 27 ml/min
Detector make-up gas 2: 27 ml/min
Back flush gas: 10 ml/min
Sample purge gas: 220 ml/min

CFCs analyses

Temperature

Analytical Column: 95 ºC
Detector (ECD): 240 ºC
Trap column: -50 ºC (at adsorbing) & 140 ºC (at desorbing)

Mass flow rate of nitrogen gas (99.99995%)

Carrier gas : 10 ml/min
Detector make-up gas : 27 ml/min
Back flush gas: 10 ml/min
Sample purge gas: 130 ml/min

Standard gas (Japan Fine Products co. Ltd.)

Cylinder No.	Base gas	CFC-11	CFC-12	CFC113	SF_6	N_2O	remarks
		ppt	ppt	ppt	ppt	ppm	
CPB20785	N_2	873	472	81.5	9.83	14.6	for SF_6/CFC/N_2O
CPB21090	N_2	891	472	82.0	9.77	15.0	for SF_6/CFC/N_2O
CPB09873	N_2	301	160	30.2	0.00	0.0	for CFC
CPB16993	N_2	300	161	29.8	0.00	0.0	Reference

4 Performance

The analytical precisions were estimated from replicate sample analyses. The estimated preliminary precisions were ± 0.014 pmol/kg (n = 69), ± 0.007 pmol/kg (n = 69), ± 0.007 pmol/kg (n = 69), ± 0.018 fmol/kg (n = 42), and ± 0.8 nmol/kg (n = 13) for CFC-11, CFC-12, CFC-113, SF_6, and N_2O, respectively. There were some problems on N_2O analysis. The peak area of N_2O was significantly increase at standard gas analysis after seawater sample analysis compared with that at continuous analysis of standard gas. This increase was not due to carryover from previous seawater sample analysis because any nitrous oxide peak does not detected in blank analysis just after a seawater sample analysis. As a possibility, a

slight moisture in the sample gas could influence the sensitivity of the detector during seawater sample analysis. Further investigations are necessary for this phenomenon. As a stopgap measure on this cruise, calibration curves for nitrous oxide were prepared as following procedure. Standard gas was introduced into the system (and concentrated on cold trap) in the usual gas analysis sequence and immediately the N_2 gas flow path was switched to the sea water line containing the blank seawater. This method can analyze the standard gas under almost same condition as the seawater analysis. In order to take a priority in the accuracy of CFCs and SF_6, this procedure was not applied to the frequent standard gas analysis for sensitivity correction during sea water sample analysis. So accurate sensitivity correction would be difficult for N_2O analyses. A peak area of N_2O always became unusually small at the first seawater analysis after the standard gas analysis by the usual gas analysis sequence. This also seems to be the same cause that could be a lack of moisture. In this case, N_2O measurement was not reported (flag "5" was given) because the correction methods for such measurement has not been found at the present time.

5 Data archive

All data will be submitted to Data Management Group (DMG) of JAMSTEC .

5 Floats, Drifters and Moorings

5.1 Argo floats

(1) Personnel

Shuhei Masuda	***(JAMSTEC/RCGC): Principal Investigator (not on board)***
Shigeki Hosoda	***(JAMSTEC/ RCGC): not on board***
Kanako Sato	***(JAMSTEC/ RCGC): not on board***
Mizue Hirano	***(JAMSTEC/ RCGC): not on board***
Shingo Oshitani	***(MWJ): Technical Staff (Operation Leader)***

(2) Objectives

The purpose of this study is to clarify the mechanisms of climate and oceanic environment variability for understanding changes of earth system through estimations of heat and material transports, by sustainably monitoring in the global ocean. To get knowledge of those changes in the ocean, it is crucial to obtain well-quality controlled observational data.

As the Southern Ocean is one of the area where the number of active Argo float is unsatisfied to the target spatial density, which had been defined by the International Argo program, oceanic change is not well-understood although the Southern Ocean is one of the key region for climate changes. Especially physical process of the oceanic change below 2000m depth and biogeochemical process associated with global carbon cycle etc. are not yet recognized because of less amount of long-term ocean observations. To obtain physical and biogeochemical data in the Southern Ocean, we launched three Argo floats for measurements of temperature and salinity above 2000m depth, one deep Argo (Deep NINJA) for measurements temperature and salinity above 4000m depth and one deep/biogeochemical Argo (DO-Deep APEX) for measurements temperature, salinity and dissolved oxygen above 6000m depth at station points where shipboard CTD cast was conducted.

The continuously obtaining data form those floats will be opened as contribution of the Argo program, after conducting real-time quality control within 24 hours by Argo data assembly center and delayed mode quality controls within one year by JAMSTEC as Argo PI. Based on the Argo and deep/biogeochemical Argo data, we will investigate spatial and temporal variability of water mass such as Antarctic Intermediate Water and amount of carbon uptake and transport, adapting those data to data assimilation systems such as JAMSTEC's 4D-VAR data synthesis system (ESTOC). Further, we will evaluate accuracy of CTD and DO sensors mounted on the floats in comparison with the high accuracy shipboard CTD data at the station points, which makes Argo and deep/biogeochemical Argo data quality improve and then largely contributes to the International Argo program.

(3) Parameters

Water temperature, salinity, pressure, and dissolved oxygen

(4) Methods

i. Profiling float deployment of Argo

We launched one Navis float with SBE41 CTD sensor and two Arvor floats with SBE41 CTD sensor. The floats usually drift at a depth of 1000 dbar (parking depth), then dive to a depth of 2000 dbar (profiling depth) and rise up to the sea surface by changing its buoyancy every ten days. The floats measure temperature, salinity, and pressure when they rise to the sea surface. During staying at the sea surface within a few ten minutes ~ several hours, observed data are transmitted to the base station via telecommunication satellites in real-time. The specifications of floats and launching points are shown in Table 5.1.1.

Table 5.1.1 Specification of Navis/Arvor floats and launching point

Float Type (manufacturer)	Navis EBR (Sea-Bird Electronics Inc.)	Arvor (nke instrumentation)
CTD sensor	SBE41 (Sea-Bird Electronics Inc.)	SBE41 (Sea-Bird Electronics Inc.)
Cycle	10 days	10 days
Iridium transmit type	Router-Based Unrestricted Digital Internetworking Connectivity Solutions (RUDICS)	Argos system
Target Profiling Pressure	2000 dbar	2000 dbar
Target Parking Pressure	1000 dbar	1000 dbar
Sampling interval	2 dbar (approximately 1000 levels)	5~20 dbar (approximately 115 levels)
Mission control after launching	Available	Not available

Launching point

Float S/N	**WMOID**	**Date and Time of Launch(UTC)**	**Location of Launch**	**CTD St. No.**
F0415 (NAVIS)	5905051	2017/02/20 22:52	58° 0.828' [S] 125° 59.688' [W]	P17E16
OIN 13JAP-ARL-78 (Arvor)	7900692	2017/2/19 14:47	60° 57.888' [S] 125° 59.772' [W]	P17E10
OIN 13JAP-ARL-79 (Arvor)	5905052	2017/2/21 21:24	55-30.69[S] 125-57.09[W]	P17E21

ii. Profiling float deployment for biogeochemical/deep Argo

We also launched one deep/biogeochemical Argo float (DO-Deep APEX) and one deep Argo float (Deep NINJA). The Deep NINJA equipped with SBE41 for deep CTD sensor, and the DO-Deep APEX equipped with SBE61 CTD sensor and Optode4831 dissolved oxygen sensor. The floats measure using above sensors when they go up to the sea surface. During staying at the sea surface within a few ten minutes, observed data are transmitted as the same style as for the Argo floats shown in (4) i. Specifications and their launching points are shown in Table 5.1.2.

Table 5.1.2 Specification of Deep NINJA/DO-Deep APEX and launching point

Float Type (manufacturer)	Deep NINJA (Tsurumi Seiki Co.,Ltd)	Deep APEX (Teledyne Webb Research)
CTD sensor	SBE41 for Deep (Sea-Bird Electronics Inc.)	SBE61 (Sea-Bird Electronics Inc.)
Dissolved Oxygen Sensor	N/A	Optode4831 (Aanderaa Data Instruments)
Cycle	5 days	5 days
Iridium transmit type	Short Burst Data Service (SBD)	Router-Based Unrestricted Digital Internetworking Connectivity Solutions (RUDICS)
Target Parking Pressure	2000 dbar	2000 dbar
Target Profiling Pressure	4000 dbar	6000 dbar
Sampling interval	5 dbar (approximately 800 levels)	5 dbar (approximately 1200 levels)
Mission control after launching	Available	Available
Ice detection	Included	Included

Launching point

Float S/N	**WMO ID**	**Date and Time of Launch(UTC)**	**Location of Launch**	**CTD St. No.**
20	7900691	2017/02/19 14:41	60° 58.008' [S] 125° 59.982' [W]	P17E-10
45	Not yet obtained	2017/02/19 14:34	60° 58.140 [S] 126° 0.258' [W]	P17E-10

(5) Data archive

With regard to NAVIS, Arvor and Deep NINJA, observed data are delivered to meteorological

organizations, research institutes, and universities etc. via Global Data Assembly Center (GDAC: http://www.usgodae.org/argo/argo.html, http://www.coriolis.eu.org/) and Global Telecommunication System (GTS). Real-time and delayed mode quality controls are conducted within 24 hours and one year after receiving the data, respectively. Both data are provided from GDACs following procedure decided by the International Argo program. With regard to SBE61 on DO-Deep APEX, the data will not delivered via GDACs for a while because quality control method is not yet fixed in the Argo Data Management Team. Instead, we will provide the data from Argo JAMSTEC HP conducting quality checks.

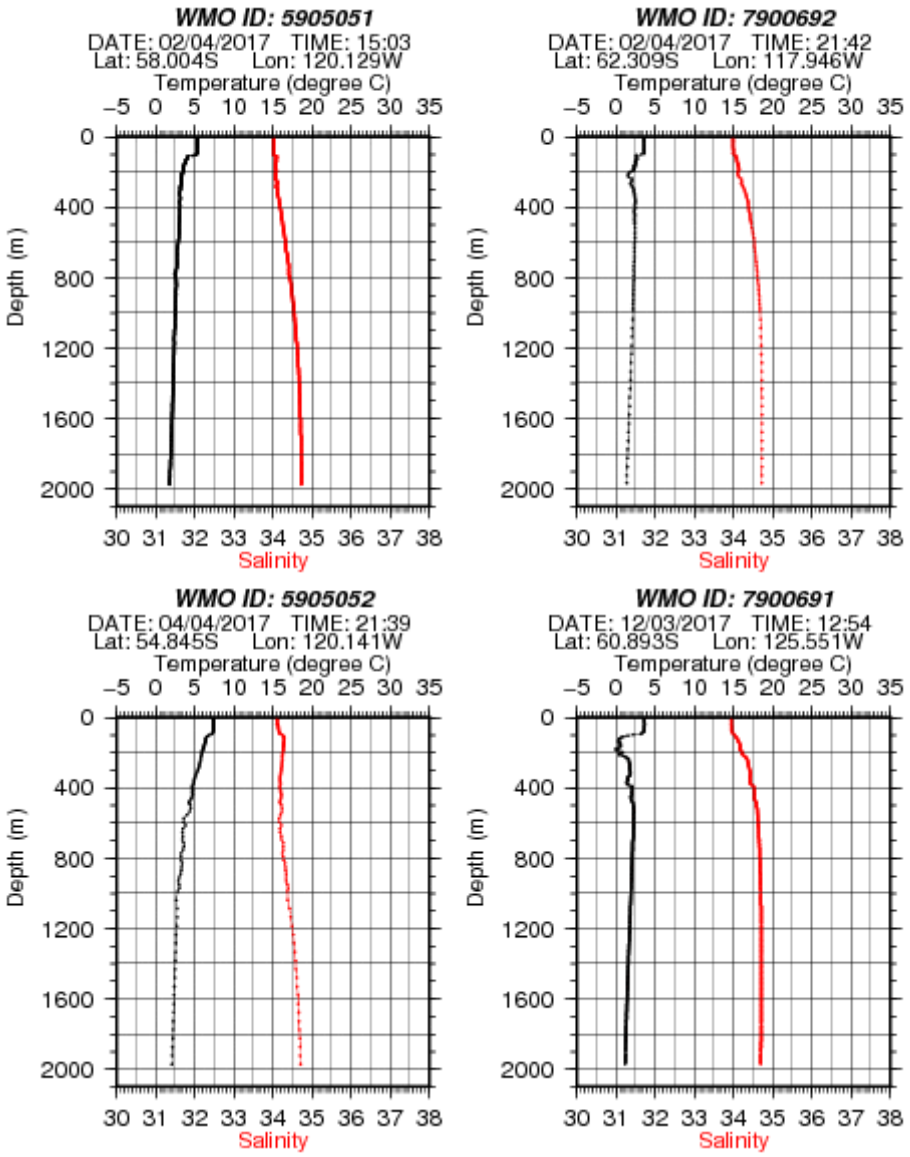

Fig. 5.1.1. First profiles of vertical temperature and salinity distribution from NAVIS (WMOID: 5905051), Arvor (WMOID: 7900692 and 5905052) and Deep NINJA (WMOID: 7900691 but only above 2000m depth).

5.2 SOCCOM biogeochemical floats

(1) Personnel

K. Katsumata (JAMSTEC), S. Riser, D. Swift (University of Washington), K. Johnson (Monterey Bay Aquarium Research Institute), E. Boss (U. Maine), L. Talley (Scripps Institution of Oceanography)

(2) Objectives

SOCCOM (Southern Ocean Carbon and Climate Observations and Modeling) is a project funded by NSF, NOAA, and NASA aiming at understanding the roles of Southern Ocean in climate change and biogeochemistry of the Earth system. Their main observational tool is a newly developed float with biogeochemical measurements. The project envisages deploying approximately 200 such floats within the Southern Ocean from 2014 to 2020. As a JAMSTEC contribution towards the project, we have deployed five floats during the P17E reoccupation. It is essential that the float deployment be accompanied with high-quality bottle data for calibrating the float sensors. GO-SHIP cruises, which strive for state-of-the-art accuracy and precision in CTD and chemistry analyses are a good platform for this purpose. In this section, we describe the float deployments. The accompanying bottle sampling is described in Section 4.26 of this report.

(3) SOCCOM BGC float

In addition to the usual temperature and salinity measurements, a SOCCOM biogeochemical Argo-type float carries sensors to measure acidity (pH), nutrient (nitrate), and oxygen. The APEX floats that were deployed in this cruise also carried a bio-optic sensor to measure ocean fluorescence and backscatter. Further references for the float specifications are available at SOCCOM (2017).

(4) Deployments

Five floats were deployed at five different CTD stations right after the CTD cast. After cleaning the FLBB and ISUS sensors with pre-moistened lens cleaning wipe and deionized water following Riser *et al.* (2017), the floats were deployed from the stern deck of *R/V Mirai* with a rope. The details of deployments are shown below. The year is 2017.

Stn	Latitude	Longitude	Depth	Time (UT)	Float Serial Num.
2	66-21.55°S	126- 1.47°W	4445 m	16 Feb 17:33	12371
4	65-1.00°S	125-56.51°W	4872 m	17 Feb 07:42	12379
8	62-20.59°S	126- 6.90°W	5055 m	19 Feb 00:43	12366
18	57-1.60°S	126- 0.12°W	4115 m	21 Feb 07:26	12386

24	54-0.00°S	125-58.42°W	3543 m	22 Feb 13:01	12542

References

Riser, S., R. Rupan, D. Swift, K. Johnson, C. Sakamoto, L. Talley, 2017, SOCCOM BGC Floats: Deployment and Cleaning Procedures, version 8 January 2017, available online at https://soccom.princeton.edu/content/manuals

SOCCOM, 2017, https://soccom.princeton.edu/content/float-specifications

5.3 CO_2 buoys

(1) Personnel

Akihiko Murata (JAMSTEC)

Kosei Sasaoka (JAMSTEC)

Tomonori Watai (MWJ)

Atsushi Ono (MWJ)

Emi Deguchi (MWJ)

Nagisa Fujiki (MWJ)

(2) Objective

It is said that the ocean takes up approx. 30% of CO_2 emitted into the atmosphere by human activities such as fossil fuel burning, deforestation, cement production, etc. Thus, accurate estimation of CO_2 uptake by the ocean is an important task in predicting global warming and related climate changes, because the ocean tends to moderate the warming by absorbing anthropogenic CO_2 from the atmosphere. Calculation of air-sea fluxes of CO_2 is one of straightforward methods to estimate the CO_2 uptake. Data for surface seawater partial pressure of CO_2 (pCO_2) are necessary for the calculation. Surface seawater pCO_2 data covering the world ocean have been collected by such an international activity as Surface Ocean Carbon Dioxide Atlas (SOCAT). However, in spite of the long-term effort over 40 years, a large data gap is still found in the Southern Hemisphere oceans, especially in the South Pacific. This is because the ocean is far away from pCO_2 observations-leading countries, i.e., difficult to do observations by research vessels due to high cost, and because there scarcely exist regular lines of cargo ships, along which pCO_2 observations have been conducted. Drifting buoys with pCO_2 sensor are free from the limitation. Therefore, we intend to deploy drifting buoys in the South Pacific during the MR16-09 cruise.

(3) Apparatus

The drifting pCO_2 buoy was constructed by NiGK Corporation. The specification of drifting CO_2 buoy is as Table 5.3.1.

Table 5.3.1 Specification of drifting CO_2 buoy.

Items	Specification
Size	Diameter: 315 mm (max.), Height: 575 mm
Weight	8.6 kg
Pressure proof	5 m
Positioning	GPS
Battery	Primary lithium battery
CO_2 range	150 – 1000 ppm
CO_2 resolution	< 1 ppm
Accuracy	< 1.5%

(4) Results

We injected 7 drifting CO_2 buoys into the South Pacific, where a large data gap exists. We injected them during the cruise of R/V *Mirai* (legs 1 and 3 of MR16-09) (Figs. 5.3.1 and 5.3.2), and started data acquisition through a satellite communication system. In addition, we introduced a server in order to stock, control and analyze data from drifting CO_2 buoys.

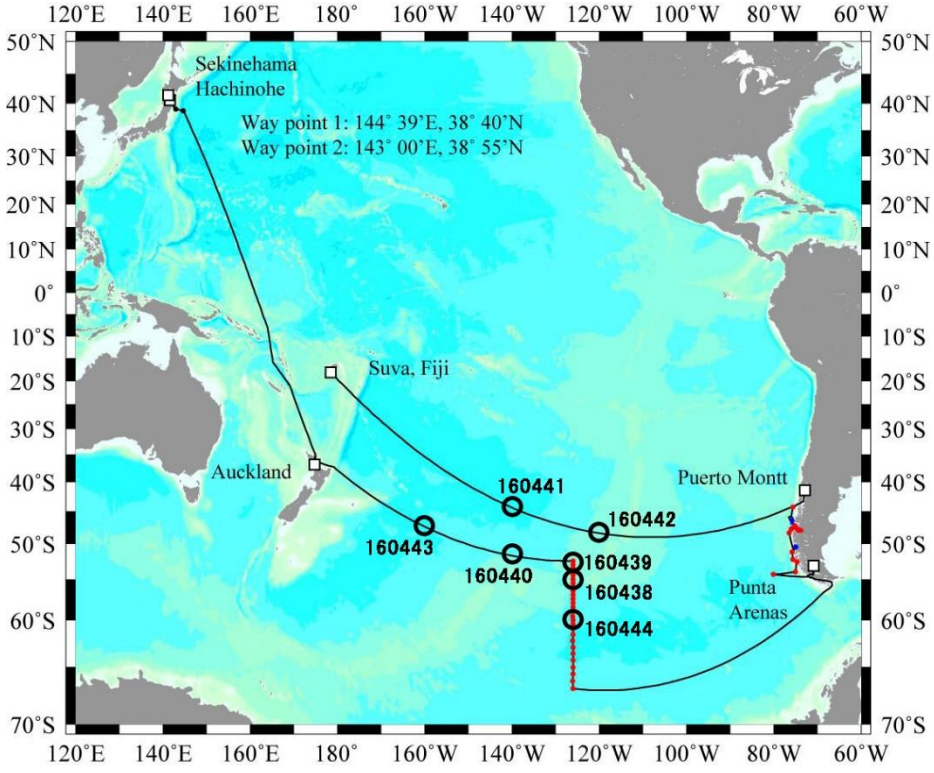

Fig. 5.3.1. Positions (circles) of drifting CO_2 buoys injected during the R/V *Mirai* cruise and the

Identification Number.

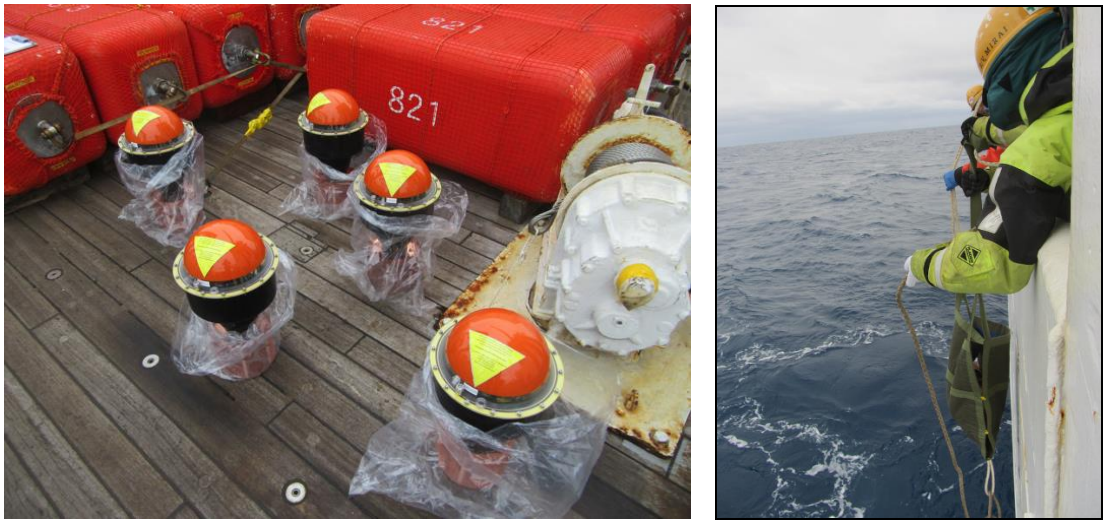

Fig. 5.3.2. Drifting CO_2 buoys on the deck of the R/V *Mirai* (left), and appearance of injection in the MR16-09 cruise (right).